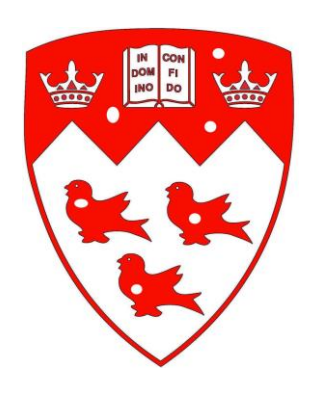
A NOVEL NANOPARTICLE FORMULATION FOR TARGETED DRUG DELIVERY IN CARDIOVASCULAR DISEASES

Nikita LomisDivision of Experimental Medicine



Biomedical Technology and Cell Therapy Research Laboratory
Division of Experimental Medicine
Faculty of Medicine
McGill University, Montreal

December 2019

A thesis submitted to McGill University in partial fulfillment of the requirements of the degree of Doctor of Philosophy

© Nikita Lomis, 2019

To my parents

ACKNOWLEDGEMENTS

The work presented in this thesis would not have been completed without the contribution of various individuals. I am immensely indebted to my thesis supervisor, Dr. Satya Prakash, for his support and guidance. He has not only provided me with an exceptional research environment, but also unique opportunities to learn and hone my skills. Constantly pushing my intellectual barriers, he has given me the freedom to design and lead my project, instilling in me confidence as an independent researcher. I feel privileged to have worked under his supervision.

I am extremely grateful to my co-supervisor, Dr. Dominique Shum-Tim. Through his vast research experience and clinical expertise in the cardiovascular field, he has supported me throughout the course of my PhD, especially while performing specialized techniques during animal studies. I extend my gratitude to my PhD committee members, Dr. Maryam Tabrizian, Dr. Giuseppe Martucci and Dr. Elena Torban for their constructive feedback and valuable questions on my project, thus shaping and improving it from its inception till the end.

I extend my gratitude to Dr. Susan Westfall, for being a supportive colleague, a confidante and wonderful friend, through the challenges of PhD life. To all my other colleagues including Umar Iqbal, Leila Farahdel, Ryan Buyting, Alicia Reyes, thank you for your words of encouragement, insightful comments and suggestions at various stages of my work. I fall short of words while thanking Dr. Meenakshi Malhotra, for being a pillar of strength and guiding me at every step of this journey. Her valuable feedback, guidance and remarks on my work have helped refine my scientific thinking, analysis and writing skills.

I thank Dr. Maryam Tabrizian and the Biomat'X laboratory for providing me complete access to their equipment which helped in generating valuable data for my PhD thesis. I also thank Mr. David Liu for his assistance with electron microscopy, Mr. Nadim Saadeh for help with Mass Spectrometry analysis, Ms. Camille Stegen for help and training with Flow cytometry, and Dr. Tara Sprules for NMR analysis. Furthermore, I would like to thank Dr. Aurore Dodelet-Devillers, Ms. Anna Choy, Ms. Annie Leblanc and Ms. Stephanie Lantosca at the McGill University Health Clinic Animal Facility for their assistance with animal training, handling and the complete animal

studies. Mr. Cleber Silveira Moraes at the Goodman Cancer Research Centre must be thanked for processing the tissue samples and preparing histology slides.

I specially acknowledge the support of the Department of Biomedical Engineering's academic staff. The Department Chair, Prof. David Juncker for his constant support, Prof. Robert Kearney for his motivation and encouragement, Prof. Ross Wagner for his technical assistance, and the department's coordinators, Trang Tran and Sabrina for their endless help and cheer over the years. I thank Mr. Pina Sorrini for her personal and academic support in both happy and challenging times during my PhD and always being available to hear me out. I am grateful to the Division of Experimental Medicine staff and coordinators, especially the Graduate Program Director, Prof. Anne-Marie Lauzon. I thank Ms. Marylin Linhares, Ms. Katerine Couvrette and Ms. Ilya Razykov for aiding and assisting me with all academic matters whenever needed.

This work was supported by the Natural Sciences and Engineering Research Council (NSERC) and Canadian Institutes of Health Research (CIHR) research grants. The funding support provided through the McGill University Faculty of Medicine Internal Studentships has been generous and was instrumental in helping me carry out my research work.

I am extremely grateful to Ms. Aditi Yadav for her friendship, endless moral support and motivation despite being continents apart, and Ms. Aishwarya Pendyala for seeing me through the motions of PhD life and beyond with her unconditional love, laughter and happiness.

Last but not the least, I am forever indebted to my family for their unwavering support throughout my academic career. My father, Dr. Kuldip Kumar Lomis, for being my backbone, role model and go-to person for everything and my mother, Mrs. Navita Lomis for tirelessly walking every step of this journey with me, always pushing me forward to pursue my dreams. To my brother, Nihit, for all the fun, amusement and cheer. Their love and blessings have kept me focused and on track, throughout. And finally, my spiritual guru, Gurudev Sri Sri Ravi Shankar, for instilling in me the zeal to reach my highest potential.

PREFACE

This thesis was prepared in accordance with the McGill University Thesis Preparation guidelines. This thesis has been presented in a manuscript-based thesis format consisting of three articles of original contribution, either published or to be submitted in peer reviewed journals. The articles in which I am the first author along with my co-authors are presented in Chapters 3, 4 and 5 of the thesis. Each chapter contains an abstract, introduction, materials and methods, results, discussion and conclusion section. The thesis also contains a common abstract, general introduction, literature review, general discussion of results, contributions to knowledge, conclusion and bibliography in accordance with the thesis guidelines.

TABLE OF CONTENTS

TABLE OF CONTENTS	6
ABSTRACT	10
LIST OF ABBREVIATIONS	12
LIST OF TABLES	
LIST OF FIGURES	
)•• 1 /
CHAPTER 1: GENERAL INTRODUCTION, RATIONALE, RESEARCH HYPOTHESIS, OBJECTIVES AND OUTLINE	20
1.1 GENERAL INTRODUCTION	
1.2 RATIONALE	
1.3 RESEARCH HYPOTHESIS	
1.4 Research Objectives	
1.5 Contributions	23
1.6 Thesis Outline	29
CHAPTER 2: BACKGROUND AND LITERATURE REVIEW	30
2.1 CARDIOVASCULAR DISEASES	
2.1.1 Congestive Heart Failure	
2.1.2 Pathophysiology of Congestive Heart Failure	
2.1.3 Neurohormonal Modulation in Congestive Heart Failure	
2.1.3.2 Role of the Angiotensin II Receptors	
2.1.3.3 Regulation of Cardiac Contractile Function in Heart Failure	34
2.1.4 Phosphodiesterase Inhibitors in Clinical Use for Heart Failure	34
2.1.4.1 Milrinone	35
2.1.4.2 Enoximone	
2.1.5 Other Inotrope Drugs in Clinical Use for Heart Failure	
2.1.6 Selecting Milrinone as Inotropic Therapy of Choice for Congestive Heart Failure	
2.1.7 Limitations to the Use of Milrinone in Heart Failure	39
2.2 NANOMEDICINE IN CARDIOVASCULAR DISEASES	39
2.2.1 Physicochemical Properties of Nanoparticles	40
2.2.1.1 Nanoparticle Size	40
2.2.1.2 Nanoparticle Surface Charge	41
2.2.1.3 Nanoparticle Shape and Surface Morphology	
2.2.2 Nanoparticle Uptake	
2.2.3 Nanoparticle Surface Functionalization and Targeting	
2.2.4 Introduction to Human Serum Albumin Nanoparticles	
2.2.4.1 Ethanol Desolvation (Coacervation)	
2.2.4.2 Emulsification	
2.2.4.4 Nano-Spray Drying	
2.2.4.5 Nab Technology	
2.2.5 Peptide-Conjugated Albumin Nanoparticles	48
PREFACE TO CHAPTERS 3 - 8	54

CONTRIBUTION OF AUTHORS	56
CHAPTER 3: NOVEL MILRINONE NANOFORMULATION FOR USE IN CARDIOVASCULAR DISEASES: PREPARATION AND IN VITRO	
CHARACTERIZATION	
3.1 Abstract	
3.2 Introduction	
3.3 Materials and Methods	
3.3.1 Materials	
3.3.2 Preparation and optimization of MRN-nanoformulation	
3.3.3 Nanoparticle characterization, yield and encapsulation efficiency	
3.3.4 Computational modelling of the HSA-MRN complex	
3.3.5 Circular Dichroism Measurement	
3.3.6 Enzymatic drug release from HSA-NPs	
3.3.7 Cellular uptake of nanoparticles by HUVEC cells and dose-dependent study	64
3.3.8 Flow cytometry	64
3.4 Results	65
3.4.1 Designing the MRN-nanoformulation	
3.4.2 Preparation and optimization of the MRN-nanoformulation	65
3.4.2.1 Effect of HSA concentration on nanoformulation	65
3.4.2.2 Effect of pH preparative solution on nanoformulation	
3.4.2.4 Effect of glutaraldehyde on nanoformulation.	
3.4.2.5 Effect of MRN concentration on nanoformulation	
3.4.2.6 Effect of glutaraldehyde polymerization time on nanoformulation	
3.4.3 SEM analysis of MRN-nanoformulation	
3.4.4 Molecular Docking study of HSA-MRN interaction	
3.4.5 Effect of MRN binding on different HSA conformations	
3.4.6 Enzymatic degradation of HSA-NPs and MRN release	
3.4.7 Intracellular nanoparticles uptake	
3.4.8 Flow cytometry analysis	
3.4.9 Cell viability analysis	
3.5 DISCUSSION	
3.6 CONCLUSION	
3.7 ACKNOWLEDGEMENTS	
3.8 References	75
CHAPTER 4: SYNTHESIS OF PEPTIDE CONJUGATED HUMAN SERUM ALB	UMIN
NANOPARTICLES FOR TARGETED MILRINONE DELIVERY	92
4.1 Abstract	93
4.2 Introduction	94
4.3 MATERIALS AND METHODS	95
4.3.1 Materials	95
4.3.2 Synthesis of the AT1-peptide	
4.3.3 Surface Modification of HSA with AT1 peptide	
4.3.4 Mass Spectrometry	
4.3.5 Nanoparticle Preparation	97
4.3.6 Nanoparticle characterization, yield and encapsulation efficiency	
4.3.7 Cell culture and viability	0.0

4.3.8 Overexpression of the AT1 Receptor	98
4.3.9 Intracellular Nanoparticle Uptake	
4.3.10 Confocal Microscopy	99
4.4 Results	100
4.4.1 Mass Spectrometry	100
4.4.2 Characterization of the AT1-nanoparticle formulation	100
4.4.3 Cell Viability Analysis	100
4.4.4 Angiotensin II Type 1 Receptor Overexpression	101
4.4.5 Intracellular Nanoparticle Uptake Analysis	101
4.4.6 Confocal Microscopy Analysis	102
4.5 DISCUSSION	102
4.6 CONCLUSION	104
4.7 ACKNOWLEDGEMENTS	104
4.8 References	105
CHAPTER 5: TARGETED MILRINONE DELIVERY USING ALBUMIN	
NANOCARRIERS IN A RAT MODEL OF CONGESTIVE HEART FAILURE	115
5.1 Abstract.	
5.2 Introduction.	
5.3 Materials and Methods	
5.3.1 Materials	
5.3.2 Synthesis of the AT1 Peptide	
5.3.3 Surface Modification of HSA with AT1 Peptide	
5.3.4 Mass Spectrometry	
5.3.5 Quantification of AT1 Peptide Attached to HSA	
5.3.6 Nanoparticle Preparation	
5.3.7 Nanoparticle Characterization	
5.3.8 In Vitro Milrinone Release from Nanoparticles	
5.3.9 In Vivo Studies	
5.3.10 Pharmacokinetics and Biodistribution Study	
5.3.11 Ligation of the Left Anterior Descending Coronary Artery to Induce CHF	
5.3.12 Animal Mortality	
5.3.13 Blood Serum and Plasma Collection	
5.3.14 Quantification of Milrinone from Rat Plasma	123
5.3.15 Echocardiography Procedure	
5.3.16 Cytokine Measurement	
5.3.17 Tissue Collection and Histological Analysis	
5.4 Results	
5.4.1 Synthesis of AT1-HSA-MRN-NPs	125
5.4.2 Mass Spectrometry Analysis of AT1-HSA	
5.4.3 Quantification of AT1 Peptide bound to HSA	
5.4.4 Characterization of the AT1-HSA-MRN-NPs	
5.4.5 In Vitro Cumulative Milrinone Release Analysis	
5.4.6 Pharmacokinetics Analysis	
5.4.7 Tissue Distribution of AT1-HSA-MRN-NPs	
5.4.8 Milrinone Quantification from Rat Plasma	128
5.4.9 Safety and Toxicity of AT1-nanoparticle formulation	128

5.4.10 Cardiac Function Assessment	129
5.4.11 Serum Cytokine Measurements	
5.4.12 Safety and Toxicity Analysis	
5.5 DISCUSSION	
5.6 CONCLUSIONS	134
5.7 ACKNOWLEDGEMENTS	134
5.8 References	134
CHAPTER 6: GENERAL DISCUSSION	150
CHAPTER 7: SUMMARY OF OBSERVATIONS, CLAIMED ORGINAL	
CONTRIBUTIONS TO KNOWLEDGE AND CONCLUSIONS	158
7. 1 SUMMARY OF COMPLETED RESEARCH OBJECTIVES	158
7.2 CLAIMED ORIGINAL CONTRIBUTIONS TO KNOWLEDGE	161
7.3 Conclusion	162
CHAPTER 8: RECOMMENDATIONS	164
BIBLIOGRAPHY	166

ABSTRACT

Cardiovascular diseases are the leading cause of mortality across the globe. Of the various cardiovascular diseases, congestive heart failure is the most prevalent. Heart failure has no permanent cure, yet certain treatments and lifestyle changes can help enhance the patients' quality of life. Congestive heart failure is commonly treated by delivering drugs which lower the blood pressure and improve the heart's pumping action. However, their use has limitations such as lack of specificity, toxicity, low retention time in the body along with side effects such as hypotension, arrhythmia, nausea, vomiting etc. It is anticipated that the targeted delivery of drugs would help address and overcome these limitations. This thesis focuses on the design and development of a nanoparticle-based formulation for the targeted delivery of the drug, milrinone, for congestive heart failure treatment. The action of milrinone helps in improving the contraction ability and functioning of the failing heart. The nanoparticles were prepared from the protein, human serum albumin, which was surface functionalized to bind the angiotensin II type 1 (AT1) peptide. The peptide-tagged nanoparticles were designed to target the AT1 receptors, found to be overexpressed on the myocardium under heart failure conditions, therefore facilitating higher nanoparticle uptake and drug delivery to the heart. The nanoparticles were spherical with a particle size between 100-200 nm and negative surface charge, indicating high physical stability. The in vitro characterization studies showed that the nanoparticle formulation was target-specific, biodegradable, biocompatible and suitable for use in vivo. The in vivo pharmacokinetics and tissue distribution studies of the targeted nanoparticle formulation revealed superior drug delivery and release, with improvement in the retention time of milrinone compared to the non-targeted drug. The treatment efficacy of this formulation was validated using a rat model of congestive heart failure, where it was found to be safe and effective in improving the cardiac function and contractility. Therefore, this targeted nanoparticle formulation delivering milrinone exhibits immense potential for use in congestive heart failure and related cardiovascular disease.

RÉSUMÉ

Les maladies cardiovasculaires sont la principale cause de mortalité dans le monde. Parmi les diverses maladies cardiovasculaires, l'insuffisance cardiaque congestive est la plus répandue. L'insuffisance cardiaque n'a pas de guérison, mais certains traitements et changements de mode de vie peuvent améliorer la qualité de vie des patients. L'insuffisance cardiaque congestive est généralement traitée en administrant des médicaments qui abaissent la tension artérielle et améliorent l'action de pompage du cœur. Cependant, leur utilisation présente des limites telles que le manque de spécificité, la toxicité, un temps de rétention court dans l'organisme, ainsi que des effets indésirables tels que l'hypotension, l'arythmie, les nausées, les vomissements, etc. L'administration ciblée de médicaments contribuerait à remédier à ces limites. Cette thèse porte sur la conception et le développement d'une formulation à base de nanoparticules pour la délivrance ciblée du médicament, la milrinone, destinée au traitement de l'insuffisance cardiaque congestive. L'action de la milrinone contribue à améliorer la capacité de contraction et le fonctionnement du cœur défaillant. Les nanoparticules ont été préparées à partir de la protéine, la sérum albumine humaine, qui a été fonctionnalisée en surface pour se lier au peptide de l'angiotensine II type 1 (AT1). Les nanoparticules à marquage peptidique ont été développées pour cibler les récepteurs AT1, surexprimées sur le myocarde dans des conditions d'insuffisance cardiaque, facilitant ainsi une absorption plus élevée de nanoparticules et une délivrance de médicaments au cœur. Les nanoparticules étaient sphériques avec une taille de particule entre 100 et 200 nm et une charge de surface négative, indiquant une stabilité physique élevée. Les études de caractérisation in vitro ont montré que la formulation de nanoparticules était spécifique à la cible, biodégradable, biocompatible et adaptée à une utilisation in vivo. Les études de pharmacocinétique et de distribution tissulaire in vivo de la formulation de nanoparticules ciblées ont révélé une libération de médicament supérieure, avec une amélioration du temps de rétention de la milrinone par rapport au médicament non ciblé. L'efficacité du traitement de cette formulation a été validée à l'aide d'un modèle d'insuffisance cardiaque congestive chez le rat, où elle s'est révélée sécuritaire et efficace pour améliorer la fonction cardiaque et la contractilité. Par conséquent, cette formulation de nanoparticules ciblée délivrant de la milrinone présente un potentiel immense en cas d'insuffisance cardiaque congestive et de maladies cardiovasculaires associées.

LIST OF ABBREVIATIONS

ACE Angiotensin Converting Enzyme

ALP Alkaline Phosphatase

ALT Alanine Aminotransferase

AMP Adenosine Monophosphate

AST Aspartate Transaminase

ATP Adenosine Triphosphate

ATPase Adenosine Triphosphatase

Ang II Angiotensin II

AT1 Angiotensin II Type 1

AT1R Angiotensin II Type 1 Receptor

Ca²⁺ Calcium ions

CAD Coronary Artery Disease

cAMP cyclic 3',5'- Adenosine Monophosphate

CD Circular Dichroism

cGMP cyclic 3',5'- Guanosine Monophosphate

CHF Congestive Heart Failure

CICR Calcium Induced Calcium Release

CRE Creatinine

CVD Cardiovascular Diseases

Da Dalton

DDQ 2,3-dichloro-5,6-dicyanobenzoquinone

DMEM Dulbecco's Modified Eagle Medium

DMSO Dimethyl Sulfoxide

DNA Deoxyribonucleic acid

DLS Dynamic Light Scattering

EDC 1-Ethyl-3-[3-dimethylaminopropyl]carbodiimide hydrochloride

EE Encapsulation Efficiency

EPR Enhanced Permeability and Retention

ET-1 Endothelin-1

FBS Fetal Bovine Serum

FITC Fluorescein Isothiocynate

g gram

gp glycoprotein

GGT gamma glutamyl transferase

HSA Human Serum Albumin

HF Heart Failure

hr hour

HUVEC Human Umbilical Vein Endothelial Cell

IBP Ibuprofen

IL Interleukin

IV Intravenous

K⁺ Potassium ions

kcal kilocalorie

kDa kilo Dalton

kg kilogram

kV kilovolt

L Litre

LAD Left Anterior Descending

LTCC L-type Calcium Channel

LV Left Ventricular

LVEDD Left Ventricular End Diastolic Diameter

LVESD Left Ventricular End Systolic Diameter

LVEDV Left Ventricular End Diastolic Volume

LVEDV Left Ventricular End Systolic Volume

LVEF Left Ventricular Ejection Fraction

LVFS Left Ventricular Fractional Shortening

MALDI Matric Assisted Laser Desorption/ Ionization

mg milligram

mL mililiter

mM milimolar

M molar

MI Myocardial Infarction

mL mililitre

MMP Matrix Metalloproteinase

MRN Milrinone

min minute

μg microgram

μL microliter

μM micromolar

μmol micromole

mmol milimole

mol mole

MTT 3-(4,5-dimethylthiazol-2-yl)-2,5-diphenyltetrazolium bromide

mV millivolt

MWCO molecular weight cutoff

Na⁺ Sodium ions

ng nanogram

NHS N-hydroxysuccinimide

nm Nanometer

nM nanomolar

NP Nanoparticle

PA Propionic Acid

PBS Phosphate Buffer Saline

PCI Percutaneous Coronary Intervention

PCWP Pulmonary Capillary Wedge Pressure

PDE Phosphodiesterase

PDI Polydispersity Index

PEG Polyethylene Glycol

pg picogram

PLGA Polylactic-co-glycolic acid

PKA Protein Kinase A

RAAS Renin Angiotensin Aldosterone System

RAS Renin Angiotensin System

RES Reticuloendothelial System

RGD Arginylglycylaspartic acid

RNA Ribonucleic Acid

rpm rotations per minute

RWF Warfarin

SD Standard Deviation

SEM Scanning Electron Microscopy

SNS Sympathetic Nervous System

SPA Succinimidyl propionate

SR Sarcoplasmic Reticulum

TEM Transmission Electron Microscopy

TnC Troponin C

TOF Time of Flight

TNF Tumour Necrosis Factor

THY Thyroxine

UV Ultraviolet

Wt. Weight

LIST OF TABLES

Table 2.1. List of Inotropic drugs for use in congestive heart failure53
Table 3.1. Encapsulation efficiency of MRN-HSA-NPs at various MRN concentrations, represented as HSA/MRN molar ratio. MRN concentrations, molar ratio.
Table 3.2. Predicted binding affinities between HSA and MRN using the Wilma and SIE scoring90
Table 3.3. HSA secondary structural content on interaction with MRN in different molar ratios. MRN in different molar m
Table 3.4. Cumulative release of MRN from MRN-HSA-NPs in the presence of different enzymes. 91
Table 4.1. Parameters for nanoparticle characterization of AT1-HSA-MRN-NPs115
Table 5.1. Nanoparticle size, charge, encapsulation efficiency and yield at various MRN/HSA (wt./wt.) ratios of nanoparticle preparation
Table 5.2. Pharmacokinetic parameters of AT1-HSA-MRN-NPs and MRN-Lactate at MRN dose 50 μg/kg
Table 5.3. Percentage LVEF measurements for Groups I, II, III, IV and V149
Table 5.4. Percentage LVFS measurements for Groups I, II, III, IV and V150

LIST OF FIGURES

Figure 2.1. Myocardial infarction leading to congestive heart failure due to plaque build up (atherosclerosis)
Figure 2.2. Mechanism of Action of Milrinone for Myocardial Contraction in Cardiomyocytes
Figure 2.3. Chemical structure of Milrinone (1,6-Dihydro-2-methyl-6-oxo(3,4'-bipyridine)-5-carbonitrile)
Figure 2.4. Advantages and limitations of milrinone treatment for congestive heart failure51
Figure 2.5. Molecular structure of Human Serum Albumin
Figure 2.6. Schematics and steps of preparation of human serum albumin nanoparticles following the ethanol desolvation method
Figure 3.1. Optimization of parameters for preparation of MRN-HSA-NPs80
Figure 3.2. Nanoparticle surface characterization using SEM analysis
Figure 3.3. Molecular docking predictions
Figure 3.4. Far-UV CD spectra of HSA at different pH and HSA/MRN molar ratios83
Figure 3.5. Cumulative release of MRN from 1 mg/mL MRN-HSA-NPs in the presence of various enzymes
Figure 3.6. Intracellular uptake of MRN-HSA-NPs and HSA-NPs in HUVEC cells85
Figure 3.7. Intracellular uptake of MRN-HSA-NPs and HSA-NPs in H9c2 cells86
Figure 3.8. Flow cytometry analysis of intracellular uptake of FITC-HSA-NPs87
Figure 3.9. Viability of HUVECs incubated with MRN-HSA-NPs compared with MRN-Lactate at different MRN concentrations
Figure 3.10. Viability of H9c2 cells incubated with MRN-HSA-NPs (black bars) compared with MRN-Lactate (grey bars) at different MRN concentrations
Figure 4.1. Schematic representation of the surface modification of the HSA molecule for binding with the AT1 peptide through a two-step chemical conjugation reaction using cross-linkers

Figure 4.2. HSA (lower) and AT1-HSA (upper) was analyzed by Matrix-Assisted Laser Desorption/Ionization Time of Flight Mass Spectrometry
Figure 4.3. Nanoparticle surface characterization using TEM analysis
Figure 4.4. Cell viability analysis on H9c2 cells treated with MRN-Lactate, AT1-HSA-MRN-NPs and AT1-HSA-NPs at 1 mM MRN concentration
Figure 4.5. Viability of H9c2 cells treated for hypoxia and hypertrophy in comparison with normal cells (non-hypoxic and non-hypertrophic)
Figure 4.6. AT1 expression in normal, hypoxic and hypertrophic H9c2 cells 112
Figure 4.7. Intracellular uptake of MRN-HSA-NPs, AT1-HSA-MRN-NPs and Scr-HSA-MRN-NPs in H9c2 cells
Figure 4.8. H9c2 cells under Normal, Hypoxic and Hypertrophic conditions demonstrate uptake of fluorescently-tagged nanoparticles
Figure 4.9. H9c2 cells treated with the FM 4-64 stain and
Figure 5.1. Schematic representation of the surface modification of the HSA molecule for binding with the AT1 peptide through a two-step chemical conjugation reaction using cross-linkers PA-(PEG) ₄ -SPA and EDC/Sulfo-NHS
Figure 5.2. HSA (lower) and AT1-HSA (upper) was analyzed by Matrix-Assisted Laser Desorption/Ionization Time of Flight Mass Spectrometry
Figure 5.3. Nanoparticle surface characterization using TEM analysis140
Figure 5.4. Cumulative drug release (mean \pm SD %, $n=3$) of AT1-HSA-MRN-NPs with starting MRN concentrations 0.8 mg/mL over predetermined time intervals of 0, 0.25, 0.5, 0.75, 1, 2, 4, 8, 18 and 24 hrs
Figure 5.5. Pharmacokinetics of AT1-HSA-MRN-NPs and MRN-Lactate at an initial MRN dose of 50 μg/kg <i>in vivo</i>
Figure 5.6. Tissue distribution of AT1-HSA-MRN-NPs and MRN-Lactate at an initial MRN dose of 50 μg/kg <i>in vivo</i>
Figure 5.7. Milrinone levels detected in plasma 24 hrs post treatment
Figure 5.8. Serum analysis performed as a safety test comparing the (a) ALP (U/L), (b) ALT (U/L) and (c) AST (U/L) as liver function tests

Figure 5.9. Serum analysis performed as a safety test comparing the (a) creatinine (μmol/L) and (b) urea (mmol/L) as kidney function tests
Figure 5.10. Percentage LVEF measurements for Groups I, II, III, IV and V at baseline, 48 hours post ligation, 60 mins, 24 hrs, 48 hrs and 1-week post injections
Figure 5.11. Percentage LVFS measurements for Groups I, II, III, IV and V at baseline, 48 hours post ligation, 60 mins, 24 hrs, 48 hrs and 1-week post injections
Figure 5.12. Serum cytokine levels for (a) IL-6 (pg/mL), (b) TNF-α (pg/mL) and (c) IL-10 (pg/mL)
Figure 5.13. Images of thin sections of H & E stained hearts

CHAPTER 1: GENERAL INTRODUCTION, RATIONALE, RESEARCH HYPOTHESIS, OBJECTIVES AND OUTLINE

1.1 General Introduction

Cardiovascular diseases (CVDs) are a significant and ever-growing problem across the world, being the leading cause of mortality in developed and developing countries ¹. As humans experience changes in lifestyle, new risk factors are introduced ranging from high blood pressure, cholesterol, diabetes, obesity to unhealthy diets and physical inactivity ². Careful reduction of the associated risk factors could thus help in prevention of CVDs. Though CVDs encompass a number of linked pathologies, these could be classified based on their underlying causes such as ischemia, hypertension, structural deformities, valvular defects, inflammation, arrhythmias and cardiomyopathy ^{1,3}. Of these CVDs, congestive heart failure (CHF) resulting from myocardial infarction (MI) or ischemia, is the most prevalent ⁴. Every year, approximately 600,000 cases of CHF are reported across Canada creating a huge economic burden, with almost 2.8 billion dollars spent in direct healthcare costs towards this disease ^{1,5,6}.

CHF is commonly treated by delivering drugs such as angiotensin converting enzyme (ACE) inhibitors, angiotensin receptor blockers, beta blockers, diuretics and inotropes ⁷. The mechanism of action of these drugs results in lowering of blood pressure, vasodilation, diuresis or changes in the myocardial contractility ⁸. However, some limitations associated with the use of the majority of these drugs include the lack of specificity, toxicity, immunogenicity and lower retention time in the body ⁷. Additionally, their use is linked with side effects such as hypotension, arrhythmia, anorexia, nausea, vomiting, renal impairment, hyperkalaemia etc. ⁹. Thus, with the ever-growing incidences of CHF, novel strategies must be introduced to effectively prevent and treat cardiovascular syndromes. Though much research undertaken for developing preventative and therapeutic strategies involves pharmacological and surgical procedures, the emergence of nanomedicine as a modality for use in CHF has displayed tremendous potential.

Nanomedicine is one of the most promising fields of research involving the development of nanoparticle formulations ranging in the size of 1-100 nm ¹⁰. The ability to multifunctionalize nanoparticles with various small molecules, ligands and peptides etc. for targeted delivery of

drugs, hormones, genes and other small molecules has enhanced their therapeutic applications. In addition, the properties of the nanoparticles may be tailored further to serve as diagnostic and imaging agents, treatment modalities and innovative therapies ¹¹⁻¹³. The surface modification of the nanoparticles plays an essential role in improving drug delivery, modulating their biodistribution, blood circulation time and permeation into inflamed tissues ^{14,15}. Although, till date, only a minor number of nanoparticle formulations have reached clinical trials, the abundance of relevant data demonstrating their advantages over existing treatments, highlights the need of continual research efforts in this direction ^{16,17}.

Recent literature suggests that nanoparticles ranging in particle sizes between 100 nm to 400 nm demonstrate an enhanced permeability and retention (EPR) effect and may therefore be used for cardiac therapy ¹⁸. It is also well known that particles with size greater than 250 nm may be eliminated from the blood circulation due to opsonization and the reticuloendothelial system (RES) effect ¹⁹. Therefore, preparation of nanoparticles of an optimal size ranging up to 250 nm is essential to maintain longer blood circulation times ^{20,21}. Additionally, the surface charge of the particles also contributes to this effect. Therefore, highly positively and negatively charged particles are known to be physically stable due to electrostatic repulsions of the individual particles ¹⁹. The features of an ideal nanoparticle include optimal particle size, physical stability, target specificity, biocompatibility, biodegradability, and non-immunogenicity ²⁰. These characteristics may be found in various bioinspired nanocarriers such as proteins, polymeric nanoparticles, liposomes, dendrimers, etc. However, nanoparticles prepared from the protein, human serum albumin (HSA) have proven to be highly malleable with a high drug binding capacity and potential for surface-functionalization to introduce target specificity features ²²⁻²⁶.

Human serum albumin nanoparticles (HSA-NPs) have been evaluated for the delivery of a variety of hydrophobic and hydrophilic drugs such as paclitaxel, docetaxel, doxorubucin etc. ²⁷⁻²⁹. However, the studies presented in this thesis are the first of its kind to demonstrate the design and development of targeted HSA-NPs for binding and delivery of the drug, milrinone (MRN), for use in CHF. MRN is a phosphodiesterase-3 enzyme (PDE3) inhibiting drug, which improves the contraction ability of the heart and its function under failure conditions ³⁰. However, with a half-life of approximately 2 hours in humans, it is rapidly cleared from the body and is therefore

clinically administered via a continuous infusion as a lactate formulation (MRN-Lactate). Thus, the targeted delivery of MRN would help overcome this limitation as HSA-NPs improve the drug retention time, solubility, delivery specificity and drug bioavailability ³¹.

To achieve targeted drug delivery to the heart, HSA-NPs could be surface-functionalized with targeting moieties such as peptides. Research has shown that the angiotensin II type 1 (AT1) receptors present on the myocardium are found to be overexpressed under CHF conditions ³²⁻³⁴. Delivering AT1-tagged HSA-NPs carrying MRN, would facilitate greater targeting, cellular uptake and delivery of MRN under CHF. In this thesis, a novel targeted nanoparticle formulation has been designed and developed for MRN binding and delivery to the heart for efficient treatment of CHF.

1.2 Rationale

Every year, thousands of patients are hospitalized because of CHF, with greater than 30% mortality within the first year of admission ^{1,5}. Additionally, the post-HF outcomes include side-effects, severity of symptoms and lower quality of life with the currently available medical and surgical treatments ³⁵. CHF is commonly treated by delivering cardiac drugs which improve the heart's contraction ability ³⁶. However, their poor bioavailability, lack of target specificity, low blood circulation and retention, immunogenicity and side effects, makes them inefficient for treatment ³¹. Despite significant advances in HF treatment, there is an unmet need to focus on developing safer and efficient therapies which offer cost-effective, lasting effects, reduced side-effects and higher quality of life for patients. Thus, the emergence of bioinspired nanomedicine-based treatments for targeted drug delivery offers tremendous potential in accomplishing the desired outcomes for prevention and treatment of CHF and related CVDs.

1.3 Research Hypothesis

The novel nanoparticle formulation designed for targeted delivery of MRN will achieve superior drug delivery and treatment efficacy in CHF and other CVDs.

1.4 Research Objectives

The thesis research objectives are to:

- 1. Perform an extensive literature review to design the most appropriate nanoparticle-based targeted drug delivery system for a therapeutic application in CVDs.
- 2. Design, prepare, optimize and characterize HSA-NPs to obtain a particle size between 100-200 nm for delivery of MRN. This objective includes determining the optimal HSA concentration, pH, MRN/HSA ratio, polymerization time, maximum yield, encapsulation efficiency, particle size and zeta potential for nanoparticle formulation development.
- 3. Investigate the binding efficiency between MRN and HSA using computational modelling, circular dichroism analysis and enzymatic drug release. Evaluate the cellular uptake and cytotoxicity of MRN-HSA-NPs in cardiomyoblasts and endothelial cells.
- 4. Synthesize and develop a targeted nanoparticle formulation, AT1-HSA-MRN-NPs, for specific delivery of MRN. The synthesis includes a novel scheme to functionalize the HSA molecule with the AT1 peptide through chemical conjugation. Perform *in vitro* characterization of the AT1-HSA-MRN-NPs through cellular uptake studies and drug release analysis.
- 5. Determine the *in vivo* pharmacokinetics and tissue distribution of the targeted AT1-HSA-MRN-NPs formulation and compare with the non-targeted MRN-Lactate.
- 6. Validate the developed targeted AT1-HSA-MRN-NPs formulation in an animal model of CHF and determining the change in cardiac function and heart contractility parameters.

1.5 Contributions

Original research contributions were made towards fulfilment of the thesis objectives included in the form of published and unpublished papers, research abstracts, presentations and awards. These have been listed below:

Original research articles included in the thesis

- Lomis, N., Gaudreault, F., Malhotra, M., Westfall, S., Shum-Tim, D., Prakash, S. (2017)
 Novel Milrinone Nanoformulation for Use in Cardiovascular Diseases: Preparation and In
 Vitro Characterization. *Mol Pharmaceut*. 15(7):2489-2502
- 2. **Lomis, N.**, Westfall, S., Shum-Tim, D., Prakash, S. (2019) Synthesis of Peptide Conjugated Human Serum Albumin Nanoparticles for Milrinone Delivery. (To Be Submitted)

3. **Lomis, N.**, Sarfaraz, Z. K., Alruwaih, A., Westfall, S., Shum-Tim, D., Prakash, S. (2019) Targeted Milrinone Delivery Using Albumin Nanocarriers in a Rat Model of Congestive Heart Failure. (To Be Submitted)

Other original research articles not included in the thesis

- 4. **Lomis, N.**, Westfall, S., Farahdel, L., Malhotra, M., Shum-Tim, D., Prakash, S. (2016) Human Serum Albumin Nanoparticles for Use in Cancer Drug Delivery: Process Optimization and *In Vitro* Characterization. *Nanomaterials*. 6(116):1-17.
- 5. **Lomis N.**, Westfall, S., Shum-Tim, D., Prakash, S. (2019) Human Serum Albumin Nanoparticles for Cardiovascular Drug Delivery. (To Be Submitted)
- 6. **Lomis N.**, Westfall, S., Shum-Tim, D., Prakash, S. (2019) Applications of Biomaterials in Cardiac Repair. (To Be Submitted)
- 7. Westfall, S., **Lomis, N.**, Prakash, S. (2019) A novel symbiotic delayes Alzheimer's disease onset via combinatorial gut-brain axis signaling in Drosophila melanogaster. *Plos One 14(4)*.
- 8. Westfall, S., **Lomis, N.**, Prakash, S. (2018) Longevity extension in Drosophila through gutbrain communication. *Scientific reports* 8 (1), 8362.
- 9. Westfall, S., **Lomis**, **N.**, Prakash, S. (2018) A novel polyphenolic prebiotic and probiotic formulation have synergistic effects on the gut microbiota influencing Drosophila melanogaster physiology. *Artificial cells*, *nanomedicine*, *and biotechnology*, *1-15*.
- 10. Westfall, S., **Lomis, N.**, Prakash, S. (2018) Ferulic Acid Produced by Lactobacillus fermentum Influences Developmental Growth Through a dTOR-Mediated Mechanism. *Molecular biotechnology*, 1-11.

- 11. Westfall, S., **Lomis, N.**, Kahouli I, Dia SY, Prakash, S. (2017) Microbiome, probiotics and neurodegenerative diseases: deciphering the gut brain axis. *Cellular and Molecular Life Sciences*. 74(14).
- 12. Westfall, S., **Lomis, N.**, Singh, S.P., Prakash, S. (2016) Ferulic acid produced by Lactobacillus fermentum NCIMB 5221 reduces symptoms of metabolic syndrome in Drosophila melanogaster. *J. Microbial Biochem. Tech.* 8(4):272-284.
- 13. Pacelli, S., Manoharan, V., Desalvo, A., **Lomis, N.**, Jodha, K.S., Prakash, S., and Paul, A., (2015) Tailoring biomaterial surface properties to modulate host-implant interactions: implication in cardiovascular and bone therapy. *Journal of Materials Chemistry B*, 4.9: 1586-1599.
- 14. Westfall, S., **Lomis**, **N.**, Singh, S.P., Prakash, S. (2015) The gut microflora and its metabolites regulate the molecular crosstalk between diabetes and neurodegeneration. *J.Diabetes Metab*, 6(8): 1-16.
- 15. Westfall, S., Lomis, N., Singh, SP., Prakash, S. (2015) The gut microflora and its metabolites regulate the molecular crosstalk between diabetes and neurodegeneration. *J Diabetes Metab* 6:577. Doi:10.4172/2155-6156.1000577.

Other Refereed Contributions (Abstracts/Presentations/Posters)

- Lomis, N., Gaudreault, F., Malhotra, M., Shum-Tim, D., and Prakash, S. "Development of a novel nanoparticle-based therapy for cardiovascular diseases". International Symposium on Blood substitutes, Oxygen Therapeutics and Nanomedicine Conference, *Montreal*, QC. Nov 2017.
- 2. **Lomis, N.**, Gaudreault, F., Malhotra, M., Shum-Tim, D., and Prakash, S. "A novel nanoparticle formulation for enhanced delivery of milrinone for cardiac applications". 3rd

- International Drug Discovery and Development Forum. *Montreal*, *QC*. April 2017. (**Best Poster Award**)
- 3. **Lomis, N.**, Gaudreault, F., Malhotra, M., Shum-Tim, D., and Prakash, S. "A novel nanoparticle formulation for enhanced delivery of milrinone in cardiac applications". Canadian Society of Pharmaceutical Sciences. *Montreal, QC.* May 2017.
- 4. **Lomis, N.,** Westfall, S., Malhotra, M., Shum-Tim, D., and Prakash, S. "Nanoparticles based delivery of 9-bromo noscapine drug: preparation and optimization". 2nd International Drug Discovery and Development Forum. *Montreal*, *OC*. Jun 2016.
- Lomis, N., Westfall, S., Farahdel, L., Shum-Tim, D., Prakash, S. "Preparation of protein nanoparticles for delivery of Paclitaxel drug for use in cancer". A Conference of New Ideas in Cancer: Challenging Dogmas, American Association for Cancer Research. *Mumbai, India*. Feb 2016.
- 6. **Lomis, N.**, Westfall, S., Faradehl, L., Shum-Tim, C., Sorreini, S., Shum-Tim, D., and Prakash., S. "Design, preparation and process optimization for development of human serum albumin nanoparticles capable of delivering Paclitaxel drug for use in cancer". 12th Annual NHPRS Conference. *London, ON*. Aug 2015. (**Best Research Abstract Award**)
- 7. **Lomis, N.**, Maclean, L., Westfall, S., and Prakash, S. "Process Optimization and Characterization of Human Serum Albumin Nanoparticles". 12th Annual World Congress on Industrial Biology. *Montreal, QC*. Jun 2015.
- 8. **Lomis, N.**, Maclean, L., Westfall, S., and Prakash, S. "The Effect of pH on Size of Human Serum Albumin Nanoparticles". Drug Discovery and Development in the Post-Genomic Era. Canadian Society for Pharmaceutical Sciences. *Toronto, ON*. May 2015.

- Lomis, N., Westfall, S., Shum-Tim, D., Prakash, S. "Design of novel drug delivery vehicles for cardiovascular & other diseases". Quebec-Ontario Biotechnology Meeting. *Montreal*, QC. May 2015.
- 10. Lomis, N., Paul, A., Westfall, S., Shum-Tim, D., Prakash, S. "A Novel Biotherapeutic Stent Technology Encapsulated Baculovirus-modified Stem Cells for Stent Coating".
 International Conference on Translational Medicine in 21st Century. *Bhopal, India*. Apr 2015.
- 11. Westfall, S., **Lomis, N.**, Iqbal, U., Prakash, S. "Elucidating microbiome-host communication: Ferulic acid is a cross-talk mediator between *L. fermentum* NCIMB 5221 and the host metabolic, anti-oxidant and immune systems". 60th Anniversary of Artificial Cells in conjunction with XVI ISBS and V ISNS. *Montreal, QC*. Nov 2017.
- 12. Westfall, S., **Lomis, N.**, Iqbal, U., Prakash, S. "Ferulic acid produced by the probiotic *Lactobacillus fermentum* NCIMB 5221 reduced developmental time through a dTOR-mediated mechanism". Artificial Cells and Blood Hematology. *Montreal, QC.* Nov 2017.
- 13. Westfall, S., **Lomis, N.**, Iqbal, U., Kahouli, I., Prakash, S. "Describing the novel prebiotic activity of Triphala extract and its impact on anti-oxidant, immune and metabolic processes". Artificial Cells and Blood Hematology. *Montreal, QC*. Nov 2017.
- 14. Westfall, S., Lomis, N., Iqbal, U., Singh, SP., Prakash, S. "Elucidating microbiome-host communication: Ferulic acid is a cross-talk mediator between *L. fermentum* NCIMB 5221 and the host metabolic, anti-oxidant and immune systems". Probiota. *Berlin, Germany* Feb 2017.
- 15. Westfall, S., **Lomis, N.**, Iqbal, U., Singh, SP., Prakash, S. "The anti-aging effects of *L. fermentum* NCIMB 5221 occurs through ferulic acid mediated metabolic, immune and anti-oxidant activities". Human Microbiome Congress. *San Diego, USA*. Jan 2017.

- 16. Westfall, S., Lomis, N., Singh, SP., Prakash, S. "Characterization of the prebiotic potential of three novel plant extracts with implications in age-related diseases including metabolic syndrome and neurodegeneration". Probiota. *Amsterdam*, *NL*. Feb 2016.
- 17. Westfall, S., **Lomis, N.**, Iqbal, U., Singh, SP., Prakash, S. "Elucidating microbiome-host communication: Ferulic acid is a cross-talk mediator between *L. fermentum* NCIMB 5221 and the host metabolic, anti-oxidant and immune systems". Keystone Symposia on Molecular and Cellular Biology. *Colorado, USA*. Feb 2016.
- 18. Westfall, S., **Lomis**, **N.**, Singh, SP., Prakash, S. "Anti-inflammatory and anti-oxidant features of *Ferula asafoetida* Rhizome Oil Resin: Potentials and Limitations". Role of Herbals in Cancer Prevention and Treatment. *JNU: New Delhi*, *India*. Feb 2016.
- 19. Westfall, S., Lomis, N., Jones, M.L., Martoni, C.J., Tomaro-Duchesneau, C., Rodes, L., Bhathena, J., Urbanska, A.M., Prakash, S. "Probiotic Biotherapies for use in Metabolic Syndrome: Innovating Science and Technology". International Conference on Innovative Trends in Engineering, Science and Management. *New Delhi, India*. May 2016.
- 20. Westfall, S., **Lomis, N.**, Prakash, S. "Prebiotics, probiotics and the gut-brain axis: Implications in neurodegeneration, metabolism, immunity and everything in between". Department of Immunology invited talk. *McGill University, Montreal, QC*. Nov 2015.
- 21. Westfall, S., **Lomis, N.**, Kahouli, I., Faradhel, L., Iqbal, U., Shum-Tim, C., Sorrini, S., Singh, SP., Prakash, S. "The role of plant extracts as prebiotics in the modulation of gut microflora: Potential and limitations in metabolic syndrome and Alzheimer's disease". NHPRS, *London, ON*. Aug 2015.
- 22. Westfall, S., **Lomis**, **N.**, Singh, SP., Prakash, S. "The prebiotic action of Trikatu defines a novel concept of agni in the gut microbiota". NHPRS, *London*, *ON*. Aug 2015.

1.6 Thesis Outline

This PhD thesis includes 8 chapters. The introduction, rationale, research hypothesis and objectives are stated in Chapter 1, followed by an extensive literature review presented in Chapter 2. Chapters 3 to 5 comprise of original research manuscripts either published or to be submitted in peer-reviewed journals. These research articles include the studies performed to evaluate the above stated research hypothesis and accomplish the mentioned research objectives. Chapter 6 summarizes the findings obtained in these studies with a general discussion. Chapter 7 elaborates the claimed contributions to knowledge and conclusions. Chapter 8 includes the recommendations for future research and potential clinical implications of the study.

CHAPTER 2: BACKGROUND AND LITERATURE REVIEW

2.1 Cardiovascular Diseases

Cardiovascular diseases are an ever-growing problem of the modern world. Though the advent of technology has brought comfort to human life, it has also introduced risk factors such as high blood pressure, cholesterol, diabetes, obesity to unhealthy diets and physical inactivity ². Today, CVDs are the leading cause of mortality across developed and developing countries claiming almost 18 million lives every year ^{37,38}. CVDs encompass a group of diseases associated with the heart and system of blood vessels, which can be segregated into coronary heart disease, peripheral arterial disease, congenital heart disease, rheumatic disease, venous thromboembolism and cerebrovascular disease ³⁸. The World Health Organization has estimated that CVDs contribute to almost 50% of the global deaths due to non-communicable diseases with coronary and cerebrovascular diseases together responsible for more than 31% mortality ³⁷. CVDs also contributed to approximately 14% of total health expenditures in 2014-15, which is expected to increase to ~\$749 billion in the next decade, thus adding to the huge economic burden ^{37,38}.

2.1.1 Congestive Heart Failure

Myocardial infarction (MI), a type of CVD is caused by the inability of the heart to receive blood and oxygen from the coronary artery due to the build up of plaque, a condition known as atherosclerosis (**Figure 2.1**). The heart muscle eventually undergoes necrosis becoming stiff and is unable to pump blood resulting in congestive heart failure (CHF) ¹. With the advent of new medical therapies and interventions, management of heart failure has rapidly evolved in the recent decades, improving the quality of life and life span of patients. However, despite significant advancements, the treatment of CHF remains a challenge for healthcare providers, which may be indicated by the rate of increase in hospital readmissions ^{4,35}. The reasons associated with hospitalization and readmission post heart failure have been found to due to lack of proper adherence, delay in reporting HF, inadequate professional help etc. ³⁵. Though some cases of rehospitalization may be due to HF re-exacerbation, majority of these cases are due to non-cardiovascular reasons ³⁹. Thus, a need exists to optimize medical therapies, which will consequently reduce hospital readmissions.

2.1.2 Pathophysiology of Congestive Heart Failure

CHF is a clinical syndrome caused by impairment of the ventricular filling and ejection of blood as a result of structural and functional deformities in the myocardium ⁴⁰. It is caused by reduction in left ventricular myocardial function resulting from obstruction of the left coronary artery, defects in heart valves, pericardium, myocardium and endocardium. Most commonly, CHF is a direct result of MI leading to an irreversible loss of contracting cardiomyocytes, replaced by the development of an akinetic scar tissue ⁴⁰. This further results in stiffness and progressive fibrosis consequently leading to ventricular remodelling and ischemia-like conditions in combination with hemodynamic overload ^{40,41}.

Depending on the time of onset, HF may be classified into acute and chronic HF. Chronic HF may develop as a long-term condition signified by a decrease in left ventricular ejection fraction 42 . Acute HF may be described by an onset or escalation of symptoms of chronic HF requiring rapid therapy and hospitalization 43,44 . About 60% of the patients hospitalized due to acute heart failure are reported to be suffering from coronary artery disease (CAD), hypertensions, atrial fibrillation, diabetes and increased serum creatinine levels 45 . The development of HF is marked by transport of monocytes, macrophages and neutrophils to the site of cardiac injury by stretched myocardial fibers, initiating a series of intracellular and neurohormonal responses, thus activating the reninangiotensin-aldosterone system and the sympathetic nervous system as a positive adaptive response to sustain blood pressure, heart rate and cardiac output 46 . If left unchecked, this will subsequently damage β -adrenergic signalling and flux of intracellular calcium further causing cardiomyocyte hypertrophy, fibroblast proliferation, collagen accumulation and apoptosis 47 .

Left ventricular remodelling can be categorized into an early phase remodelling (within 72 hours) and a late phase remodelling (after 72 hours) ⁴⁸. The early phase remodelling is characterized by expansion of the infarct size within a few hours of cardiomyocyte injury. The expansion is caused by degradation of type I and III interstitial collagen, responsible for structural integrity and alignment of cardiomyocytes, by matrix metalloproteinase 1 (MMP-1) and neutrophil collagenase ⁴⁹. As a consequence, the fibrillar collagen loses integrity causing myocyte slippage and misalignment, sarcomere distension, wall thinning and dyskinesia, all responsible for increase in infarct size ⁴⁹. The infarct size expansion begins within a few hours of the cardiac injury and

continues for weeks or months until the appearance of a collagen scar, which also deforms the border zone and remote myocardium. Further, the wall-thinning and ventricular dilation cause systolic and diastolic wall stress which induces an intracellular signalling for gene regulation. As a result, the non-infarcted myocardium is involved in adaptive responses to preserve the stroke volume ⁵⁰.

Late phase heart remodelling involves myocyte hypertrophy, myocyte apoptosis and/or necrosis, however the distribution of wall stresses in the infarcted myocardium is relatively proportionate as the collagen scar is formed ^{45,51}. Reportedly, many patients with reduced systolic function have a viable non-contractile myocardium, which may be a result of hemodynamic overload, excessive neurohumoral stimulation and ischemia. The reduced contractile ability of the myocardium is anticipated to compensate for the energy use in the failing myocardium, thus allowing greater survival of cardiac cells ⁵².

2.1.3 Neurohormonal Modulation in Congestive Heart Failure

In heart failure, the pathophysiological process of damage to the myocardium mostly begins with a MI which creates structural and functional changes in the cardiomyocyte. Simultaneously, neurohormonal modulation begins with vasoconstrictor and vasodilator hormones as the reninangiotensin system and the sympathetic nervous system are activated ⁵³. The vasoconstrictor hormones are anti-natriuretic and anti-diuretic and growth promoting whereas the vasodilator hormones are natriuretic and diuretic with anti-mitogenic properties. As the CHF progresses, the vasoconstrictor hormones overshadow the effect of the vasodilator hormones ⁵⁴.

2.1.3.1 Role of the Renin-Angiotensin Aldosterone System in Heart Failure

The local tissue renin-angiotensin system is activated under myocyte hypertrophy, causing sympathetic activation, increase in production of catecholamine by the adrenal medulla and the secretion of natriuretic peptides 53 . Enhanced norepinephrine release stimulates the α 1-adenoreceptors leading to myocyte hypertrophy via the G α q-dependent signalling pathway 55 . Also, renin is an enzyme released by granular cells in the juxtaglomerular apparatus, due to the activation of β 1-adenoreceptors. It breaks down the circulating angiotensinogen produced by the liver, forming angiotensin I. The angiotensin I is converted into angiotensin II by endothelial cells

primarily from the pulmonary vasculature ⁵⁶. The angiotensin II (Ang II) is a key component of RAAS cascade, which stimulates release of aldosterone from the adrenal glands. Ang II is initially produced as a compensatory product and is later detrimental with the progression of heart failure. The stretch activation of smooth muscle cells induces increased Ang II production, which promotes presynaptic release of norepinephrine, blocking its re-uptake and increases catecholamine synthesis, bringing into effect its postsynaptic action ⁵⁷. Initially, the increase in catecholamine production, increases the cardiac output through inotropic and chronotropic mechanisms however this effect is temporary and subsequently, myocardial ischemia is exacerbated ⁵⁸. The elevated adrenaline and noradrenaline levels promote sympathetic nervous system activity, another temporary compensatory mechanism that maintains perfusion pressure, however prolonged exposure to catecholamines results in hypertrophy, ischemia and ventricular arrhythmias ⁵⁸. Further, Ang II and norepinephrine may augment release of endothelin-1 (ET1), another stimulus for myocyte hypertrophy which induces the secretion of A-type natriuretic peptide. The RAAS and SNS causing myocardial wall stretching are opposed by the natriuretic peptides A-type and B-type natriuretic peptides, secreted as counterregulatory mediators responsible for vasodilation and natriuresis, which in turn, inhibit the production of catecholamines, Ang II, ET-1, and aldosterone ⁵⁹⁻⁶¹.

2.1.3.2 Role of the Angiotensin II Receptors

The Ang II receptors are G-protein coupled receptors which induce the myocardial wall stretch induced hypertrophic response resulting in increased production of Ang II. Through the activation of these G-protein coupled receptors, various signalling pathways are activated such as the tyrosine kinase pathway through calcium dependent activation, protein kinase C (via phospholipase $C\beta$), MAP kinase and S6 kinase ⁵⁵. The intracellular calcium is essential for Ang II mediated activation of protein kinases in cardiomyocytes. Many components of the RAAS such as angiotensinogen, angiotensin converting enzyme (ACE) and angiotensin II type I and type II receptors are found to be upregulated under heart failure mode. In fact, the overexpression of angiotensin II type 1 receptors (AT1R) present on the myocardium is found to be directly related with cardiomyocyte hypertrophy ^{32,33}. The AT1R are coupled with the G α q receptors and thus a similar cardiac phenotype is observed from their overexpression.

2.1.3.3 Regulation of Cardiac Contractile Function in Heart Failure

The cyclic adenosine 3',5'- monophosphate (cAMP) is the second messenger of the β-adrenergic receptors signalling (a type of G-protein coupled receptors), which induces phosphorylation of the calcium channels and ryanodine receptors to increase the amount of intracellular Ca²⁺concentration for myocardial contractile ability ⁶². In order to maintain proper cardiac function, it is essential to modulate the cAMP concentration by balancing the cAMP synthesis and degradation. cAMP is produced by adenyl cyclases in mammals, the activity of which can be controlled by extracellular stimuli such as hormones, neurotransmitters, chemokines, drugs etc. by binding with various G-protein coupled receptors ⁶³. Production of cAMP activates various proteins such as cAMP dependent protein kinase A (PKA). PKA in turn promotes opening of the voltage dependent L-type calcium ion channel allowing influx of calcium ions into the cell, which further provides stimulus for calcium release from the sarcoplasmic reticulum (SR) via ryanodine receptors (Figure 2.2). This process is termed as calcium induced calcium release (CICR) and is responsible for myofilament contraction ^{62,64,65}. One of the functions of the catecholamine stimulated β-adrenergic receptors is cAMP effector dependent troponin -1 phosphorylation for quicker contraction force development and shortening during systole and faster force relaxation and re-lengthening during diastole. It also mediates phosphorylation of cAMP effector dependent phospholamban and calmodulin proteins to allow Ca²⁺ re-uptake by SR for myofilament relaxation ^{62,66}. However, the PKA dependent calcium release from the SR may be independent of the CICR mechanism and may occur through voltage-sensitive release. This mechanism of calcium release from SR independent of the LTCC appears to be more relevant for phosphodiesterase III inhibitors. cAMP is hydrolyzed to form AMP by phosphodiesterase.

2.1.4 Phosphodiesterase Inhibitors in Clinical Use for Heart Failure

Phosphodiesterase is a ubiquitous enzyme comprising a family of enzymes responsible for the hydrolysis of phosphodiesterase bonds. It can hydrolyze both cAMP and cGMP (cyclic 3',5' guanosine monophosphate) ⁶⁷. Primarily cAMP and to a lesser extent cGMP, have a crucial role in the inotropic mechanism for proper cardiac function Both cAMP and cGMP demonstrate effects in numerous other tissues ⁶⁴. Various drugs have been identified as phosphodiesterase inhibitors which inhibit specific types of the enzyme within the superfamily to improve cardiac function, although they may have effects on the lungs, vasculature, platelet function and other inflammatory

mechanisms. Though numerous drugs are available known to improve cardiac function, those under clinical practice are known to inhibit phosphodiesterase isozymes III and IV. These compounds are amrinone, milrinone and the imidazolone derivative, enoximone.

2.1.4.1 *Milrinone*

Milrinone is a positive inotrope and vasodilator structurally represented as a bipyridine methyl carbonitrile derivative of amrinone (**Figure 2.3**). It selectively inhibits the phosphodiesterase 3 enzyme activity, thus preventing the hydrolysis of cAMP and increasing the cAMP concentration 30,68 . This allows greater Ca^{2+} release from the SR and increased force generation by the actin-myosin. In the vascular smooth muscle, cAMP promotes muscle contraction by preventing myosin light chain phosphorylation by the myosin light chain kinase enzyme. Increased concentration of cAMP due to MRN use promotes smooth muscle contraction, justifying its vasodilator effects 36 . Milrinone commonly treats low cardiac output, lowers the pulmonary arterial pressure, pulmonary capillary wedge pressure, left ventricular filling pressure, decreases systemic vascular resistance and improves overall cardiac function $^{69-71}$. The primary advantage of using MRN therapy is that it bypasses effects on β -adrenergic receptors to exhibit its potency. Also, compared to other drugs, it has a longer half-life and clearance rate 70 .

Clinically, MRN is administered as MRN-Lactate either intravenously or orally to both adult and pediatric patients ⁷². Orally administered MRN has less predictable outcomes and therefore has now been abandoned ⁷³. The intravenously injected loading dose of MRN may vary between 20-50 µg/kg over 10 minutes followed by an infusion of 0.2-0.75 µg/kg per minute ⁷⁴. Milrinone has an elimination half life of 2 to 2.5 hours, a volume distribution of 0.4 to 0.45 L/kg and a mean clearance of 0.13 and 0.14 L/kg/hr. It is excreted in urine at a renal clearance rate of 0.3 L/min such at 90% of the dose can be recovered within 8 hours of administering the initial dose. As MRN is renally excreted, it's observed that its half-life is prolonged in patients with renal dysfunction, hence the applicability in clinical use is subjected to adjustment of dose on a case by case basis ⁷².

Milrinone may also be given by nebuliser at a dose concentration of 1 mg/mL and the most common dose regimen has been a single dose of 5 mg. In cases of cardiopulmonary bypass, inhaled

MRN has been found to be more effective than an intravenous dose as it prevents endothelial dysfunction in the pulmonary arterial system, reducing the pulmonary reperfusion syndrome ⁷⁵. Inhaled MRN has also been used to treat acute lung injury and severe pulmonary tensions in several studies ⁷⁶⁻⁸⁰.

2.1.4.2 *Enoximone*

Enoximone is a substituted imidazolone derivative which inhibits the action of phosphodiesterase III. It possesses both inotropic and vasodilatory properties like MRN and the action of enoximone is due to an increase in the intracellular cAMP and increased calcium ion mobilizataion ⁸¹. It is administered as a loading dose of 0.5-1.0 mg/kg over 10-30 minutes as a continuous infusion followed with a maintenance infusion of 5-20 μg/kg/min ⁸². The half-life of enoximone is up to 10 hours and upon administration in cases of congestive heart failure. As enoximone is metabolized to enoximone sulfoxide by oxidation, about 75% of the enoximone intravenously administered is excreted through urine as the sulfoxide metabolite. It has been found that even though lower dosage of enoximone appears to be safer in patients, it does not improve the heart failure outcomes ⁸³. Also, it follows a non-linear pharmacokinetics with plasma concentrations increasing exponentially over a prolonged infusion, as a result of which the enoximone metabolite accumulates resulting is serious toxicity ⁸³.

2.1.5 Other Inotrope Drugs in Clinical Use for Heart Failure

Apart from MRN there are some other positive inotrope drugs that have been used clinically for treatment of the heart failure syndrome (**Table 2.1**). These drugs improve the myocardial contractility by increasing the intracellular Ca²⁺ concentration or by enhancing the myofilament sensitivity towards Ca²⁺. These drugs may act either by elevating the cAMP levels to enhance the re-uptake of Ca²⁺ by the SR under diastole or by acting on the Na⁺/K⁺-ATPase pump present on the cell membrane ⁸⁴.

Digoxin, also known as *Digitalis glycoside*, are compounds originally isolated from *Digitalis purpura*. Digoxin is the oldest and yet the most widely used cardiac glycoside in contemporary medicine ⁸⁵. It binds to the Na⁺/K⁺-ATPase pump in the cardiomyocyte membrane, which maintains the Na⁺ and K⁺ gradient across the cell producing low Na⁺ intracellular concentrations

and higher K^+ intracellular concentrations. Driven by the Na^+ concentration, another exchange occurs between the Na^+ and Ca^{2+} with entry of Na^+ into the cell and translocation of the Ca^{2+} out of the cell 81 . Digoxin can partially inhibit the Na^+/K^+ -ATPase pump causing an increase in the Na^+ intracellular concentration which lowers the gradient for Na^+ across the cell further lowering the exchange between Na^+ and Ca^{2+} . Thus, the intracellular Ca^{2+} concentration is elevated which releases excess Ca^{2+} during cell membrane excitation, causing contraction 86,87 .

Levosimendan is a calcium sensitizer drug in clinical use that works differently than other inotropes ⁸⁸. It works by binding with the N-terminal of the cardiac troponin C (TnC), to stabilize the Ca²⁺ bound form of the protein, which thus increases the force of contraction by prolonging the systolic interaction between actin and myosin. Since the function of levosimendan is based on its binding with the TnC which is Ca²⁺ concentration dependent, it acts only during systole leaving diastole unaffected ⁸⁹.

Other drugs which act on adrenergic (α 1, α 2, β 1, β 2) and dopaminergic (D1, D2) receptors are catecholamines 90,91 . The α 1 receptor increases the systemic vascular resistance and the β 1 increases myocardial contractility 92 . Dopamine and dobutamine are two catecholamines most widely used in current clinical practices 93,94 . Dopamine is a neurotransmitter, precursor to epinephrine and norepinephrine. It creates a vasodilation effect by acting on the D1 and D2 receptors 95,96 . It may bind with the β 1 and β 2 receptors at intermediate doses to increase myocardial contractility and stimulate α 1 receptors to increase systemic vascular resistance at higher doses 97 . At lower doses it can decrease the systemic vascular resistance however it is also associated with tachycardia, arrhythmias and myocardial infarction 98 .

Dobutamine is also used clinically for short term treatment of CHF 99,100 . It acts by improving the myocardial contractility and ventricular ejection similar to MRN, however is associated with higher incidences of arrhythmias due to stimulation of both $\beta 1$ and $\beta 2$ adrenoreceptors and the reflex response to $\beta 2$ -adrenoreceptor mediated peripheral arterial dilation 97,101 . Dobutamine binds to $\beta 1$ receptors to create a direct vasodilatory effect. It decreases the systemic vascular resistance and lowers the mean arterial pressure, offset by the increase in cardiac output and can significantly increase the heart rate in certain cases 102 .

Omecamtiv mecarbil increases the number of active myosin-actin interactions to prolong myocardial contraction ¹⁰³. It reported increases in the left ventricular ejection fraction in individuals with normal ventricular function ¹⁰⁴. It can also improve the LVEF, stroke volume, left ventricular systolic and diastolic volumes ¹⁰⁵.

2.1.6 Selecting Milrinone as Inotropic Therapy of Choice for Congestive Heart Failure

The selection of the appropriate therapy for treatment of congestive heart failure depends on the desired physiological effects guided by the clinical scenario. Milrinone is a positive inotrope agent which serves as a bridging as well as palliative therapy. Compared to dobutamine, a tough competitor as heart failure therapy, MRN exhibits greater improvement of the syndrome ¹⁰⁶. Milrinone decreases the pulmonary capillary wedge pressure, systemic vascular resistance and pulmonary arterial pressure to an extent greater than dobutamine and other drugs ¹⁰⁷. Milrinone also improves the heart rate and lowers requirement for oxygen consumption during myocardial infarction (**Figure 2.4**).

One of the main advantages of MRN over other drugs targeting the β -adrenergic receptor is its ability to bypass the need to block the β -receptors to exhibit its potency and effect thus allowing it to be used in conjunction with β -blocker drugs as well ¹⁰⁸. This significantly lowers the risk of arrhythmias which is associated with the use of MRN. Also, in case of patients suffering from severe renal impairment, caution is exercised while selecting the appropriate MRN dosage given its longer half-life and renal clearance time in these patients ^{74,109}.

Milrinone exhibits a comparatively better safety profile as compared with other drugs with lower risk of re-hospitalization, when weaning off inotrope therapy in cases of congestive heart failure 110 . The side effects to MRN are arrhythmia and hypotension, which may be addressed by combination with another β -blocker therapy 111 . Overall, MRN therapy has been effective in alleviating symptoms of acute myocardial infarction and heart failure, reducing length of end-stage heart failure, reducing re-hospitalizations and improving the quality of life of patients 112 .

2.1.7 Limitations to the Use of Milrinone in Heart Failure

Like the use of other drug therapies, the effectiveness of MRN could be improved further by addressing its limitations. The lack of target specificity of the drug causes it to be accumulated in various organs other than the heart. Also, intravenous injection of MRN results in a bolus release which also explains for the reasons of its side effects such as arrhythmia and hypotension ¹¹³. Improving the target specificity of MRN along with a controlled drug release profile would allow for usage of lower doses, higher retention, site-specific delivery and elimination of side effects. Given the lower retention time of MRN, it is cleared from the body rapidly. This could also be addressed by targeted delivery of MRN which will not only improve the clearance rate of the drug but also limit the need for continuous infusions. Further, the toxicity of the drug would need to be enhanced further to eliminate any inflammatory or other effects.

The use of safe, targeted and biocompatible drug delivery vehicles could ameliorate majority of the above concerns. In fact, the introduction of nanomedicine for applications in cardiovascular diseases has set the path for development of novel and more effective drug delivery therapies.

2.2 Nanomedicine in Cardiovascular Diseases

Nanomedicine is emerging as one of the most promising fields of research owing to its relevancy in various areas of medicine especially drug delivery ¹¹⁴. The concept of nanomedicine is based on the intentional design, characterization, production and application of materials, structures, devices and systems by controlling their size and shape in the nanoscale range (1-100 nm) ^{115,116}. Though the field of nanomedicine has seen an enormous explosion in the last decades, it has not as actively been explored in the field of cardiovascular diseases and especially heart failure. Since the last decade, there has been ongoing research focused on finding new and effective ways for treatment of cardiovascular diseases especially for cardiac targeting of drugs using nanomedicine. With the currently available methods of treatment, the outcomes for CHF have been poor with only few patients receiving access to gold standard treatments such as ventricular assist devices, pacemakers or heart transplantation ¹¹⁷⁻¹¹⁹. Some of the surgical interventions include percutaneous coronary intervention and coronary artery bypass surgery ¹²⁰⁻¹²².

Though majority of the research efforts have been focused on developing methods, mechanisms and strategies of direct cardiac regeneration, fewer studies have been directed towards improving the current drug delivery approaches. The use of nanomedicine first as a cancer therapy offers a new therapeutic perspective in the context of cardiovascular diseases where the development of targeted drug delivery vehicles may offer tremendous benefits for treatment of CHF ¹²³⁻¹²⁵. As stated above, one of the major limitations of traditional medicine or drug therapies is the lack of specificity in recognition of diseases cells and interactions with the specific cells and tissues resulting in side-effects and treatment dropout ¹²⁶. Besides this, some of the other limitations of drugs include lower solubility, poor biodistribution and unfavourable pharmacokinetics behaviour ¹²⁷⁻¹²⁹. Therefore, nanoparticle-based drug carriers could allow for delivery of small molecules and drugs in a controlled manner with a sustained release profile, maximizing the therapeutic effects and minimizing the side effects ¹³⁰⁻¹³².

2.2.1 Physicochemical Properties of Nanoparticles

The interaction of the nanoparticles with different cells and tissues is dependent on its physical characteristics ¹³³. Keeping in view these interactions, the nanoparticle parameters to be considered during design and development include the size, surface charge and morphology ^{134,135}. These have been explained in detail below.

2.2.1.1 Nanoparticle Size

The size of the nanoparticle is one of the most crucial parameters to be taken into consideration during nanoparticle preparation. Nanoparticle size is usually tailored as per the target's characteristics to facilitate internalization by the cells or to interact with the blood vessels ¹³⁶. Research has shown that usually nanoparticles of size up to a maximum diameter of 4µm are suitable for delivery. However, based on various studies, the ideal nanoparticle diameter would be up to 250 nm ^{137,138}. Nanoparticles prepared in the size range of 10-100 nm enter the lymphatic capillaries to undergo clearance whereas nanoparticles in the range of 250 nm – 1µm are usually eliminated by the reticuloendothelial system (RES) by the process of opsonization ¹³⁹. This is a process by which macrophages and monocyte bind to the particles to identify them for removal from the body ^{19,140}.

2.2.1.2 Nanoparticle Surface Charge

The surface charge of the nanoparticle is another important property which determines the interaction of the particle with target cells as well as particle aggregation while in the bloodstream ¹⁴¹. It is known that positively charged particles interact well with negatively charged cell membranes and may be well suited for internalization. However, positively charged particles also bind to opsonin molecules for removal from the blood circulation ^{142,143}. On the other hand, negative surface charge on the nanoparticle prevents nanoparticle aggregation and accumulation and exhibit greater physical stability ¹⁴⁴. Neutral or negative charged particles have a relatively longer circulation half-life as compared to positively charged nanoparticles ¹⁴⁵.

2.2.1.3 Nanoparticle Shape and Surface Morphology

The shape and surface morphology of the nanoparticle have an impact on its internalization with the cell target ^{146,147}. The shape of the nanoparticle determines its binding with the cell surface, its angle of interaction with the target, speed of internalization and the contact surface area ¹⁴⁸. It has been observed that particles with spherical surface morphology are more likely to internalized by the target cells as than those with cylindrical, rod-like or cubic shape ¹⁴⁹⁻¹⁵¹.

2.2.2 Nanoparticle Uptake

Upon reaching the target cells, the nanoparticles interact with components of the plasma membrane and are internalized mainly through endocytosis ¹⁵². Endocytosis is the process of engulfment of the nanoparticle by membrane invaginations which bud off from the membrane to form endocytic vesicles. These vesicles are then transported off for intracellular trafficking. The mechanism of endocytosis can be classified into several types depending on the cell type and molecules involved in the process ¹⁵³. These mechanisms of endocytosis are clathrin mediated endocytosis, caveolae mediated endocytosis, clathrin/caveolae independent endocytosis, phagocytosis and micropinocytosis. The process of pinocytosis includes macropinocytosis, clathrin and caveolae meditated endocytosis ¹⁵⁴⁻¹⁵⁶. The engulfment of large particles (greater than 1μm) by formation of membrane protrusions due to actin polymerization is micropinocytosis, which is independent of vesicle formation. Phagocytosis on the other hand is the removal of pathogens and other larger particles by opsonization ¹⁵⁷.

Clathrin and caveolae mediated endocytosis involve interaction of the nanoparticle with the cell membrane either through cell surface receptors or through receptor-independent absorption mechanisms that trigger uptake of the nanoparticles ¹⁵⁸⁻¹⁶⁰. In receptor-independent endocytosis, the nanoparticles interact with the cell membrane through surface charges and the nanoparticle uptake is initialized through hydrophobic or electrostatic interactions. In receptor mediated endocytosis, also known as clathrin mediated endocytosis, ligands present on the nanoparticle surface identify the targeting receptor present on the cell-surface. Clathrin mediated endocytosis involves adapter proteins on the side of the plasma membrane and accessory proteins, which are together responsible for the nucleation at the site of internalization in the membrane. Accessory proteins generate membrane curvature and stability. The vesicle buds of from the membrane engulfing the nanoparticles, ending up in degradative lysosomes ¹⁵³.

Caveolae dependent endocytosis plays an active role in various biological processes such as cell signalling ^{161,162}. Caveolae are present in endothelial cells as membrane invaginations and cover a substantial area of the cell membrane in case of non-endothelial cells. Caveolin is a dimeric protein responsible for the formation of flask-shaped and caveolin 2 is involved in giving stability to vesicle structure. Particles entering the cell through caveolae dependent processes may also escape the lysosomal degradation, a mechanism that has been explored by various nanoparticle-based therapeutics ^{163,164}.

The use of receptor dependent endocytosis is widely explored for targeted drug delivery to improve the delivery and drug release profiles and reduce side effects ^{165,166}. Although, theoretically the nanoparticle uptake mechanism can be easily established *in vitro*, it is challenging to prove the delivery of ligand bound nanoparticles via receptor-mediated endocytosis *in vivo* ¹⁶⁷. Towards this, the first step would involve targeting a suitable receptor that has high affinity for a specific ligand to enhance cellular uptake of nanoparticles ^{168,169}. Unlike *in vitro*, uptake mechanisms do not occur in isolation in *in vivo* settings and the delivery mechanisms are usually competing with other nonspecific mechanisms such as opsonization, RES, clearance, EPR etc. Irrespective of the given challenges, the design and development of targeted nanoparticle-based therapies remain continually in active research.

2.2.3 Nanoparticle Surface Functionalization and Targeting

Ligands may be coupled with the nanoparticles through chemical covalent linkages present on the surfaces of the nanoparticles and the active functional groups used for the cross-linking ¹⁷⁰. Various ligands used for conjugation with the nanoparticles such as peptides, small molecules, antibodies, aptamers, proteins ^{15,171-174}. This property has been widely explored in the field of targeted drug delivery in order to improve the uptake of drug conjugates which otherwise show lower binding affinity towards the target. Receptor targeting ligands for specific uptake by cardiomyocytes can be incorporated on various nanoparticles ^{23,26,173,175,176}. This does not necessarily enhance the biodistribution of nanoparticles but can improve the ligand-density dependent cellular uptake of nanoparticles. This can be seen in case of the AT1R, which is found to be overexpressed in diseased tissues especially under HF, as well as at physiological levels in non-diseases tissues ³²⁻³⁴. The AT1R-targeted nanoparticles are taken up with greater specificity than non-targeted nanoparticles ¹⁷⁷. This has been shown in AT1 ligand bound PEGylated quantum dots which showed receptor-mediated uptake via AT1R present on cardiomyocytes ¹⁷⁸. Similarly, liposome-based nanoparticles have been developed as potential drug delivery vehicles to the infarcted heart by tagging with the AT1 peptide, showing specificity for the AT1Rs ¹⁷⁹.

Thus, nanoparticles exhibit unique physical properties which make them attractive materials for diagnostic and therapeutic applications. Specially designed nanoparticle structures may impart improved stability, non-cytotoxicity, cellular internalization, binding capacity, improved payload and effective delivery characteristics. Additionally, the functionalized nanoparticles offer better properties such as anti-corrosive, non-agglomerating and non-invasive characteristics. When utilizing any of the ligands for nanoparticle surface modification, it is essential to chemically modify the surface of the nanoparticles with appropriate chemistry to introduce reactive moieties providing functional groups for conjugation with the targeting ligand of choice. Some of the commonly utilized covalent reactions for nanoparticle conjugation with targeting ligands include carbonyl reactive groups, amine reactive groups, sulfhydryl reactive groups, azide/alkyne conjugation ¹⁸⁰. These conjugations allow better control over ligand density and orientation, especially by incorporation of amino groups for introducing specific functional groups for site-specific binding ^{15,170,181}.

Each ligand has unique properties, attributes, conjugation strategies, advantages and disadvantages. Coating of polyethylene glycol (PEG) chains on the nanoparticle surface on one hand improves the biocompatibility and on the other hand may lower chances of cellular internalization ¹⁸²⁻¹⁸⁴. This may also impact the targeting capability of the peptide conjugated nanoparticles if coated with biomolecules ¹⁸⁵. Modification of nanoparticle surface with peptides or proteins allows binding with cell surface receptors providing targeted delivery. Though adding protein monolayers to the nanoparticle surface may increase the particle size, it provides stability to the nanoparticle structure ^{181,186,187}. Adding multiple ligands to the nanoparticle surface can further improve the efficacy while delivery ^{188,189}.

For effective treatment of cardiovascular diseases, it is crucial that the nanoparticle formulation is not only efficacious, targeted and stable, but also safe and non-cytotoxic for delivery to cardiomyocytes. Additionally, developing high quality targeting ligands is one of the most challenging problems in site specific delivery of nanoparticles. These ligands can be selected from a variety of options and their successful conjugation with nanoparticles will significantly impact their applications in imaging, diagnostics and therapeutics.

2.2.4 Introduction to Human Serum Albumin Nanoparticles

Albumin is the most abundant plasma protein (35-50 g/L human serum) with an average half life of 19 days ¹⁹⁰. It is a soluble globular monomeric protein with a molecular weight of approximately 66500 Da consisting of 585 amino acid residues with 35 cysteinyl residues forming 1 sulfhydryl group and 17 disulphide bridges. Human serum albumin (HSA) comprises of 3 homologous domains numbered I, II and III. Each domain is divided into two helical sub-domains A and B that possess common structural motifs ²⁵. The two-principal ligand-binding sites present on HSA are known as Sudlow Site I and II, located at sites IIA and IIIA (**Figure 2.5**) ^{191,192}. Albumin is extremely robust as a protein being stable in the range of pH 4-9 and at temperatures up to 60 °C for 10 hours, and in organic solvents. When albumin is broken into its amino acid residues, they provide nutrition to the peripheral tissue. The above properties as well as the site-specific uptake of albumin, biocompatibility, biodegradability and non-immunogenicity make it an ideal candidate for drug delivery applications.

Human serum albumin nanoparticles (HSA-NPs) offer several advantages such as lack of toxicity, easy of production and reproducibility, apart from those mentioned above. Due to the presence of multiple binding sites on the albumin molecule, HSA-NPs can be used for binding a variety of drugs, hormones, growth factors, genes and other molecules ^{193,194}. The presence of functional groups such as amino and carboxylic groups allows covalent chemical conjugation with crosslinking agents and other targeting ligands ^{22,23,175}. Known for its exceptional drug loading and binding capacity, various compounds may bind to it reversibly as non-covalent interactions. Sudlow Site I located in sub-domain IIA binds bulky heterocyclic anions such as bilirubin, warfarin anticoagulants, anti-inflammatory drugs like azapropazone, phenylbutazone and salicylate. Sudlow Site II located in sub-domain IIIA binds aromatic carboxylate compounds such as ibuprofen, ketoprofen, fenoprofen and benzodiazepines such as diazepam ^{190,195-197}. Both these sites are stable high-affinity binding sites which can load most hydrophobic and hydrophilic drugs at therapeutics concentrations. Presence of lower-affinity sites can accommodate extra drug molecules with lower selectivity. HSA-NPs are capable of binding fatty acids with different affinities at multiple binding sites. Thyroxine binds to a region between domain I and III ^{198,199}.

Several albumin binding proteins and receptors have been identified in various tissue and cell lines. Of these, the most widely known are albondin/glycoprotein 60 (gp60), glycoprotein 18 (gp18) and glycoprotein 30 (gp30) ²⁰⁰. Albondin (gp60) is a 60kDa glycoprotein that is widely distributed but selectively expressed on the surface of the plasma membrane of endothelial cells and helps to increase capillary permeability ^{201,202}. Upon interaction with the gp60 receptor, HSA-NPs are selectively targeted and internalized and undergo transcytosis ²⁰³. The albondin is taken up by caveolin mediated endocytosis and therefore may even escape lysosomal degradation. On the other hand, both gp18 and gp30 bind with conformationally modified HSA-NPs such as peptide labelled, gold-labelled or chemically conjugated albumin and do not interact with native albumin.

The methods for preparation of HSA-NPs may be classified into the following main techniques: (i) Ethanol Desolvation, (ii) Emulsification, (iii) Thermal Gelation, (iv) Nano-spray Drying and (v) Nab Technology.

2.2.4.1 Ethanol Desolvation (Coacervation)

In the ethanol desolvation process, also known as coacervation, HSA-NPs are formed by addition of ethanol into the albumin solution (**Figure 2.6**) ^{204,205}. The albumin may be dissolved in deionized/distilled water or sodium chloride followed by adjustment of solution pH at the desired value. Ethanol is then added in a drop-wise manner until the solution turns turbid due to precipitation of albumin nanoparticles. This is a result of the phase separation of albumin due to its diminished water solubility. The coacervated nanoparticles are however unstable and may redissolve again after dispersion with water. Therefore, this step is followed by addition of glutaraldehyde, which hardens the nanoparticles by undergoing a condensation reaction between the aldehyde-group of glutaraldehyde and amino-groups present on the lysine moieties and arginine moieties present on the guanidino side chains of the albumin protein.

The desolvation process can be optimized for preparation of albumin nanoparticles to achieve a particle size up to 250 nm and negative zeta potential ^{204,206}. The nanoparticle size, surface charge and morphology can be monitored by changing the albumin concentration, solution pH and amount of desolvating agent. Additionally, the polymerization time with glutaraldehyde also has a role to play in preparation of nanoparticles with optimal particle size. Washing the particles by ultracentrifugation can further help control the polydispersity to obtain a narrower size distribution.

The presence of free thiol groups present on the albumin molecule creates dimers and aggregates. At pH below 8.0, the aggregates may interfere with the nanoparticle, whereas at pH 8.0 and above, monodisperse particles between 200-300 nm could be obtained. Monodisperse HSA-NPs could be degraded in the presence of different enzymes such as trypsin, pepsin, proteases, cathepsin, proteinase K etc. ²⁰⁶. The enzymatic degradation further confirms the biodegradability of the nanoparticles as a crucial prerequisite for drug release after cellular uptake.

2.2.4.2 Emulsification

The emulsification technique has been found to be useful primarily for preparation of polymeric particles ²⁰⁷. Albumin nanoparticles can be formed by homogenizing the oil phase containing albumin droplets and then stabilizing with thermal treatment ²⁰⁸. The heated mixture is then cooled and diluted with ethyl ether to reduce the oil viscosity. Stabilizing the albumin nanoparticles by

chemical treatment involves emulsification of the albumin solution in cottonseed oil followed by denaturation by suspension in ether containing the cross-linking agent.

2.2.4.3 Thermal Gelation

The process of thermal gelation involves thermally induced unfolding of the albumin protein which is followed by various protein-protein interactions such as hydrogen bonding, electrostatic, hydrophobic interactions, disulfide-sulfhydryl interchange reaction. This technique has been used to effectively form nanoparticle conjugates, for loading drugs onto the nanoparticle and for forming nanogels ^{209,210}.

2.2.4.4 Nano-Spray Drying

Nano-spray dryers use a novel vibrating mesh technology for generating fine droplets. This is a well-established method used by the pharmaceutical industry to produce dry powder from liquid phase ²¹¹. The collection of fine particles or droplets is achieved with an electrostatic particle collector comprising of a grounded star electrode (cathode) and cylindrical particle collecting electrode (anode). A voltage is applied to the particle collector which creates an electrostatic field to accelerate the deposition of negatively charged particles onto the inner wall of the particle collecting electrode. This is followed by discharging. This method could be used for preparation of spherical and stable albumin nanoparticles ²¹².

2.2.4.5 Nab Technology

A novel albumin-based nanoparticle technology has been developed by American Biosciences, Inc. to encapsulate hydrophobic drugs into the nanoparticles ^{213,214}. This technology though developed for use in cancer may be extended to other applications as well. The lipophilic drug mixed with an organic solvent is then homogenized with HSA to form a suspension. This suspension containing albumin droplets is passed through a tiny nozzle at high pressure using a high-pressure homogenizer to form nano-sized albumin droplets. The organic solvent is then evaporated to obtain solidified drug-containing albumin nanoparticles. Nab-technology, Abraxane[®] is the first FDA approved nanoparticle based chemotherapeutic using paclitaxel drug that has shown significant effects in treatment of metastatic breast cancer ²¹⁵. This method of preparation has been extended to other lipophilic drugs and molecules for HSA binding.

2.2.5 Peptide-Conjugated Albumin Nanoparticles

Albumin nanoparticles offer a wide possibility for surface modification due to the presence of various functional groups such as amino and carboxylic groups, on the primary structure of albumin ^{23,24,26,27}. Ligands may bind to the albumin surface through covalent chemical conjugation methods as well as through electrostatic adsorption methods. The role of the ligand typically is to enhance nanoparticle internalization, improve pharmacokinetic parameters, prolong the circulating time, enhance nanoparticle stability and control the drug release profile, whereas the albumin nanoparticles act as biodegradable delivery vehicles ^{14,15}.

There are several ligands that may be bound to the albumin surface such as peptides, polyethylene glycol, cationic polymers, surfactants, thermosensitive polymers, apolipoprotein, folate, transferrin and monoclonal antibodies ¹⁹⁰. Peptide-anchored stable albumin nanoparticles have been developed as cancer treatments incorporating arginine-glycine-aspartic acid (RGD) peptide which has a high binding affinity towards sterically stabilized albumin ^{23,26}. Similarly, RGD peptide conjugated with PEG chains on the albumin nanoparticles has been developed for sustained release of doxorubicin ²¹⁶. In fact, given the various binding sites on the albumin surface, a dual-peptide targeted delivery using cyclic RGD and KALA peptides was designed for intracellular doxorubicin delivery ¹⁷⁵. Gene delivery is also one of the applications of albumin nanoparticles that has been explored by loading plasmid DNA onto targeting peptides cRGD and TAT, showing great transfection potential ²¹⁷. Peptide-Abraxane[®] conjugates have also been prepared by coupling CREKA and LyP-1 peptides to Abraxane® through the cysteinyl sulfhydryl group using the cross-linker SMCC ²¹⁸. Thus, majority of albumin nanoparticle formulations have been developed as effective cancer therapies. However, the immense potential for albumin surface functionalization gives rise to a wide possibility of diverse peptide-conjugated albumin nanoparticle formulations for use in cardiovascular and other diseases as well.

2.3 Conclusions

Cardiovascular diseases one of the most important medical issues for concern in today's world. Despite the availability of treatments modalities and the continual research efforts to refine these technologies, there is an unmet need for efficient and potent cardiovascular therapies. The most prominent of the CVDs is congestive heart failure. Having affected millions of people worldwide,

it creates and enormous economic burden on both individual as well society. One of the treatments of CHF involve delivery of inotropic drugs, of which MRN is known to be the most effective. However, the delivery of drugs for CHF treatment has its own limitations such as a lower half-life, low bioavailability, low retention time, lack of target specificity along with side effects. These limitations could be ameliorated by introducing target specificity to drug delivery. Thus, the inefficiency of existing drug delivery treatments has given rise to the field of nanomedicine.

Nanomedicine is rapidly evolving as a field of immense interest to the scientific community as it offers a wide possibility of solutions to existing medical issues that may overtake conventional treatment strategies. It has the potential to offer safe, efficient and cost-effective treatments as the drug dosage may be reduced with a sustained and controlled release effect. Thus, diseases and medical conditions could be overcome in an effective manner with minimum intervention. Using nanomedicine-based treatments also offers an advantage of developing multifunctional nanoparticles which could customized to offer target specific solutions with better resource utilization. The nanoparticle systems could be surface functionalized with a variety of therapeutic drugs, chemicals, peptides, small molecules etc. to enhance the intended functionality of the nanoparticle formulation and extend the possibility of current pharmacotherapy in cardiovascular disease. Use of nano-sized drug delivery vehicles allows better interaction with cell-surface receptors promoting enhanced cellular uptake, intracellular pathways and monitoring of the targeted cells, thus serving as essential tools in imaging, diagnostic and therapeutic applications.

Human serum albumin nanoparticles offer unique strategies for customization of medicine. Owing to unique properties such as biodegradability, biocompatibility, non-immunogenicity and potential for target specificity through surface functionalization, they are an excellent choice of targeted drug delivery vehicles. HSA-NPs bind a variety of peptides through covalent conjugation to achieve specialized effects, showing potential for use as a therapeutic tool in cardiovascular diseases. Thus, enhancing knowledge and increasing use of targeted nanoparticles as personalized therapies would enable clinicians to achieve objectives that would otherwise seem unattainable. These developments represent the commencement of significant advancements in the field of nanomedicine with use in cardiovascular diseases.

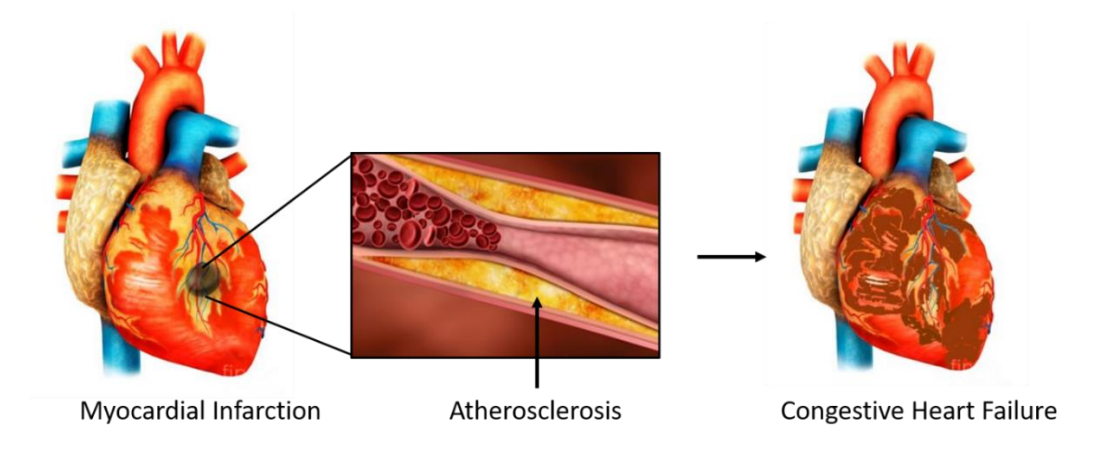


Figure 2.1. Myocardial infarction leading to congestive heart failure due to plaque build up (atherosclerosis).

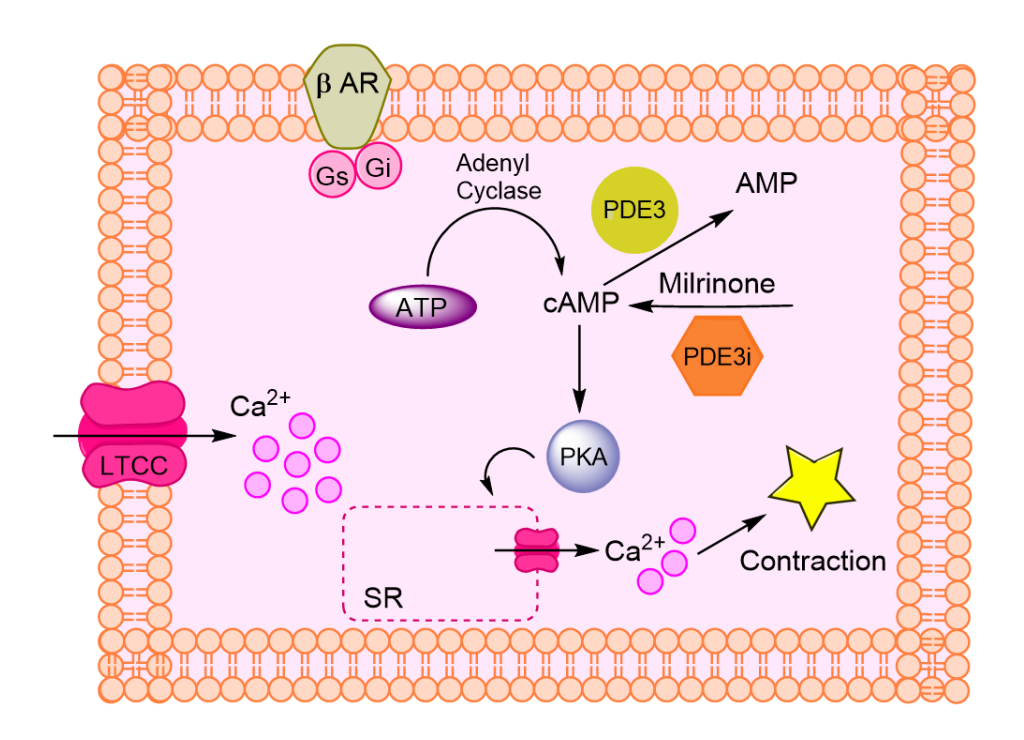


Figure 2.2. Mechanism of Action of Milrinone for Myocardial Contraction in Cardiomyocytes. ATP: Adenosine Triphosphate; βAR: Beta Adrenergic Receptor; cAMP: 3',5'- cyclic Adenosine Monophosphate, LTCC L-Type Calcium Channel; PDE Phosphodiesterase; PDEi Phosphodiesterase inhibitor; PKA Protein Kinase A; SR Sarcoplasmic Reticulum.

Figure 2.3. Chemical structure of Milrinone (1,6-Dihydro-2-methyl-6-oxo(3,4'-bipyridine)-5-carbonitrile) with molecular weight 211.219 g/mol.

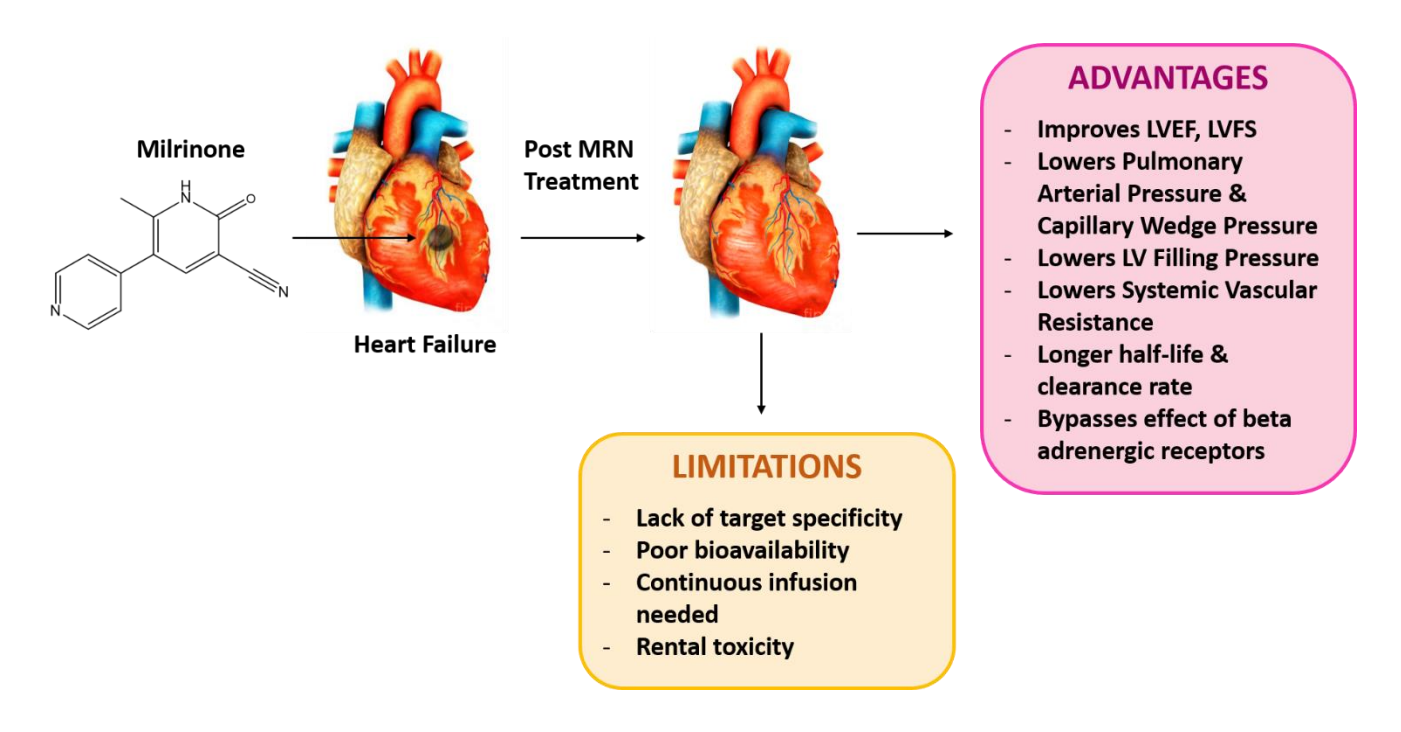


Figure 2.4. Advantages and limitations of milrinone treatment for congestive heart failure.

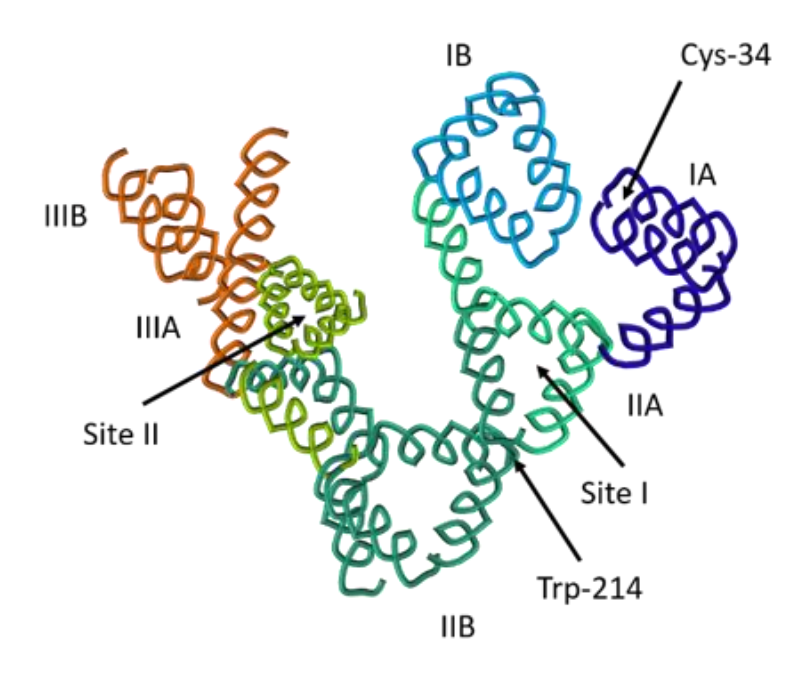


Figure 2.5. Molecular structure of Human Serum Albumin.

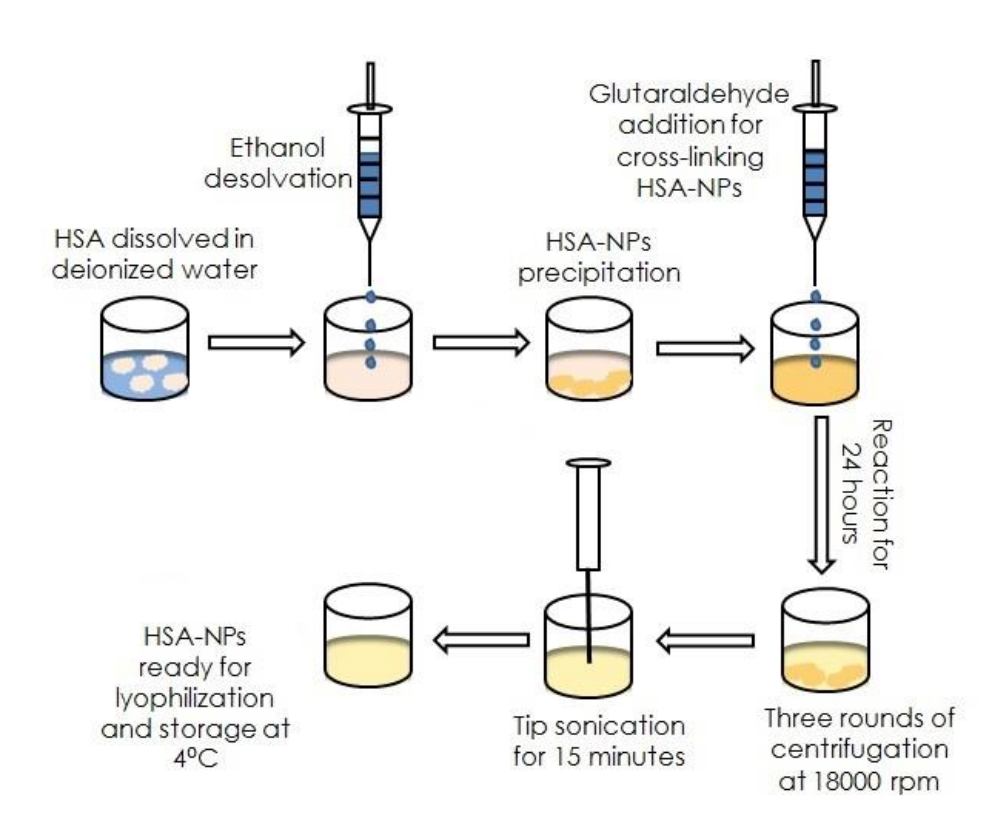


Figure 2.6. Schematics and steps of preparation of human serum albumin nanoparticles following the ethanol desolvation method.

 Table 2.1. List of Inotropic drugs for use in congestive heart failure

Name of Drug	Delivery Route	Mechanism of Action	Half- Life	Loading Dose	Repeated Dose	Limitations
Milrinone 30,36,74,113	IV	PDE III Inhibitor	2-2.5 hrs	0.1-0.5 μg/kg/min	Yes	- May induce cardiac arrhythmia
Enoximone 36,82,83	IV	PDE III Inhibitor	4-10 hrs	0.5-1.0 mg/kg	Yes	- Does not improve HF even with low doses - Metabolite accumulation
Digoxin 86,87,219,220	IV, Oral	Na ⁺ /K ⁺ pump	36-48 hrs	0.01-0.02 mg/kg or 0.125-0.25 mg/day	Yes	 Narrow therapeutic index Toxicity due to multiple drug interactions Cardiac arrhythmias
Dobutamine 70,100,101,107	IV	Targets β1 adrenergic receptor	< 5 mins	1-20 μg/kg/min	Yes	 Rise in BP and HR Hypotension Higher hospital readmission rate & in-hospital mortality
Dopamine ^{36,93,98}	IV	Targets β1 & β2 adrenergic receptors	1-2 mins	0.5-20 μg/kg/min	Yes	- Undesirable increase in PCWP - Dose-dependent effects of use
Levosimendan 36,88,89	IV	Binds N- terminal of cardiac TnC	~ 80 hrs	0.05-0.1 μg/kg/min	Yes	- Cardiac arrhythmias - Hypotension
Omecamtiv Mecarbil 103,104,221	Oral, IV	Increased actin-myosin cross-bridge formation	0.5-1.0 hr (Oral); 17-21 hrs (IV)	Under clinical trials	-	- Possible encroaching of diastole duration - Potential effects of use still unknown

PREFACE TO CHAPTERS 3 - 8

Presented in the following chapters is original research work. These studies were performed to investigate and accomplish the stated research hypothesis and research objectives.

Chapter 3: In this chapter, a novel nanoparticle formulation was developed from the HSA protein, to bind and deliver MRN. MRN is a cardiac inotrope and vasodilator drug, which improves myocardial contractility during CHF. For the first time, the binding efficiency between HSA and MRN was studied using computational modelling and circular dichroism techniques. The MRN-nanoformulation was optimized to obtain a particle size between 100-200 nm, negative zeta potential and high MRN encapsulation. The parameters optimized were HSA concentration, pH, MRN/HSA (weight/weight) ratio, ethanol volume, cross-linker concentration and polymerization time. The MRN-HSA-NPs were characterized by dynamic light scattering, electrophoretic doppler anemometry and scanning electron microscopy. The MRN release from the nanoformulation was investigated in the presence of various enzymes. Further, the cellular uptake of the MRN-nanoformulation and cytotoxicity were evaluated in cardiomyoblasts and endothelial cells.

Chapter 4: This chapter describes a novel synthesis scheme for surface functionalization of HSA with the AT1 peptide to develop AT1 peptide-tagged nanoparticles. The main aim of this study was to synthesize an AT1 receptor-targeted nanoparticle formulation for specific delivery of MRN. Attaching the AT1 peptide on the HSA surface was achieved by following a two-step covalent chemical conjugation reaction with heterobifunctional cross-linkers 5(6)-Carboxyfluorescein-NHS (N-hydroxysuccinimide) and EDC/Sulfo-NHS. The AT1-HSA binding was confirmed using mass spectrometry. The AT1-HSA-MRN-NPs were formed following the ethanol desolvation methodology mentioned in Chapter 3. The safety and uptake of the AT1-nanoparticle formulation was evaluated in cardiomyoblasts by fluorescence studies and confocal microscopy and compared with the non-targeted MRN-nanoformulation prepared in Chapter 3.

Chapter 5: In this chapter, the targeted nanoparticle formulation for MRN delivery was evaluated *in vivo*. First, the synthesis scheme for attaching the AT1 peptide to the HSA surface, given in chapter 4, was modified by replacing 5(6)-Carboxyfluorescein-NHS with PA-(PEG)₄-SPA

(propionic acid-PEG₄-succinimidyl propionate), followed by addition of EDC/Sulfo-NHS. The fluorescein molecule is known to be mildly cytotoxic and hence was removed from the nanoparticles to avoid toxicity to the animals. Instead, PA-(PEG)₄-SPA was used since addition of PEG imparts non-immunogenicity to the resulting nanoparticle formulation. This chapter investigates MRN pharmacokinetics and tissue distribution, comparing the targeted AT1-HSA-MRN-NPs formulation with MRN-Lactate in an animal model. Further, the treatment efficacy of the AT1-HSA-MRN-NPs vs MRN-Lactate was evaluated in a rat model of CHF. The changes in cardiac function and contractility were determined by measuring the parameters such as ejection fraction, fractional shortening, liver and kidney function, and serum cytokine levels.

Chapter 6: This chapter discusses the findings of the research work presented above.

Chapter 7: Claims of original contributions to knowledge and conclusions.

Chapter 8: Recommendations for future research

CONTRIBUTION OF AUTHORS

The work presented in Chapters 3 to 5 are original research articles (published and unpublished). As first author of these articles, I was responsible for conceptualization, planning and execution of each study. This includes conducting an extensive literature review, specifying the research objectives, performing experiments and analyzing the obtained results from *in vitro* and *in vivo* studies and preparing the research manuscripts. My research supervisor, Dr. Satya Prakash contributed to experiment design and manuscript review, and is the corresponding author for each of the research articles. My research co-supervisor, Dr. Dominique Shum-Tim, helped with data analysis and manuscript review for each chapter. Susan Westfall helped with lab techniques, troubleshooting and manuscript review in Chapters 3, 4 and 5. Meenakshi Malhotra contributed to experiment design, execution and editing the manuscript in Chapter 3. Francis Gaudreault helped with computational modelling studies in Chapter 3. Ziyab K. Sarfaraz performed animal surgeries mentioned in Chapter 5. Aiman Alruwaih assisted with animal echocardiography procedures mentioned in Chapter 5.

CHAPTER 3: NOVEL MILRINONE NANOFORMULATION FOR USE IN CARDIOVASCULAR DISEASES: PREPARATION AND IN VITRO CHARACTERIZATION

Nikita Lomis^{1,2}, Francis Gaudreault³, Meenakshi Malhotra⁴, Susan Westfall¹, Dominique Shum-Tim⁵, Satya Prakash^{1,2,*}

¹Biomedical Technology and Cell Therapy Research Laboratory, Department of Biomedical Engineering, 3775 University Street, Montreal, QC, H3A 2B4, Canada ²Division of Experimental Medicine, 1110 Pins Avenue, Montreal, QC, H3A 1A3, Canada ³Human Health Therapeutics, National Research Council Canada, 6100 Royalmount Avenue, Montreal, QC, H4P 2R2, Canada

⁴Department of Radiology, Stanford University School of Medicine, Stanford, CA, 94305, USA ⁵Division of Cardiac Surgery and Surgical Research, Royal Victoria Hospital, 1001 Boulevard Décarie, Montréal, QC, H4A 3J1, Canada

*Corresponding author: Satya Prakash

Tel: 514-398-2736; Fax: 514-398-7461

Email: satya.prakash@mcgill.ca

Preface: In this chapter, a novel nanoparticle formulation was developed from the HSA protein, to bind and deliver MRN. MRN is a cardiac inotrope and vasodilator drug, which improves myocardial contractility during CHF. For the first time, the binding efficiency between HSA and MRN was studied using computational modelling and circular dichroism techniques. The MRN-nanoformulation was optimized to obtain a particle size between 100-200 nm, negative zeta potential and high MRN encapsulation. The parameters optimized were HSA concentration, pH, MRN/HSA (weight/weight) ratio, ethanol volume, cross-linker concentration and polymerization time. The MRN-HSA-NPs were characterized by dynamic light scattering, electrophoretic doppler anemometry and scanning electron microscopy. The MRN release from the nanoformulation was investigated in the presence of various enzymes. Further, the cellular uptake of the MRN-nanoformulation and cytotoxicity were evaluated in cardiomyoblasts and endothelial cells.

Article published in ACS Molecular Pharmaceutics. 2017; 15(7), 2489-2502.

3.1 Abstract

Cardiovascular diseases are the leading causes of mortality across the globe. Over the years, various drug formulations and delivery methods have been tested, for cardiac repair. Milrinone (MRN) is a widely known cardiac inotrope drug, used for the treatment of congestive heart failure in patients, however, its efficacy is limited. This study is the first to report the design of a novel MRN-nanoformulation using human serum albumin nanoparticles (HSA-NPs). The HSA-NPs exhibit promising drug delivery characteristics such as target specificity, non-immunogenicity, biocompatibility, and enhanced bioavailability. This article describes a MRN-nanoformulation design for in vitro drug release, cellular uptake, biocompatibility and other features. The MRNnanoformulation was prepared by the ethanol desolvation technique and key parameters were optimized to obtain a desired particle size of 154.2±5.8 nm, zeta potential of -29.5±2.9 mV and a drug encapsulation efficiency of 41.1±1.7 %. Molecular docking studies have revealed that MRN binds in the hydrophobic cavity of HSA, which has also been indicated by circular dichroism and enzyme-mediated drug release studies in the presence of trypsin, pepsin, proteinase K, protease and cathepsin D. The intracellular uptake of fluorescently tagged MRN-HSA-NPs using HUVEC and H9c2 cells, was evaluated by flow cytometry. The nanoparticle toxicity results indicated that MRN-HSA-NPs show significantly lower cytotoxicity and higher cell viability (P<0.0001) as compared to the MRN-Lactate drug, in HUVEC (61.6±3.7% vs 36.2±2.9%) and H9c2 (58.8±5.7% vs 18.8±4.9%) cells. These studies indicate that the novel MRN-nanoformulation offers better drug delivery procedures than currently used methods and has potential in treatment of congestive heart failure and other cardiovascular diseases.

Keywords: Heart, human serum albumin, nanoparticles, milrinone, targeting, drug delivery

3.2 Introduction

Cardiovascular diseases (CVDs) are the leading causes of mortality across the developed and developing world, primarily due to unhealthy lifestyles and lack of physical activity ¹. More than 50% of the global CVD occurrences are due to congestive heart failure (CHF), in which buildup of plaque in the coronary artery obstructs the flow of blood to the heart, causing irreversible cardiac necrosis ². CHF is commonly treated using drugs such as ACE inhibitors, inotropes, beta blockers etc., which lower blood pressure and treat arrhythmias ³.

Milrinone, a cardiac inotrope and vasodilator, is widely used for the treatment of CHF. It selectively inhibits the action of the phosphodiesterase III enzyme, increasing the intracellular cAMP concentration, and providing high calcium influx to create a positive inotropic effect ⁴⁻⁶. Milrinone increases myocardial contractility and decreases systemic vascular resistance, left ventricular filling pressure and pulmonary arterial pressure, thus improving overall cardiac function ⁷. It offers an advantage over other cardiac inotropes such as dobutamine, nitroprusside and captopril, in significantly reducing right atrial pressure, pulmonary capillary wedge pressures, left-ventricular end-diastolic pressure along with increase in stroke work index ⁷. MRN is commercially available as a lactate formulation (MRN-Lactate) and clinically administered either intravenously or orally to adult as well as pediatric patients for heart failure and related cardiac conditions ⁸⁻⁹. However, its efficacy may be limited due to lack of target specificity and low bioavailability with other side effects such as renal dysfunction, palpitations and arrhythmias ^{3, 10}.

To improve the target specificity of MRN, we have prepared a MRN-nanoformulation using HSA-NPs. The presence of multiple unique binding pockets on the HSA molecule, promotes the use of HSA-NPs for delivery of various hydrophilic and hydrophobic drugs such as paclitaxel, doxorubicin etc. ¹¹⁻¹³. Milrinone has a half-life of approximately 1-2 hours in humans and is therefore administered as a continuous intravenous infusion or repeated oral dose^{7, 14}. It is widely known that binding the drug to HSA-NPs improves its blood circulation time as compared to that of the free drug itself ¹⁵. Therefore, it is hypothesized that MRN-carrying HSA-NPs will demonstrate superior pharmacokinetics than free MRN, *in vivo*. Previous studies have shown that MRN carrying PLGA-NPs were utilized for the treatment of myocardial infarction (MI) in rats, however no *in vivo* pharmacokinetics study was performed ¹⁶. Also, the particle size of the PLGA-

NPs was approximately 7.4 μ m, which is larger than the diameter of the smallest capillaries (approximately 5-6 μ m) in the body ¹⁷. A large particle size (> 1 μ m) lowers nanoparticle suitability for intravenous delivery. Moreover, HSA-NPs of size less than 250 nm and approximately ± 30 mV zeta potential have shown greater physical stability and prolonged blood circulation times ¹⁸⁻²⁰. Further, unique characteristics like biocompatibility, biodegradability, and non-immunogenicity, have led HSA-NPs to emerge as an excellent choice for delivery of MRN to the heart ²¹.

In this study, we demonstrate the preparation and optimization of the MRN-HSA-NPs. For the first time, molecular docking has predicted binding between MRN and HSA, also indicated by circular dichroism (CD) spectroscopy. Enzyme mediated drug release studies have been performed to validate MRN encapsulation in HSA-NPs. The cellular uptake of MRN-HSA-NPs was evaluated by fluorescence and flow cytometry studies using HUVEC and H9c2 cells, followed by cell viability analysis comparing the MRN-HSA-NPs with the commercial MRN-Lactate. This novel MRN-nanoformulation is anticipated to be an excellent choice for use in cardiovascular diseases.

3.3 Materials and Methods

3.3.1 Materials

Human serum albumin (> 97% lyophilized) was purchased from Sigma Aldrich (Oakville, ON, Canada). Glutaraldehyde (25% aq. solution) was purchased from Alfa Aesar (Cedarlane, Burlington, ON, Canada). Fluorescein isothiocynate human serum albumin (FITC-HSA) was purchased from Sigma Aldrich (Oakville, ON, Canada). Milrinone was purchased from Selleck Chemicals (Burlington, ON, Canada). Bradford reagent was purchased Bio-Rad (St. Laurent, QC, Canada). Trypsin from bovine pancreas, Pepsin from porcine mucosa, Proteinase K, Cathepsin D from bovine liver and Protease were purchased from Sigma Aldrich (Oakville, ON, Canada). Other chemicals were purchased from Fisher Scientific (Nepean, ON, Canada). LysoTracker Deep Red dye (Thermo Fisher, Mississauga, ON, Canada).

3.3.2 Preparation and optimization of MRN-nanoformulation

HSA-NPs bound to MRN were prepared and optimized by following the ethanol desolvation technique ²². Briefly, an aqueous solution of HSA was prepared by dissolving 10, 20, 30, 40 and 50 mg of HSA, each, in 1 mL of deionized water and stirred for 10 minutes. The range of these concentrations were selected based on the maximum solubility of HSA in deionized water (50 mg/mL). A stock solution of 1mg/mL MRN was prepared by dissolving MRN in minimum amount of DMSO and deionized water for 1 mL volume. The 1 mg/mL solution was diluted by mixing with the preparatory HSA solution in HSA/MRN (μ M/ μ M) ratios of 1:1, 1:5, 1:10 and 1:15. The range of concentrations of MRN selected for optimization were based on the maximum solubility of MRN in DMSO (20 mg/mL). Apart from the solubility of MRN alone, there was a limit to the binding of MRN with HSA in solution. Dissolving higher amounts of MRN with the HSA solution led to precipitation of the drug. The pH of the solution was adjusted to 7.0, 7.5, 8.0, 8.5 and 9.0 by addition of 0.1 M NaOH, while stirring at 800 rpm. The pH of the preparative solution was maintained in the basic range in order to have particles with more negative zeta potential. Ethanol was added per volume of the HSA solution (1.0, 1.5, 2.0, 2.5 and 3.0) in a dropwise manner, until it turned turbid. The minimum amount of ethanol needed to turn the preparative solution turbid, was to be determined. Glutaraldehyde (8% v/v aq. solution) concentrations of 0.235, 0.588 and 1.175 μL/mg HSA, were added, which correspond to saturation of 40%, 100% and 200% of amino bonds present on the HSA molecule ²³. The mixture was reacted for 4, 8, 18 & 24 hours at room temperature to determine the optimal time needed for glutaraldehyde polymerization to form > 200 nm sized particles. For preparation of fluorescently tagged FITC-HSA-NPs, regular HSA was replaced by FITC-HSA.

The nanoparticles were washed by three rounds of ultracentrifugation at 16500 rpm for 15 minutes each at 25°C ²². After the final round, the supernatant was collected, and pellet was re-dispersed in phosphate buffer saline (PBS). The nanoparticle solution was tip-sonicated for 15 minutes and stored at 4°C until further use.

3.3.3 Nanoparticle characterization, yield and encapsulation efficiency

The average particle size of the nanoparticles was measured by Dynamic Light Scattering (DLS) using a Particle Size Analyzer (Brookhavens Instruments Corporation, NY, USA). The samples

were diluted in a 1:20 ratio using deionized water and measured at a scattering angle of 90° and at a temperature of 25°C. The Polydispersity Index (PDI) estimated the size distribution of the nanoparticles. The surface charge of the particles was measured by a Zeta Potential Analyzer (Brookhavens Instruments Corporation, NY, USA), which uses electrophoretic laser Doppler anemometry. The nanoparticle size, shape and surface morphology was examined by Scanning Electron Microscopy (SEM) using Hitachi S-4700 FE-SEM. The nanoparticles were diluted with deionized water and a drop of the diluted suspension was deposited on the polished surface of an aluminum sample holder. The samples were dried under vacuum and the morphology of the nanoparticles was observed at 5 kV and 50k X magnification.

The nanoparticle yield was measured by UV-Visible spectrophotometry. A standard curve of HSA solution dissolved in Bradford reagent was used as a reference and absorbance was measured at 595 nm. For calculation of yield, the following equation was used:

Yield% = (final amount of HSA in suspension/initial amount of HSA added) * 100.

To measure the encapsulation efficiency, nanoparticles were spin concentrated using Amicon centrifugal filters with a molecular weight cut off (MWCO) of 10,000 Da for non-encapsulated MRN to be eluted out into the collection tube. The concentration of non-encapsulated MRN was determined by UV-Visible spectrophotometry. A standard curve of MRN in a mixture containing DDQ/Ethanol was used as a reference ^{16, 24}. The absorbance values were measured at 356 nm. The MRN bound to the MRN-HSA-NPs was calculated using the following equation:

Encapsulation Efficiency (EE%) =

(amount of MRN encapsulated/initial amount of MRN added) * 100

3.3.4 Computational modelling of the HSA-MRN complex

Molecular Docking was used to predict the nature of binding, if any, between MRN and HSA. The Protein Data Bank (PDB) was searched to identify target structures of HSA unbound and bound to fatty acids ²⁵. PDB entries 1HK4, 2BXD and 2BXG bound to the small molecules Thyroxin (THY), Warfarin (RWF) and Ibuprofen (IBP) were used as controls in validating the docking

procedure. Fatty acids from the protein target structures were removed before docking the small molecules to allow docking in all interior cavities of HSA. The docking calculations were performed through the Wilma engine version 0.93 and the predicted conformations were re-scored using SIE (Solvated Interaction Energy) scoring function ²⁶⁻²⁷. Conformations of the small molecules were generated in-house. AM1BCC charges (small molecules) were calculated by MolCharge. Sybyl was used to cap N- and C-terminal ends and chain breaks of the targets with NME/ACE groups, rebuild missing side-chain atoms and add explicit Hydrogen atoms ²⁸. Water molecules were assumed to be non-essential and removed. The protonation and tautomerization states of side chains of the targets were corrected using the minH algorithm followed by a minimization.

3.3.5 Circular Dichroism Measurement

Circular Dichroism (CD) measurements were carried out on a JASCO spectropolarimeter (model J-810) equipped with a thermoelectrically controlled cell holder under a constant flow of nitrogen gas. The measurements were acquired using a 0.05 mm quartz cell. The spectra were recorded as an average of three scans from 180-260 nm, acquired with a scan rate of 20 nm/min at 25° C. The averaged spectra were smoothed with a Savitzky-Golay window of five or seven points. The secondary structure was determined using a CDPro with the CDNN and Deconvolution software $^{29-30}$. For CD measurements, an HSA concentration of 0.2 mg/mL (3 μ M) was prepared in deionized water. The HSA/MRN concentrations were in the ratio of 0, 1:1, 1:5, 1:10, 1:15 and 1:20, analyzed at pH 7.0, 8.0 and 9.0. DMSO content (solvent to dissolve MRN) never exceeded 1.0 % (v/v).

3.3.6 Enzymatic drug release from HSA-NPs

The enzymatic drug release from MRN-HSA-NPs was carried out using the following enzymes: trypsin, proteinase K, pepsin, protease and cathepsin D 31 . The MRN-HSA-NPs were divided into aliquots of 1 mL each, with a final nanoparticle concentration of 1 mg/mL and diluted with the respective enzyme buffers. The final enzyme concentration, in the nanoparticle suspension, for trypsin was 100 μ g/mL, protease 10 μ g/mL, proteinase K 10 μ g/mL, pepsin 0.2 mg/mL and cathepsin D 10 μ g/mL 31 . The mixture was incubated at 37°C and 120 rpm. After pre-determined time intervals, the amount of MRN released due to nanoparticle degradation was measured

photometrically at 356 nm and the percentage of cumulative release of MRN over time, was calculated.

3.3.7 Cellular uptake of nanoparticles by HUVEC cells and dose-dependent study

The HUVEC cells were received as a kind gift from Dr. Maryam Tabrizian (Dept. of Biomedical Engineering, McGill University, Montreal, QC, Canada). HUVECs were grown in Medium 200 (Thermo Fisher, Mississauga, ON, Canada) supplemented with Low supplement growth serum (Thermo Fisher, Mississauga, ON, Canada). The H9c2 cells (rat cardiomyoblasts) were received as a kind gift from Dr. Renzo Cecere, M.D. (Montreal General Hospital, Montreal, QC, Canada). The H9c2 cells were grown in DMEM (Gibco, Thermo Fisher, Mississauga, ON, Canada) supplemented with 10% FBS (Gibco, Thermo Fisher, Mississauga, ON, Canada). Both the cell lines were maintained in a humidified incubator at 37°C and 5% CO₂.

Intracellular uptake of nanoparticles and their cytotoxic effect was determined by culturing HUVECs at an initial density of 5 x 10^3 cells/well and H9c2 cells at 10 x 10^3 cells/well in black clear bottom 96-well plates. The cells were replaced with fresh media after 24 hours of incubation and treated with MRN-FITC-HSA-NPs and MRN-Lactate. The concentration of MRN in the MRN-FITC-HSA-NPs and MRN-Lactate, was $1000\mu\text{M}$, $100\mu\text{M}$, $10\mu\text{M}$, $1\mu\text{M}$, $0.1\mu\text{M}$ and $0.01\mu\text{M}$, diluted with serum-free medium. After 4, 24 and 48 hours of incubation, the cells were washed with PBS and fresh cell culture medium was added. The fluorescence intensity was measured at 489nm/535nm using a Victor3V 1420 Multilabel Counter spectrophotometer (Perkin Elmer, Woodbridge, ON, Canada). After fluorescence measurement, $20~\mu\text{L}$ of MTT reagent was added to each well containing $100~\mu\text{L}$ of fresh cell culture medium and incubated in a humidified chamber at 37°C with 5% CO₂. After 4 hours, the cells were lysed using $100~\mu\text{L}$ of DMSO and incubated at room temperature for 15 minutes. The absorbance was measured at 570 nm using the Victor3V 1420 Multilabel Counter spectrophotometer

3.3.8 Flow cytometry

Flow cytometry analysis was performed on HUVEC and H9c2 cells. The cells were seeded in 6-well plates at an initial density of $5x10^5$ cells/well with their respective growth media for 48 hours in a humidified incubator at 37°C and 5% CO₂. Post incubation, both the HUVEC and H9c2 cells

were exposed to the following treatments: 1) FITC-HSA-NPs (0.2 mg/mL in serum free media), 2) 50 nM of LysoTracker Deep Red dye and 3) FITC-HSA-NPs and LysoTracker Deep Red dye double staining and 4) Untreated ³². The cells were incubated with the treatments for 1 hour followed by twice washing with PBS. The cells were trypsinized and centrifuged at 1000 rpm for 5 minutes. Flow cytometry was performed on a FACSCanto II (BD Biosciences, San Jose, CA, USA) and data analysis was performed using FlowJo Version 10 (Tree Star Inc., OR, USA) software.

3.4 Results

3.4.1 Designing the MRN-nanoformulation

HSA is a α-helical protein, most abundantly found in human plasma, with a molecular weight of 66kDa ^{21, 33}. It consists of three homologous domains, which are further divided into A and B subdomains. The subdomains IIA and IIIA allow binding of various acidic drugs such as warfarin, diazepam, paclitaxel etc. at either Site 1 or 2, respectively ³³. MRN is a positive inotrope with a bipyridine structure, represented as 2-methyl-6-oxo-1,6-dihydro-3,4'-bipyridine-5-carbonitrile ³⁴. Studies indicate that the potency of MRN results from the interaction of the methyl moiety with the hydrogen atoms ³⁴⁻³⁵. The MRN structure with its electronegative features was anticipated to bind at the Site 1 of the HSA molecule for formation of MRN-HSA-NPs.

3.4.2 Preparation and optimization of the MRN-nanoformulation

In this study, MRN-HSA-NPs were prepared by the ethanol desolvation method ²². Key parameters were optimized to obtain nanoparticles of size less than 250 nm and zeta potential varying between -15 mV to -40 mV. The parameters considered for optimization were HSA concentration, MRN concentration, pH of preparative solution, amount of ethanol per volume of HSA solution, glutaraldehyde concentration and glutaraldehyde polymerization time.

3.4.2.1 Effect of HSA concentration on nanoformulation

The effect of HSA concentration on nanoparticle size and surface charge was determined by preparing nanoparticles at pH 7.0, ethanol/HSA (v/v) ratio 2.0, glutaraldehyde concentration 1.175 μ L/mg of HSA and polymerization time of 24 hours. HSA is a negatively charged protein. Thus,

increasing the amount of HSA in solution from 10 mg/mL to 50 mg/mL, the particle size increased from 213.2±3.6 nm to 281.8±4.8 nm, due to enhanced formation of intermolecular disulfide bonds (**Figure 3.1(a**)). Further, the zeta potential increased from -22.8±1.8 mV to -29.5±2.4 mV (**Figure 3.1(b**)) ^{13, 36}. The polydispersity index (PDI) for all the preparations was less than 0.15, indicating the homogeneity of the suspension. From this study, the 20 mg/mL HSA concentration, resulting in particle size of 241.8±3.7 nm and zeta potential of -25.5±2.4 mV, was selected for further optimization.

3.4.2.2 Effect of pH preparative solution on nanoformulation

The pH of the preparative solution was found to influence the size and zeta potential of the nanoparticles. The starting HSA concentration was 20 mg/mL, ethanol/HSA (v/v) ratio was 2.0, glutaraldehyde concentration 1.175 μ L/mg HSA and polymerization time of 24 hours. The pH of preparative solution was raised by addition of 0.1 M NaOH, which increases in the negative charges (OH ions) in solution. Thus, due to greater repulsion between charges, when pH of the preparative solution varied from 7.0 to 9.0, particle size decreased from 219.8 \pm 0.4 nm to 147.4 \pm 1.1 nm (**Figure 3.1(c**)). As particle aggregation was lowered, the zeta potential of the particles increased from -23.8 \pm 0.8 mV to -26.5 \pm 0.2 mV (**Figure 3.1(d**)) ²². There was no significant difference in the PDI of the particles and was less than 0.15, which indicated homogeneity of the suspension. At pH 8.0, the particle size was 169.1 \pm 0.6 nm and zeta potential was -24.1 \pm 0.4 mV, and hence, was selected for further optimizations.

3.4.2.3 Effect of ethanol volume on nanoformulation

The ratio of ethanol/HSA (v/v) was also optimized. The nanoparticles were prepared with a starting HSA concentration of 20 mg/mL, pH 8.0, glutaraldehyde concentration of 1.175 μ L/mg HSA and 24 hours polymerization time. Results showed that increasing the ethanol/HSA (v/v) ratio from 1.0 to 3.0 resulted in higher precipitation of the nanoparticles, thus increasing particle aggregation and size from 200.5 \pm 2.2 nm to 293.9 \pm 5.1 nm, respectively (**Figure 3.1(e)**). However, since HSA concentration and pH of solution remained constant throughout this optimization, there were no significant differences in the zeta potentials (**Figure 3.1(f)**). The PDI for all samples was less than 0.15. The ethanol/HSA (v/v) ratio of 1.0 was selected as optimal resulting in particle size of 200.5 \pm 2.2 nm and a zeta potential of -27.1 \pm 1.8 mV.

3.4.2.4 Effect of glutaraldehyde on nanoformulation

Glutaraldehyde (8% v/v aqueous solution) concentrations of 0.235, 0.588 and 1.175 μ L/mg of HSA, saturating 40%, 100% and 200%, respectively, of the amines present on the HSA molecule, were chosen for optimization 23 . The nanoparticles were prepared at a starting HSA concentration of 20 mg/mL, pH 8.0, ethanol/HSA (v/v) ratio of 1.0 and polymerization time of 24 hours. It was observed that at glutaraldehyde concentration of 0.235 and 0.588 μ L/mg of HSA, the particle size was significantly different from that obtained at 1.175 μ L/mg of HSA (155.0±0.8, 152.2±2.4 to 175.7±1.6 nm, respectively) (**Figure 3.1(g**)). However, there was no significant difference between the zeta potentials of different samples (**Figure 3.1(h**)). The PDI for all samples was less than 0.15. The glutaraldehyde concentration 0.588 μ L/mg of HSA was considered as optimal.

3.4.2.5 Effect of MRN concentration on nanoformulation

MRN was added to the HSA solution in the HSA/MRN (μ M/ μ M) ratio of 1:1, 1:5, 1:10 and 1:15. The starting HSA concentration was 20 mg/mL, pH 8.0, ethanol/HSA (v/v) ratio of 2.0, glutaraldehyde 0.588 μ L/mg of HSA and polymerization time of 24 hours. It was observed that on increasing the amount of MRN in the HSA solution, the particle size reduced from 384.1±2.9 nm at HSA/MRN (μ M/ μ M) ratios of 1:1 to 224.4±6.3 nm at HSA/MRN (μ M/ μ M) ratios of 1:15, however, there was no significant difference among particle sizes at 1:5, 1:10 and 1:15 (**Figure 3.1(i)**). This could be due to the electronegative features of the bipyridine rings in the MRN structure. With increasing MRN concentration in the preparative solution, the repulsion between molecules would prevent particle aggregation, thus forming smaller sized particle. Significant differences in the zeta potential of different samples were not observed (**Figure 3.1(j)**). The PDI of the nanoparticle suspensions was less than 0.15 for all samples. The MRN concentration at HSA/MRN (μ M/ μ M) ratio of 1:15 was selected as optimal.

3.4.2.6 Effect of glutaraldehyde polymerization time on nanoformulation

The last parameter optimized was the glutaraldehyde polymerization time. The nanoparticles were prepared at 20 mg/mL HSA concentration, HSA/MRN (μ M/ μ M) ratio of 1:15, pH 8.0, ethanol/HSA (v/v) ratio of 2.0 and glutaraldehyde concentration of 0.588 μ L/mg of HSA. The MRN-HSA-NPs were reacted for 4, 8, 18 and 24 hours. Results showed that after 24 hours of polymerization, the particle size was 269.5±3.9 nm, which was lower than the particle sizes

obtained at other reaction times (**Figure 3.1(k**)). Glutaraldehyde forms a mesh-like network by undergoing a condensation reaction with the amine groups present on lysine or hydroxylysine residues present on the albumin ³⁷. Thus, higher polymerization time possibly allows complete formation of intermolecular bonds and stable nanoparticles. The zeta potential of nanoparticles reacted for 24 hours was -29.0±0.6 mV, which was significantly higher than that of the other samples (**Figure 3.1(l**)). The PDI for the HSA-NPs reacted for 24 hours was less than that of the other preparations. Thus, the polymerization time of 24 hours was selected as optimized.

3.4.3 SEM analysis of MRN-nanoformulation

MRN-HSA-NPs were prepared by following the ethanol desolvation method and compared with HSA-NPs without MRN, for SEM characterization ²²⁻²³. The size of the MRN-HSA-NPs was 154.2±5.8 nm with a polydispersity index of approximately 0.08 and zeta potential of -29.5±2.9 mV (**Figure 3.2(a**)). The size of the HSA-NPs was 148.5±6.2 nm with a polydispersity index of approximately 0.19 and zeta potential of -27.1±3.3 mV (**Figure 3.2(b**)). The yield of the MRN-HSA-NPs was 86.2±2.6% and that of the HSA-NPs was 85.3±2.5%. The MRN encapsulation efficiency at 1:15 HSA/MRN ratio was 41.7±1.7%, as mentioned in **Table 3.1**. The particle size for FITC-HSA-MRN-NPs was 130.2±2.0 nm, polydispersity approximately 0.11 and zeta potential was -27.0±0.3 mV. For FITC-HSA-NPs, the particle size was 118.8±1.4 nm, polydispersity index approximately 0.14 and zeta potential was -30.6±1.9 mV.

3.4.4 Molecular Docking study of HSA-MRN interaction

To evaluate the nature of binding between the MRN and HSA, docking simulations were performed with the Wilma software across the entire surface and interior cavities of HSA ²⁷. The literature data was reproduced by docking the control ligand molecules THY, IBP and RWF (**Figure 3.3 (a-c)**). All molecules were docked as shown in **Table 3.2**, i.e. the most energetically favorable conformation as per the Wilma scoring function, a function that quantifies the protein-ligand interactions to estimate binding affinity. To precisely estimate binding affinities, the analysis was combined with a more elaborate scoring function called SIE scoring function ²⁶. Docking performed by the SIE-software predicted that MRN was bound to HSA in the sub-pocket that also binds RWF. The MRN molecule was found to exhibit 3-H bond acceptors and a single H-bond donor. The sub-pocket contained the following residues with their side-chains interacting

with MRN: GLU292, ALA291, ILE290, SER287, ILE264, ALA261, ILE260, ARG257, HIS242, VAL242, LEU238, LEU234, PHE223, ARG222, LEU219, ARG218, ALA215, TRP214, PHE211, LYS199, GLN196, LYS195, SER192, GLU153 and TYR150. The predictions can be grouped into 2 distinct flipped binding modes: where the nitrogen of the nitrile of MRN interacts with LYS195 (Figure 3.3(d)) and where the oxygen of the hydroxyl is highly stabilized via 3 H-bonds formed with ARG257 and TYR150 (Figure 3.3(e)). Predictions also suggest that MRN binds to HSA with a binding affinity similar as that between RWF and HSA. Using the Wilma scoring function, MRN is predicted to bind the strongest to a form of HSA which is bound to fatty acids, in a sub-pocket close to that for RWF (Figure 3.3(f)). However, SIE re-scoring indicates that the MRN binds stronger to a form of HSA which is unbound to fatty acids at the same location (Figure 3.3(g)).

3.4.5 Effect of MRN binding on different HSA conformations

Circular Dichroism is one of the most promising tools for studying various aspects of protein structure ³⁸. The conformational changes in the secondary structure of HSA have been studied with Far-UV CD, in the range of 180-260 nm at pH 7.0, 8.0 and 9.0. The CD spectra of HSA at pH 7.0, 8.0 and 9.0 exhibits two negative bands in the UV region at 208 nm ($\pi \rightarrow \pi^*$) transition and 222 nm $(n \rightarrow \pi^*)$ transition, which is characteristic of an α -helical protein ³⁹. The conformational states of HSA at pH 7.0, 8.0 and 9.0 contained α-helical content of 58.7%, 62.2% and 59.8%, respectively, which is in alignment with values reported in the literature ⁴⁰. The effect of MRN binding on HSA was studied using Far-UV CD spectra, recorded with MRN/HSA molar ratios of 0, 1:1, 1:5, 1:10, 1:15 and 1:20. At pH 7.0 (Figure 3.4(a-b)) and pH 9.0 (Figure 3.4(c-d)), no change in the HSA secondary structure was observed on binding with different MRN concentrations. However, at pH 8.0, a significant reduction in the α -helical content from 62% to 36% at the expense of random coil with 30.7%, was observed at MRN/HSA ratio 1:5. The α-helical content in the remaining preparations with HSA/MRN ratios 1:1, 1:10, 1:15 and 1:20 remained 62.2%, 60.9%, 60.1% and 57.8% respectively (**Figure 3.4(e-f)**). Similar reduction in helical content of human serum albumin on binding with other drugs has also been reported ⁴¹⁻⁴³. These results demonstrated the interaction between MRN on binding with HSA at pH 8.0 and have been summarized in Table 3.3.

3.4.6 Enzymatic degradation of HSA-NPs and MRN release

The intracellular delivery of nanoparticles is of utmost importance. In this study, the enzyme mediated release of MRN from MRN-HSA-NPs has been evaluated in the presence of different enzymes such as trypsin, protease and proteinase K which are functionally active at the neutral pH and pepsin, cathepsin D, which are functionally active at acidic pH ³¹. The enzyme concentrations in the nanoparticle suspension were set to obtain a rapid nanoparticle degradation and release of MRN. It was observed that trypsin caused rapid degradation of the nanoparticles, releasing 72.5±1.9% of MRN within 24 hours (**Figure 3.5(a)**) whereas pepsin released 87.5±0.9% of MRN within just 2 hours of incubation (**Figure 3.5(b)**). Proteinase K, protease and cathepsin D exhibited a relatively slower release of 33.4±2.5%, 14.2±2.7% and 5.9±1.3%, respectively, over 24 hours (**Figure 3.5(c-e)**). A summary of these results is presented in **Table 3.4**.

3.4.7 Intracellular nanoparticles uptake

It is known that HSA is transported across the endothelial cells by receptor mediated endocytosis via the albondin glycoprotein receptor (gp60) on the surface of endothelial cells ⁴⁴. Albumin transports fatty acids across cardiac cells, however, the exact method of HSA uptake by these cells is uncertain ⁴⁵. In this study, the uptake of HSA-NPs by HUVECs and H9c2 cells was studied by using FITC-HSA. The HUVECs and H9c2 cells were treated with different concentrations of HSA-NPs with and without MRN, for 4, 24 and 48 hours. The HUVECs treated with MRN-HSA-NPs with nanoparticle concentration of 8000 μ g/mL (M-8000) exhibited significantly higher (P<0.0001) fluorescence intensity as compared to the other treatments after 4 hours (**Figure 3.6(a)**). An increase in the fluorescence intensity at nanoparticles concentrations of 600 μ g/mL, represented by M-600 (MRN-HSA-NPs) and H-600 (HSA-NPs alone) was observed between 4 hours and 24 hours (**Figure 3.6(b**)), after which there was no significant increase until 48 hours (**Figure 3.6(c**)).

The H9c2 rat cardiomyoblasts treated with M-600 and H-600 exhibited higher nanoparticle uptake than M-8000 after 4 hours of treatment (**Figure 3.7(a**)). The fluorescence intensity further increased significantly (P<0.0001) in the M-8000, M-600 and H-600 treatments as compared to rest of the treatments from 4 to 24 hours (**Figure 3.7(b**)) after which there was no significant

increase until 48 hours (**Figure 3.7(c**)). However, no significant cellular uptake of nanoparticles was observed in other treatment conditions.

3.4.8 Flow cytometry analysis

Flow cytometry analysis was performed to validate the uptake of FITC-HSA-NPs (0.2 mg/mL) by HUVECs and H9c2 cells. The treatments were divided as: FITC-HSA-NPs, LysoTracker Deep Red labeled (control), FITC-HSA-NPs and Lysotracker double stained and untreated cells. Results suggested that the for the HUVECs treated with both FITC-HSA-NPs and LysoTracker Deep Red, approximately 98% of the cell population exhibited fluorescence for both the FITC as well as LysoTracker Deep Red dye (Figure 3.8(a)). For H9c2 cells treated with both FITC-HSA-NPs and LysoTracker Deep Red, approximately 41.3% of the cell population exhibited fluorescence for both FITC and LysoTracker Deep Red dye (Figure 3.8(b)). These results validated the intracellular uptake of the FITC-HSA-NPs.

3.4.9 Cell viability analysis

For evaluating the safety and efficacy of MRN-HSA-NPs on HUVECs and H9c2 cells, the MTT assay was performed. The cells were treated with MRN-HSA-NPs and MRN-Lactate at MRN concentrations 0.01 μ M, 0.1 μ M, 10 μ M, 100 μ M and 1000 μ M for 4, 24 and 48 hours. Results suggested that the HUVECs incubated with the two treatments containing 1000 μ M MRN displayed cell viabilities of 82.4±14.3%, 60.1±3.8%, and 61.6±3.7% at 4, 24 and 48 hours, respectively, in the presence of MRN-HSA-NPs. In comparison, cell viabilities in the presence of MRN-Lactate were 42.5±5.8%, 35.4±0.9% and 36.2±2.9%, respectively (**Figure 3.9**). When MRN concentration was 100 μ M, the cell viability in the presence of MRN-HSA-NPs was 85.9±12.3%, 71.9±9.6% and 65.1±1.5% at 4, 24 and 48 hours, respectively, whereas for MRN-Lactate treatment was 59.4±4.1%, 49.6±1.1% and 55.7±2.8%, respectively. There were no significant differences in the other MRN-HSA-NPs and MRN-Lactate treatments containing 0.01, 0.1, 1 and 10 μ M MRN.

Similarly, the safety of MRN-HSA-NPs as compared to the MRN-Lactate was also evaluated in H9c2 cells. Results suggested that at $1000 \,\mu\text{M}$ MRN concentration, the cell viability due to MRN-HSA-NPs was $74.7\pm3.9\%$, $74.9\pm2.2\%$, and $58.8\pm5.7\%$ at 4, 24 and 48 hours, respectively, in comparison to that of MRN-Lactate with $52.6\pm4.9\%$, $46.1\pm2.5\%$ and $18.8\pm4.9\%$, respectively

(**Figure 3.10**). At 100 μ M MRN concentration, cell viability in the presence of MRN-HSA-NPs was 79.0±0.9%, 88.3±4.1% and 64.9±5.6% at 4, 24 and 48 hours, respectively, whereas in the presence of MRN-Lactate was 62.3±2.1%, 50.1±3.8% and 42.3±10.4%, respectively. Also, there were no significant differences in the remaining MRN-HSA-NPs and MRN-Lactate treatments containing 0.01, 0.1, 1 and 10 μ M MRN. Therefore, it was concluded that the MRN-HSA-NPs exhibited greater cell biocompatibility than MRN-Lactate.

3.5 Discussion

HSA-NPs are widely used for the delivery of drugs, genes, hormones, and various other molecules ²¹. This study is the first to report the use of HSA-NPs as vehicles for carrying the cardiac inotrope and vasodilator drug, MRN. MRN is a phosphodiesterase-III inhibitor, which through the action of protein kinase A, improves myocardial contractility. It is commonly administered as a lactate formulation to patients suffering from CHF ^{5, 34}.

This study demonstrates the development of a novel MRN-nanoformulation. Following the ethanol desolvation technique, stable MRN-HSA-NPs were prepared by optimizing key parameters such as HSA and MRN concentration, pH of preparative solution, ethanol volume, glutaraldehyde content and polymerization time ²³. This resulted in achieving an encapsulation efficiency of approximately 41%, which is the highest reported so far. Nanoparticle characterization was performed by the DLS, laser Doppler anemometry and SEM techniques. Molecular docking analysis using the Wilma software predicted a strong binding affinity of -27.6 kcal/mol between MRN and HSA bound to fatty acids, similar to that between warfarin and HSA (-26.6 kcal/mol) ⁴⁶. The SIE-rescoring predicted a HSA-MRN binding affinity of -8.6 kcal/mol, when HSA is unbound to fatty acids. MRN is predicted to bind with the Lys195, Arg257 and Tyr150 residues in sub-domain IIA at Site 1 of the HSA molecule, which is also known to bind other hydrophobic drugs ^{13, 33}. Circular dichroism spectroscopy determined a change in the secondary structure of HSA on interaction with MRN in a 1:5 molar ratio. However, this change in secondary structure was not observed at other HSA/MRN molar ratios and at other different pH conditions. This can be compared with changes observed in the HSA secondary structure on binding with drug molecules such as virstatin or cisplatin 42-43. This could be explained due to the changes in molecular conformation of albumin on binding with small molecules, which also change with the

pH of solution leading to increased formation of β -sheets and random coil structures at the expense of the α -helix. ⁴⁷⁻⁴⁸. This may also suggest formation of more inter and intra-domain structures when MRN interacts or binds with HSA. This test was a supplement to our molecular docking studies to indicate that there was an interaction between the MRN and HSA, given that this has not been reported in literature earlier.

An enzyme-mediated drug release study was performed to confirm that MRN was bound to HSA-NPs. The enzymes trypsin, pepsin, proteinase K, protease and cathepsin D were used to evaluate the cumulative MRN release from MRN-HSA-NPs ³¹. However, these enzymes may not be physiologically involved when nanoparticles are administered in the body as the drug is expected to be released into the cytosol by receptor mediated endocytosis of the nanoparticles. The rate of degradation of nanoparticles varies due to the difference in the type of peptide bonds cleaved by the enzymes. Trypsin, known to cleave at the carboxyl end of lysine and arginine residues of the protein, released approximately 70-75% of the drug. Pepsin, which cleaves the peptide bonds between phenylalanine, tyrosine and tryptophan residues, released approximately 85-90% of the MRN. However, the drug release in the presence of other enzymes was relatively slower. Cathepsin D, a lysosomal enzyme known for HSA degradation, was unable to completely release MRN from the nanoparticles, possibly due to the high glutaraldehyde concentration ³¹. Also, the *in vitro* conditions cannot completely simulate the conditions of a lysosomal vesicle inside the cell.

During *in vivo* treatment, MRN-HSA-NPs are anticipated to be up-taken by endothelial cells as well as cardiomyocytes. Therefore, the intracellular uptake and cell biocompatibility of MRN-HSA-NPs was studied using HUVECs and H9c2 cells. Fluorescence studies have revealed that the nanoparticle uptake by both HUVECs and H9c2 cells was time-dependent. This was demonstrated by an increase in fluorescence intensity from 4 to 24 hours at nanoparticle concentrations of 600 and 8000 μg/mL, post which there was no significant increase until 48 hours. Fluorescence intensity at lower nanoparticle concentrations was significantly lower due to high dilution. Further, the presence of MRN in the NPs did not affect their cellular uptake. A flow cytometry analysis confirmed the intracellular uptake of the nanoparticles by both cell types. HUVECs (endothelial cells) are known to interact with HSA through the presence of albondin (gp60) receptors present on the cell surface, which allows receptor mediated endocytosis of the nanoparticles ⁴⁴. Also, H9c2

cells (cardiomyoblasts) are anticipated to interact with HSA through the gp18 and gp31 receptors present on the cell surface ⁴⁵.

Cell viability due to MRN-HSA-NPs and MRN-Lactate was analyzed by performing the MTT assay. The MTT assay is a commonly used colorimetric assay using the dye 3-(4,5-dimtheylthiazol-2-yl)-2,5-diphenltetrazoliumbromide (MTT) for the rapid determination of cell viability/cytotoxicity ¹². The overall cytotoxicity of the MRN-Lactate treatments was significantly higher than the MRN-HSA-NPs in both HUVEC and H9c2 cells. The treatments which showed very low cytotoxicity, could be attributed to the higher dilution and hence lower nanoparticle uptake as revealed by the fluorescence studies. Therefore, it may be concluded that the MRN-nanoformulation is safer and more biocompatible as compared to the MRN-Lactate.

3.6 Conclusion

The growing incidence of CVDs across the world has also increased the need for developing effective novel technologies. This study is the first to report the development of a novel MRN-nanoformulation using HSA-NPs as vehicles for delivery of MRN, a cardiac inotrope drug that treats congestive heart failure. MRN-HSA-NPs exhibit a final particle size less than 200 nm and zeta potential of approximately -30 mV, which is ideal for *in vivo* drug delivery. This study is also the first to report predictions for MRN binding to the hydrophobic pocket present on sub-domain IIA (Site I) of the HSA molecule, by molecular docking studies.

Future studies will include the determination of the therapeutic effect of the MRN-nanoformulation. Currently, MRN with a retention time of 1-2 hours, is administered clinically as a continuous intravenous infusion ^{7, 14}. Hence, pharmacokinetic-pharmacodynamic studies with the MRN-nanoformulation will be useful in determining an increase in the body circulation time of MRN. Since the MRN-nanoformulation is target-specific, it is anticipated to have reduced dose requirements as compared to that of the currently used MRN-Lactate. The intracellular uptake of MRN-HSA-NPs by endothelial cells and cardiomyoblasts as well as their high biocompatibility are indicative that this novel nanoformulation will work better and may potentially be used in CHF and other cardiac applications. Since the presented study is the first of its kind, these results need

extrapolation into *in vivo* data. Therefore, further animal studies will be required to evaluate the complete clinical potential of the MRN-nanoformulation.

3.7 Acknowledgements

This work is supported by the research funding granted to Dr. Satya Prakash from Canadian Institute of Health Research (CIHR) and the Natural Sciences and Engineering Research Council (NSERC). The authors would like to acknowledge the Canadian Graduate Scholarship from NSERC to Ms. Susan Westfall. The authors are grateful to Dr. Enrico Purisima (National Research Council Canada) for supervising the molecular docking study and Hervé Hogues (National Research Council Canada) for performing docking and re-scoring calculations. The authors would like to thank Mr. Xue Dong Liu for assistance in F-50 SEM imaging (Facility for Electron Microscopy Research, Materials Engineering, McGill University).

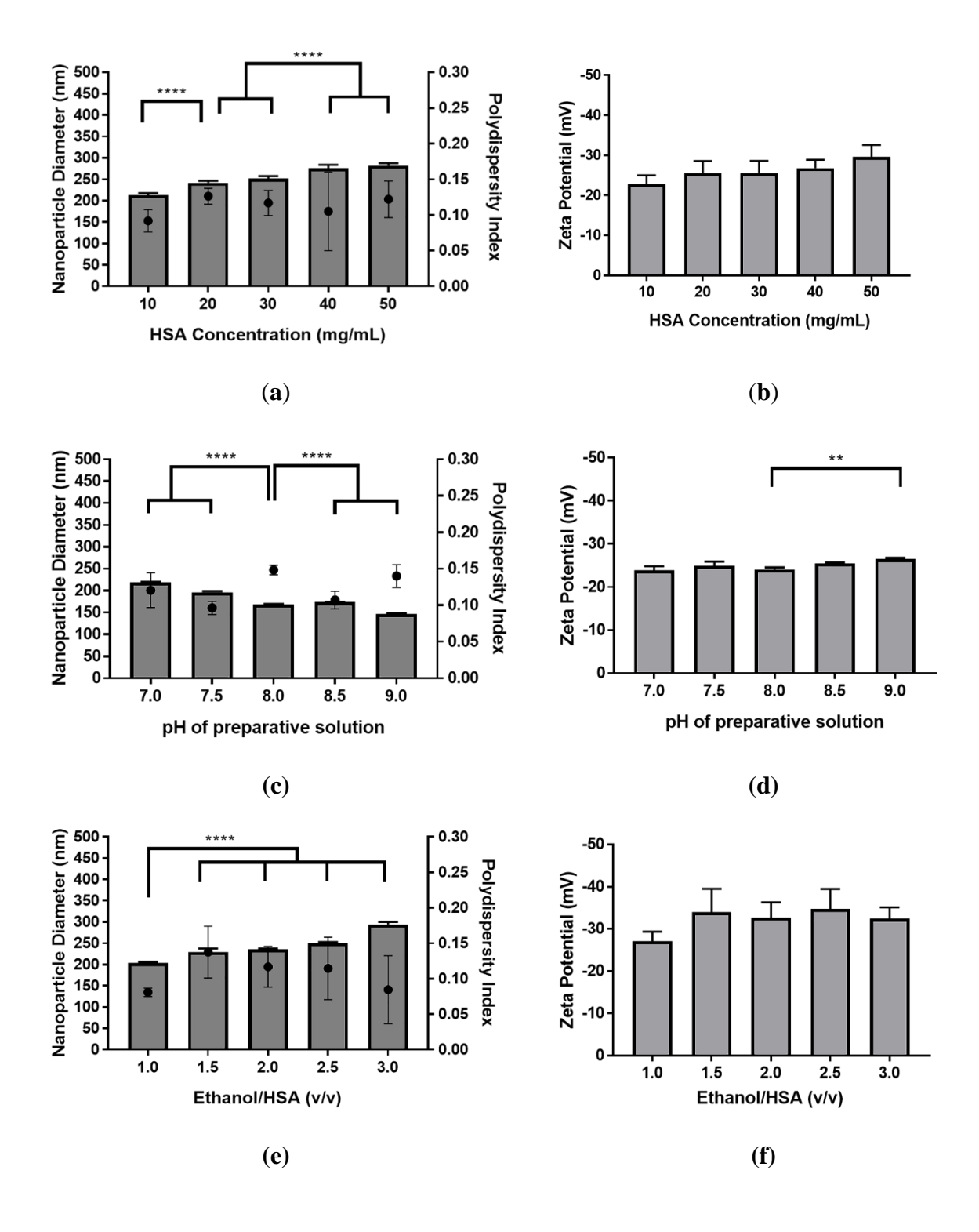
3.8 References

- Go, A. S. *et al.* Heart disease and stroke statistics--2014 update: a report from the American Heart Association. *Circulation* **129**, e28-e292, doi:10.1161/01.cir.0000441139.02102.80 (2014).
- Nabel, E. G. & Braunwald, E. A Tale of Coronary Artery Disease and Myocardial Infarction. *New England Journal of Medicine* **366**, 54-63, doi:doi:10.1056/NEJMra1112570 (2012).
- de Boer, R. A. & van Veldhuisen, D. J. ACE-inhibitors, Beta-blockers or the Combination in Heart Failure: Is It Just an A–B–C? *Cardiovascular Drugs and Therapy* **22**, 261-263 (2008).
- Feneck, R. Phosphodiesterase inhibitors and the cardiovascular system. *Continuing Education in Anaesthesia, Critical Care & Pain* **7**, 203-207 (2007).
- 5 Alousi, A. & Johnson, D. Pharmacology of the bipyridines: amrinone and milrinone. *Circulation* **73**, III10-24 (1986).
- Baim, D. S. *et al.* Evaluation of a new bipyridine inotropic agent—milrinone—in patients with severe congestive heart failure. *New England journal of medicine* **309**, 748-756 (1983).
- 7 Young, R. A. & Ward, A. Milrinone. *Drugs* **36**, 158-192, doi:10.2165/00003495-198836020-00003 (1988).
- 8 Barton, P. *et al.* Hemodynamic effects of iv milrinone lactate in pediatric patients with septic shock: A prospective, double-blinded, randomized, placebo-controlled, interventional study. *CHEST Journal* **109**, 1302-1312 (1996).
- Wang, Z., Wu, Q., Nie, X., Guo, J. & Yang, C. Combination therapy with milrinone and esmolol for heart protection in patients with severe sepsis: a prospective, randomized trial. *Clinical drug investigation* **35**, 707-716 (2015).

- 10 Cuffe, M. S. *et al.* Short-term intravenous milrinone for acute exacerbation of chronic heart failure: a randomized controlled trial. *Jama* **287**, 1541-1547 (2002).
- Abbasi, S., Paul, A., Shao, W. & Prakash, S. Cationic albumin nanoparticles for enhanced drug delivery to treat breast cancer: preparation and in vitro assessment. *Journal of drug delivery* **2012** (2011).
- Sebak, S., Mirzaei, M., Malhotra, M., Kulamarva, A. & Prakash, S. Human serum albumin nanoparticles as an efficient noscapine drug delivery system for potential use in breast cancer: preparation and in vitro analysis. *International journal of nanomedicine* 5, 525 (2010).
- Lomis, N. *et al.* Human Serum Albumin Nanoparticles for Use in Cancer Drug Delivery: Process Optimization and In Vitro Characterization. *Nanomaterials* **6**, 116 (2016).
- Edelson, J. *et al.* Pharmacokinetics of the bipyridines amrinone and milrinone. *Circulation* **73**, III145-152 (1986).
- Wang, F. *et al.* Combined image guided monitoring the pharmacokinetics of rapamycin loaded human serum albumin nanoparticles with a split luciferase reporter. *Nanoscale* **8**, 3991-4000, doi:10.1039/c5nr07308a (2016).
- Al Kindi, H. *et al.* Sustained release of milrinone delivered via microparticles in a rodent model of myocardial infarction. *The Journal of thoracic and cardiovascular surgery* **148**, 2316-2324 (2014).
- 17 Singh, R. & Lillard, J. W. Nanoparticle-based targeted drug delivery. *Experimental and molecular pathology* **86**, 215-223 (2009).
- Hawkins, M. J., Soon-Shiong, P. & Desai, N. Protein nanoparticles as drug carriers in clinical medicine. *Advanced drug delivery reviews* **60**, 876-885 (2008).
- 19 Grislain, L. *et al.* Pharmacokinetics and distribution of a biodegradable drug-carrier. *International Journal of Pharmaceutics* **15**, 335-345 (1983).
- Müller, R., Maaben, S., Weyhers, H. & Mehnert, W. Phagocytic uptake and cytotoxicity of solid lipid nanoparticles (SLN) sterically stabilized with poloxamine 908 and poloxamer 407. *Journal of drug targeting* **4**, 161-170 (1996).
- Elzoghby, A. O., Samy, W. M. & Elgindy, N. A. Albumin-based nanoparticles as potential controlled release drug delivery systems. *Journal of controlled release* **157**, 168-182 (2012).
- Langer, K. *et al.* Optimization of the preparation process for human serum albumin (HSA) nanoparticles. *International Journal of Pharmaceutics* **257**, 169-180 (2003).
- Weber, C., Coester, C., Kreuter, J. & Langer, K. Desolvation process and surface characterisation of protein nanoparticles. *International journal of pharmaceutics* **194**, 91-102 (2000).
- Siddiqui, M. *et al.* Application of DDQ and p-chloranilic acid for the spectrophotometric estimation of milrinone in pharmaceutical formulations. *Asian Journal of Scientific Research* **2**, 135-145 (2009).
- Berman, H. M. et al. The protein data bank. Nucleic acids research 28, 235-242 (2000).
- Sulea, T. & Purisima, E. O. The solvated interaction energy method for scoring binding affinities. *Computational Drug Discovery and Design*, 295-303 (2012).
- Hogues, H., Sulea, T. & Purisima, E. O. Exhaustive docking and solvated interaction energy scoring: lessons learned from the SAMPL4 challenge. *Journal of computer-aided molecular design* **28**, 417-427 (2014).

- Clark, M., Cramer, R. D. & Van Opdenbosch, N. Validation of the general purpose Tripos 5.2 force field. *Journal of Computational Chemistry* **10**, 982-1012 (1989).
- Sreerama, N. & Woody, R. W. On the analysis of membrane protein circular dichroism spectra. *Protein Science* **13**, 100-112 (2004).
- Böhm, G., Muhr, R. & Jaenicke, R. Quantitative analysis of protein far UV circular dichroism spectra by neural networks. *Protein engineering* **5**, 191-195 (1992).
- Langer, K. *et al.* Human serum albumin (HSA) nanoparticles: reproducibility of preparation process and kinetics of enzymatic degradation. *International journal of pharmaceutics* **347**, 109-117 (2008).
- Fan, F. *et al.* Labeling lysosomes and tracking lysosome-dependent apoptosis with a cell-permeable activity-based probe. *Bioconjugate chemistry* **23**, 1309-1317 (2012).
- Ghuman, J. *et al.* Structural basis of the drug-binding specificity of human serum albumin. *Journal of molecular biology* **353**, 38-52 (2005).
- Robertson, D. W. *et al.* Bipyridine cardiotonics: the three-dimensional structures of amrinone and milrinone. *Journal of medicinal chemistry* **29**, 635-640 (1986).
- Cody, V., Wojtczak, A., Davis, F. B., Davis, P. J. & Blas, S. D. Structure-activity relationships of milrinone analogues determined in vitro in a rabbit heart membrane Ca (2+)-ATPase model. *Journal of medicinal chemistry* **38**, 1990-1997 (1995).
- Jun, J. Y., Nguyen, H. H., Chun, H. S., Kang, B.-C. & Ko, S. Preparation of size-controlled bovine serum albumin (BSA) nanoparticles by a modified desolvation method. *Food Chemistry* **127**, 1892-1898 (2011).
- Damink, L. O. *et al.* Glutaraldehyde as a crosslinking agent for collagen-based biomaterials. *Journal of materials science: materials in medicine* **6**, 460-472 (1995).
- Kelly, S. M., Jess, T. J. & Price, N. C. How to study proteins by circular dichroism. *Biochimica et Biophysica Acta (BBA)-Proteins and Proteomics* **1751**, 119-139 (2005).
- 39 Ahmad, B., Parveen, S. & Khan, R. H. Effect of albumin conformation on the binding of ciprofloxacin to human serum albumin: a novel approach directly assigning binding site. *Biomacromolecules* **7**, 1350-1356 (2006).
- 40 Peters, T. Serum albumin. *Advances in protein chemistry* **37**, 161-245 (1985).
- 41 Bian, Q., Liu, J., Tian, J. & Hu, Z. Binding of genistein to human serum albumin demonstrated using tryptophan fluorescence quenching. *International journal of biological macromolecules* **34**, 275-279 (2004).
- Neault, J. & Tajmir-Riahi, H. Interaction of cisplatin with human serum albumin. Drug binding mode and protein secondary structure. *Biochimica et Biophysica Acta (BBA)-Protein Structure and Molecular Enzymology* **1384**, 153-159 (1998).
- Chatterjee, T., Pal, A., Dey, S., Chatterjee, B. K. & Chakrabarti, P. Interaction of virstatin with human serum albumin: spectroscopic analysis and molecular modeling. *PLoS One* **7**, e37468 (2012).
- Tiruppathi, C., Song, W., Bergenfeldt, M., Sass, P. & Malik, A. B. Gp60 activation mediates albumin transcytosis in endothelial cells by tyrosine kinase-dependent pathway. *Journal of Biological Chemistry* **272**, 25968-25975 (1997).
- Popov, D., Hasu, M., Ghinea, N., Simionescu, N. & Simionescu, M. Cardiomyocytes express albumin binding proteins. *Journal of molecular and cellular cardiology* **24**, 989-1002 (1992).
- Carter, D. C. & Ho, J. X. Structure of serum albumin. *Advances in protein chemistry* **45**, 153-203 (1994).

- Wilting, J. *et al.* The effect of albumin conformation on the binding of warfarin to human serum albumin. The dependence of the binding of warfarin to human serum albumin on the hydrogen, calcium, and chloride ion concentrations as studied by circular dichroism, fluorescence, and equilibrium dialysis. *Journal of Biological Chemistry* **255**, 3032-3037 (1980).
- Graciani, F. S. & Ximenes, V. F. Investigation of human albumin-induced circular dichroism in dansylglycine. *PloS one* **8**, e76849 (2013).



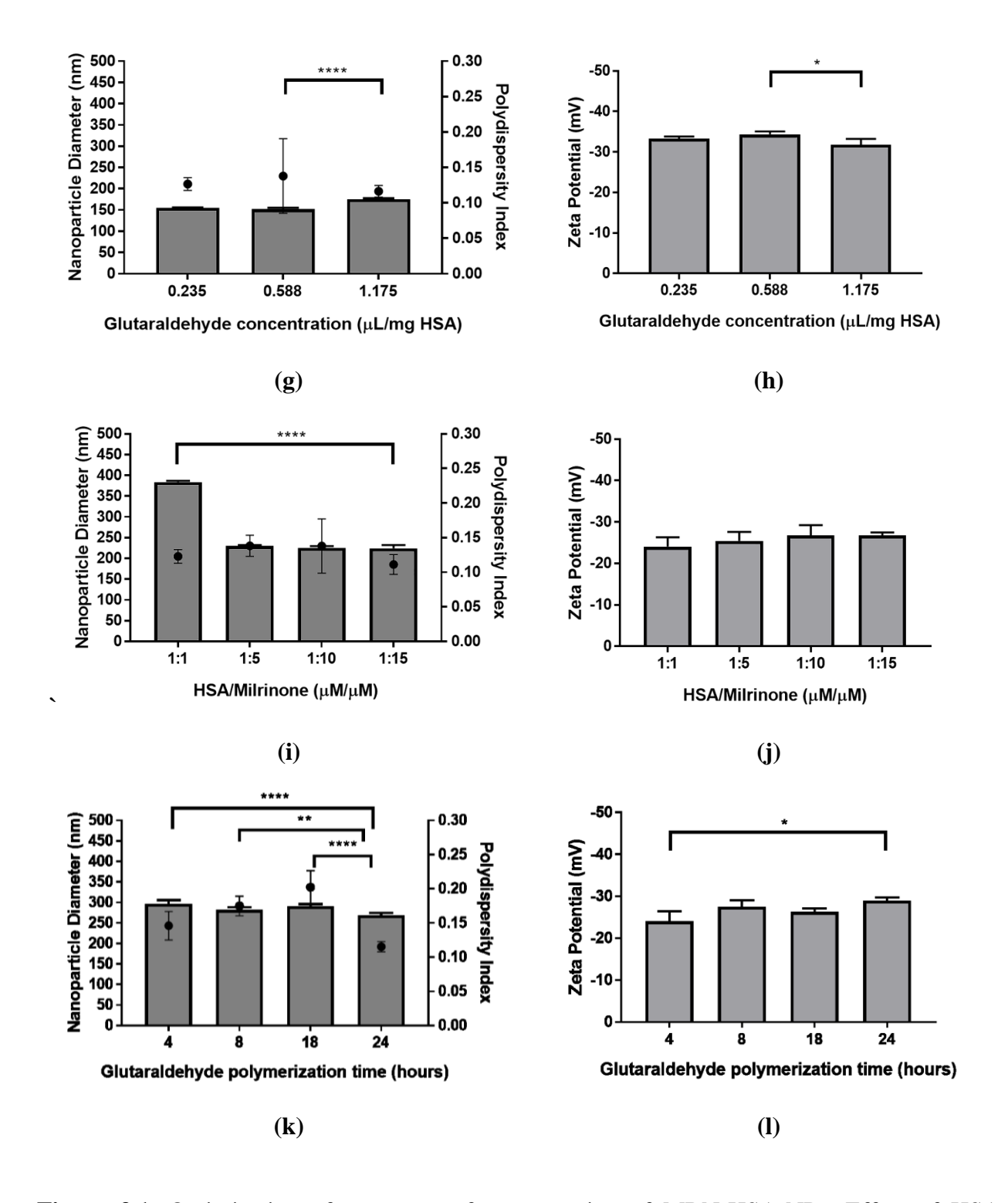


Figure 3.1. Optimization of parameters for preparation of MRN-HSA-NPs. Effect of HSA concentration (mg/mL) on (a) nanoparticle diameter and polydispersity index and (b) nanoparticle zeta potential; Effect of pH of preparative solution on (c) nanoparticle diameter and polydispersity index and (d) nanoparticle zeta potential; Effect of ratio of ethanol/HSA (v/v) on (e) nanoparticle

diameter and polydispersity index and (**f**) nanoparticle zeta potential; Effect of glutaraldehyde concentration (μ L/mg HSA) on (**g**) nanoparticle diameter and polydispersity index and (**h**) nanoparticle zeta potential; Effect of HSA/Milrinone (μ M/ μ M) ratio on (**i**) nanoparticle diameter and polydispersity index and (**j**) nanoparticle zeta potential; Effect of glutaraldehyde polymerization time (hours) on (**k**) nanoparticle diameter and polydispersity index and (**l**) nanoparticle zeta potential. The nanoparticle diameter is represented as the dark grey bar, polydispersity index as symbol and zeta potential as light grey bar. The graphs show a representative result of mean \pm SD (n=3). ****P<0.001 was considered highly significant and ***P<0.001, **P<0.05 were considered significant based on Tukey's posthoc analysis, when compared with other groups.

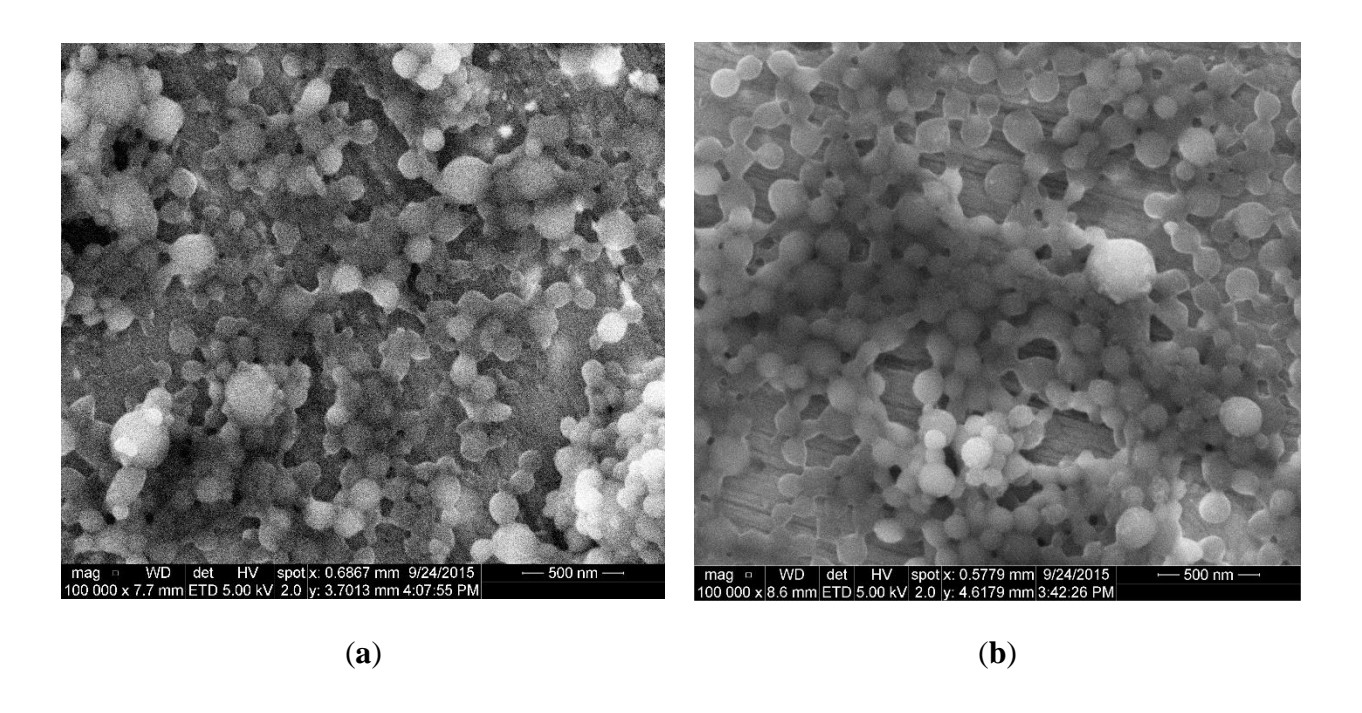


Figure 3.2. Nanoparticle surface characterization using SEM analysis: (a) MRN-HSA-NPs of size 154.2 ± 5.8 nm, polydispersity index of approximately 0.08 and zeta potential of -29.5 ± 2.9 mV (Scale = 500 nm); (b) HSA-NPs of size 148.5 ± 6.2 nm, polydispersity index of approximately 0.19 and zeta potential of -27.1 ± 3.3 mV (Scale = 500 nm).

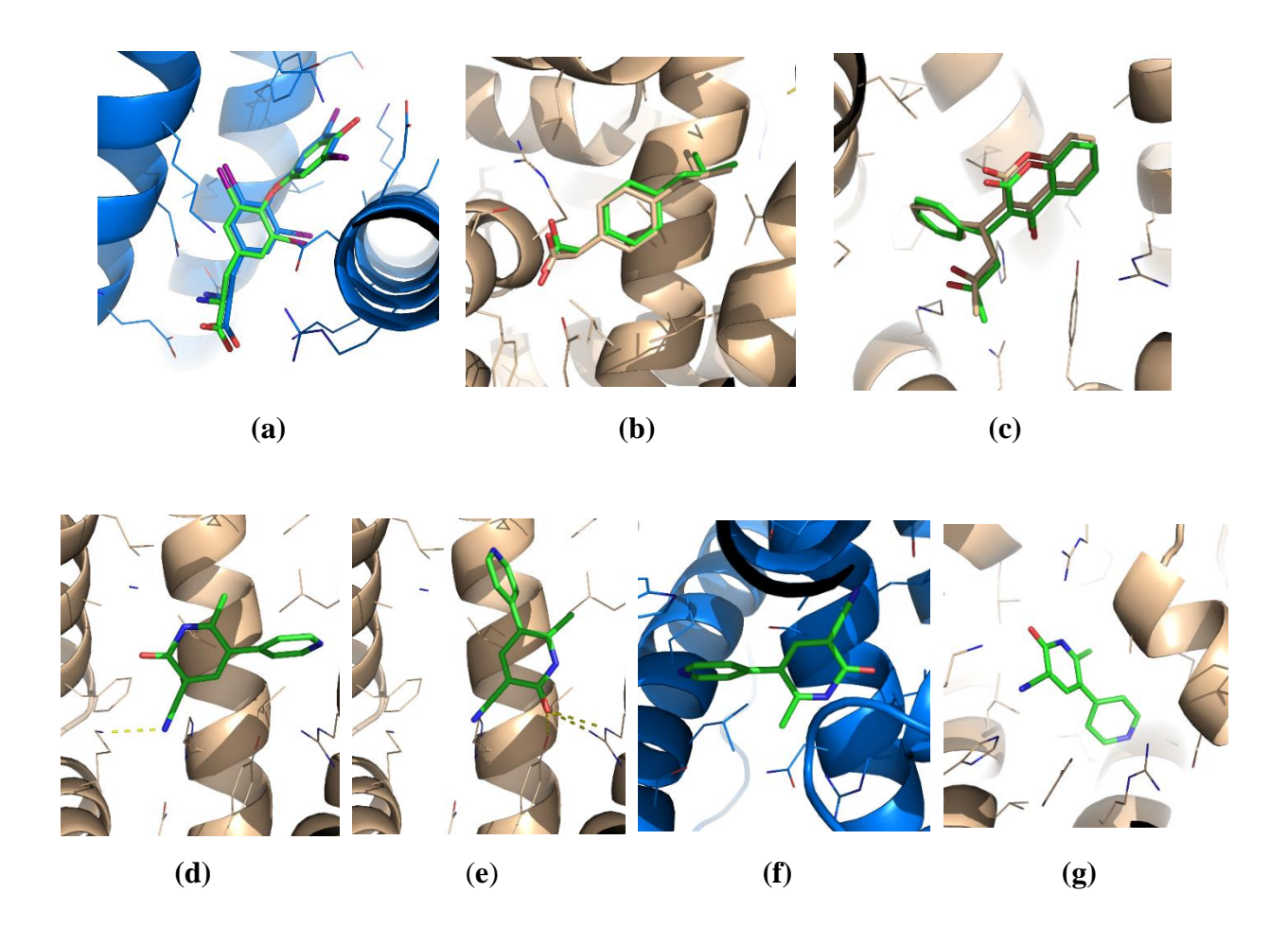


Figure 3.3. Molecular docking predictions for (a) Thyroxine (green) relative to its cognate conformation (blue); (b) Ibuprofen (green) relative to its cognate conformation (beige); (c) Warfarin (green) relative to its cognate conformation (beige); (d) MRN (green) docked against HSA, where the nitrile group on MRN forms 1 H-bond (yellow dashed line) with Lys195 on HSA; (e) MRN docked against HSA, where the hydroxyl group forms 3 H-bonds (yellow dashed lines) with Arg257 and Tyr150; (f) MRN (green) predicted to bind the strongest to forms of HSA bound to fatty acids, in the same sub-pocket as Warfarin when considering Wilma scoring results; (g) MRN (green) predicted to bind the strongest to forms of HSA unbound to fatty acids when considering SIE re-scoring results.

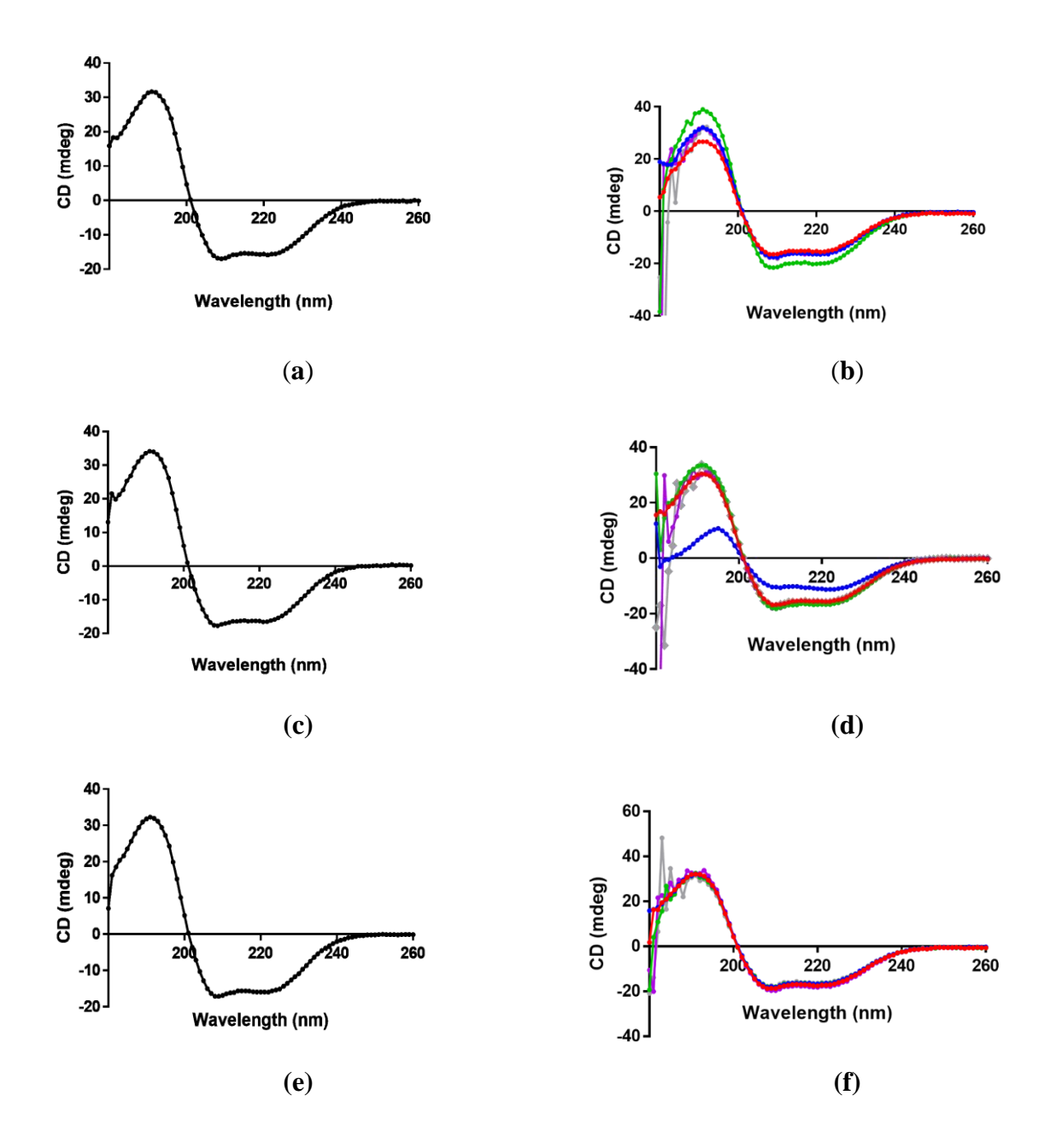


Figure 3.4. Far-UV CD spectra of HSA at different pH and HSA/MRN molar ratios. (a) HSA at pH 7.0 (b) HSA at HSA/MRN molar ratios of 0 (dark blue), 1:1 (red), 1:5 (green), 1:10 (purple), 1:15 (light blue) and 1:20 (orange); (c) HSA at pH 8.0; (d) HSA at HSA/MRN molar ratios of 0 (dark blue), 1:1 (red), 1:5 (green), 1:10 (purple), 1:15 (light blue) and 1:20 (orange); (e) HSA at pH 9.0; (f) HSA at HSA/MRN molar ratios of 0 (dark blue), 1:1 (red), 1:5 (green), 1:10 (purple), 1:15 (light blue) and 1:20 (orange).

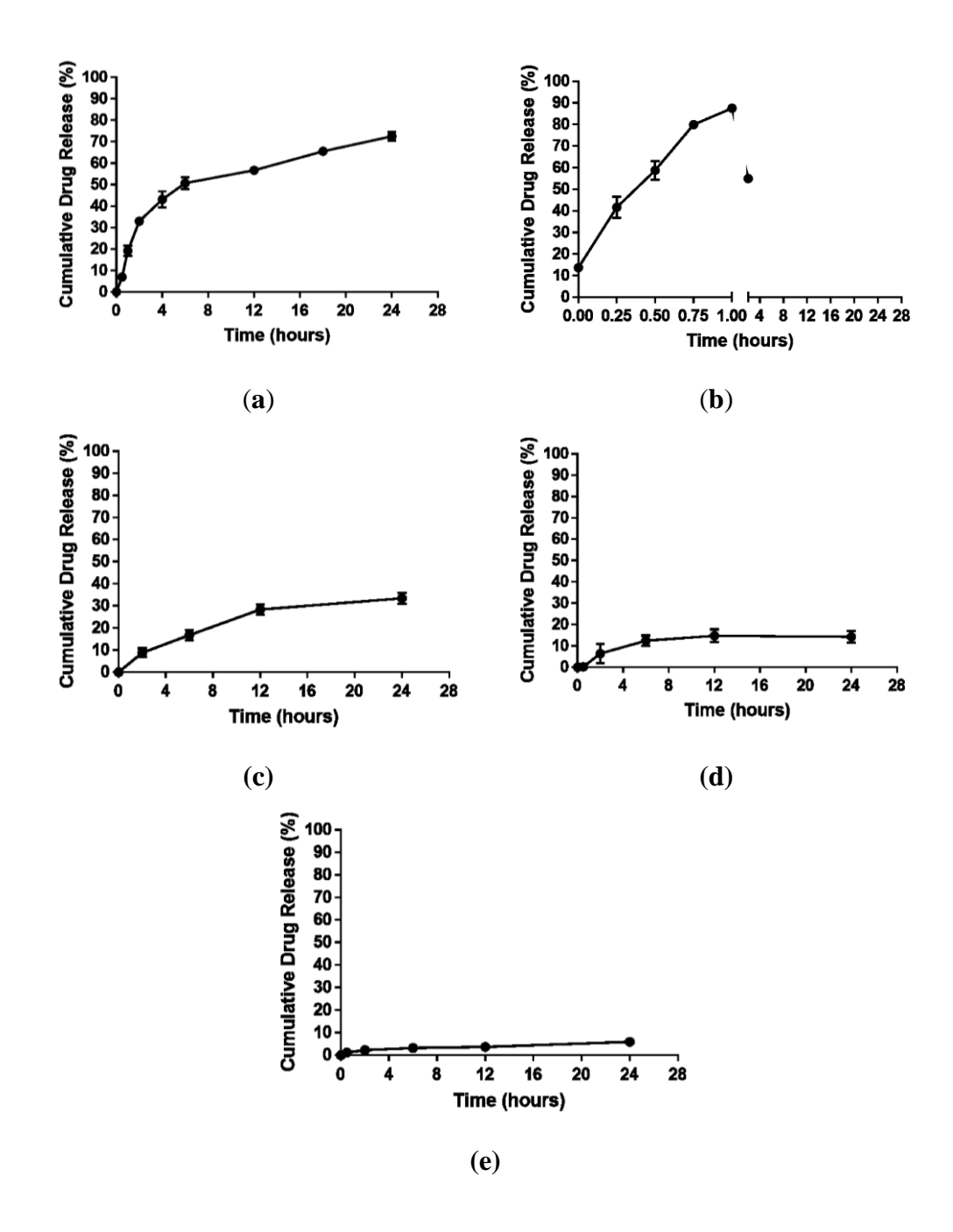


Figure 3.5. Cumulative release of MRN from 1 mg/mL MRN-HSA-NPs in the presence of various enzymes: (a) trypsin, (b) pepsin, (c) proteinase K, (d) protease and (e) cathepsin D. The graphs show a representative result of mean \pm SD (n=3).

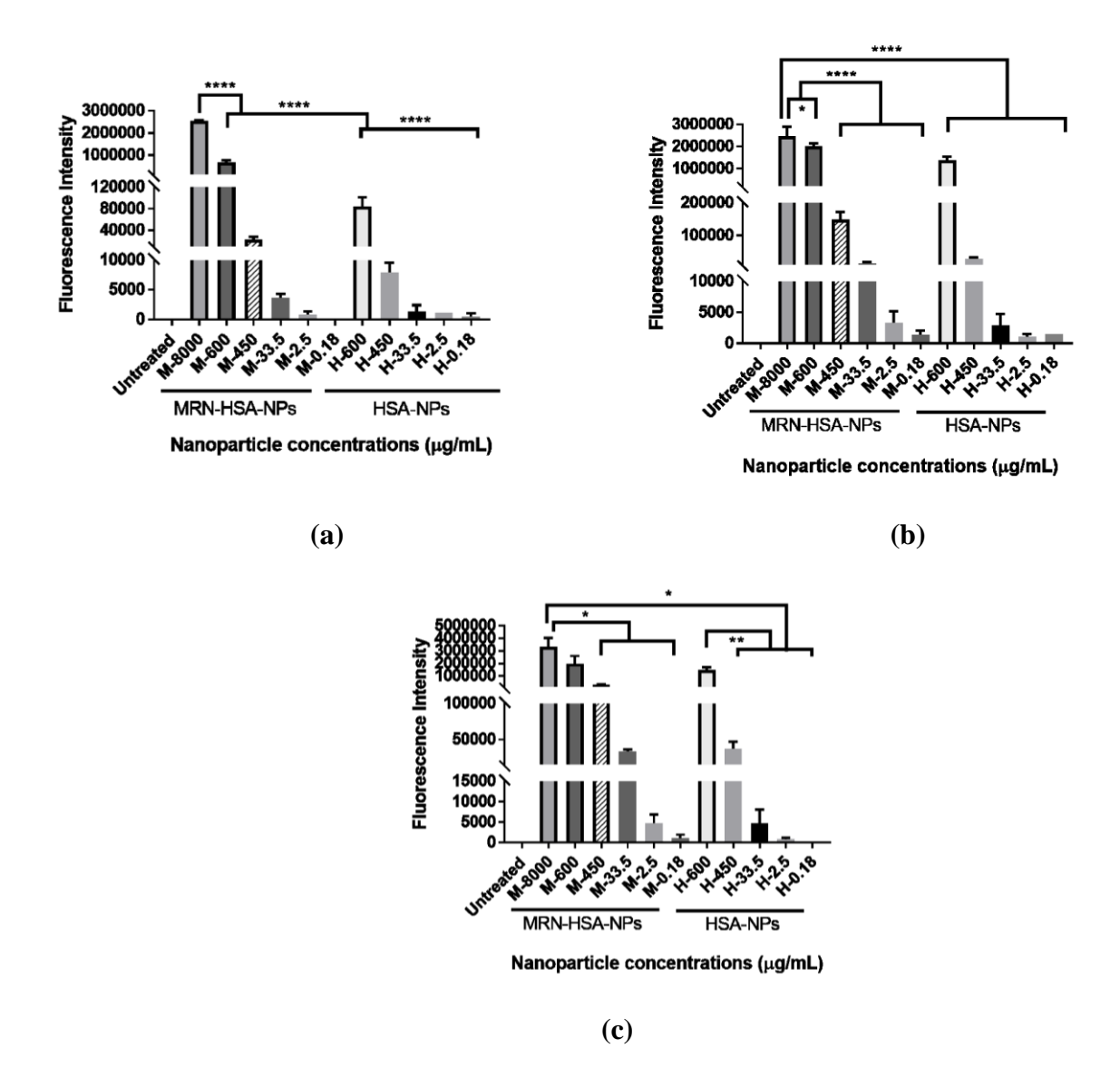


Figure 3.6. Intracellular uptake of MRN-HSA-NPs and HSA-NPs in HUVEC cells at (a) 4 hours, (b) 24 hours and (c) 48 hours. HUVEC cells were treated with different nanoparticle concentrations: 8000, 600, 450, 33.5, 2.5 and 0.18 μ g/mL, represented as M-8000, M-600, M-450, M-33.5, M-2.5 and M-0.18 in case of MRN-HSA-NPs; and H-8000, H-600, H-450, H-33.5, H-2.5 and H-0.18 in case of HSA-NPs alone. The graph shows a representative result of mean \pm SD (n=3). ****P<0.0001 was considered highly significant and ***P<0.001, **P<0.005 were considered significant based on Tukey's posthoc analysis, when compared with other groups.

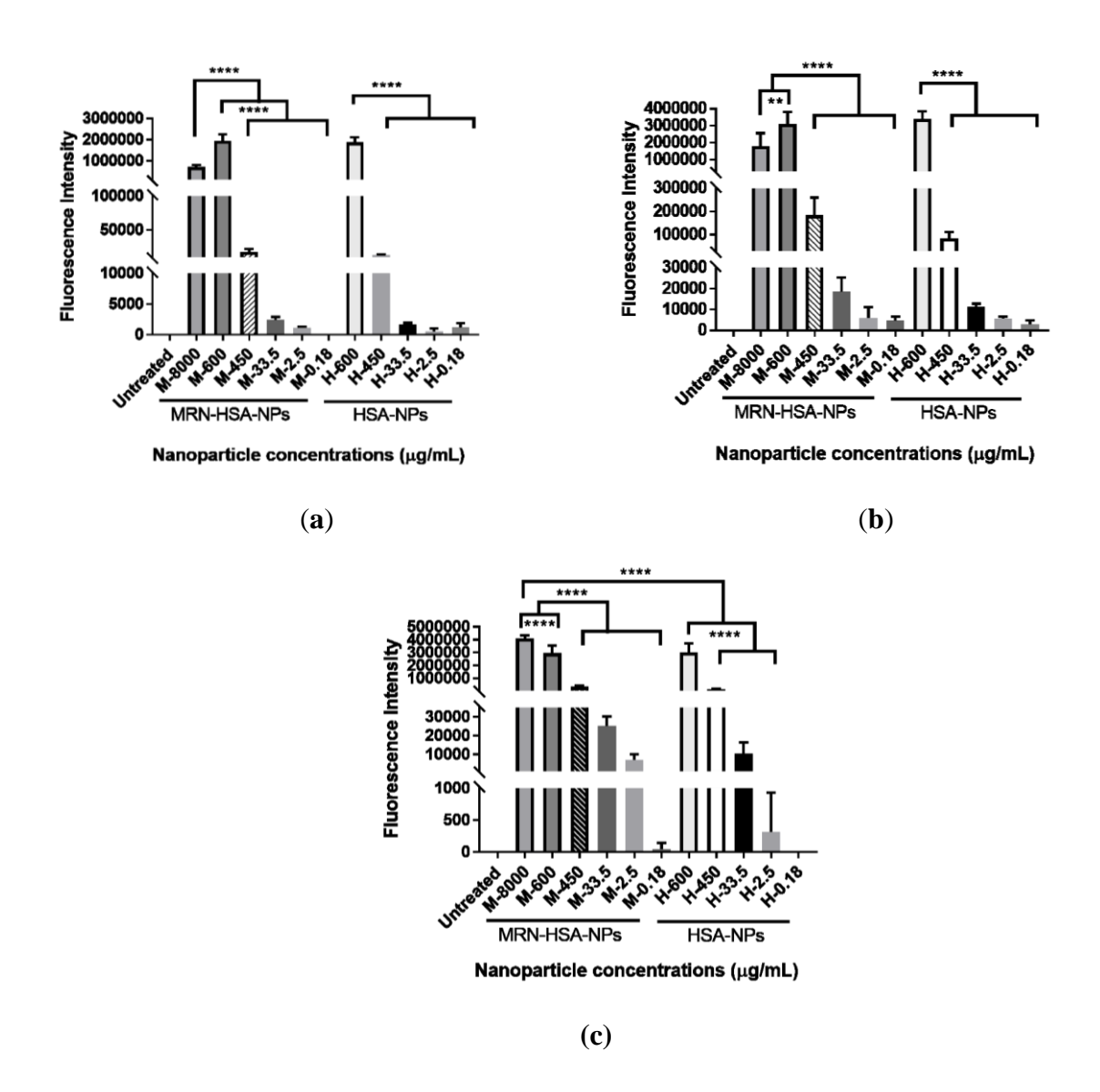


Figure 3.7. Intracellular uptake of MRN-HSA-NPs and HSA-NPs in H9c2 cells at (a) 4 hours, (b) 24 hours and (c) 48 hours. H9c2 cells were treated with different nanoparticle concentrations: 8000, 600, 450, 33.5, 2.5 and 0.18 μ g/mL, represented as M-8000, M-600, M-450, M-33.5, M-2.5 and M-0.18 in case of MRN-HSA-NPs; and H-8000, H-600, H-450, H-33.5, H-2.5 and H-0.18 in case of HSA-NPs alone. The graph shows a representative result of mean \pm SD (n=3). ****P<0.0001 was considered highly significant and ***P<0.001, **P<0.05 were considered significant based on Tukey's posthoc analysis, when compared with other groups.

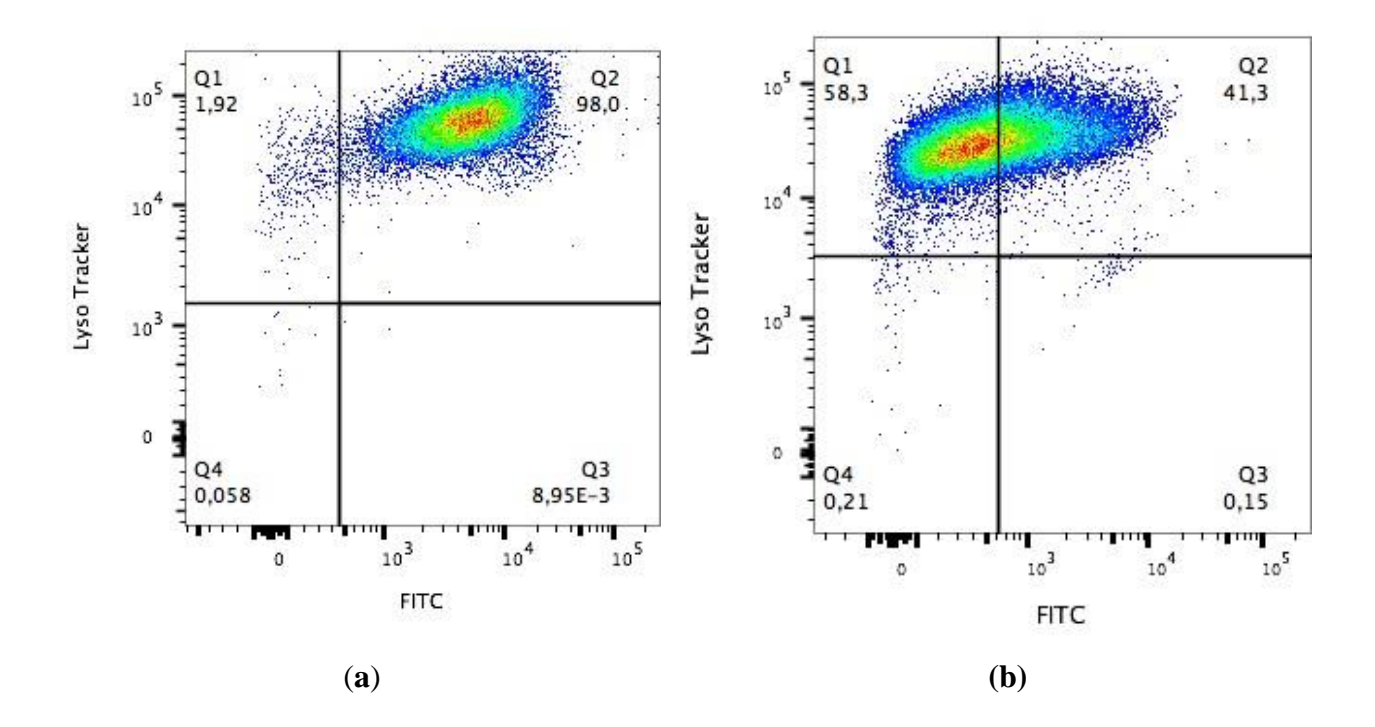


Figure 3.8. Flow cytometry analysis of intracellular uptake of FITC-HSA-NPs. Gated on single cells and quadrants were set as per FMO controls. (a) HUVEC cells treated with both FITC-HSA-NPs and LysoTracker Deep Red exhibiting double staining in approximately 98% cell population (Q2 quadrant); (b) H9c2 cells treated with both FITC-HSA-NPs and LysoTracker Deep Red exhibiting double staining in approximately 41.3% cell population (Q2 quadrant) with approximately 58.3% cells displaying Lysotracker Deep Red staining (Q1 quadrant). Data is represented for n=3 experiments.

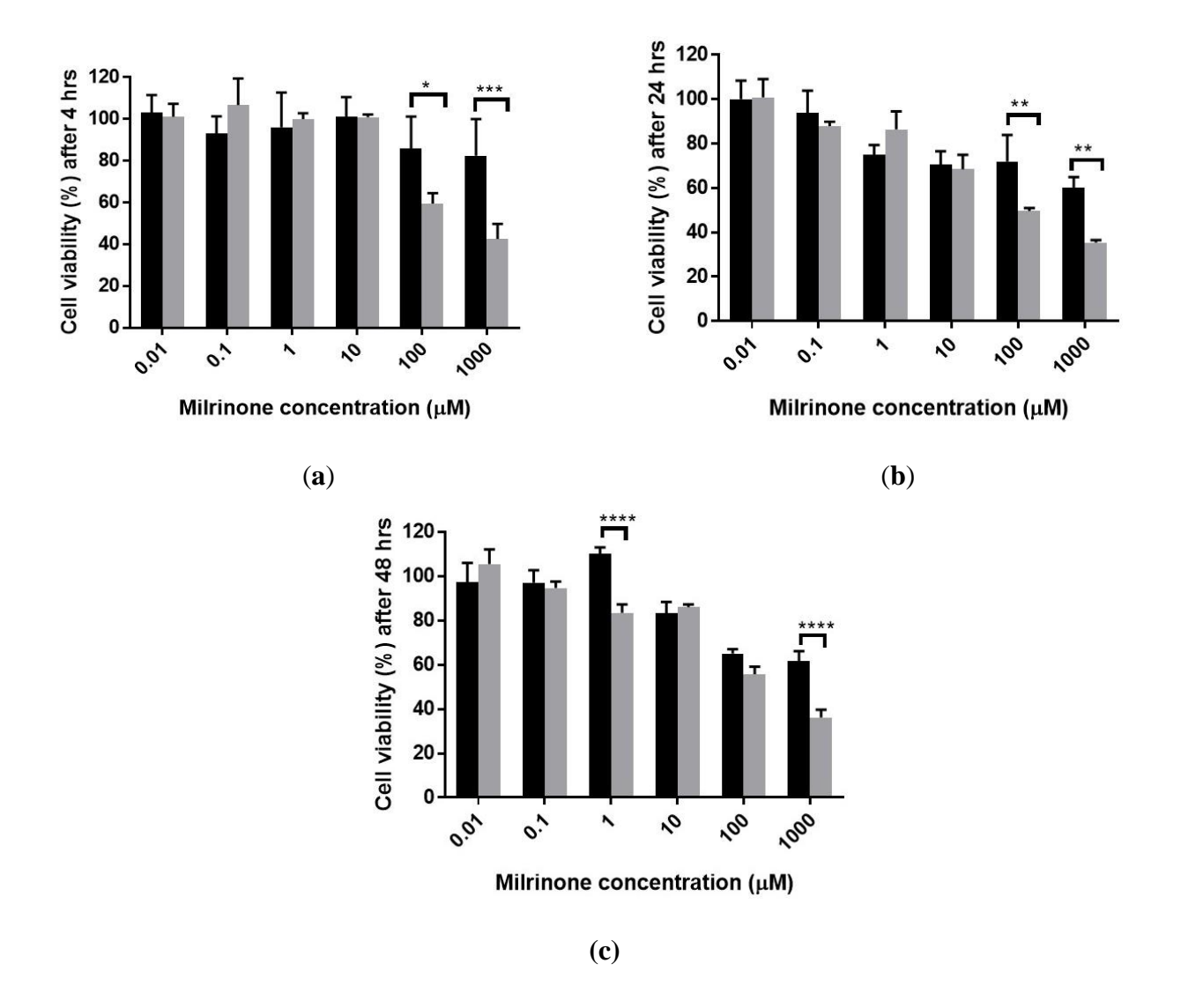


Figure 3.9. Viability of HUVECs incubated with MRN-HSA-NPs (black bars) compared with MRN-Lactate (grey bars) at different MRN concentrations, at (a) 4 hours, (b) 24 hours and (c) 48 hours. The graph shows a representative result of mean \pm SD (n=3). ****P<0.001 was considered highly significant and ***P<0.001, **P<0.01 and *P<0.05 were considered significant based on Sidak's posthoc analysis.

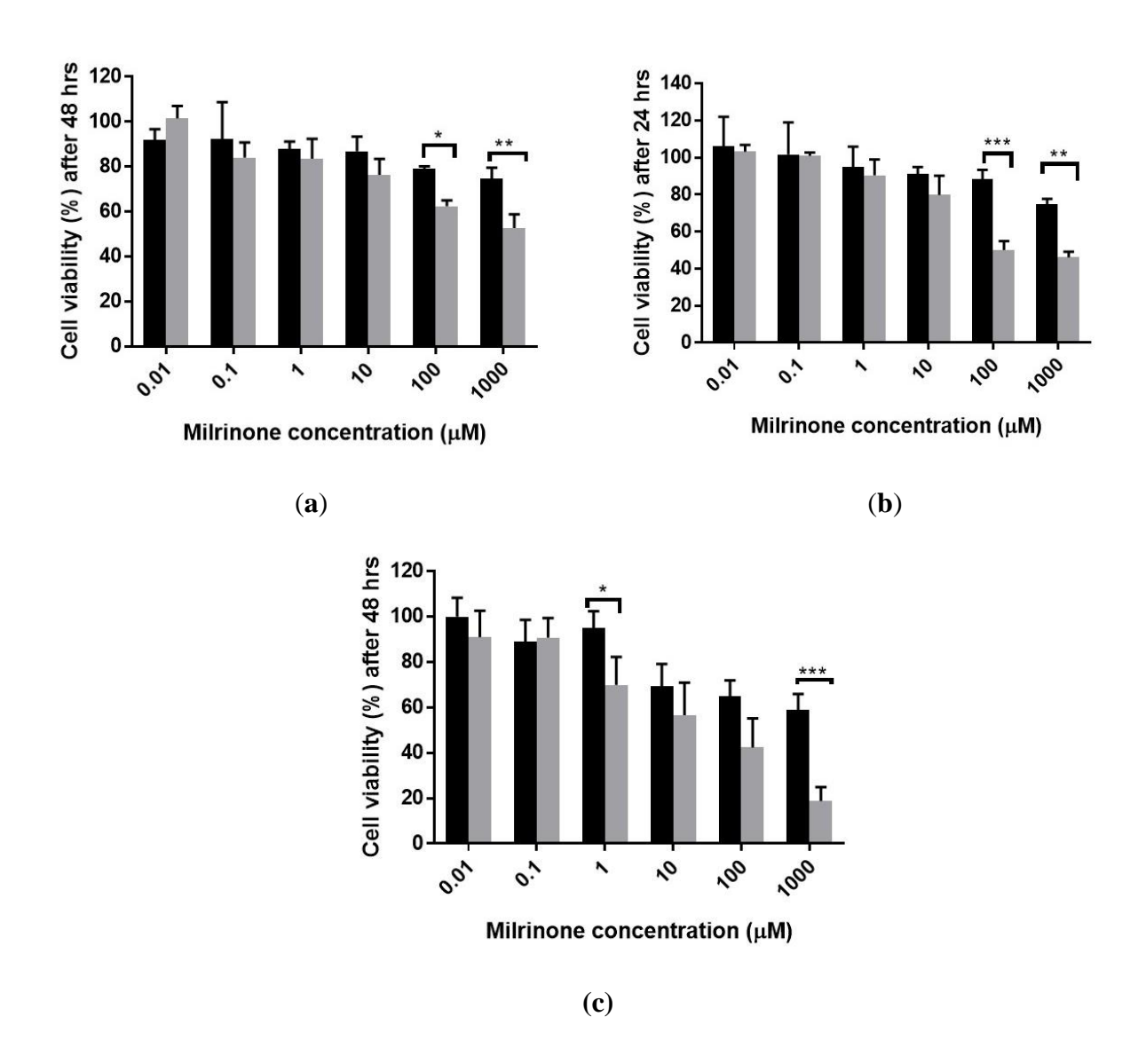


Figure 3.10. Viability of H9c2 cells incubated with MRN-HSA-NPs (black bars) compared with MRN-Lactate (grey bars) at different MRN concentrations, at (a) 4 hours, (b) 24 hours and (c) 48 hours. The graph shows a representative result of mean \pm SD (n=3). ****P<0.0001 was considered highly significant and ***P<0.001, **P<0.01 and *P<0.05 were considered significant based on Sidak's posthoc analysis.

Table 3.1. Encapsulation efficiency of MRN-HSA-NPs at various MRN concentrations, represented as HSA/MRN molar ratio.

HSA/MRN	Encapsulation				
molar ratio	efficiency (%)				
1:1	86.9±13.8				
1:5	23.4±4.9				
1:10	30.2±5.9				
1:15	41.8±1.7				

Table 3.2. Predicted binding affinities between HSA and MRN using the Wilma and SIE scoring.

Ligand hound to	SIE	Wilma		
Ligand bound to	Predicted	Predicted		
HSA	(kcal/mol)	(kcal/mol)		
MRN (best	-5.7	-27.6		
Wilma)	-3.1			
MRN (best SIE)	-8.6	-26.5		
THY (control)	-6.7	-26.2		
RWF (control)	-8.3	-26.6		
IBP (control)	-7.6	-23.6		

Table 3.3. HSA secondary structural content on interaction with MRN in different molar ratios.

200 - 260 nm									
Molar ratio	HSA (at pH 7.0)		HSA (at pH 8.0)			HSA (at pH 9.0)			
(HSA/MRN)									
	α-	β-	Random	α-	β-	Random	α-	β-	Random
	helix	sheet	coil (%)	helix	sheet	coil (%)	helix	sheet	coil (%)
	(%)	(%)		(%)	(%)		(%)	(%)	
0	58.7	13.1	17.8	62.2	12.6	16.4	59.8	13.0	17.3
1:1	54.0	13.8	19.9	56.3	13.4	19.1	62.4	12.6	16.1
1:5	59.9	12.9	17.3	36.0	16.3	30.7	61.2	12.8	16.7
1:10	72.8	11.2	11.9	60.9	12.8	17.0	59.7	13.0	17.3
1:15	58.80	13.1	17.7	60.1	12.9	17.1	65.5	12.2	14.8
1:20	59.10	13.1	17.6	57.8	13.2	18.3	59.1	13.1	17.6

Table 3.4. Cumulative release of MRN from MRN-HSA-NPs in the presence of different enzymes.

Enzyme present with	Cumulative			
MRN-HSA-NPs	MRN release			
WIKIN-MSA-INPS	(%)			
Trypsin	72.5±1.9			
Pepsin	87.5±0.9			
Proteinase K	33.4±2.5			
Protease	14.2±2.7			
Cathepsin D	5.9±1.3			

CHAPTER 4: SYNTHESIS OF PEPTIDE CONJUGATED HUMAN SERUM ALBUMIN NANOPARTICLES FOR TARGETED MILRINONE DELIVERY

Nikita Lomis^{1,2}, Susan Westfall³, Dominique Shum-Tim⁴, Satya Prakash^{1,2,*}

¹Biomedical Technology and Cell Therapy Research Laboratory, Department of Biomedical

Engineering, 3775 University Street, Montreal, QC, H3A 2B4, Canada

²Division of Experimental Medicine, 1001 Boulevard Décarie, Montréal, QC, H4A 3J1, Canada

³Department of Neurology, Icahn School of Medicine Mount Sinai, New York, NY, 10029, USA

⁴Division of Cardiac Surgery and Surgical Research, Royal Victoria Hospital, 1001 Boulevard

Décarie, Montréal, QC, H4A 3J1, Canada

*Corresponding author: Satya Prakash

Tel: 514-398-2736; Fax: 514-398-7461

Email: satya.prakash@mcgill.ca

Preface: This chapter describes a novel synthesis scheme for surface functionalization of HSA

with the AT1 peptide to develop AT1 peptide-tagged nanoparticles. The main aim of this study

was to synthesize an AT1 receptor-targeted nanoparticle formulation for specific delivery of MRN.

Attaching the AT1 peptide on the HSA surface was achieved by following a two-step covalent

chemical conjugation reaction with heterobifunctional cross-linkers 5(6)-Carboxyfluorescein-

NHS and EDC/Sulfo-NHS. The AT1-HSA binding was confirmed using mass spectrometry. The

AT1-HSA-MRN-NPs were formed following the ethanol desolvation methodology mentioned in

Chapter 3. The safety and uptake of the AT1-nanoparticle formulation was evaluated in

cardiomyoblasts by fluorescence studies and confocal microscopy and compared with the non-

targeted MRN-nanoformulation prepared in Chapter 3.

(Article to be submitted)

92

4.1 Abstract

Congestive heart failure is a significant health problem across the globe. It occurs when a reduced cardiac output is unable to meet the demands of the body. It may result due to numerous reasons however the most common cause is myocardial infarction or ischemia. Though, there are various medical therapies for heart failure involving drug delivery, one of the most widely used treatments is milrinone (MRN) drug delivery. Milrinone helps in improving the heart's contractile ability, cardiac function and vasodilation. The efficiency of MRN is challenged due to its non-targeted delivery, low bioavailability and low body retention time necessitating its use as a continuous infusion. Previously, the delivery of MRN using human serum albumin nanoparticles (HSA-NPs) has shown to improve its delivery, uptake and biocompatibility. The delivery and release of MRN could be further enhanced by targeted delivery of the MRN-HSA-NPs. This study is the first to report the synthesis of surface functionalized HSA-NPs carrying MRN, covalently conjugated to the AT1 peptide (Asp-Arg-Val-Tyr-Ile-His-Pro-Phe). The AT1 peptide-tagged MRN-HSA-NPs will bind specifically to the AT1 receptors present on the myocardium and found to be overexpressed under CHF conditions, facilitating higher nanoparticle uptake and drug delivery. The AT1 peptide was first attached to the HSA surface through a two-step reaction scheme involving crosslinking with heterobifunctional crosslinkers. The targeted AT1-HSA-MRN-NPs formulation was developed with particle size of 215.2±4.7 nm and zeta potential -28.8±2.7 mV. The cellular uptake of the nanoparticles was determined by fluorescence and confocal microscopy which showed that the uptake of AT1-HSA-MRN-NPs was significantly higher as compared with non-targeted nanoparticles (P<0.0001), tested in H9c2 cells under hypoxia, hypertrophy and normal conditions. Also, a higher cell viability and lower cytotoxicity was observed when H9c2 cells were treated with AT1-MRN-HSA-NPs vs the control non-targeted drug, MRN-Lactate (73.4±1.4% vs 44.9±1.4%). Therefore, it may be concluded that AT1-HSA-MRN-NPs will be safe for *in vivo* use and will potentially exhibit superior targeting and drug delivery characteristics when used in CHF and other CVDs.

Keywords: Heart failure, drug delivery, nanoparticles, peptide, angiotensin, receptor

4.2 Introduction

The incidences of CVDs are constantly on the rise across the developed and developing world. The total projected cost associated with cardiovascular healthcare is greater than 1 trillion USD, which causes a huge economic burden. The occurrences of myocardial infarction (MI) and congestive heart failure (CHF) are responsible for more than 50% of the global cases of CVDs with high rates of readmission and re-hospitalization ¹. Currently, the most common treatments for CHF include surgical interventions such as transplantation, stenting, bypass surgeries, ventricular assist devices and medical treatments which include clinical administration of drugs such as ACE inhibitors, beta blockers, vasodilators etc. ²⁻³. However, despite these common treatment modalities, average survival rate for more than 50% of patients who have suffered a first heart failure is less than 5 years ⁴. Therefore, there is an urgent need for development of effective therapies to target these diseases.

CHF is typically caused by blockage of the coronary artery, which results in ischemia and leads to an irreversible necrosis of the cardiomyocytes. It is widely suggested that under MI and CHF, an overexpression of the angiotensin II type 1 receptors (AT1Rs) on the myocardium may be an underlying cause for cardiac remodeling ⁵⁻⁸. This property facilitates the underlying mechanism of ACE inhibitor drugs, which block the overexpressed AT1 receptors to prevent cardiac hypertrophy ⁹⁻¹⁰. The condition of overexpression of AT1Rs has been explored by a study in which superior AT1R targeting was reportedly achieved for delivery of AT1 bound quantum dot nanoparticles ¹¹. Another study investigated the use of AT1-conjugated liposomes in a mouse model of MI, demonstrating their specific internalization ⁵. This will be the first study demonstrating a new synthesis scheme for development of a novel nanoparticle formulation, AT1-HSA-MRN-NPs, for targeted drug delivery to the heart.

In a previous study, we demonstrated the preparation and binding of HSA-NPs with MRN, a cardiac inotrope and vasodilator drug, widely used for the treatment of CHF ¹². Milrinone is a phosphodiesterase III enzyme inhibitor which increases the intracellular cAMP concentration, providing higher calcium influx to create a positive inotropic effect ¹³⁻¹⁵. Clinically administered as a lactate formulation (MRN-Lactate), MRN is known to improve the overall cardiac function by increasing myocardial contractility and decreases systemic vascular resistance ¹⁶⁻¹⁷. However,

the lack of target specificity, lower bioavailability and a half-life of approximately 1-2 hours in humans, necessitates its use as a continuous infusion, also causing other side effects such as renal dysfunction, palpitations and arrhythmias ¹⁸⁻¹⁹.

The enhanced targeting and delivery of MRN could be achieved by loading it on nanoparticles targeted to the intended site of action. One of the most widely used nanoparticles are HSA-NPs owing to unique features like biocompatibility, biodegradability and non-immunogenicity. The HSA molecule possesses multiple pockets to promotes binding of various hydrophilic and hydrophobic drugs such as paclitaxel, doxorubicin etc. ²⁰⁻²². Computational modeling and enzyme release studies have shown that MRN binds hydrophobically to the HSA molecule ²³. HSA-NPs are known to improve the blood circulation time of otherwise insoluble or free drugs and are anticipated to improve the bioavailability of MRN as well ²⁴⁻²⁵.

The presence of active functional groups on the HSA allows opportunities for surface-modification to bind additional ligands such as peptides, antibodies, genes and other molecules ²⁶⁻²⁹. This would be useful in enhancing receptor mediated nanoparticle internalization and drug delivery characteristics of HSA-NPs. In this study, for the first time, HSA was surface modified through a novel two-step reaction scheme to bind the AT1 peptide to form AT1-HSA. The AT1-HSA was further bound to the cardiac inotrope and vasodilator, MRN, to form AT1-HSA-MRN-NPs. A cell viability analysis was performed to compare the safety of AT1-HSA-MRN-NPs with MRN-Lactate, the clinically used drug for CHF treatment. The cellular uptake of AT1-HSA-MRN-NPs was confirmed with fluorescence and confocal microscopy studies in hypoxic and hypertrophic H9c2 cells, mimicking conditions of MI and CHF. These studies indicate that the novel AT1-HSA-MRN-NPs can deliver MRN in a targeted manner to treat heart failure and related cardiovascular diseases.

4.3 Materials and Methods

4.3.1 Materials

Human serum albumin (> 97% lyophilized) was purchased from Sigma Aldrich (Oakville, ON, Canada). Glutaraldehyde (25% aq. solution) was purchased from Alfa Aesar (Cedarlane,

Burlington, ON, Canada). Fluorescein isothiocynate human serum albumin (FITC-HSA) was purchased from Sigma Aldrich (Oakville, ON, Canada). Milrinone was purchased from Selleck Chemicals (Burlington, ON, Canada). Bradford reagent was purchased from Bio-Rad (St. Laurent, QC, Canada). The 5(6)-Carboxyfluorescein *N*-hydroxysuccinimide was purchased from Thermo Fisher Scientific (ON, Canada) Other chemicals were purchased from Fisher Scientific (Nepean, ON, Canada). All antibodies were purchased from Abcam (Toronto, ON, Canada)

4.3.2 Synthesis of the AT1-peptide

The Angiotensin II Type 1 (AT1) receptor targeting peptide is a chain of 8 amino acids Asp-Arg-Val-Tyr-Ile-His-Pro-Phe, and was synthesized by CanPeptide (Pointe-Claire, QC, Canada) as NH₂-Gly-Gly-Gly-Asp-Arg-Val-Tyr-Ile-His-Pro-Phe-NH₂ along with a Scrambled Peptide NH₂- Gly-Gly-Gly-Gly-Phe-His-Tyr-Arg-Asp-Val-Ile-Pro-NH₂ as mentioned by Dvir et al.⁵.

4.3.3 Surface Modification of HSA with AT1 peptide

The surface of HSA was modified for attachment of the AT1 peptide in a two-step reaction. An aqueous solution of 20 mg/mL of HSA dissolved in deionized water (0.3 mM) was prepared and reacted with a 10-fold molar excess of 5(6)-Carboxyfluorescein-NHS ester, for 1 hour. This was further reacted with EDC/Sufo-NHS for 30 minutes followed by reaction with either the AT1 or scrambled peptide (Scr) for 4 hours (**Figure 4.1**). The AT1 and Scr peptide was added in a 10-fold molar excess than HSA. The AT1-HSA and Scr-HSA were purified by dialysis using the Slide-a-Lyze dialysis cassette (10,000 Da MWCO). The purified sample was then lyophilized and stored at 4°C.

4.3.4 Mass Spectrometry

The AT1-HSA, HSA and AT1 peptide samples were analyzed by the Matrix-Assisted Laser Desorption/Ionization Time of Flight Mass Spectrometry (MALDI-TOF-MS) MALDI Autoflex III- TOF-(BRUKER) SMARTBEAM) (Dept. of Chemistry, McGill University, Montreal, QC, Canada) in linear positive mode. Dihydroxybenzoic Acid was used as the Matrix and the AT1-HSA, HSA and AT1 peptide samples were dissolved in water at concentrations of approximately 7 mg/mL.

4.3.5 Nanoparticle Preparation

The AT1-HSA-MRN-NPs were prepared by the ethanol desolvation technique ³⁰⁻³¹. Briefly, an aqueous solution of 20 mg/mL of AT1-HSA was prepared in deionized water. The pH of the solution was adjusted to pH 8.0 using 0.1 M NaOH. MRN was dissolved in DMSO and added to the AT1-HSA solution with a final MRN/HSA ratio of 1:20 by weight. Ethanol was added in a dropwise manner resulting in solution turbidity. Glutaraldehyde (8% v/v aq. solution) was added to the reaction mixture at a concentration of 0.588 µl/mg HSA and polymerized for 24 hours. AT1-HSA was substituted with Scr-HSA for preparation of Scr-HSA-NPs and HSA was replaced with FITC-HSA for preparation of fluorescently tagged MRN-HSA-NPs. The nanoparticles were washed by three rounds of ultracentrifugation at 16500 rpm for 15 minutes each at 25°C. After each round, the supernatant was collected for detection of unbound MRN. The pellet was washed with deionized water and finally re-dispersed in phosphate buffer saline (PBS). The nanoparticles were tip-sonicated for 10 minutes and stored at 4°C.

4.3.6 Nanoparticle characterization, yield and encapsulation efficiency

The average particle size of the nanoparticles was measured by Dynamic Light Scattering (DLS) using a Particle Size Analyzer (Brookhavens Instruments Corporation, NY, USA). The samples were diluted 1:20 with deionized water and measured at a scattering angle of 90° and temperature of 25 °C. The Polydispersity Index (PDI) estimated the size distribution of the nanoparticles. The zeta potential was measured by a Zeta Potential Analyzer (Brookhavens Instruments Corporation, NY, USA) using electrophoretic laser Doppler anemometry. The size and shape of the nanoparticles were examined by Transmission Electron Microscopy (TEM) (FEI Tecnai G² Spirit Twin 120 kV Cryo-TEM, Gatan Ultrascan 4000 4k x 4k CCD Camera System Model 895).

The yield of the nanoparticles was measured by the UV-spectrophotometric method. A standard curve of HSA solution dissolved in Bradford reagent was used as a reference and absorbance was measured at 595 nm. For calculation of yield, the following equation was used:

Yield
$$\% = (\frac{\text{weight of HSA in solution}}{\text{initial weight of HSA}}) * 100.$$

For measuring encapsulation efficiency, nanoparticles were spin concentrated using centrifugal filters with molecular weight cut off (MWCO) of 10,000 Da for eluting the non-encapsulated MRN into the collection tube. The concentration of non-encapsulated MRN was determined by UV-spectrophotometry. A standard curve of MRN in a mixture containing DDQ/Ethanol was used as a reference ³². The absorbance was measured at 356 nm. The MRN bound to the AT1-HSA-MRN-NPs was calculated using the following equation:

Encapsulation Efficiency
$$\% = (\frac{\text{concentration of MRN encapsulated}}{\text{starting concentration of MRN used}}) * 100.$$

4.3.7 Cell culture and viability

Rat cardiomyoblasts (H9c2) cells were received as a kind gift from Dr. Renzo Cecere, M.D. (Montreal General Hospital, QC, Canada). The H9c2 cells were grown in Dulbecco's Modified Eagle Medium (DMEM) supplemented with 10% fetal bovine serum (FBS). The cytotoxic effect due to nanoparticle treatment was determined by seeding H9c2 cells at an initial density of 5000 cells/well in clear bottom 96-well black plates. Post incubation for 24 hours in a humidified incubator at 37°C and 5% CO₂, the cell media was replaced with AT1- HSA-MRN-NPs, AT1- HSA-NPs, MRN-HSA-NPs and MRN-Lactate treatments, diluted in serum-free cell culture medium. The MRN concentration in the nanoparticles and MRN-Lactate were 1 mM, as optimized from previous studies 33 . After 4, 24 and 48 hours of incubation, the cells were washed thrice with PBS. Cells were treated with 100 μ L of fresh cell culture medium and 20 μ L of MTT reagent and incubated at 37°C and 5% CO₂ for 4 hours. The media was removed, and cells were lysed by addition of 100 μ L of DMSO for 15 minutes at room temperature. The absorbance was measured at 570 nm using the Victor3V 1420 Multilabel Counter spectrophotometer.

4.3.8 Overexpression of the AT1 Receptor

The H9c2 cells were seeded at an initial density of 5,000 cell/well in 96-well plates, separated into three groups: Normal, Hypoxic and Hypertrophic. Hypoxia was induced by treatment with 100 μ M of CoCl₂.6H₂O for 24 hours, which simulated the conditions of MI, through induction of hypoxic markers such as hypoxia inducible factor (HIF)-1 α ³⁴. Hypertrophy was induced by treatment with 20 μ M H₂O₂ for 48 hours to simulate conditions of heart failure ³⁵. The cells in each group were treated with the anti-AT1 antibody (Abcam, Canada) for 1 hour followed by a goat

polyclonal secondary antibody conjugated to Alexa 488 for an additional 1 hour. The cells were fixed with 4% paraformaldehyde in PBS for 10 mins and thrice washed with PBS and stored at 4°C. The fluorescence was measured at 495 nm excitation/519 nm emission wavelengths.

4.3.9 Intracellular Nanoparticle Uptake

The H9c2 cells were seeded at an initial density of 5,000 cell/well in 96-well plates, separated into three groups: Normal, Hypoxic and Hypertrophic. Cells were subjected to hypoxia by treatment with 100 μM of CoCl₂.6H₂O for 24 hours, to simulate MI ³⁴. Cells were subjected to hypertrophy by treatment with 20 μM H₂O₂ for 48 hours to simulate HF ³⁵. The H9c2 cells in each group were treated with 0.5 mg/mL of fluorescently tagged AT1-HSA-MRN-NPs, Scr-HSA-MRN-NPs and MRN-HSA-NPs for 4 hours. The Scr peptide was the same amino acid chain as AT1 peptide but in a scrambled order ²⁰. The Scr peptide-tagged NPs were used to confirm the targeting efficiency of the AT1 peptide-tagged NPs. The cells were washed thrice with PBS and fresh media was added. The fluorescence intensity was measured at 489nm/535nm using a Victor3V 1420 Multilabel Counter spectrophotometer (Perkin Elmer, Woodbridge, ON, Canada).

4.3.10 Confocal Microscopy

The H9c2 cells were seeded into 35 mm μ-dishes for cell imaging (ibidi, USA) at an initial density of 4x10⁴ cells/mL and incubated for 24 hours at 37°C and 5% CO₂. The cells were separated into Normal, Hypoxic and Hypertrophic cells. Hypoxia was induced by treatment with 100 μM of CoCl₂.6H₂O for 24 hours ³⁴. Hypertrophy was induced by treatment with 20 μM H₂O₂ for 48 hours ³⁵. Further, the cells were treated with AT1-HSA-MRN-NPs and MRN-HSA-NPs for 4 hours and with the FM 4-64 dye (5 μg/mL working solution) for 1 minute and washed with HBSS solution (as per manufacturer's instructions). The cells were washed thrice with PBS and fixed using 4% paraformaldehyde for 15 minutes and washed again with PBS. The cells were imaged by confocal microscopy (LSM 710 Confocal Microscope). Image processing and analysis was performed in the McGill University Life Sciences Complex Advanced BioImaging Facility (ABIF, McGill University, Montreal, QC, Canada).

4.4 Results

4.4.1 Mass Spectrometry

To validate the AT1-conjugation with HSA, MALDI-TOF-MS was used to compare the average molecular weight change between HSA and AT1-HSA. The mass-to-charge ratio (m/z) of the green peak (AT1-HSA) was approximately 7000 higher than the red peak (HSA). The molecular weights of the AT1 peptide, 5(6)-Carboxyfluorescein-NHS, EDC and Sulfo-NHS is 1274, 376.32, 190 and 217 g/mol, respectively. Results suggest that at least 3 AT1 molecules are successfully conjugated to the surface of each HSA molecule (**Figure 4.2**).

4.4.2 Characterization of the AT1-nanoparticle formulation

The nanoparticles were characterized by DLS for size determination and laser Doppler anemometry for zeta potential analysis, respectively. The particle size of AT1-HSA-MRN-NPs was 215.2±4.7 nm with a zeta potential of -28.8±2.7 mV, and size of MRN-HSA-NPs was 189.6±3.8 nm with zeta potential of -27.5±4.6 mV. The morphology of the nanoparticles as observed by TEM techniques under 13500X (**Figure 4.3(a)**) and 55,000X magnification exhibited a near spherical shape with moderately uniform particle size and even distribution (**Figure 4.3(b)**). Under 250,000X magnification, the AT1-HSA-MRN-NPs had a dark core surrounded by a bright membrane, which confirmed the distinct layer (**Figure 4.3(c)**). The yield of the MRN-HSA-NPs was 86.2±2.6% and for AT1-MRN-HSA-NPs was 75.6±2.5%, The drug encapsulation efficiency of the AT1-HSA-MRN-NPs was 40.5±1.5% (**Table 4.1**).

4.4.3 Cell Viability Analysis

For evaluating the safety and efficacy of AT1-HSA-MRN-NPs on H9c2 cells, the MTT assay was performed. The cells were treated with AT1-HSA-MRN-NPs, AT1-HSA-NPs, MRN-HSA-NPs and MRN-Lactate containing 1mM MRN concentrations (optimized previously) for 4, 24 and 48 hours ³³. Results showed that the H9c2 cells treated with AT1-HSA-MRN-NPs, AT1-HSA-NPs and MRN-Lactate for 4 hours showed cell viability of 73.4±1.4%, 101.7±2.9% and 44.9±1.4%, respectively (**Figure 4.4(a**)). At 24 hours, the cell viability was 55.5±3.7%, 70.8±11.2% and 41.2±3.8%, respectively (**Figure 4.4(b**)), and at 48 hours, 52.4±2.1%, 65.9±11.2% and 35.3±7.7%, respectively (**Figure 4.4(c**)). Thus, the AT1-HSA-MRN-NPs exhibit higher cell compatibility and

lesser cytotoxicity as compared to MRN-Lactate at 4 hrs (p=0.0016), 24 hrs (p=0.0474) and 48 hrs (p=0.0385).

The *in vitro* cytotoxicity was also investigated for the hypoxia and hypertrophy inducing treatments. The H9c2 cells were treated with 100 µM of CoCl₂.6H₂O for 24 hours to induce hypoxia, whereas to induce hypertrophy, the cells were treated with 20 µM H₂O₂ for 48 hours. These were compared to normal H9c2 cells, which were non-hypoxic and non-hypertrophic. It was observed that there was no significant difference in the cell viabilities of normal, hypoxic or hypertrophic cells especially due to the treatments (**Figure 4.5**). Thus, the methods of inducing hypoxia and hypertrophy were safe.

4.4.4 Angiotensin II Type 1 Receptor Overexpression

The AT1R receptor overexpression was studied in hypoxic, hypertrophic and normal H9c2 cells. Results showed that hypoxic and hypertrophic cells exhibited a significantly higher expression of the AT1 receptors as compared to normal cells (P<0.0001). The fluorescence intensity displayed by the hypoxic and hypertrophy was almost twice higher than that observed in the normal cells (**Figure 4.6**).

4.4.5 Intracellular Nanoparticle Uptake Analysis

Since AT1 receptors are overexpressed on cardiomyocytes during HF, conjugating the nanoparticles with the AT1 peptide was anticipated to demonstrate higher uptake of the AT1-HSA-MRN-NPs through receptor-mediated endocytosis. Results suggested that in normal (non-hypoxic, non-hypertrophic) cells, the AT1-HSA-MRN-NPs exhibited significantly higher fluorescence intensity as compared to the non-targeted MRN-HSA-NPs (p=0.0001) and Scr-HSA-MRN-NPs (p=0.0079) (Figure 4.7(a)). Similarly, for hypoxic cells, the cellular uptake of the AT1-HSA-MRN-NPs was significantly higher (P<0.0001) than that of MRN-HSA-NPs and Scr-HSA-MRN-NPs was significantly greater (P<0.0001) than that of MRN-HSA-NPs and Scr-HSA-MRN-NPs was significantly greater (P<0.0001) than that of MRN-HSA-NPs and Scr-HSA-MRN-NPs (Figure 4.7(c)).

It was also observed that the H9c2 cells under hypoxia and hypertrophy demonstrated greater uptake of AT1-HSA-MRN-NPs as compared to normal conditions (Figure 4.8(a)). The MRN-

HSA-NPs (**Figure 4.8(b**)) and Scr-HSA-MRN-NPs (**Figure 4.8(c**)) also exhibited a similar trend, however, it was significantly less than that observed by AT1-HSA-MRN-NPs.

4.4.6 Confocal Microscopy Analysis

The uptake of AT1-HSA-MRN-NPs vs Scr-HSA-MRN-NPs by normal and hypertrophic H9c2 cells was analyzed by confocal microscopy. Results indicate that the uptake of AT1-HSA-MRN-NPs was approximately 45% in normal cells in comparison to approximately 30% uptake of MRN-HSA-NPs. However, the cellular uptake of the AT1-HSA-MRN-NPs increased to approximately 66% in hypoxic cells and to almost 78% in hypertrophic cells (**Figure 4.9**).

4.5 Discussion

The urgent need to effectively treat MI and HF has led to the research and innovation of various new strategies and treatment modalities. These include delivery of drugs, growth factors, cytokines and other molecules for myocardial regeneration or treatment ³⁶⁻³⁷. However, due to inherent limitations with most treatment strategies such as lack of target specificity, low bioavailability, cardiac rejection while heart pumping, or non-specific distribution, the therapeutic effect is lessened ³⁸. The emerging studies on nanoparticles and targeted drug delivery systems have displayed promising results, however, their efficacy remains dependent on the drug binding capacity, solubility, nanoparticle degradability and plasma retention time ³⁹. In this study, keeping in view the intended features of ideal drug delivery systems, a targeted nanoparticle formulation was synthesized. The HSA surface was modified to attach a targeting ligand, AT1 peptide, to achieve superior delivery characteristics. The AT1 peptide shows specificity for the AT1 receptor present on the myocardium, which is found to be overexpressed under CHF conditions ⁶⁻⁸. Using the AT1 peptide as the targeting moiety will facilitate receptor-mediated nanoparticle uptake.

The AT1 peptide was conjugated to the HSA surface through a two-step covalent chemical reaction. The 5(6)-Carboxyfluorescein-NHS targets primary amines such as in the side chain of lysine residues, to form stable amide bonds. This allows the carboxylic group to undergo a carbodiimide reaction with EDC, at pH 5.5, forming an unstable amine-reactive O-acylisourea intermediate. This unstable intermediate is further reacted with the Sulfo-NHS and the amine groups on AT1 peptide to release urea as a byproduct and form stable AT1-HSA. The premodification of the HSA by conjugation with the AT1 peptide was preferred over post-

modification of the HSA-NPs as the latter may cause drug loss and leakage during the synthesis and purification. MALDI-TOF confirmed the binding of AT1 peptide to the HSA surface. The spectrum on the x-axis represents the m/z (mass/charge) ratio which was 73869.546 for AT1-HSA and 67918.163 for HSA, which was 7000 higher. Considering the mass of the AT1 peptide, the HSA and the cross-linkers, at least 3 AT1 peptide molecules were bound to the HSA surface.

The AT1-HSA-MRN-NPs were formed by the ethanol desolvation process ^{12, 30}. The nanoparticles exhibited a spherical structure as observed under TEM. The AT1-HSA-MRN-NP size was 215.2±4.7 nm with a zeta potential of -28.8±2.7 mV, in comparison with AT1-HSA-NPs with a size of 189.6±3.8 nm and zeta potential of -27.5±4.6 mV. The nanoparticles were less than 250 nm with a negative zeta potential. Negative zeta potential is indicative of greater physical stability as nanoparticle aggregation is prevented due to presence of negative charges ⁴⁰. The particle size being less than 250 nm indicates a prolonged blood circulation time as the particles are not removed easily through opsonization ⁴¹⁻⁴².

Next, the *in vitro* cytotoxicity was evaluated on H9c2 cells treated with MRN-Lactate, AT1-HSA-MRN-NPs and AT1-HSA-NPs. MRN is clinically administered as a lactate formulation intravenously to adult as well as pediatric patients for HF and associated cardiac conditions ⁴³. However, the use of MRN-Lactate is linked with side effects such as palpitation, cardiac arrythmia and renal dysfunction ⁴⁴. This may be attributed to the non-targeted delivery of MRN-Lactate and hence the need for a continuous infusion to meet the dosage requirements. Using the targeted nanoparticle formulation, synthesized in this study, as drug carriers this limitation would be overcome, given their higher biocompatibility, higher retention time, drug binding capacity and characteristics of controlled drug release ⁴⁵. The cell viability of H9c2 cells was investigated at 4, 24 and 48 hours, with MRN-Lactate exhibiting higher cytotoxicity as compared to AT1-HSA-MRN-NPs and AT1-HSA-NPs. The safety of the nanocarriers is as essential a feature as their efficacy, which makes them suitable for use in future pre-clinical and clinical studies.

The intracellular uptake of the nanoparticles was investigated in normal (non-hypoxic, non-hypertrophic), hypoxic and hypertrophic H9c2 cells. H9c2 cells have been found to be more suitable for cardiac ischemia studies ⁴⁶. Inducing hypoxia and hypertrophy in cells closely mimics

MI and HF conditions ^{35, 47-48}. The cell viability analysis comparing the normal cell viability with that of hypoxic and hypertrophic H9c2 cells suggested that the hypoxia and hypertrophy inducing treatments were safe and did not cause cytotoxicity. Literature has widely suggested that under HF, the AT1 receptors present on the cardiomyocytes are overexpressed and these receptors could be blocked to reverse cardiac remodeling ⁷⁻⁸. Therefore, targeting the overexpressed AT1 receptors with the targeted AT1-HSA-MRN-NPs to hypoxic and hypertrophic cardiac cells allowed higher uptake of the AT1-HSA-MRN-NPs as compared to the non-targeted MRN-HSA-NPs and Scr-HSA-MRN-NPs. The Scr peptide-tagged nanoparticles were used as a negative control to ensure that the higher uptake of AT1-HSA-MRN-NPs was a direct result of AT1 peptide mediated targeting and not passive uptake ⁵. Also, the uptake of the AT1-HSA-MRN-NPs was significantly higher in hypoxic and hypertrophic cells vs the normal cells. This effect was further confirmed by confocal microscopy. These studies confirm the targeting abilities of the AT1 peptide under MI and HF conditions and demonstrate that AT1-HSA-MRN-NPs can safely be used as targeted drug delivery systems for congestive heart failure and related conditions.

4.6 Conclusion

We have synthesized and developed stable AT1 peptide-tagged albumin nanoparticles to deliver MRN in a targeted manner for heart failure treatment. This novel drug delivery system demonstrates physical stability, biocompatibility, specific targeting ability and higher cellular uptake. Also, as compared to the non-targeted MRN-Lactate, AT1-HSA-MRN-NPs show greater biocompatibility in cardiomyoblasts. In future, the performance of AT1-HSA-MRN-NPs will be evaluated in a rat model of CHF along with MRN pharmacokinetics. This targeted therapy is anticipated to be more effective in improve the cardiac function in CHF as compared to the currently available treatments.

4.7 Acknowledgements

This work is supported by the research funding granted to Dr. Satya Prakash from Canadian Institute of Health Research (CIHR) and the Natural Sciences and Engineering Research Council (NSERC). The authors are grateful to Mr. Xue Dong Liu for assistance in TEM imaging (Facility for Electron Microscopy Research, Materials Engineering, McGill University) and Mr. Nadim

Saadeh for help with Mass Spectroscopy (Mass Spectroscopy Facility, Department of Chemistry, McGill University).

4.8 References

- Benjamin, E. J. *et al.* Heart disease and stroke statistics—2018 update: a report from the American Heart Association. *Circulation* **137**, e67-e492 (2018).
- Inamdar, A. A. & Inamdar, A. C. Heart Failure: Diagnosis, Management and Utilization. *Journal of clinical medicine* **5**, 62, doi:10.3390/jcm5070062 (2016).
- Doenst, T. *et al.* PCI and CABG for Treating Stable Coronary Artery Disease: JACC Review Topic of the Week. *Journal of the American College of Cardiology* **73**, 964-976 (2019).
- 4 Taylor, C. J. *et al.* Survival following a diagnosis of heart failure in primary care. *Family practice* **34**, 161-168 (2017).
- 5 Dvir, T. *et al.* Nanoparticles targeting the infarcted heart. *Nano letters* **11**, 4411-4414 (2011).
- Rivard, K. *et al.* Overexpression of type I angiotensin II receptors impairs excitation-contraction coupling in the mouse heart. *American Journal of Physiology-Heart and Circulatory Physiology* (2011).
- Paradis, P., Dali-Youcef, N., Paradis, F. W., Thibault, G. & Nemer, M. Overexpression of angiotensin II type I receptor in cardiomyocytes induces cardiac hypertrophy and remodeling. *Proceedings of the National Academy of Sciences of the United States of America* **97**, 931-936 (2000).
- 8 Xu, J. *et al.* Role of cardiac overexpression of angiotensin II in the regulation of cardiac function and remodeling post-myocardial infarction. *American Journal of Physiology-Heart and Circulatory Physiology* (2007).
- Tai, C. *et al.* Effect of angiotensin-converting enzyme inhibitors and angiotensin II receptor blockers on cardiovascular events in patients with heart failure: a meta-analysis of randomized controlled trials. *BMC cardiovascular disorders* **17**, 257-257, doi:10.1186/s12872-017-0686-z (2017).
- 10 Khan, M. S. *et al.* Dose of angiotensin-converting enzyme inhibitors and angiotensin receptor blockers and outcomes in heart failure: a meta-analysis. *Circulation: Heart Failure* **10**, e003956 (2017).
- Hennig, R., Pollinger, K., Tessmar, J. & Goepferich, A. Multivalent targeting of AT1 receptors with angiotensin II-functionalized nanoparticles. *J Drug Target* **23**, 681-689, doi:10.3109/1061186x.2015.1035276 (2015).
- Lomis, N. *et al.* Novel Milrinone Nanoformulation for Use in Cardiovascular Diseases: Preparation and in Vitro Characterization. *Molecular pharmaceutics* **15**, 2489-2502 (2017).
- Feneck, R. Phosphodiesterase inhibitors and the cardiovascular system. *Continuing Education in Anaesthesia, Critical Care & Pain* **7**, 203-207 (2007).
- 14 Alousi, A. & Johnson, D. Pharmacology of the bipyridines: amrinone and milrinone. *Circulation* **73**, III10-24 (1986).

- Baim, D. S. *et al.* Evaluation of a new bipyridine inotropic agent—milrinone—in patients with severe congestive heart failure. *New England journal of medicine* **309**, 748-756 (1983).
- Barton, P. *et al.* Hemodynamic effects of iv milrinone lactate in pediatric patients with septic shock: A prospective, double-blinded, randomized, placebo-controlled, interventional study. *CHEST Journal* **109**, 1302-1312 (1996).
- Wang, Z., Wu, Q., Nie, X., Guo, J. & Yang, C. Combination therapy with milrinone and esmolol for heart protection in patients with severe sepsis: a prospective, randomized trial. *Clinical drug investigation* **35**, 707-716 (2015).
- de Boer, R. A. & van Veldhuisen, D. J. ACE-inhibitors, Beta-blockers or the Combination in Heart Failure: Is It Just an A–B–C? *Cardiovascular Drugs and Therapy* **22**, 261-263 (2008).
- 19 Cuffe, M. S. *et al.* Short-term intravenous milrinone for acute exacerbation of chronic heart failure: a randomized controlled trial. *Jama* **287**, 1541-1547 (2002).
- Abbasi, S., Paul, A., Shao, W. & Prakash, S. Cationic albumin nanoparticles for enhanced drug delivery to treat breast cancer: preparation and in vitro assessment. *Journal of drug delivery* **2012** (2011).
- Sebak, S., Mirzaei, M., Malhotra, M., Kulamarva, A. & Prakash, S. Human serum albumin nanoparticles as an efficient noscapine drug delivery system for potential use in breast cancer: preparation and in vitro analysis. *International journal of nanomedicine* 5, 525 (2010).
- Lomis, N. *et al.* Human Serum Albumin Nanoparticles for Use in Cancer Drug Delivery: Process Optimization and In Vitro Characterization. *Nanomaterials* **6**, 116 (2016).
- Lomis, N. *et al.* Novel Milrinone Nanoformulation for Use in Cardiovascular Diseases: Preparation and in Vitro Characterization. *Mol Pharm* **15**, 2489-2502, doi:10.1021/acs.molpharmaceut.7b00360 (2018).
- Jithan, A., Madhavi, K., Madhavi, M. & Prabhakar, K. Preparation and characterization of albumin nanoparticles encapsulating curcumin intended for the treatment of breast cancer. *International journal of pharmaceutical investigation* **1**, 119 (2011).
- Yu, H., Nguyen, M.-H., Cheow, W. S. & Hadinoto, K. A new bioavailability enhancement strategy of curcumin via self-assembly nano-complexation of curcumin and bovine serum albumin. *Materials Science and Engineering: C* **75**, 25-33 (2017).
- Ji, S. *et al.* RGD-conjugated albumin nanoparticles as a novel delivery vehicle in pancreatic cancer therapy. *Cancer biology & therapy* **13**, 206-215 (2012).
- Yu, X. *et al.* Enhanced tumor targeting of cRGD peptide-conjugated albumin nanoparticles in the BxPC-3 cell line. *Sci Rep* **6**, 31539 (2016).
- Look, J. *et al.* Ligand-modified human serum albumin nanoparticles for enhanced gene delivery. *Molecular pharmaceutics* **12**, 3202-3213 (2015).
- Ruan, C. *et al.* Substance P-modified human serum albumin nanoparticles loaded with paclitaxel for targeted therapy of glioma. *Acta Pharmaceutica Sinica B* **8**, 85-96 (2018).
- Langer, K. *et al.* Optimization of the preparation process for human serum albumin (HSA) nanoparticles. *International Journal of Pharmaceutics* **257**, 169-180 (2003).
- Langer, K. *et al.* Human serum albumin (HSA) nanoparticles: reproducibility of preparation process and kinetics of enzymatic degradation. *International journal of pharmaceutics* **347**, 109-117 (2008).

- Siddiqui, M. *et al.* Application of DDQ and p-chloranilic acid for the spectrophotometric estimation of milrinone in pharmaceutical formulations. *Asian J Sci Res* **2**, 135-145 (2009).
- Lomis, N. *et al.* A novel milrinone nanoformulation for use in cardiovascular diseases: preparation and in vitro characterization. *Molecular pharmaceutics*, doi:10.1021/acs.molpharmaceut.7b00360 (2017).
- Wu, D. & Yotnda, P. Induction and testing of hypoxia in cell culture. *Journal of visualized experiments: JoVE* (2011).
- Song, R. *et al.* H2O2 induces myocardial hypertrophy in H9c2 cells: a potential role of Ube3a. *Cardiovascular toxicology* **15**, 23-28 (2015).
- Rebouças, J. d. S., Santos-Magalhães, N. S. & Formiga, F. R. Cardiac regeneration using growth factors: advances and challenges. *Arquivos brasileiros de cardiologia* **107**, 271-275 (2016).
- Tang, Y. *et al.* Targeted delivery of vascular endothelial growth factor improves stem cell therapy in a rat myocardial infarction model. *Nanomedicine: Nanotechnology, Biology and Medicine* **10**, 1711-1718 (2014).
- Feric, N. T. & Radisic, M. Strategies and challenges to myocardial replacement therapy. *Stem cells translational medicine* **5**, 410-416 (2016).
- Mudshinge, S. R., Deore, A. B., Patil, S. & Bhalgat, C. M. Nanoparticles: emerging carriers for drug delivery. *Saudi pharmaceutical journal* **19**, 129-141 (2011).
- 40 Xiao, K. *et al.* The effect of surface charge on in vivo biodistribution of PEG-oligocholic acid based micellar nanoparticles. *Biomaterials* **32**, 3435-3446 (2011).
- Aderem, A. & Underhill, D. M. Mechanisms of phagocytosis in macrophages. *Annual review of immunology* **17**, 593-623, doi:10.1146/annurev.immunol.17.1.593 (1999).
- Owens III, D. E. & Peppas, N. A. Opsonization, biodistribution, and pharmacokinetics of polymeric nanoparticles. *International journal of pharmaceutics* **307**, 93-102 (2006).
- Tang, X. *et al.* Milrinone for the Treatment of Acute Heart Failure After Acute Myocardial Infarction: A Systematic Review and Meta-Analysis. *Basic & clinical pharmacology & toxicology* **117**, 186-194 (2015).
- Stewart, D. & McPherson, M. L. Symptom management challenges in heart failure: pharmacotherapy considerations. *Heart failure reviews* **22**, 525-534 (2017).
- Loureiro, A., G Azoia, N., C Gomes, A. & Cavaco-Paulo, A. Albumin-based nanodevices as drug carriers. *Current pharmaceutical design* **22**, 1371-1390 (2016).
- Kuznetsov, A. V., Javadov, S., Sickinger, S., Frotschnig, S. & Grimm, M. H9c2 and HL-1 cells demonstrate distinct features of energy metabolism, mitochondrial function and sensitivity to hypoxia-reoxygenation. *Biochimica et Biophysica Acta (BBA)-Molecular Cell Research* **1853**, 276-284 (2015).
- Dickhout, J. G., Carlisle, R. E. & Austin, R. C. Interrelationship between cardiac hypertrophy, heart failure, and chronic kidney disease: endoplasmic reticulum stress as a mediator of pathogenesis. *Circulation Research* **108**, 629-642 (2011).
- Zhang, Z. *et al.* Knockdown of MicroRNA-122 Protects H9c2 Cardiomyocytes from Hypoxia-Induced Apoptosis and Promotes Autophagy. *Medical science monitor : international medical journal of experimental and clinical research* **23**, 4284-4290, doi:10.12659/MSM.902936 (2017).

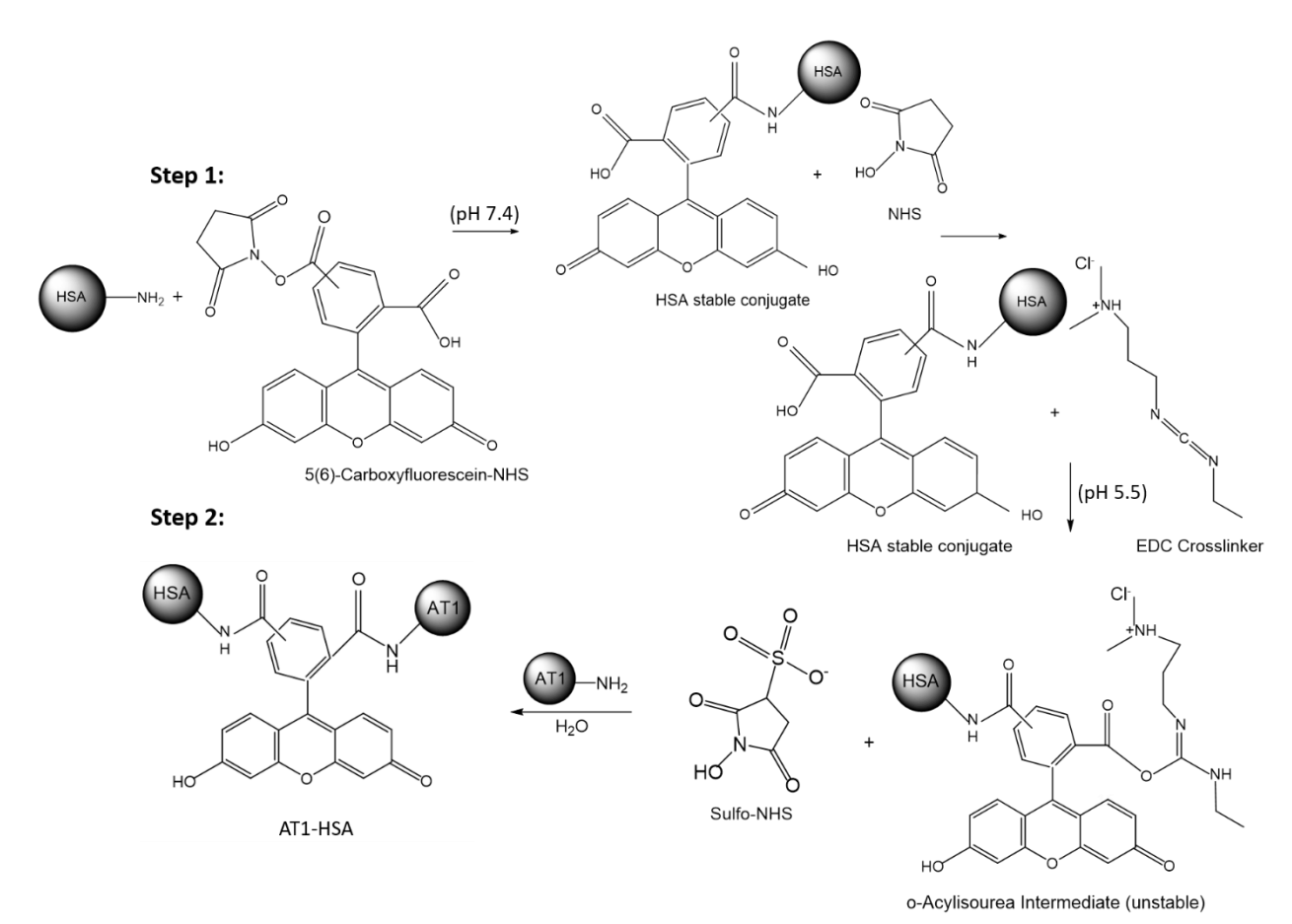


Figure 4.1. Schematic representation of the surface modification of the HSA molecule for binding with the AT1 peptide through a two-step chemical conjugation reaction using cross-linkers.

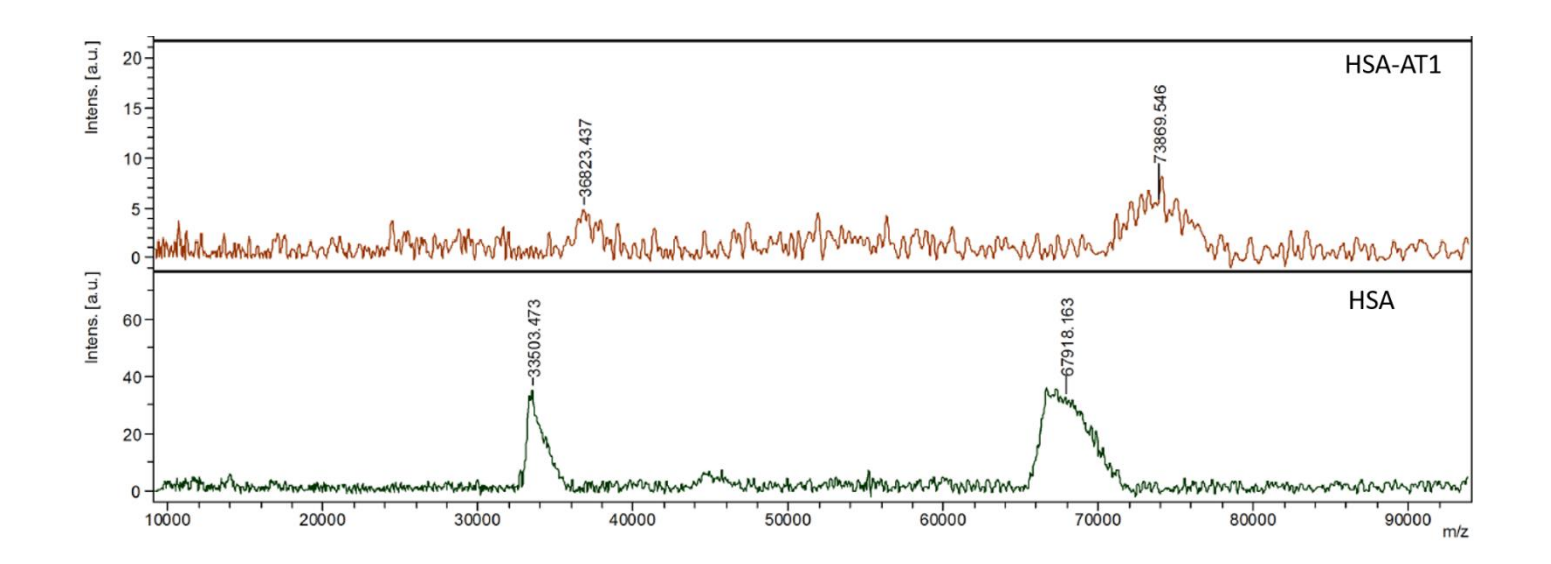


Figure 4.2. HSA (lower) and AT1-HSA (upper) was analyzed by Matrix-Assisted Laser Desorption/Ionization Time of Flight Mass Spectrometry. The m/z ratio of the AT1-HSA peak was at least 7000 higher than that of the HSA peak, which demonstrated that AT1 was successfully conjugated to the surface of HSA.

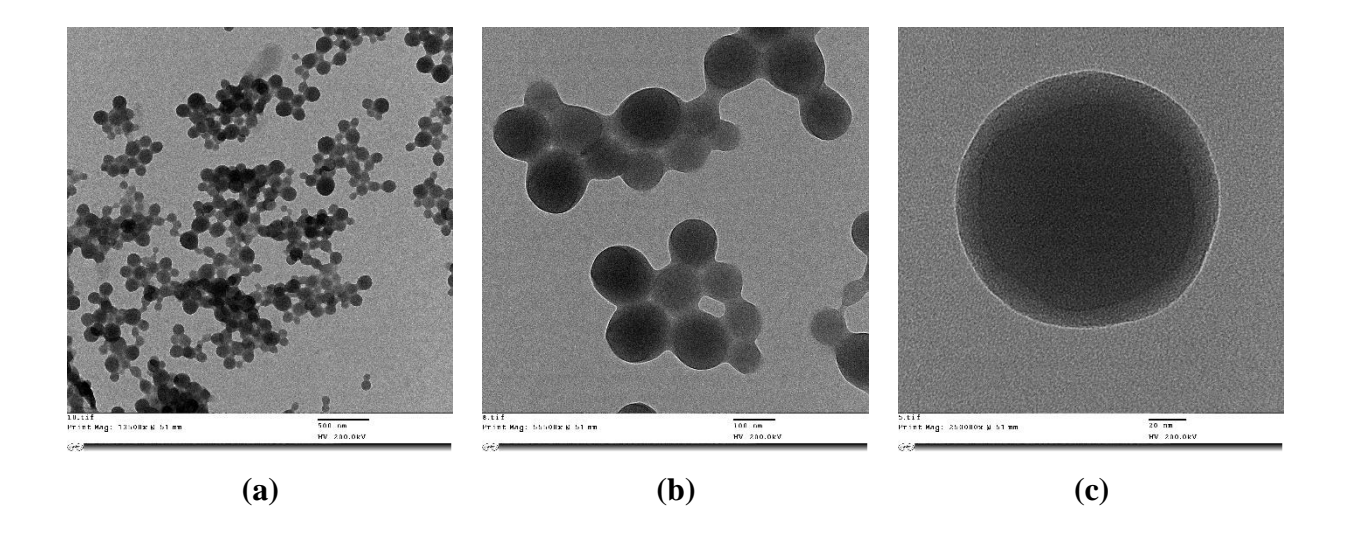


Figure 4.3. Nanoparticle surface characterization using TEM analysis (a) Under magnification of 13,500X, AT1-HSA-MRN-NPs of size 215.2±4.7 nm and zeta potential of -28.8±2.7 mV (Scale = 500 nm) (b) Under magnification of 55,000X, AT1-HSA-MRN-NPs with moderately uniform particle size (Scale = 100 nm); (c) Under 250,000X magnification, the AT1-HSA-MRN-NPs display a dark core surrounded by a bright membrane, which confirmed the distinct peptide layer (Scale = 20 nm).

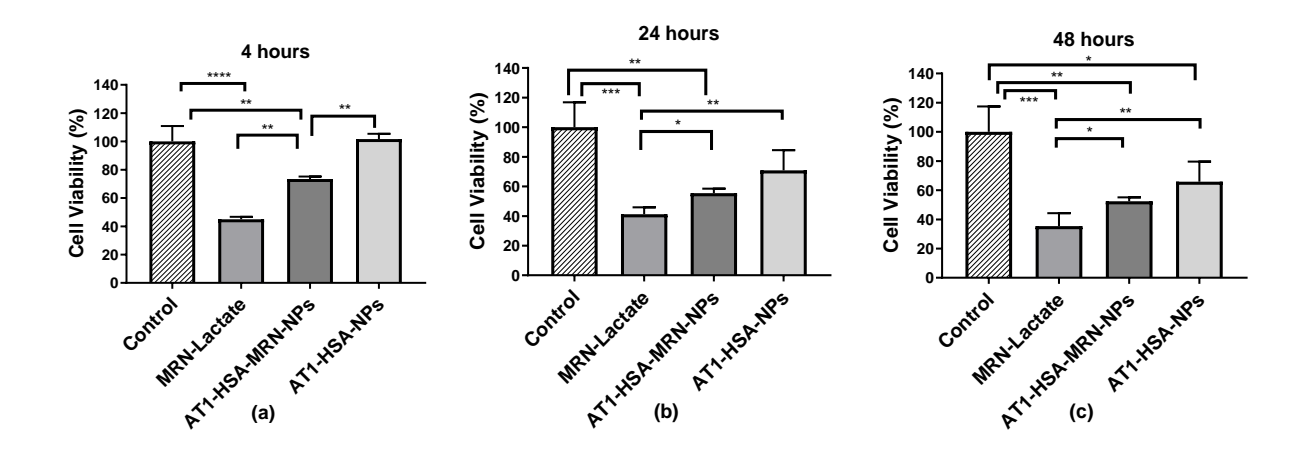


Figure 4.4. Cell viability analysis on H9c2 cells treated with MRN-Lactate, AT1-HSA-MRN-NPs and AT1-HSA-NPs at 1 mM MRN concentration at (a) 4 hours, (b) 24 hours and (c) 48 hours. The graph shows a representative result of mean \pm SD (n=5). ****P<0.0001 was considered highly significant and ***P<0.001, **P<0.01 and *P<0.05 were considered significant based on Tukey's posthoc analysis.

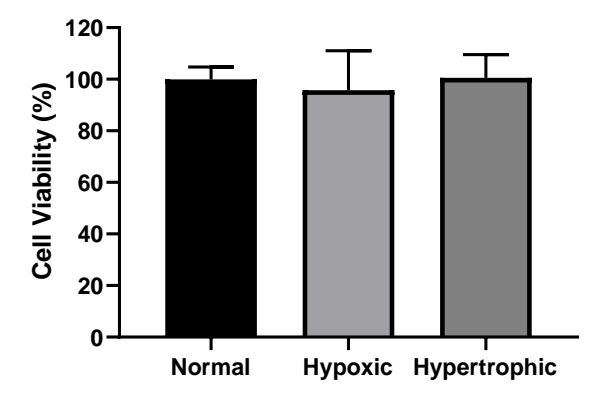


Figure 4.5. Viability of H9c2 cells treated for hypoxia and hypertrophy in comparison with normal cells (non-hypoxic and non-hypertrophic). There were no significant differences (*P*>0.1) in cell viability amongst the groups.

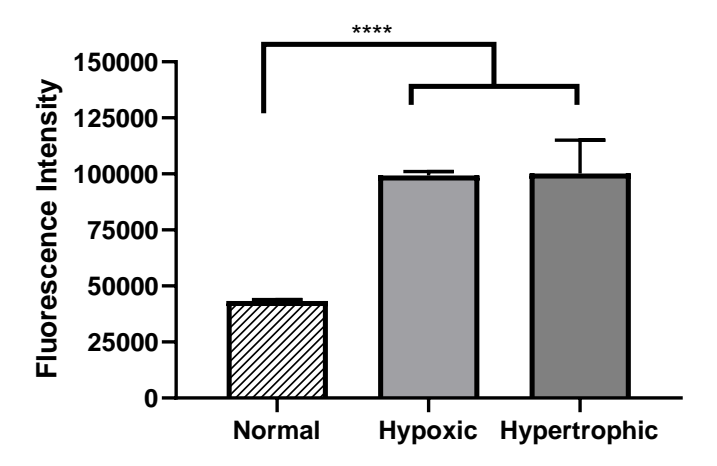


Figure 4.6. AT1 expression in normal, hypoxic and hypertrophic H9c2 cells. Results are represented as mean \pm SD (n=5). ****P<0.0001 was considered highly significant based on Tukey's posthoc analysis.

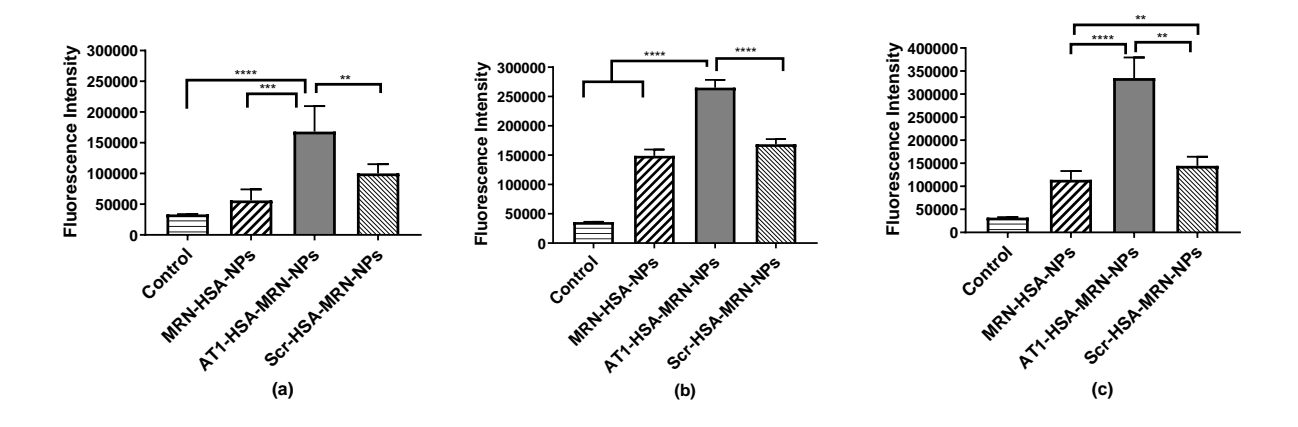


Figure 4.7. Intracellular uptake of MRN-HSA-NPs, AT1-HSA-MRN-NPs and Scr-HSA-MRN-NPs in H9c2 cells (a) Normal cells (non-hypoxic, non-hypertrophic), (b) Hypoxic cells and (c) Hypertrophic cells. The nanoparticle concentration was 0.5 mg/mL. The graph shows a representative result of mean \pm SD (n=5). ****P<0.0001 was considered highly significant and ***P<0.001, **P<0.01 were considered significant based on Tukey's posthoc analysis.

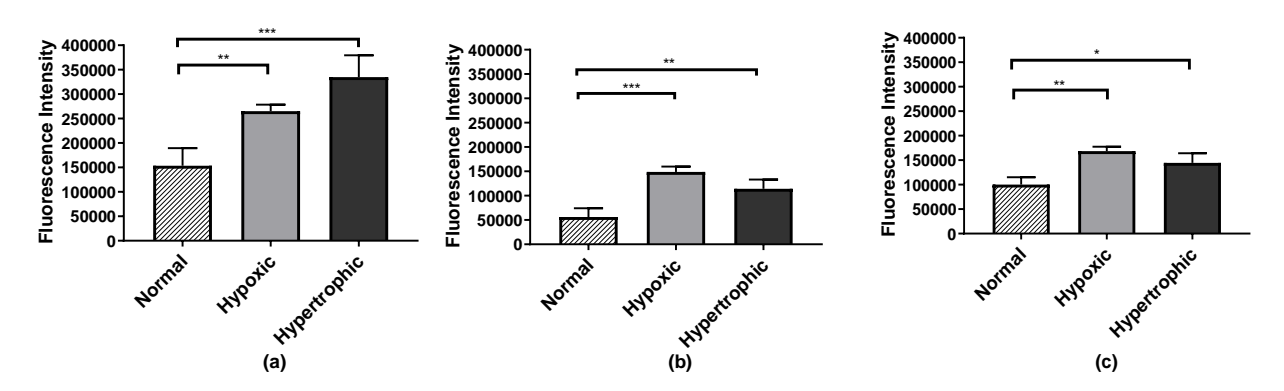


Figure 4.8. H9c2 cells under Normal, Hypoxic and Hypertrophic conditions demonstrate uptake of nanoparticles: (a) AT1-HSA-MRN-NPs, (b) MRN-HSA-NPs and (c) Scr-HSA-MRN-NPs. The nanoparticle concentration for all three samples was 0.5 mg/mL. The graph shows a representative result of mean \pm SD (n=5). ***P<0.001, **P<0.01, *P<0.05 were considered significant based on Tukey's posthoc analysis.

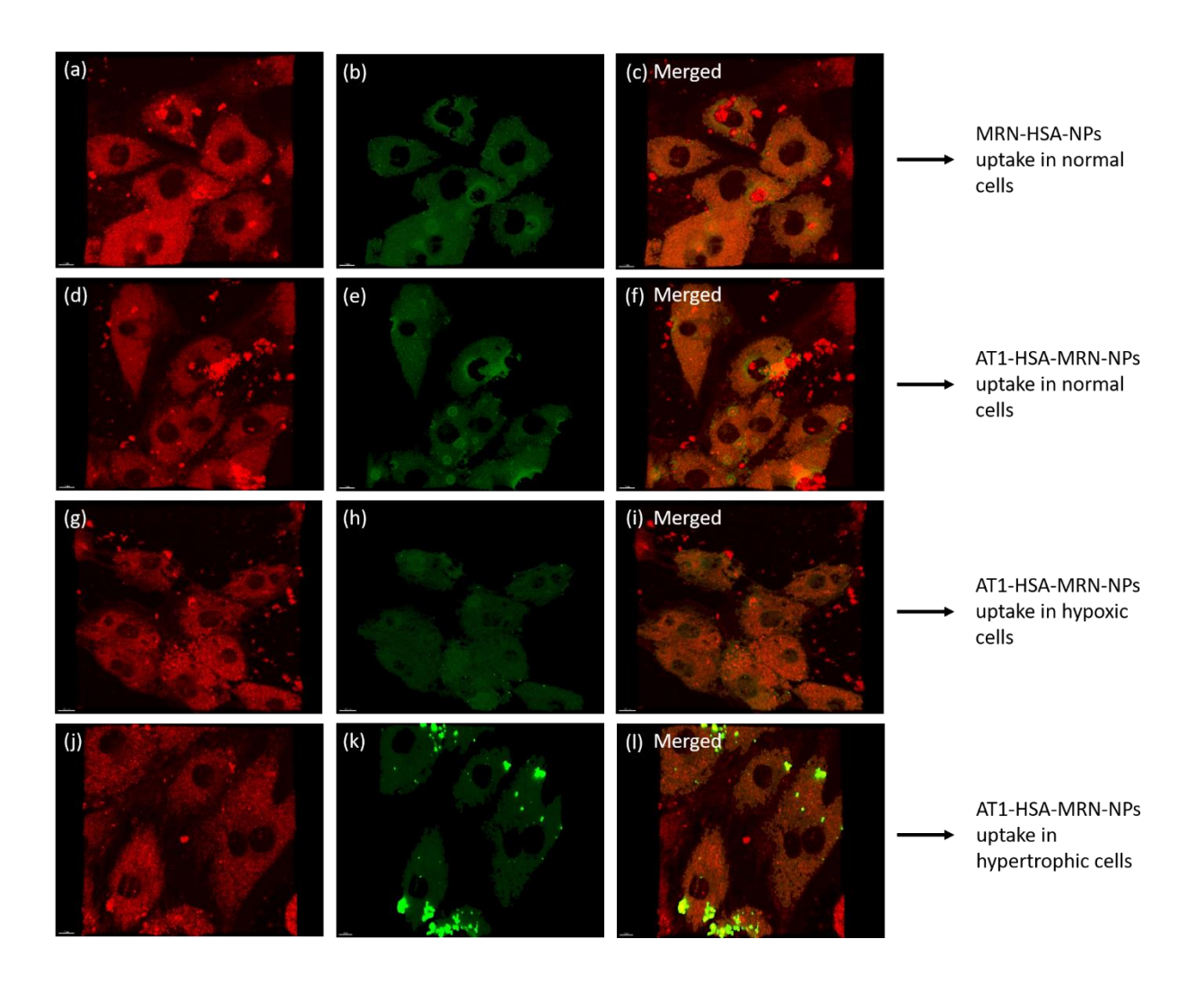


Figure 4.9. H9c2 cells treated with the FM 4-64 stain (red) and fluorescently tagged nanoparticles (green). (a-c) Uptake of MRN-HSA-NPs by normal H9c2 cells; (d-f) Uptake of AT1-HSA-MRN-NPs by normal H9c2 cells; (g-i) Uptake of AT1-HSA-MRN-NPs by hypoxic H9c2 cells; (j-l) Uptake of AT1-HSA-MRN-NPs by hypertrophic H9c2 cells.

Table 4.1. Parameters for nanoparticle characterization of AT1-HSA-MRN-NPs.

Nanoparticle Size	215.2±4.7 nm
Zeta Potential	-28.8±2.7 mV
Polydispersity Index	0.15+0.003
Yield	75.6±2.5%
Encapsulation Efficiency	40.5±1.5%

CHAPTER 5: TARGETED MILRINONE DELIVERY USING ALBUMIN NANOCARRIERS IN A RAT MODEL OF CONGESTIVE HEART FAILURE

Nikita Lomis^{1,2}, Ziyab K. Sarfaraz³, Aiman Alruwaih³, Susan Westfall⁴, Dominique Shum-Tim³, Satya Prakash^{*}

¹Biomedical Technology and Cell Therapy Research Laboratory, Department of Biomedical Engineering, 3775 University Street, Montreal, QC, H3A 2B4, Canada ²Division of Experimental Medicine, 1110 Pins Avenue, Montreal, QC, H3A 1A3, Canada ³Division of Cardiac Surgery and Surgical Research, Royal Victoria Hospital, 1001 Boulevard Décarie, Montréal, QC, H4A 3J1, Canada

⁴Department of Neurology, Icahn School of Medicine Mount Sinai, New York, NY, 10029, USA

*Corresponding author: Satya Prakash

Tel: 514-398-2736; Fax: 514-398-7461

Email: satya.prakash@mcgill.ca

Preface: In this chapter, the targeted nanoparticle formulation for MRN delivery was evaluated *in vivo*. First, the synthesis scheme for attaching the AT1 peptide to the HSA surface, given in chapter 4, was modified by replacing 5(6)-Carboxyfluorescein-NHS with PA-(PEG)₄-SPA (propionic acid-PEG₄-succinimidyl propionate), followed by addition of EDC/Sulfo-NHS. The fluorescein molecule is known to be mildly cytotoxic and hence was removed from the nanoparticles to avoid toxicity to the animals. Instead, PA-(PEG)₄-SPA was used since addition of PEG imparts non-immunogenicity to the resulting nanoparticle formulation. This chapter investigates MRN pharmacokinetics and tissue distribution, comparing the targeted AT1-HSA-MRN-NPs formulation with MRN-Lactate in an animal model. Further, the treatment efficacy of the AT1-HSA-MRN-NPs vs MRN-Lactate was evaluated in a rat model of CHF. The changes in cardiac function and contractility were determined by measuring the parameters such as ejection fraction, fractional shortening, liver and kidney function, and serum cytokine levels.

(Article to be submitted)

5.1 Abstract

Congestive heart failure is primarily caused by ischemia or myocardial infarction, leading to lower cardiac output and the loss of contraction ability of cardiac tissue. CHF is typically treated by administering inotropic drugs such as milrinone (MRN) to improve the myocardial contractility and therefore the overall cardiac function. The action of inotropic drugs could be enhanced further by delivering drugs specifically to the target site. Hence, the use of targeted drug delivery vehicles could help achieve the desired effect. Human serum albumin nanoparticles (HSA-NPs) are known to be biodegradable, biocompatible with drug binding pockets. HSA-NPs bind with various drugs to help improve their bioavailability, target specificity and blood circulation time in the body, also eliminating potential side effects. In this study, a targeted nanoparticle formulation using albumin nanoparticles has been developed for site-specific MRN delivery. The HSA-NPs carrying MRN were tagged with the angiotensin II (AT1) peptide to form AT1-HSA-MRN-NPs, which show specificity for the AT1 receptors overexpressed on infarcted cardiomyocytes during CHF. The targeted nanoparticle formulation has been tested both in vitro and in vivo. The MRN pharmacokinetics and biodistribution studies compared the AT1-HSA-MRN-NPs with MRN-Lactate, the clinically used drug for CHF patients. It was found that AT1-HSA-MRN-NPs showed targeted delivery of MRN and improved its retention time. Further, the treatment efficiency of AT1-HSA-MRN-NPs was evaluated in a rat model of CHF where the delivery of AT1-HSA-MRN-NPs showed significant improvement in myocardial contractility parameters. The targeted nanoparticle formulation did not exhibit toxicity towards the liver an increase the creatinine levels indicated renal impairment due to heart injury. The serum levels of IL-6 and TNF-α of the AT1-HSA-MRN-NPs animal group were significantly higher and IL-10 levels were significantly lower than the MRN-Lactate animal group. Thus, the sustained release of MRN from AT1-HSA-MRN-NPs with targeted drug delivery features and a superior treatment efficiency make it a successful formulation for CHF.

Keywords: Albumin, Milrinone, Heart Failure, Rat, Targeted, Drug Delivery

5.2 Introduction

Cardiovascular diseases (CVDs) are responsible for disability and mortality across the developed and developing world, of which congestive heart failure (CHF) is an ever-expanding issue ¹. The more commons treatments for CHF include surgical measures such as heart transplant, ventricular assist devices, bypass surgeries and stents ². The medical treatments involve drug delivery using ACE inhibitors, beta blockers, diuretics, inotropes etc. To prevent and treat cardiovascular syndromes, promising research has been undertaken especially in the field of nanomedicine ³⁻⁴. The application of nanomedicine in cardiac therapy represents a promising approach for efficient delivery of therapeutic agents such as drugs, genes, growth factors, cytokines and other molecules ⁵⁻⁸. However, despite the prominent advances on the use of nanoparticles as drug delivery systems for cancer therapy, fewer such studies have been reported for treatment of CVDs, which claim millions of lives annually, also causing a huge economic burden 9-10. The development of an effective nanoparticle formulation would entail the use of biocompatible and biodegradable materials, optimal particle size, surface charge, surface modifiable characteristics, targeting features and longer blood circulation time 11. This would help overcome limitations associated with current pharmacological treatments for CVDs resulting in more unique, specific and efficient therapies.

Currently, the treatment of myocardial infarction (MI) and HF involves administration of drugs either intravenously or orally in both adults and pediatric patients. However, lower retention times call for a continuous infusion of drugs with lack of target specificity, potentially causing toxicity and other side effects such as arrythmias, palpitations for off-target organs ¹². Though some studies have suggested strong cardioprotective effects due to growth factor delivery through direct myocardial injection, retaining the nanoparticles remains a challenge ^{6, 13-14}. The novel nanoparticle system reported in this study, developed from human serum albumin (HSA-NPs) protein addresses the above issues, by packaging the MRN drug molecule ¹⁰. This improves the pharmacokinetics profile, improves drug delivery at the infarcted site and enhances the therapeutic effect of the drug. Further, the controlled release of the MRN from the nanoparticles at the targeted site would allow for a single dose injection as opposed to a continuous supply. Also, being biodegradable, non-toxic and non-immunogenic, they are a more favourable option ¹⁵. Thus, many

albumin-based nanocarriers are being developed due to their increased specificity, biocompatibility and ability for surface functionalization for enhanced drug delivery ^{5, 16}.

It is widely known that under MI and HF, the angiotensin II type 1 (AT1) receptors are overexpressed on the myocardium. These receptors are specific for the angiotensin molecule, an 8-amino acid chain peptide (Asp-Arg-Val-Tyr-Ile-His-Pro-Phe). The overexpression of the AT1 receptors has been correlated directly with cardiac remodelling due to HF, explaining the use of drugs to block these receptors ¹⁷. Similarly, downregulation of AT1R expression using a siRNA delivery systems have shown significant improvement in cardiac function ^{7, 18}. Emerging strategies on functionalized AT1 receptor-targeted nanoparticles such as liposomes, quantum dots, PLGA microcapsules as novel drug delivery systems have suggested a modern outlook on treatment of MI and HF conditions ^{8, 16-17}. Thus, the study of AT1 receptors as targets for the delivery and uptake of drugs, nanoparticles and other biomolecules has immense potential for development for potent cardiac therapies.

In this study, we report the development of AT1 peptide-tagged HSA-NPs for delivery of the MRN drug to treat CHF. The targeted AT1-HSA-MRN-NP formulation has been characterized *in vitro*. The release of MRN from the targeted nanoparticles formulation, over time, was evaluated. An *in vivo* pharmacokinetics and tissue distribution study has been reported comparing the pharmacokinetic parameters of the AT1-HSA-MRN-NPs with the control non-targeted drug, MRN-Lactate. In another *in vivo* study, the treatment efficacy of the AT1-HSA-MRN-NPs vs MRN-Lactate has been evaluated in a rat model of congestive heart failure.

5.3 Materials and Methods

5.3.1 Materials

Human serum albumin (> 97% lyophilized) was purchased from Sigma Aldrich (Oakville, ON, Canada). Glutaraldehyde (25% aq. solution) was purchased from Alfa Aesar (Cedarlane, Burlington, ON, Canada). Milrinone was purchased from Selleck Chemicals (Burlington, ON, Canada). The PA-(PEG)₄-SPA (propionic acid-PEG₄-succinimidyl propionate) was purchased from JenKem (TX, USA), EDC, Sulfo-NHS were purchased from Thermo Fisher Scientific (ON,

Canada) Other chemicals were purchased from Fisher Scientific (Nepean, ON, Canada). The ELISA kits were purchased from Abcam (Toronto, ON, Canada)

5.3.2 Synthesis of the AT1 Peptide

The Angiotensin II Type 1 (AT1) receptor targeting peptide is a chain of 8 amino acids Asp-Arg-Val-Tyr-Ile-His-Pro-Phe, synthesized by CanPeptide (Pointe-Claire, QC, Canada) as NH₂-Gly-Gly-Gly-Asp-Arg-Val-Tyr-Ile-His-Pro-Phe-NH₂ ¹⁶.

5.3.3 Surface Modification of HSA with AT1 Peptide

The surface of HSA was modified for attachment of the AT1 peptide in a two-step reaction. An aqueous solution of 20 mg/mL of HSA dissolved in deionized water (0.3 mM) was prepared and reacted with PA-(PEG)₄-SPA (10-fold molar excess), for 1 hour. The solution was further mixed with EDC/Sufo-NHS for 30 minutes followed by reaction with the AT1 peptide (10-fold molar excess) for 4 hours. The AT1-HSA was purified by dialysis using the Slide-a-Lyzer dialysis cassette (10K Da MWCO). The purified sample was lyophilized and stored at 4°C.

5.3.4 Mass Spectrometry

The AT1-HSA, AT1 peptide and HSA samples were analyzed by the Matrix-Assisted Laser Desorption/Ionization Time of Flight Mass Spectrometry (MALDI-TOF-MS) MALDI Autoflex III- TOF-(BRUKER) SMARTBEAM) (Dept. of Chemistry, McGill University, Montreal, QC, Canada) in linear positive mode. Dihydroxybenzoic Acid was used as the Matrix and the AT1-HSA, HSA and AT1 peptide samples were dissolved in water at concentrations of 7 mg/mL

5.3.5 Quantification of AT1 Peptide Attached to HSA

The amount of AT1 peptide attached to the HSA molecule was determined by UV-Visible spectrophotometry. Post surface modification of HSA with AT1 by chemical conjugation and prior to dialysis, the reaction mixture was centrifuged using Amicon centrifugal filters with 30 KDa MWCO. The unbound AT1 peptide (Mol. Wt. 1292 g/mol) was collected as the filtrate at the bottom of the tube and quantified by UV-Visible spectrophotometry at 280 nm. A standard curve was prepared by making serial dilutions of AT1 to measure the unknown quantity of AT1 in solution.

5.3.6 Nanoparticle Preparation

The AT1-HSA-MRN-NPs were prepared by the ethanol desolvation technique ¹⁹⁻²⁰. Briefly, an aqueous solution AT1-HSA (20 mg/mL) was prepared in deionized water and solution pH was adjusted to pH 8.0 using 0.1 M NaOH. MRN was dissolved in DMSO and added to the AT1-HSA, with MRN/HAS (wt./wt.) at 1:10, 1:20, 1:40 and 1:80 ¹⁰. Ethanol was added in a dropwise manner resulting in solution turbidity. Glutaraldehyde (8% v/v aq. solution) was added at a concentration of 0.588 μl/mg HSA and reacted for 24 hours. The nanoparticles were washed by three rounds of ultracentrifugation at 16500 rpm for 15 minutes each at 25°C. The supernatant was collected for detection of unbound MRN. The pellet was washed with deionized water and resuspended in PBS.

5.3.7 Nanoparticle Characterization

The average size of the nanoparticles was measured by Dynamic Light Scattering (DLS) using a Particle Size Analyzer (Brookhavens Instruments Corporation, NY, USA). The samples were diluted 1:20 with deionized water and measured at a scattering angle of 90° and temperature of 25°C. The Polydispersity Index (PDI) estimated the size distribution of the nanoparticles. The zeta potential was measured by a Zeta Potential Analyzer (Brookhavens Instruments Corporation, NY, USA) using electrophoretic laser Doppler anemometry. The size, shape and surface morphology of the nanoparticles were examined by SEM and TEM techniques.

The yield of the nanoparticles was measured by the UV-spectrophotometric method ⁹⁻¹⁰. A standard curve of HSA solution dissolved in Bradford reagent was used as a reference and absorbance was measured at 595 nm. For calculation of yield, the following equation was used:

Yield
$$\% = (\frac{\text{weight of HSA in solution}}{\text{initial weight of HSA}}) * 100.$$

For measuring encapsulation efficiency, nanoparticles were spin concentrated using centrifugal filters (10K Da MWCO) for eluting the non-encapsulated MRN into the collection tube. The concentration of non-encapsulated MRN was determined by UV-spectrophotometry at 356 nm. A standard curve of MRN in a DDQ/Ethanol mixture was used as reference ²¹. The encapsulation efficiency was calculated using the following equation:

Encapsulation Efficiency
$$\% = (\frac{\text{concentration of MRN encapsulated}}{\text{starting concentration of MRN used}}) * 100.$$

5.3.8 In Vitro Milrinone Release from Nanoparticles

The *in vitro* drug release was studied by UV-visible spectrophotometry ⁹. In brief, 40 mg of AT1-HSA-MRN-NPs were suspended in 10 mL of PBS at 37°C and 120 rpm in a shaking incubator. At predetermined time intervals of 0, 15 mins, 30 mins, 45 mins, 1 h, 2 h, 4h, 8h, 18h and 24 h, 0.5 mL of the nanoparticle suspension was withdrawn and re-substituted with 0.5 mL of fresh PBS. The withdrawn suspension was centrifuged using Amicon centrifugal filters (10K MWCO) and supernatant was used to determine the amount of MRN released. The MRN was detected at 356 nm using a colorimetric assay and a cumulative MRN release over time was calculated ²¹.

5.3.9 *In Vivo* Studies

All experiments were performed on female Lewis Rats (200–250 g; Charles River Laboratories, Senneville, Canada) in accordance with the guidelines set forth by the Canadian Council on Animal Care and were approved by the institutional ethics committee. Rats were housed in groups of two to three per cage.

Two *in vivo* studies were performed. The first study includes pharmacokinetics and tissue distribution analyses on rats not having undergone the coronary artery ligation surgery. The second study evaluated the treatment efficacy of the targeted nanoparticle formulation in a rat model of CHF by performing ligation surgery of the left anterior descending (LAD) coronary artery.

5.3.10 Pharmacokinetics and Biodistribution Study

The animals were randomized into three groups in a blinded manner. Group 1 (n=6) was intravenously injected with 1 c.c. saline. Group II (n=12) was intravenously injected with 250 μ L of AT1-HSA-MRN-NPs containing 50 μ g/kg MRN. Group III (n=12) was intravenously injected with 250 μ L of MRN-Lactate containing 50 μ g/kg MRN. Blood was collected from the jugular vein at the following timepoints: 0, 5, 15, 30, 45, 60, 120 and 360 mins (n=4 per time point). The animals were euthanized by isoflurane/CO₂. Organ tissues (heart, lungs, liver and kidneys) were

collected, washed, rinsed and snap-frozen in liquid nitrogen. MRN was detected in the organs at 120 mins for the tissue distribution study.

5.3.11 Ligation of the Left Anterior Descending Coronary Artery to Induce CHF

The surgery was performed in a blinded manner as previously mentioned ²²⁻²³. Briefly, rats were anesthetized using 5% isoflurane, intubated, and mechanically ventilated at 80 breaths/minute. Via a left thoracotomy (through the fourth intercostal space), the LAD coronary artery was permanently ligated 2 mm from its origin with a 7/0 polypropylene suture (Ethicon Inc, Somerville, NJ). The ischemic myocardial segment rapidly became identifiable through its pallor and akinesia corresponding to the distribution of the LAD coronary artery territory distal to the occlusion, which resulted in MI of the free left ventricle (LV) and subsequently heart failure. About 48 hours after ligation of the artery, injections were performed using a 27-G needle. Rats were randomized into five groups: Control group I (n=5) received an intravenous injection of 1 c.c. saline. Group II (n=8) received 250 μL intravenous injection of AT1-HSA-MRN-NPs containing 50 μg/kg of MRN. Group III (n=8) received 250 μL bolus intravenous injection of 50 μg/kg MRN-Lactate ²⁴⁻²⁵. Group IV (n=5) received 250 µL intravenous injection of empty NPs in the same concentration as group I. Group V (n=8) received 250 μL subcutaneous injection of 50 μg/kg of AT1-HSA-MRN-NPs. The reason for using empty NPs as a control was to ensure that these particles had no effect on cardiac function or other inadvertent toxicity. Blood was collected 24 hours post injection for MRN quantification. Various endpoint measurements were taken as described in subsequent paragraphs. At 5 days post injection, all rats were killed by euthanasia. The hearts were washed with saline solution to remove excess blood and clots and then fixed in neutral-buffered 4% formalin.

5.3.12 Animal Mortality

Forty female Lewis rats were included in the study, with a total of thirty-four rats surviving till the 1-week experimental end point of the study. All mortalities occurred during surgery. There was no difference in mortality among the different groups. No mortality was observed in surviving rats.

5.3.13 Blood Serum and Plasma Collection

Blood was collected via the jugular vein from the animals using a sterile 23G/25mm needle in the Microtainer® serum separator tubes (Becton Dickinson, NJ, USA) for serum separation and in Plasma-EDTA tubes (Becton Dickinson, NJ, USA) for plasma collection. The blood was allowed to clot at room temperature for 30 minutes and subsequently placed on ice until centrifugation. Serum was separated by low-speed centrifugation at 1500 rpm for 15 min at 4°C and was frozen at -80°C until analysis. Serum was used to test for C-reactive protein (CRP) and liver function tests, alkaline phosphatase (ALP), alanine aminotransferase (ALT) and aspartate transaminase (AST). Urea, creatinine (CRE) and uric acid (UA) were also tested for renal functionality in the animals using a conventional enzymatic method on Hitachi 911 automated clinical chemistry autoanalyzer (Roche Diagnostics, USA). The plasma was separated by low-speed centrifugation at 2500 rpm for 10 mins at 4°C and was frozen at -80°C until analysis. Plasma was used to detect MRN levels using High Performance Liquid Chromatography (HPLC).

5.3.14 Quantification of Milrinone from Rat Plasma

The MRN in plasma samples was quantified using High Performance Liquid Chromatography (HPLC). For sample preparation, stock solutions of MRN (1 mg/mL) and amrinone (1 mg/mL) were prepared in DMSO. Amrinone was used as an internal standard. A working solution of amrinone at 250 ng/mL was prepared by serial dilution with deionized water. Further, 50 μ L of plasma was mixed with 10 μ L of internal standard and 500 μ L of ethyl acetate was added. The sample was vortexed and centrifuged at 13000 rpm for 5 minutes and 400 μ L supernatant was separated. The samples were dried and analyzed at PhenoSwitch Biosciences, QC. A standard curve was generated using rat plasma that was spiked with 1000 ng/ml MRN and serially diluted. The standard curve samples were then spiked with 10 μ l of internal standard working solution (0.25 ng/ml amrinone) and extracted with 500 μ l of ethyl acetate and 400 μ l of supernatant was dried. All samples were reconstituted in 40 μ l of mobile phase A and analysed by LC-MS/MS.

The acquisition was performed with an LCMS-8060 (Shimadzu) equipped with an electrospray interface, coupled to a Nexera Labsolution software was used to control the instrument. Separation was performed on a reversed phase Kinetex XB 50mm x 2.1 mm column which was maintained at 40°C. Samples were injected by loop overfilling into a 5µL loop. For the 6 min LC gradient, the

mobile phase consisted of the following solvent A (5 mM ammonium formate at pH 4.5 in water) and solvent B (5mM ammonium formate in methanol) at a flow rate of 400 μ L/min. The gradient started at 95:5 A:B. Samples were quantified using the area under the curve (AUC) and a standard curve. Samples were integrated using the Browser extension from the Labsolution suite.

5.3.15 Echocardiography Procedure

Echocardiographic examinations were performed under inhaled isoflurane anesthesia (2.5% in oxygen, 500–700 mL/minute). Transthoracic echocardiography was performed for each rat as a baseline before the surgery, 48 hrs post surgery, 60 mins post injection, 24 hrs post injection, 48 hrs post injection and 1-week post injection. Echocardiograms were obtained with a commercially available system (Micromaxx P04224; SonoSite, Bothell, WA), equipped with a linear probe 7–13 MHz 25 mm footprint turbo transducer (P06519.11; SonoSite). Briefly, LV end-diastolic diameters (LVEDD) and end-systolic diameters (LVESD) were measured with M-mode tracings between the anterior and posterior walls from the parasternal short-axis view just below the level of the papillary muscles of the mitral valve ¹³. The time of end-diastole was defined as time of maximum diameter of the LV in one heart cycle. Accordingly, end-systole was defined as the minimum diameter. Following the American Society of Echocardiology leading-edge method, two images on average were obtained in each view and averaged over three consecutive cycles ²⁶⁻²⁷.

The left-ventricular end-diastolic volume (LVEDV) and left-ventricular end-systolic volume (LVESV) were measured using the Teichholz formula ^{13, 27}:

LVEDV =
$$(\frac{7.0 \times \text{LVEDD}^3}{2.4 + \text{LVEDD}})$$

LVESV = $(\frac{7.0 \times \text{LVESD}^3}{2.4 + \text{LVESD}})$

Left ventricular ejection fraction (LVEF) was determined as:

Ejection Fraction
$$\% = (\frac{LVEDV - LVESV}{LVEDV}) * 100$$

Left-ventricular fractional shortening (LVFS) was determined as:

Fractional Shortening
$$\% = (\frac{LVEDD - LVESD}{LVEDD}) * 100$$

5.3.16 Cytokine Measurement

The cytokine analysis for levels of IL-6, IL-10 and tumor necrosis factor-alpha (TNF- α) was performed using commercially available ELISA kits according to the manufacturer's instructions. Microtiter plates were precoated with a murine monoclonal antibody against the rat cytokine being measured. Standards of the analyte and serum samples were added in triplicate. The absorbance was read at 450 nm within 30 minutes of stopping the reaction and standard curves were plotted.

5.3.17 Tissue Collection and Histological Analysis

After 1 week of treatment, the animals were anesthetized and sacrificed using pentobarbital sodium (100 mg/kg) overdose. The heart, lungs, liver and kidney were excised rapidly and washed with cold saline to remove excess blood and then fixed in neutral-buffered 10% formalin for 48 hrs. The tissues were trimmed to 3 mm thickness and stored in 70% ethanol in histology cassettes. The tissues were paraffin-embedded and processed into 4-5 μm thick sections on slides (The Rosalind and Morrison Goodman Cancer Research Institute, McGill University). The tissue slides were stained with hematoxylin-eosin following manufacturer's instructions and observed by confocal microscopy at 400X.

5.4 Results

5.4.1 Synthesis of AT1-HSA-MRN-NPs

The AT1-nanoformulation was developed for targeted delivery of MRN to the site of heart failure in animals. The overexpression of the AT1 receptors in cardiomyocytes allows for improved targeting of the AT1 peptide and hence greater uptake of the nanoparticle ²⁸. The AT1 peptide is an 8-amino acid peptide chain of Asp-Arg-Val-Tyr-Ile-His-Pro-Phe. On the N-terminal of the chain, 4 Gly residues were added to serve as a spacer to form NH₂-Gly-Gly-Gly-Gly-Asp-Arg-Val-Tyr-Ile-His-Pro-Phe-NH₂ as given in a study by Dvir et al ¹⁶. The synthesis of the AT1-HSA was through a two-step chemical reaction using heterobifunctional cross-linkers. In the first step, the primary amines present on the surface of HSA molecules react with the amines on PA-(PEG)₄-SPA. In the second step, EDC (pH 5.5) and Sulfo-NHS were added followed by addition of the AT1 peptide. The EDC reacts with the carboxyl group on one end and Sulfo-NHS reacts with

amine present on the AT1 peptide, releasing the unstable intermediates and forming AT1-HSA (**Figure 5.1**).

The targeted nanoparticle formulation was prepared as mentioned earlier, following the ethanol desolvation procedure ^{10, 19-20}. Here, the HSA was replaced with AT1-HSA to form nanoparticles. AT1-HSA was mixed with MRN in AT1-HSA/MRN (wt./wt.) ratio of 1:10, 1:20, 1:40 and 1:80.

5.4.2 Mass Spectrometry Analysis of AT1-HSA

To validate the conjugation of AT1 with HSA, MALDI-TOF-MS was performed to compare the average molecular weight change between HSA and AT1-HSA. The mass-to-charge ratio (m/z) of the green peak (AT1-HSA) was approximately 5600 higher than the red peak (HSA) (**Figure 5.2**). Since the molecular weights of the AT1, PA-(PEG)₄-SPA, EDC and Sulfo-NHS are 1274, 435.4, 190 and 217 g/mol, respectively, at least 2 molecules of the AT1 peptide may be successfully conjugated to the surface of each HSA molecule.

5.4.3 Quantification of AT1 Peptide bound to HSA

The quantity of AT1-peptide attached to the HSA molecule was determined by UV-visible spectrophotometry. Results suggested that approximately 82.9 ± 1.6 % of the starting concentration of the AT1-peptide remained bound to the surface of HSA after the chemical conjugation reaction. This translates to approximately 2.57 µmoles of peptide bound to approximately 0.22 µmoles of HSA.

5.4.4 Characterization of the AT1-HSA-MRN-NPs

The size of the nanoparticles was determined by DLS and zeta potential was measured by laser Doppler anemometry. The particle size and zeta potential of AT1-nanoparticle formulation at AT1-HSA/MRN (wt./wt.) ratio of 1:10 was 190.2±5.7 nm with a zeta potential of -29.5±3.7 mV. The size of the nanoparticles at AT1-HSA/MRN (wt./wt.) ratio of 1:20 was 205.6±3.8 nm with zeta potential of -27.5±4.6 mV. The size of the nanoparticles at AT1-HSA/MRN (wt./wt.) ratio of 1:40 was 225.4±2.8 nm with zeta potential of -20.5±4.4 mV. The size of the nanoparticles at AT1-HSA/MRN (wt./wt.) ratio of 1:80 was 245.6±3.5 nm with zeta potential of -18.7±6.6 mV. These results suggest that as the quantity of MRN bound to the nanoparticles increased, there was

reduction in the size of the nanoparticles and the zeta potential became more negative, indicating greater physical stability of the particles. The yield and drug encapsulation efficiency of the AT1-nanoparticles has been summarized in **Table 5.1**.

The morphology of the nanoparticles observed by TEM under 17800X (**Figure 5.3(a**)) and 105000X magnification exhibited a near spherical shape with moderately uniform particle size and distribution (**Figure 5.3(b**)). Under 135000X magnification, the AT1-HSA-MRN-NPs had a dark core surrounded by a bright membrane, which confirmed the distinct layer of peptide bound to the surface (**Figure 5.3(c**)).

5.4.5 In Vitro Cumulative Milrinone Release Analysis

The drug release from AT1-HSA-MRN-NPs was studied by suspending 40 mg of nanoparticles in 10 mL PBS at 37 °C and 120 rpm, with a starting MRN concentration of 0.8 mg/mL prepared from MRN/AT1-HSA (wt./wt.) ratio of 1:10. Results suggested that MRN showed a sustained release with about 50% of the MRN released between 4-6 hrs after which the release became slower with up to 75% of the MRN being released by 24 hrs (**Figure 5.4**).

5.4.6 Pharmacokinetics Analysis

To determine MRN pharmacokinetics, female Lewis rats were divided into three groups. Group I received an injection of saline, Group II was injected with AT1-HSA-MRN-NPs at MRN dose of 50 μg/kg and Group III received MRN-Lactate at MRN concentration of 50 μg/kg. The MRN plasma concentration-time curves of the intravenously administered formulations has been represented in **Figure 5.5**. Results suggest that the MRN-Lactate was removed from circulation much quicker than the AT1-HSA-MRN-NPs. The MRN-Lactate concentration 6 hours post injection was extremely low, however MRN released from the AT1-nanoparticles was detected even 6 hours post injection. The clearance of the AT1-HSA-MRN-NPs was significantly delayed. The mean pharmacokinetic parameters were calculated using a non-compartmental method and have been listed in **Table 5.2**. For AT1-HSA-MRN-NPs, the MRT was 123.7 min, AUC was 183.9 ng*h/mL, half-life was 101.3 min and clearance rate was 0.24 L/kg*h. For MRN-Lactate, the MRT was 49.1 min, AUC was 104.3 ng*h/mL, half-life was 64.7 min and clearance rate was 0.47 L/kg*h.

5.4.7 Tissue Distribution of AT1-HSA-MRN-NPs

The concentration of MRN in AT1-HSA-MRN-NPs and MRN-Lactate was investigated after intravenous administration of the formulations in female Lewis rats. The amounts of MRN detected at 2 hrs time point in different tissues such as heart, lungs, kidneys and liver have been shown in **Figure 5.6**. For lungs, the MRN detected in the MRN-Lactate group vs AT1-HSA-MRN-NPs was 7.55±0.01 vs 7.88±0.09 ng/mL, for kidneys was 4.80±0.6 vs 2.64±0.30 ng/mL, and for liver was 2.44±0.23 vs 1.27±0.14 ng/mL. This may be due to the passive targeting of albumin nanoparticles. Interestingly, the amount of MRN detected in the heart was significantly higher (*P*<0.01) in case of the AT1-HSA-MRN-NPs group (7.88±1.4 ng/mL) vs the MRN-Lactate (2.00±1.01 ng/mL). The MRN uptake by the heart was significantly greater than the MRN detected in other tissues for Group II, which indicates the target specificity of the nanoparticles towards the AT1 receptors present on the myocardium. For the same group, there was no significant difference in MRN uptake between the heart and lungs.

5.4.8 Milrinone Quantification from Rat Plasma

Both MRN and amrinone were detected by LC-MS. Results showed that at 24 hours post treatment, the MRN detected in plasma in Group II was significantly greater than in Groups III (p=0.0007) and V (p=0.0010) (Group II 16.5±4.6 ng/mL vs Group III 0.3±0.1 ng/mL and Group V 1.2±0.1 ng/mL) (**Figure 5.7**).

5.4.9 Safety and Toxicity of AT1-nanoparticle formulation

The serum samples collected from the animals were analyzed for markers of safety and toxicity. The liver function and toxicity analysis were performed by analysing alkaline phosphatase (ALP), aspartate aminotransferase (AST) and alkaline aminotransferase (ALT), respectively (**Figure 5.8**). Results show that there were no significant differences in the ALP levels between the groups and all values fall in the normal range of 16 - 302 U/L for rats. The levels of ALT enzyme for group III were lower than group V (p=0.0350), but were within the normal range of 20 - 61 U/L. The AST enzyme levels of group II were elevated as compared to group I (p=0.0273), however, were well within the normal range of 39 - 111 U/L and did not differ significantly between the control and other treatment groups. The GGT levels were also measured and were found to be in range (0 - 6 U/L) for all groups. To evaluate the renal function, creatinine and urea were analyzed (**Figure**

5.9). It was found that though there was no significant difference in the creatinine levels amongst the groups, these values were lower than the normal range of $50 - 73 \,\mu\text{mol/L}$. This is indicative of renal dysfunction which is commonly associated with heart disease. There were significant differences in urea levels between the Groups I and IV (p=0.0096) and Groups IV and V (p=0.0096), however the levels were found to be in the normal range overall (3.2 – 7.5 mmol/L).

5.4.10 Cardiac Function Assessment

The echocardiographic parameters were analyzed by comparing the baseline values with the subsequent echocardiographic measurements taken post surgery and injection. The percentage left ventricular ejection fraction (LVEF %) and percentage left ventricular fractional shortening (LVFS %) were measured for all the groups at pre-operation/ligation, 48 hours post ligation, 60 mins post treatment injections, 24 hrs post injections, 48 hrs post injections and 1-week post injection (Tables 5.3 & 5.4). The EF was not significantly different between the groups preoperatively (baseline) and 48 hrs post ligation (**Figure 5.10**). A two-way ANOVA determined that the EF at 60 mins post injection for Group II (84.3±2.9 %) was higher than Group I (68.6±2.2 %) (p=0.0003) and Group IV (70.1±2.3 %) (p=0.0006) however, not significantly different than Groups III (p=0.3846) and V (p=0.1744). At 24 hrs post injection, the EF for Group II remained consistent until 1-week post ligation. At 24 hrs post treatment, there was a reduction in EF for Group III $(70.6\pm3.6\%)$, which was significantly lower (p=0.0152) than Group II (84.2±4.8%) in addition to Groups I and IV. This effect stayed consistent at 48 hrs post injection with a reduction in Group V $(72.7\pm2.3\%)$ EF as well, which was lower (p=0.0114) than that of Group II $(83.1\pm3.6\%)$. This indicates that the intravenous delivery route worked better for targeted drug delivery as compared to the subcutaneous route of delivery in terms of sustained drug release. At 1-week post injections, there was no significant differences between Groups II, III and V, however EF of Groups II was higher than Group I (p=0.0038) and IV (p=0.0259).

Similarly, for FS measurements (**Figure 5.11**) there was no significant differences amongst the groups either pre-ligation or 48 hrs post ligation. However, in accordance with EF measurements, the FS for Group II (50.1 ± 3.8 %) was significantly higher than that of Groups I (32.8 ± 1.7 %) (p=0.0016) and IV (34.7 ± 4.0 %) (p=0.0037) at 60 mins post injection, with no significant difference from groups III and V. The FS of group III was reduced at 24 hrs (33.6 ± 3.9 %) and 48

hrs (30.2 \pm 3.9 %) post injection, which was significantly lower (p=0.0014) than that of Group II at those time points (50.4 \pm 3.1 % and 46.5 \pm 3.1 %, respectively). A similar effect was observed for Group V as well in which the FS was reduced significantly in comparison to Group II at 24 hrs (40.5 \pm 2.8 %) (p=0.0107) and 48 hrs (34.8 \pm 1.7 %,) (p=0.0029). At 1-week post injections, there was reduction in FS of Group II with no significant differences amongst the groups, except with Group IV (p=0.0182).

5.4.11 Serum Cytokine Measurements

The serum cytokine levels of IL-6, IL-10 and TNF- α were measured at 1-week post treatment (**Figure 5.12**). Serum TNF- α levels were significantly different amongst the groups with control Groups I at 40.7±3.8 pg/mL and Group IV at 40.3±1.8 pg/mL, which was higher (P<0.0001) than that of Group II (9.2±0.6 pg/mL), Group III (17.1±2.8 pg/mL) and Group V (11.1±0.9 pg/mL) (Figure). The Group II and Group V TNF- α levels were significantly higher (P<0.05) than the serum TNF- α levels of Group III (p=0.0442), with no significant difference between Groups II and V. Serum IL-6 levels were significantly different between the groups. Group I and Group IV IL-6 levels (58.2±11.3 pg/mL and 57.1±12.8 pg/mL) were significantly higher (P<0.05) than that of Group II (24.9±6.2 pg/mL), Group III (39.3±2.7 pg/mL) and Group V (22.6±5.4 pg/mL) (p=0.0137). There were no significant differences between Groups I and IV and between Groups II, III and V. However, the anti-inflammatory cytokine IL-10 levels in Group II (67.3±15.5 pg/mL) and IV (71.1±12.1 pg/mL) were significantly lower (P<0.05) than Group II (184.4±32.7 pg/mL), Group III (146.1±24.7 pg/mL) and Group V (181.6±77.3 pg/mL).

5.4.12 Safety and Toxicity Analysis

The hematoxylin-eosin staining was performed to analyze the inflammation caused due to coronary artery ligation in all groups. The cardiomyocytes observed on the heart sections showed varying sizes and uneven staining. Additionally, the cell diameter was enlarged with higher intercellular space and an irregular arrangement of cardiac muscle fibers was observed. There was no significant differences in the mean percentage of the inflamed area due to infarction in Group I (13.6±3.2 %), Group II (14.6±3.1 %), Group III (10.8±2.3 %), Group IV (12.8±1.7 %) and Group V (9.6±1.5 %) (**Figure 5.13**). This confirmed the occurrence of heart failure due to coronary artery ligation surgery.

5.5 Discussion

Nanoparticle-based technology has advanced significantly in the last few decades with numerous applications in the field of medicine and healthcare. The use of nanoparticle-based drug delivery systems has shown innovative strategies of loading and delivering drugs, genes, hormones, small molecules etc. in both targeted and non-targeted ways ^{12, 29}. Delivering drugs using nanoparticles as delivery vehicles allows for targeted and site-specific delivery, controlled drug release, enhanced bioavailability, improved safety and reduced toxicity ^{5-6, 30}. Though most of these formulations have been tested and approved for use in cancer, their use in cardiovascular applications such as congestive heart failure is equally promising with maximum focus on in-stent restenosis and the use of microparticles for drug delivery ³¹.

In the present study, AT1-HSA-MRN-NPs have been successfully prepared as a novel heart-targeted formulation for site-specific delivery of the MRN using albumin nanoparticles, surface functionalized with the ligand, AT1 peptide. Under conditions of MI and HF, AT1 receptors, present on the myocardium, are found to be overexpressed ³²⁻³⁴. Thus, the AT1 receptors specific for the angiotensin II peptide, facilitates uptake of the AT1-HSA-MRN-NPs through receptor mediated endocytosis allowing for site-specific unloading of the MRN drug. The albumin protein is a heterodimer with sites for binding many hydrophobic and hydrophilic molecules along with active functional groups such as amino and carboxylic groups for covalent conjugation ³⁵⁻³⁶. Exploiting these properties, the HSA molecule was first surface-modified to bind the AT1 ligand using PA-(PEG)₄-SPA, EDC and Sulfo-NHS as crosslinkers. This was confirmed through mass spectrometry which suggested that at least 2 molecules of AT1 were bound to the HSA molecule (Figure). Also, UV-visible spectrophotometry analysis revealed that approximately 83% of the AT1 peptide remained bound to albumin post the covalent chemical conjugation treatment and purification.

The newly synthesized AT1-HSA was used to bind MRN and prepare AT1-HSA-MRN-NPs of particle size 190.2±5.7 nm and zeta potential of -29.5±3.7 mV. It is known that the optimal nanoparticle size to avoid rapid clearance from the body by the RES and macrophages is up to 250 nm with a highly positive or highly negative surface charge ³⁷⁻³⁸. Therefore, the particles developed in this study were reproducible with the intended nanoparticle diameter. The release of MRN from

the nanoparticles was also tested in vitro at different MRN/HSA (w/w) concentrations. The nanoparticles prepared at MRN/HSA (w/w) ratio of 1:10 were found to have a more sustained drug release in comparison with the other formulations. Typically, post IV injections, a controlled and sustained drug release is desired as opposed to a burst release effect. A sustained nanoparticle-drug release may thus eliminate the requirement of a continuous drug infusion or multiple drug injections for treatment.

The pharmacokinetics of the AT1-HSA-MRN-NPs and MRN-Lactate were studied in a rat model at MRN dose of 50 µg/kg in a 0.25 mL IV injection at 0, 5, 15, 30, 45, 120 and 360 minutes. Compared to MRN-Lactate, the AT1-HSA-MRN-NPs showed a higher AUC and prolonged residence of the MRN in blood. Further, the higher accumulation of the drug in the heart at 2 hrs demonstrated that the nanoparticles could be targeted to the heart and reduce the side effects of the drug to other organs. When MRN-Lactate is intravenously injected, the direct interaction of the drug results in its fast elimination, however, loading the drug onto nanoparticles prevents exposure of the drug to blood components, acting as a reservoir for a maintaining a controlled release over time. Thus, it may be concluded that the nanoparticles improve the bioavailability of MRN with prolonged drug retention and targeted uptake by the tissue, *in vivo*.

Milrinone has been widely used for the treatment congestive heart failure resulting in a low cardiac output, right ventricular failure and pulmonary tension. For patients with end stage heart failure, awaiting heart transplantation or ventricular assist devices, MRN is used as a long-term continuous infusion ³⁹⁻⁴⁰. In this study, administering the AT1-HSA-MRN-NPs led to significant recovery of the left ventricular contractility as compared to MRN Lactate and other controls. At 24 hrs, approximately 16.5 ng/mL of MRN was detected in plasma of group II as opposed to 0.3 ng/mL in Group III. The recovery of heart function was evaluated by measuring both LVEF and LVFS. Both LVEF and LVFS first decreased in response to the infarction created for 48 hours. On injecting the formulations, the LVEF increased significantly for Groups II, III and group V, when observed at 60 mins post treatment, with no significant difference in Groups I and IV. There was no significant change in the LVEF of Group II until 48 hrs post treatment, however, the effect of MRN Lactate began to decrease with a reduction in LVEF over 48 hrs and 1 week. There were no significant variations between Groups II and V. Thus, the subcutaneous route of delivery did not

show any difference from the intravenous delivery route. There was a similar trend in the LVFS parameter as well. It can be concluded that the AT1-HSA-MRN-NPs helped improve the overall cardiac function post heart failure. These results were in alignment with a similar study done using microparticles containing MRN Lactate 23 . In fact, in the current study, the effect of the sustained MRN release from the nanoparticles was visible for up to 7 days post treatment, indicated by the ejection fraction and fractional shortening. The administered MRN dose of 50 μ g/kg in nanoparticles and MRN Lactate was also consistent with previous studies. Though, it is anticipated that injecting a higher dose of MRN in the nanoparticles will allow present an improved drug release behaviour and thus deliver a larger quantity of drug in lesser time, without a cytotoxic effect.

To verify the model of congestive heart failure in rats, H&E staining of the heart tissue was performed. Further, a cytokine analysis was performed. Previous studies were mainly focused on determining the tissue levels of cytokines post infarction and not the serum levels. Hence the cytokine levels in serum were determined with a focus on IL-6, IL-10 and TNF-α. The IL-6 and TNF-α levels were elevated in the infarcted myocardium as a result of remodelling, whereas the IL-10 levels were reduced. The groups treated with AT1-HSA-MRN-NPs had significantly reduced IL-6 and TNF-α, whereas the cardioprotective anti-inflammatory cytokine IL-10 was higher. Though, it is usual to observe higher pro-inflammatory cytokine levels even 1-week post infarction ¹³. So, a beneficial effect of the novel nanoparticle formulation could be observed with the reduction in pro-inflammatory cytokines and elevation of the anti-inflammatory cytokines.

Thus, this novel targeted nanoparticle formulation presents a new approach towards the treatment of congestive heart failure. This is the first study to deliver a cardiac inotropic drug in a targeted manner using biodegradable nanoparticles, displaying the effectiveness of the nanoparticle formulation in comparison with the free drug. Though, the nanoparticle formulation was delivered intravenously and subcutaneously in this study, an intranasal route of delivery could be evaluated as a non-invasive procedure for future work. Though in the current study, targeted albumin nanoparticles were synthesized to deliver a drug, it is anticipated that the effect of this treatment could be further enhanced by using this nanoparticle system to also deliver genes or growth factors in addition to drugs, promoting myocardial regeneration. Additionally, it has been reported that

the phosphodiesterase-3 varies across different species. Thus, investigating the effects of this novel nanoparticle formulation would be useful in developing a comprehensive understanding of the species variation.

5.6 Conclusions

A novel nanoparticle formulation was developed for targeted MRN delivery. The HSA was surface-modified to form the new AT1-HSA compound, which was used to develop the AT1-HSA-MRN-NPs. As compared to the non-targeted MRN drug, the AT1-HSA-MRN-NPs exhibited prolonged drug release *in vitro* and superior pharmacokinetics and tissue distribution of MRN *in vivo*, improved cardiac function recovery, lesser toxicity, and better pro-inflammatory/anti-inflammatory serum cytokine levels (IL-6, TNF-α and IL-10) when evaluated in a rat model of congestive heart failure. Thus, this presents a new strategy of delivering hemodynamically stable drugs in a prolonged manner with a sustained release profile with negligible side effects. This also presents the feasibility and effectiveness of nanoparticle-based formulations in cardiovascular medicine. This novel nanoparticle formulation could thus be used as a potent, safe and non-toxic heart failure medication, with potential for use in other cardiovascular diseases.

5.7 Acknowledgements

This work is supported by the research funding granted to Dr. Satya Prakash from Canadian Institute of Health Research (CIHR) and the Natural Sciences and Engineering Research Council (NSERC). The authors are grateful to Mr. Xue Dong Liu for assistance in TEM imaging (Facility for Electron Microscopy Research, Materials Engineering, McGill University) and Mr. Nadim Saadeh for help with Mass Spectroscopy (Mass Spectroscopy Facility, Department of Chemistry, McGill University). The authors are also thankful to Dr. Aurore Dodelet-Devillers, Ms. Anna Choy, Ms. Annie Leblanc and Ms. Stephanie Lantosca at the Animal Resource Division, RI-MUHC, Montreal. The authors acknowledge Dr. Hugo Gagnon and Dr. Jean-Philippe Couture at PhenoSwitch Bioscience Inc. for their assistance with quantification of milrinone.

5.8 References

Benjamin, E. J. *et al.* Heart disease and stroke statistics—2018 update: a report from the American Heart Association. *Circulation* **137**, e67-e492 (2018).

- 2 Benetis, R. Surgical treatment of congestive heart failure in coronary artery disease. (2005).
- Giardiello, M. *et al.* Accelerated oral nanomedicine discovery from miniaturized screening to clinical production exemplified by paediatric HIV nanotherapies. *Nature communications* **7**, 13184 (2016).
- 4 Martín Giménez, V. M., Kassuha, D. E. & Manucha, W. Nanomedicine applied to cardiovascular diseases: latest developments. *Therapeutic advances in cardiovascular disease* **11**, 133-142 (2017).
- Ferreira, M. P. *et al.* Drug-Loaded Multifunctional Nanoparticles Targeted to the Endocardial Layer of the Injured Heart Modulate Hypertrophic Signaling. *Small* **13**, 1701276 (2017).
- 6 Chang, M.-Y. *et al.* Functionalized nanoparticles provide early cardioprotection after acute myocardial infarction. *Journal of controlled release* **170**, 287-294 (2013).
- Diao, J. *et al.* PEG–PLA nanoparticles facilitate siRNA knockdown in adult zebrafish heart. *Developmental biology* **406**, 196-202 (2015).
- 8 Hennig, R., Pollinger, K., Tessmar, J. & Goepferich, A. Multivalent targeting of AT1 receptors with angiotensin II-functionalized nanoparticles. *Journal of drug targeting* **23**, 681-689 (2015).
- 9 Lomis, N. *et al.* Human Serum Albumin Nanoparticles for Use in Cancer Drug Delivery: Process Optimization and In Vitro Characterization. *Nanomaterials* **6**, 116 (2016).
- Lomis, N. *et al.* Novel Milrinone Nanoformulation for Use in Cardiovascular Diseases: Preparation and in Vitro Characterization. *Molecular pharmaceutics* **15**, 2489-2502 (2017).
- Mudshinge, S. R., Deore, A. B., Patil, S. & Bhalgat, C. M. Nanoparticles: emerging carriers for drug delivery. *Saudi pharmaceutical journal* **19**, 129-141 (2011).
- Blanco, E., Shen, H. & Ferrari, M. Principles of nanoparticle design for overcoming biological barriers to drug delivery. *Nature biotechnology* **33**, 941 (2015).
- Binsalamah, Z. M., Paul, A., Khan, A. A., Prakash, S. & Shum-Tim, D. Intramyocardial sustained delivery of placental growth factor using nanoparticles as a vehicle for delivery in the rat infarct model. *International journal of nanomedicine* **6**, 2667 (2011).
- Paul, A. *et al.* Genipin-cross-linked microencapsulated human adipose stem cells augment transplant retention resulting in attenuation of chronically infarcted rat heart fibrosis and cardiac dysfunction. *Cell transplantation* **21**, 2735-2751 (2012).
- Loureiro, A., G Azoia, N., C Gomes, A. & Cavaco-Paulo, A. Albumin-based nanodevices as drug carriers. *Current pharmaceutical design* **22**, 1371-1390 (2016).
- Dvir, T. *et al.* Nanoparticles targeting the infarcted heart. *Nano letters* **11**, 4411-4414 (2011).
- Nakano, Y. *et al.* Nanoparticle-mediated delivery of irbesartan induces cardioprotection from myocardial ischemia-reperfusion injury by antagonizing monocyte-mediated inflammation. *Scientific reports* **6**, 29601 (2016).
- Liu, J. *et al.* Functionalized dendrimer-based delivery of angiotensin type 1 receptor siRNA for preserving cardiac function following infarction. *Biomaterials* **34**, 3729-3736 (2013).
- Langer, K. *et al.* Optimization of the preparation process for human serum albumin (HSA) nanoparticles. *International Journal of Pharmaceutics* **257**, 169-180 (2003).

- 20 Langer, K. *et al.* Human serum albumin (HSA) nanoparticles: reproducibility of preparation process and kinetics of enzymatic degradation. *International journal of pharmaceutics* **347**, 109-117 (2008).
- Siddiqui, M. *et al.* Application of DDQ and p-chloranilic acid for the spectrophotometric estimation of milrinone in pharmaceutical formulations. *Asian J Sci Res* **2**, 135-145 (2009).
- Abbasi, S., Paul, A., Shao, W. & Prakash, S. Cationic albumin nanoparticles for enhanced drug delivery to treat breast cancer: preparation and in vitro assessment. *Journal of drug delivery* **2012** (2011).
- Al Kindi, H. *et al.* Sustained release of milrinone delivered via microparticles in a rodent model of myocardial infarction. *The Journal of thoracic and cardiovascular surgery* **148**, 2316-2324 (2014).
- Drexler, H., Höing, S., Faude, F., Wollschläger, H. & Just, H. Central and regional vascular hemodynamics following intravenous milrinone in the conscious rat: comparison with dobutamine. *Journal of cardiovascular pharmacology* **9**, 563-569 (1987).
- Huang, M.-H. *et al.* Heart Protection by Combination Therapy with Esmolol and Milrinone at Late-Ischemia and Early Reperfusion. *Cardiovascular Drugs and Therapy* **25**, 223, doi:10.1007/s10557-011-6302-z (2011).
- Davani, S. *et al.* Mesenchymal progenitor cells differentiate into an endothelial phenotype, enhance vascular density, and improve heart function in a rat cellular cardiomyoplasty model. *Circulation* **108**, II-253-II-258 (2003).
- Wykrzykowska, J. J. *et al.* Autologous cardiomyotissue implantation promotes myocardial regeneration, decreases infarct size, and improves left ventricular function. *Circulation* **123**, 62-69 (2011).
- Paradis, P., Dali-Youcef, N., Paradis, F. W., Thibault, G. & Nemer, M. Overexpression of angiotensin II type I receptor in cardiomyocytes induces cardiac hypertrophy and remodeling. *Proceedings of the National Academy of Sciences* **97**, 931-936 (2000).
- Friedman, A. D., Claypool, S. E. & Liu, R. The smart targeting of nanoparticles. *Current pharmaceutical design* **19**, 6315-6329 (2013).
- Chen, B., He, X. Y., Yi, X. Q., Zhuo, R. X. & Cheng, S. X. Dual-peptide-functionalized albumin-based nanoparticles with ph-dependent self-assembly behavior for drug delivery. *ACS applied materials & interfaces* **7**, 15148-15153, doi:10.1021/acsami.5b03866 (2015).
- Bobo, D., Robinson, K. J., Islam, J., Thurecht, K. J. & Corrie, S. R. Nanoparticle-based medicines: a review of FDA-approved materials and clinical trials to date. *Pharmaceutical research* **33**, 2373-2387 (2016).
- Hennig, R., Pollinger, K., Tessmar, J. & Goepferich, A. Multivalent targeting of AT1 receptors with angiotensin II-functionalized nanoparticles. *J Drug Target* **23**, 681-689, doi:10.3109/1061186x.2015.1035276 (2015).
- Paradis, P., Dali-Youcef, N., Paradis, F. W., Thibault, G. & Nemer, M. Overexpression of angiotensin II type I receptor in cardiomyocytes induces cardiac hypertrophy and remodeling. *Proceedings of the National Academy of Sciences of the United States of America* **97**, 931-936 (2000).

- Rivard, K. *et al.* Overexpression of type I angiotensin II receptors impairs excitation-contraction coupling in the mouse heart. *American Journal of Physiology-Heart and Circulatory Physiology* (2011).
- Fasano, M. *et al.* The extraordinary ligand binding properties of human serum albumin. *IUBMB life* **57**, 787-796 (2005).
- Merlot, A. M., Kalinowski, D. S. & Richardson, D. R. Unraveling the mysteries of serum albumin—more than just a serum protein. *Frontiers in physiology* **5**, 299 (2014).
- Hirn, S. *et al.* Particle size-dependent and surface charge-dependent biodistribution of gold nanoparticles after intravenous administration. *European journal of pharmaceutics and biopharmaceutics* **77**, 407-416 (2011).
- Suen, W. L. L. & Chau, Y. Size-dependent internalisation of folate-decorated nanoparticles via the pathways of clathrin and caveolae-mediated endocytosis in ARPE-19 cells. *Journal of Pharmacy and Pharmacology* **66**, 564-573 (2014).
- 39 Ayres, J. K. & Maani, C. V. in *StatPearls [Internet]* (StatPearls Publishing, 2019).
- Chong, L. Y. Z., Satya, K., Kim, B. & Berkowitz, R. Milrinone dosing and a culture of caution in clinical practice. *Cardiology in review* **26**, 35-42 (2018).

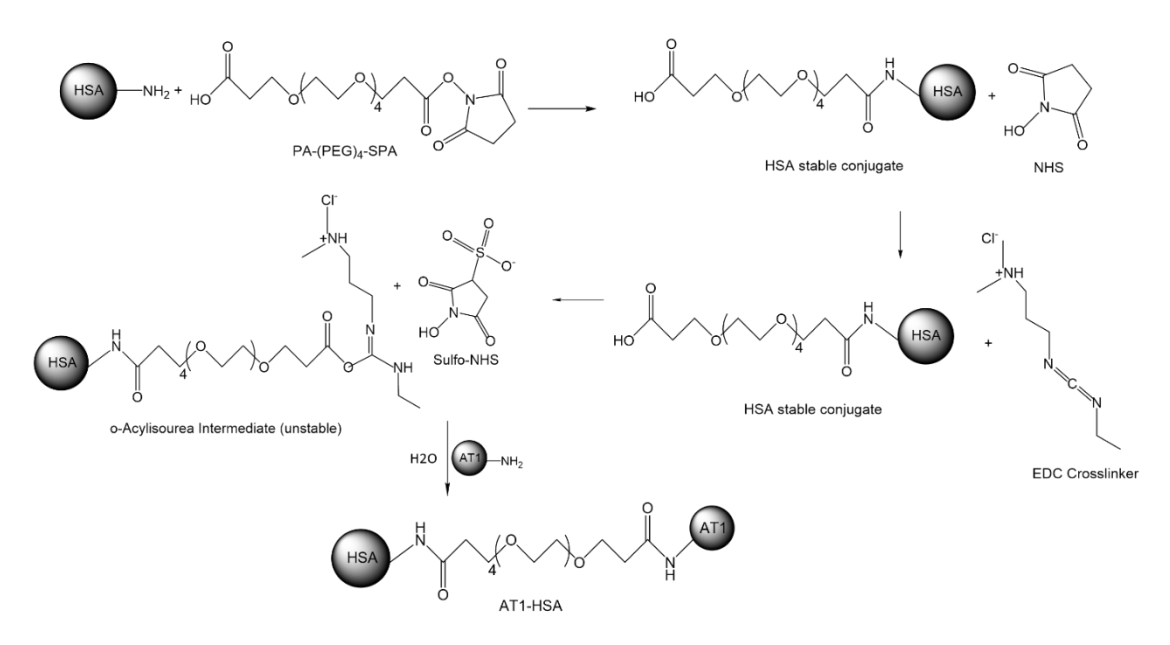


Figure 5.1. Schematic representation of the surface modification of the HSA molecule for binding with the AT1 peptide through a two-step chemical conjugation reaction using cross-linkers PA-(PEG)₄-SPA and EDC/Sulfo-NHS.

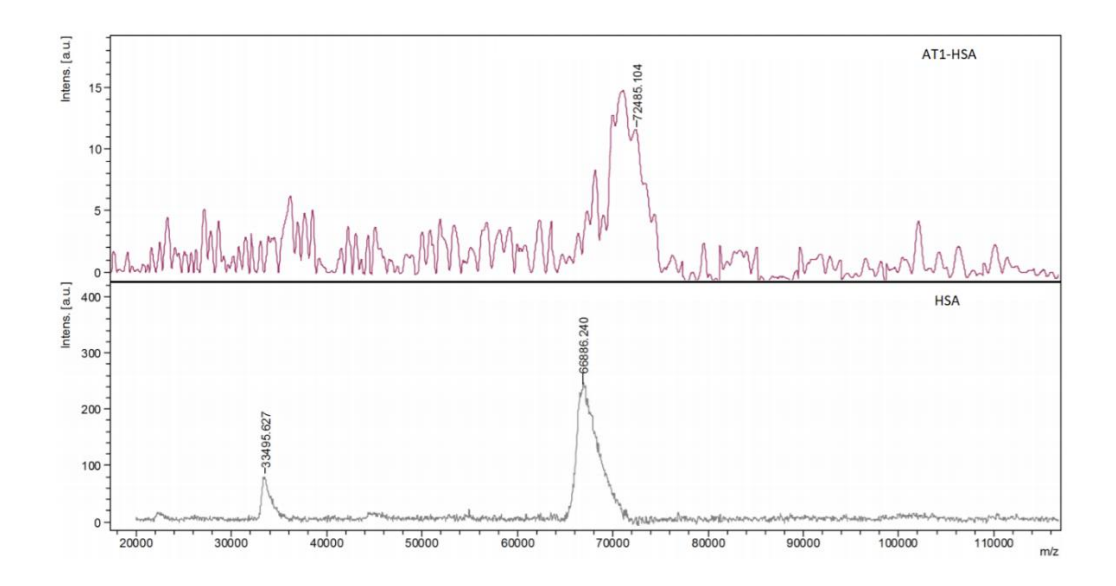


Figure 5.2. HSA (lower) and AT1-HSA (upper) was analyzed by Matrix-Assisted Laser Desorption/Ionization Time of Flight Mass Spectrometry. The m/z ratio of the AT1-HSA peak was at least 5600 higher than that of the HSA peak, which demonstrated that AT1 was successfully conjugated to the surface of HSA.

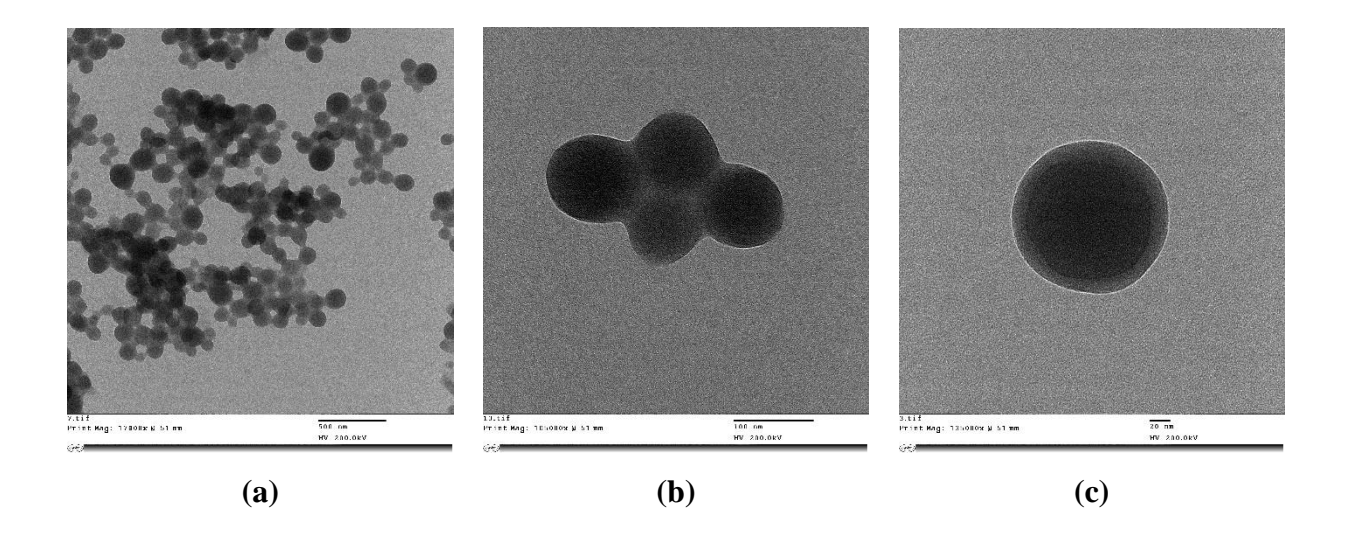


Figure 5.3. Nanoparticle surface characterization using TEM analysis: (a) Under magnification of 17800X, AT1-HSA-MRN-NPs of size 190.2±5.7 nm with a zeta potential of -29.5±3.7 mV (Scale = 500 nm) (b) Under magnification of 105000X, AT1-HSA-MRN-NPs with moderately uniform particle size (Scale = 100 nm); (c) Under 135000X magnification, the AT1-HSA-MRN-NPs display a dark core surrounded by a bright distinct membrane layer (Scale = 20 nm).

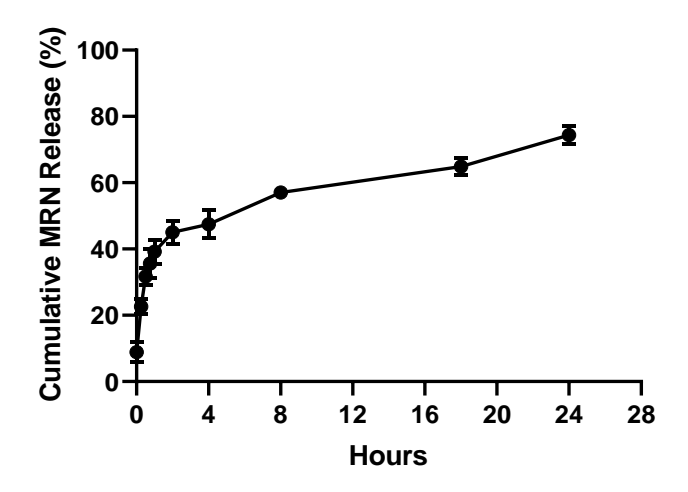


Figure 5.4. Cumulative drug release (mean \pm SD %, n = 3) of AT1-HSA-MRN-NPs with starting MRN concentrations 0.8 mg/mL over predetermined time intervals of 0, 0.25, 0.5, 0.75, 1, 2, 4, 8, 18 and 24 hrs.

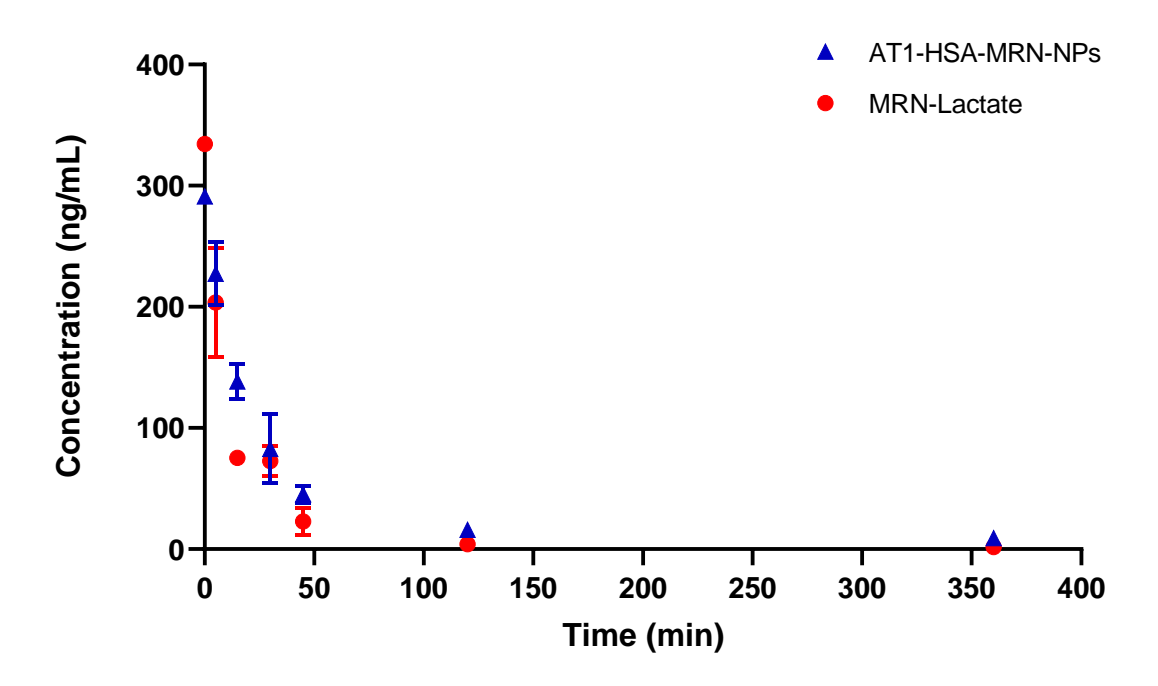


Figure 5.5. Pharmacokinetics of AT1-HSA-MRN-NPs and MRN-Lactate at an initial MRN dose of 50 μg/kg *in vivo*.

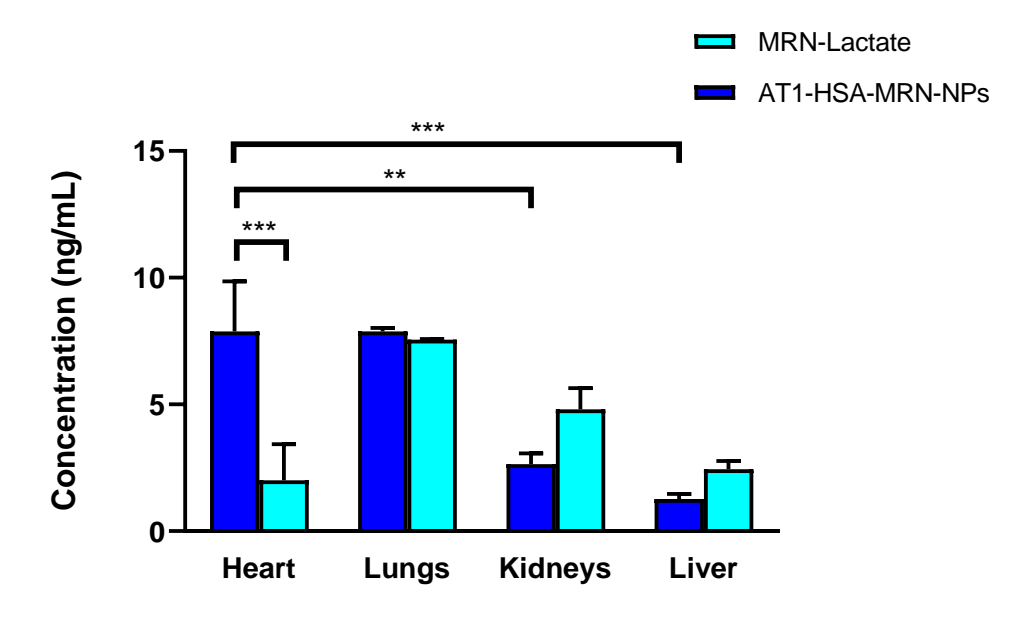


Figure 5.6. Tissue distribution of AT1-HSA-MRN-NPs and MRN-Lactate at an initial MRN dose of 50 μ g/kg *in vivo*. The graph shows a representative result of mean \pm SD (n=4). ***P<0.001 was considered highly significant and **P<0.01 was considered significant based on Tukey's posthoc analysis.

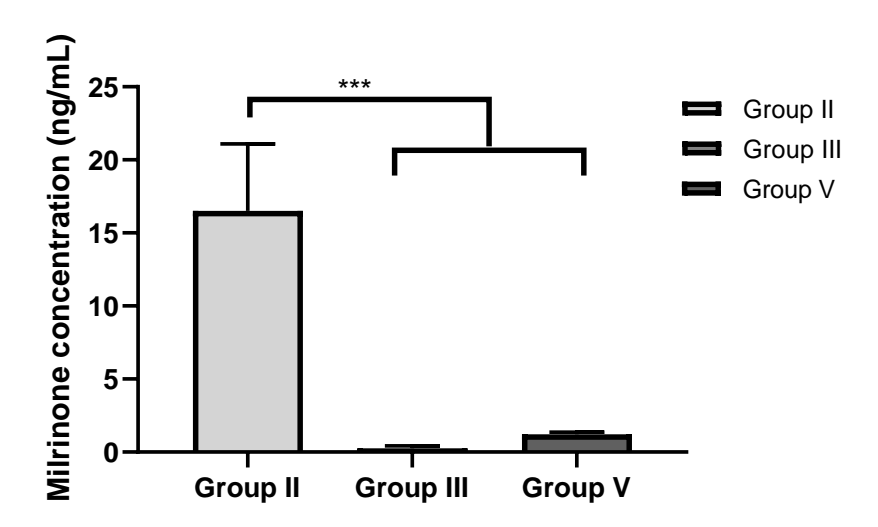


Figure 5.7. Milrinone levels detected in plasma 24 hrs post treatment for Groups II, III and V. The graph shows a representative result of mean \pm SD (n=3). ***P<0.001 was considered significant based on Tukey's posthoc analysis.

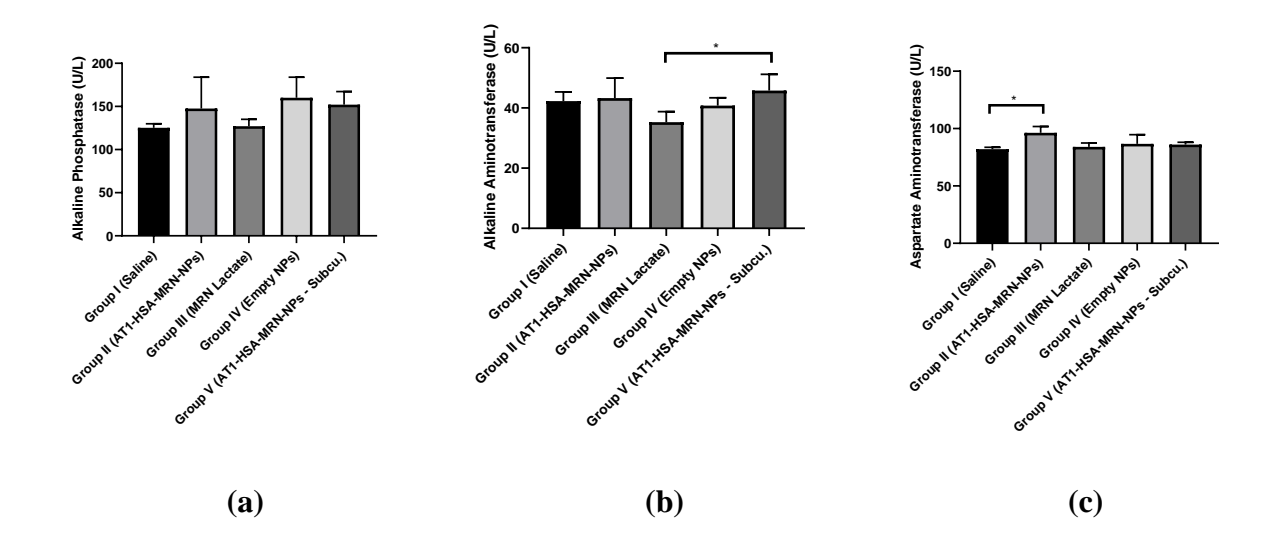


Figure 5.8. Serum analysis performed as a safety test comparing the (a) ALP (U/L), (b) ALT (U/L) and (c) AST (U/L) as liver function tests. The graph shows a representative result of mean \pm SD (n=5). *P<0.05 was considered significant based on Tukey's posthoc analysis.

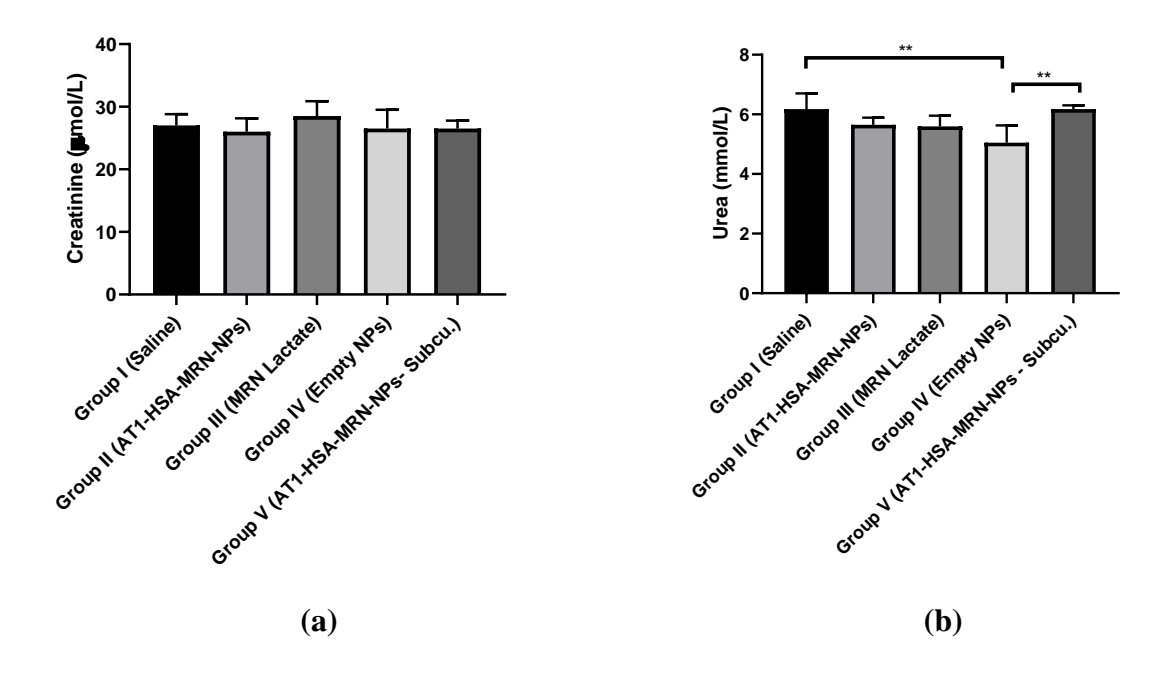


Figure 5.9. Serum analysis performed as a safety test comparing the (a) creatinine (μ mol/L) and (b) urea (mmol/L) as kidney function tests. The graph shows a representative result of mean \pm SD (n=5). **P<0.01 was considered significant based on Tukey's posthoc analysis.

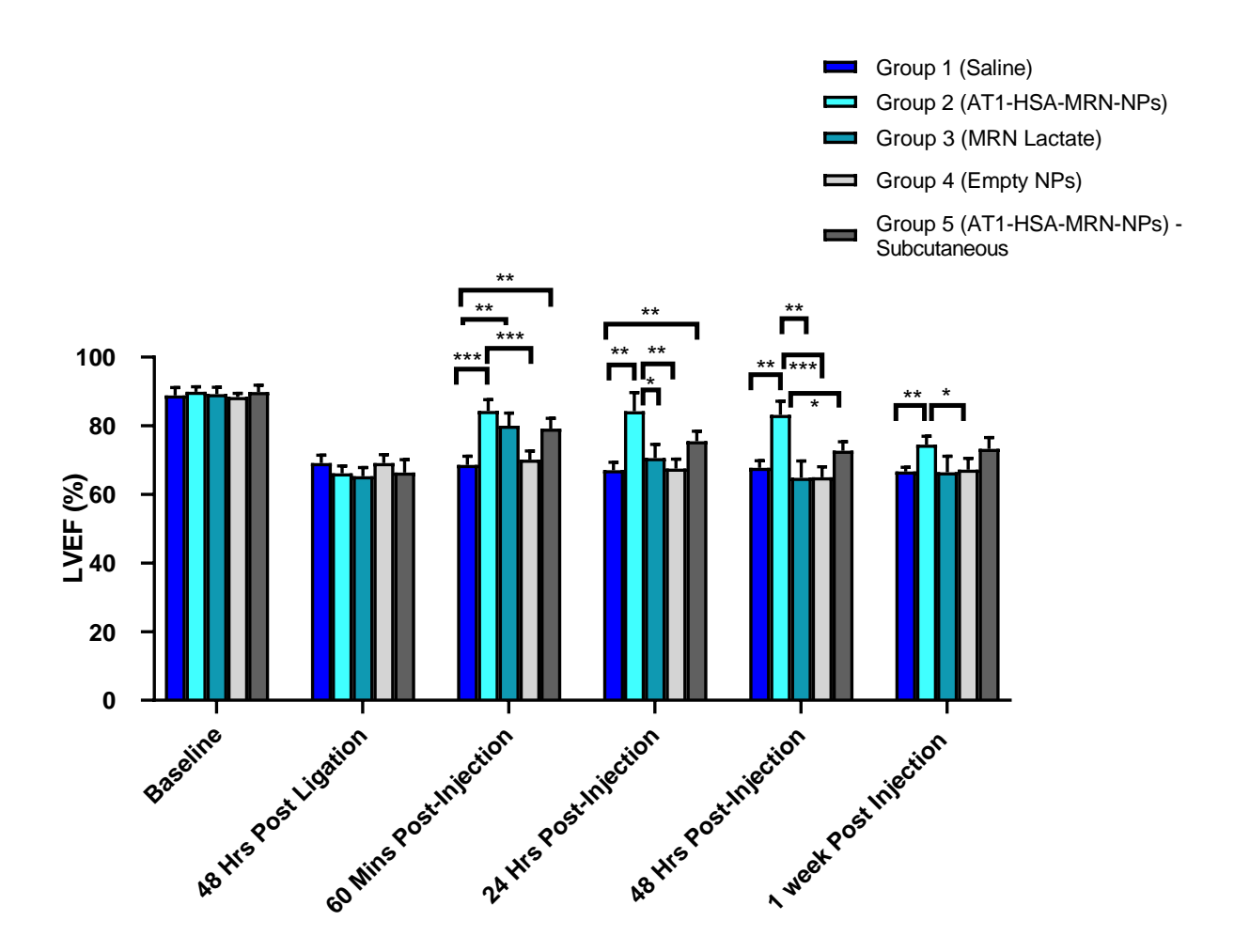
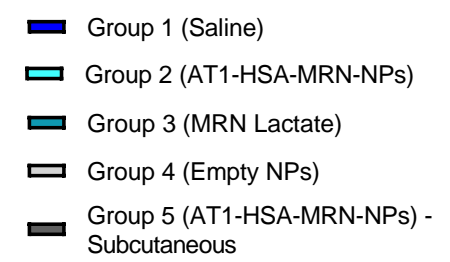


Figure 5.10. Percentage LVEF measurements for Groups I, II, III, IV and V at baseline, 48 hours post ligation, 60 mins, 24 hrs, 48 hrs and 1-week post injections. The graph shows a representative result of mean \pm SD (n=5). ***P<0.001, **P<0.01 and *P<0.05 were considered significant based on Tukey's posthoc analysis.



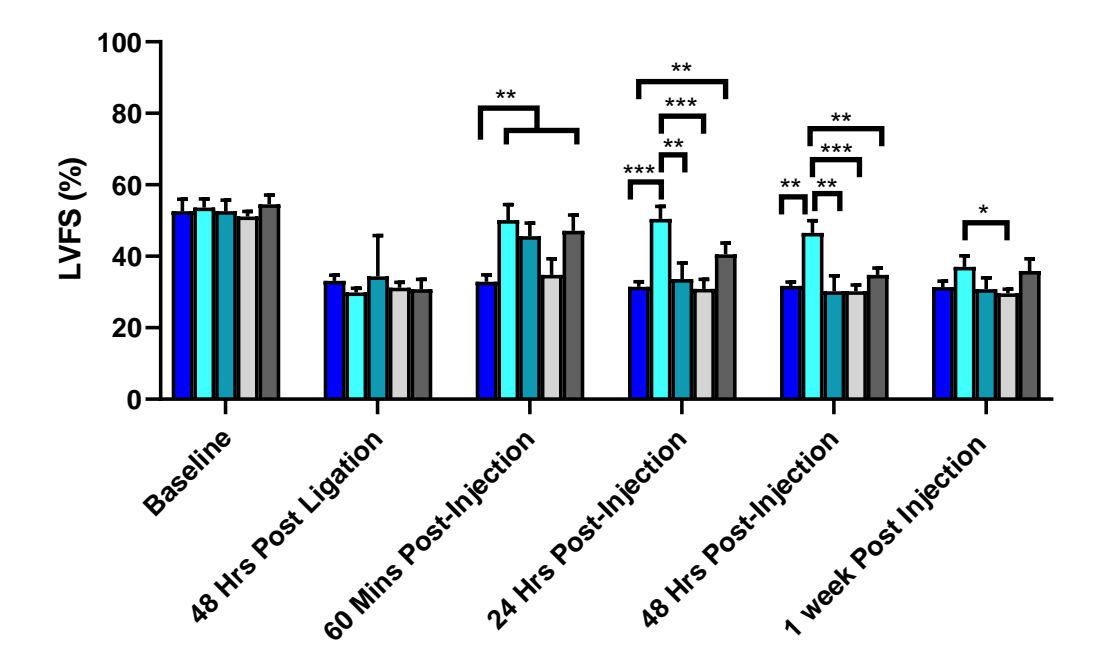


Figure 5.11. Percentage LVFS measurements for Groups I, II, III, IV and V at baseline, 48 hours post ligation, 60 mins, 24 hrs, 48 hrs and 1-week post injections. The data has been presented as mean \pm SD (n=5). ***P<0.001, **P<0.01, *P<0.05 were considered significant based on Tukey's posthoc analysis.

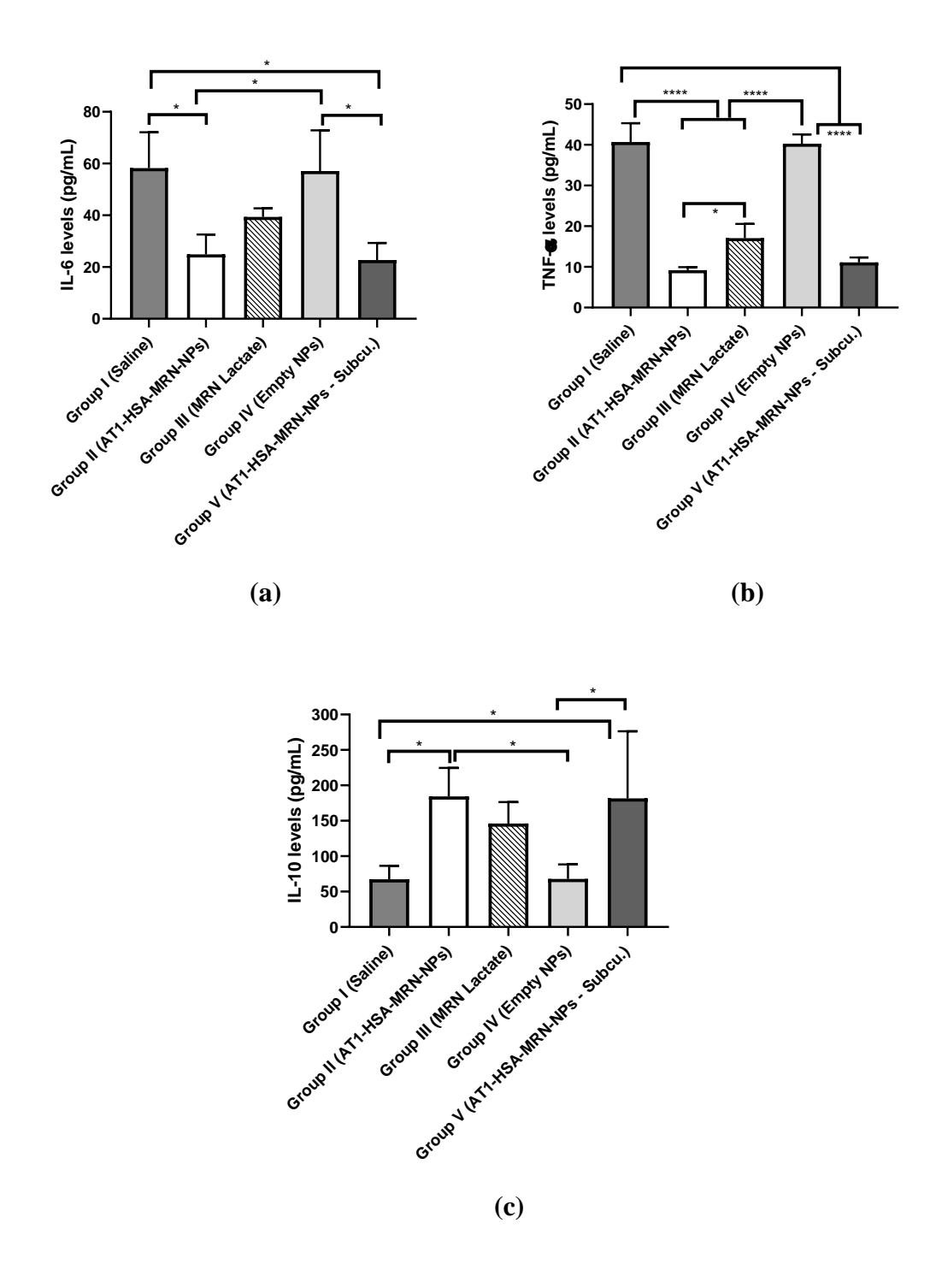


Figure 5.12. Serum cytokine levels for (a) IL-6 (pg/mL), (b) TNF- α (pg/mL) and (c) IL-10 (pg/mL). Groups II and V had significantly lower levels of IL-6 and TNF- α and significantly higher levels of IL-10 compared with other groups. The data has been presented as mean \pm SD (n=5). ****P<0.0001 was considered highly significant and *P<0.05 was considered significant based on Tukey's posthoc analysis.

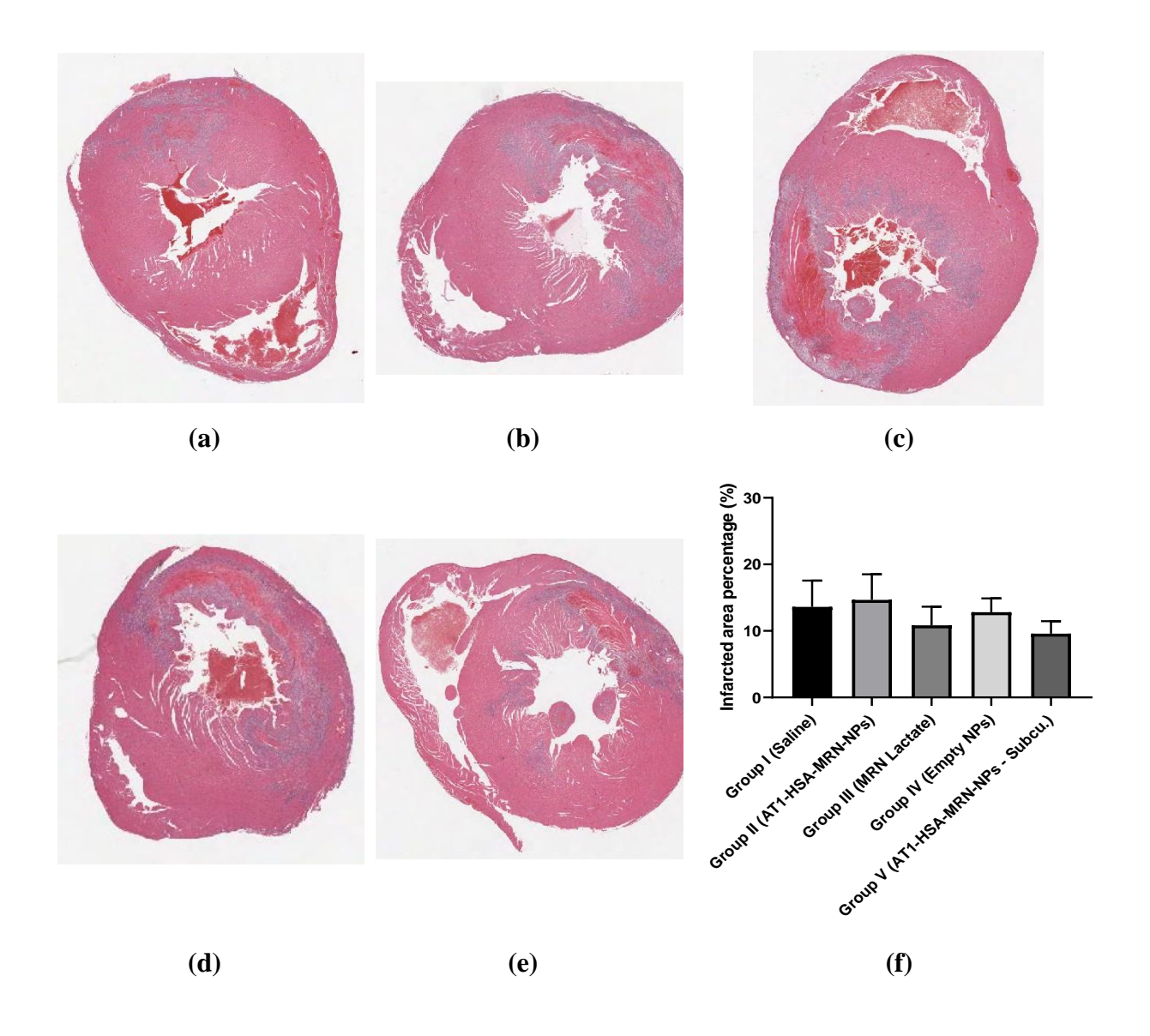


Figure 5.13. Images of thin sections of H & E stained hearts 1-week post heart failure in (a) Group I (control), (b) Group II (AT1-HSA-MRN-NPs IV injection), (c) Group III (MRN Lactate), (d) Group IV (empty NPs) and (e) Group V (AT1-HSA-MRN-NPs subcutaneous injection). Red indicated the viable myocardium and blue represents the infarcted area. (f) The percentage of infarcted left ventricular area for all groups represented as mean \pm SD (n=5).

Table 5.1. Nanoparticle size, charge, encapsulation efficiency and yield at various MRN/HSA (wt./wt.) ratios of nanoparticle preparation.

MRN/HSA	Nanoparticle Size	Zeta Potential	Encapsulation	Yield (%)
(wt./wt.)	(nm)	(mV)	Efficiency (%)	Tielu (70)
1:10	190.2±5.7	-29.5±3.7	41.8 ± 2.2	77 ± 2.3
1:20	205.6 ± 3.8	-27.5±4.6	40.4 ± 1.5	75 ± 2.6
1:40	225.4 ± 2.8	-20.5±4.4	54.1 ± 0.7	70 ± 3.5
1:80	245.6±3.5	-18.7±6.6	83.2 ± 1.2	68±4.6

Table 5.2. Pharmacokinetic parameters of AT1-HSA-MRN-NPs and MRN Lactate at MRN dose 50 μ g/kg. C0: concentration at time 0; Cmax: maximum concentration; $t_{1/2}$: half-life of plasma; MRT: mean residence time, AUC: area under the curve, Vz: apparent volume of distribution at elimination; Vss: apparent volume of distribution at steady state; CL: clearance.

Pharmacokinetic	MRN Dose: 50 ug/kg			
Parameters	MRN-Lactate	AT1-HSA-MRN-NPs		
C ₀ (ng/mL)	203.5	291.2		
$C_{max}\left(ng/mL\right)$	334.3	227.3		
$t_{1/2}$ (min)	64.7	101.3		
MRT (min)	49.1	123.7		
AUC _{0-t} (ng*h/mL)	104.3	183.9		
$AUC_{0-\infty}(ng*h/mL)$	106.7	206.1		
Vz (L/kg)	0.73	0.59		
Vss (L/kg)	0.38	0.5		
CL (L/kg*h)	0.47	0.24		

Table 5.3. Percentage LVEF measurements for Groups I, II, III, IV and V at various timepoints.

	Left Ventricular Ejection Fraction (LVEF) shown as %				
	Group I	Group II	Group III	Group IV	Group V
	(Control)	(AT1-HSA- MRN-NPs – IV injection)	(MRN Lactate – IV injection)	(Empty NPs)	AT1-HSA- MRN-NPs – Subcutaneous injection)
Baseline – Pre-Ligation	88.8±2.1	89.9±1.3	88.2±1.8	88.4±0.9	74.9±1.7
48 hrs Post Ligation	69.1±2.0	66.1±1.9	65.3±2.3	69.1±2.2	66.4±3.3
60 mins Post Injection	68.6±2.2	84.3±2.9***	80.1±3.3**	70.1±2.3	79.2±2.7**
24 hrs Post Injection	67.1±2.1	84.2±4.8**	70.6±3.6	67.5±2.5	75.5±2.6**
48 hrs Post Injection	67.7±1.8	83.1±3.6**	64.8±4.3	64.9±2.7	72.7±2.3
1-week Post Injection	66.7±1.1	74.5±2.1**	66.1±4.2	67.2±2.9	73.3±2.9*

The data has been presented as mean \pm SD (n=5). ***P<0.001, **P<0.01 was considered significant based on Tukey's posthoc analysis. The comparisons are with respect to the control Group I.

Table 5.4: Percentage LVFS measurements for Groups I, II, III, IV and V at various timepoints.

	Left Ventricular Fractional Shortening (LVFS) shown as %				
	Group I (Control)	Group II (AT1-HSA- MRN-NPs – IV injection)	Group III (MRN Lactate - IV injection)	Group IV (Empty NPs)	Group V AT1-HSA- MRN-NPs – Subcu. injection)
Baseline – Pre-Ligation	52.6±2.9	53.6±2.1	52.6±2.7	51.1±1.3	54.6±2.2
48 hrs Post Ligation	33.1±1.5	29.8±1.0	34.3±2.7	31.2±1.3	30.7±2.5
60 mins Post Injection	32.8±1.7	50.1±3.8**	45.6±3.2**	34.7±4.0	47.1±3.9**
24 hrs Post Injection	31.5±1.2	50.4±3.1***	33.6±3.9	30.9±2.4	40.5±2.8**
48 hrs Post Injection	31.7±1.0	46.5±3.1**	30.2±3.9	30.1±1.5	34.8±1.7
1-week Post Injection	31.3±1.5	37.0±2.7	30.8±2.8	29.6±1.1	35.9±3.1

The data has been presented as mean \pm SD (n=5). ***P<0.001, **P<0.01, *P<0.05 were considered significant based on Tukey's posthoc analysis. The comparisons are with respect to the control Group I.

CHAPTER 6: GENERAL DISCUSSION

Cardiovascular diseases are a global occurrence with high rates of mortality despite the significant measures taken for their prevention and treatment ^{6,7,35}. Congestive heart failure is prevalent in the general population making up for more than 50% of the global cases of CVDs, resulting in a huge economic and healthcare burden ^{37,38}. It usually represents the end-stage in the progression of the MI and CAD. Therefore, only a few patients with access to the gold standard treatments meet success in overcoming this challenge. The current treatments for CHF include both medical and surgical treatments. Medical treatments involve the administration of various drugs, either through injection or orally, and surgical treatments include bypass surgery, assist devices, heart transplant, angioplasty and stenting procedures ^{120,122,222}. Though there are a variety of drugs used in CHF, some of the common limitations with drug delivery include inefficiency in treatment, toxicity, lower bioavailability and most importantly the lack of target specificity ²²³. This limitation may be overcome by developing targeted drug delivery vehicles or nanoparticles, which bind drugs for site specific delivery ¹⁴². The functionality of these nanoparticles may be further improved through surface modification and cross-linking with ligands specific for receptors present on the myocardium ^{14,15,186}.

In this thesis, a novel nanoparticle formulation was conceived and developed for targeted drug delivery to the heart for use in CHF. Milrinone was the model drug evaluated for binding and delivery with the nanoparticles. This nanoparticle formulation demonstrated high drug binding, superior drug delivery characteristics and treatment efficacy *in vivo*. The enhanced therapeutic effect of the nanoparticle formulation delivering MRN, in comparison with the non-targeted MRN-Lactate can be attributed to the AT1 peptide attached to the surface of the HSA-NPs for specifically targeting the infarcted heart. Further, the release of MRN across the cell membrane enables greater calcium ion influx into the cardiomyocytes, causing the heart to pump again ^{113,224}. Thus, this new nanoparticle delivery system using active cardiac targeting is the first of its kind capable of delivering cardiac drugs in a targeted manner for the treatment of CHF.

The first chapter in this thesis gives a general introduction on the application of nanomedicine in cardiovascular diseases. This chapter highlights the importance and rationale behind developing

new strategies for treatment of CHF and other CVDs, with a special focus on nanoparticle based targeted drug delivery systems. The research hypothesis, research objectives and thesis outline mentioned in this chapter give direction to the experimental work elaborated further in the thesis.

The second chapter in this thesis is a review of the current and previous literature on the advancements of nanomedicine in CVDs. It describes the current status of CHF management. The presently available treatment modalities for CHF have been elaborated along with their limitations, including latest updates on the use of inotropes and phosphodiesterase III inhibitor drugs. This review focuses on the applications of nanomedicine as part of cardiac therapy for drug delivery. This review also focuses on the use of surface-functionalized nanoparticles for drug binding and delivery with a potential for enhanced functionality through surface modification with different ligands and discusses nanoparticle uptake. Further, the benefits of using HSA-NPs for targeted drug delivery have been explained, especially peptide-tagging for site-specific delivery.

The third chapter in this thesis elaborates on the preparation and optimization of HSA-NPs carrying MRN. The idea behind this study was to ensure the formation of spherical, stable, reproducible and homogenously dispersed nanoparticles bound to MRN. This was achieved by following the ethanol desolvation technique and optimizing parameters of the preparation process such as the HSA concentration, pH, MRN/HSA (wt./wt.) ratio, ethanol volume, glutaraldehyde concentration and polymerization time (**Figure 3.1**) ^{204,206}. In this technique, ethanol is added to the HSA-MRN solution in a continuous dropwise manner which lowers the solubility of the solution causing albumin nanoparticles to be precipitated out of solution. However, the precipitate is unstable and may easily solubilize and disintegrate back into the solution. Therefore, glutaraldehyde is added as a stabilizing agent, which undergoes a condensation reaction with the amino groups present on the albumin to form stable and rigid nanoparticles carrying the MRN drug ²²⁵. In this process, the pH of the solution plays an essential role in the final polydispersity of the particles ²²⁶. Having a starting solution greater than pH 7.5 results in formation of highly negatively charged nanoparticles, thus preventing aggregation of particles ²⁰⁴. Optimizing the parameters allows flexibility of formation of nanoparticles with the desired shape, morphology and surface charge characteristic. In this study, the nanoparticles were of less than 200 nm size and negative zeta potential with a spherical surface morphology when observed with electron

microscopy (**Figure 3.2**). Different MRN concentrations were tested to obtain the highest encapsulation efficiency and nanoparticle yield. In parallel, the binding efficiency of MRN with HSA was evaluated using molecular docking techniques ²²⁷. This was the first study to determine the nature of binding between HSA and MRN using computational modelling. Molecular docking simulation were performed on HSA, both with and without the presence of fatty acids (**Figure 3.3**). Milrinone was found to bind to both HSA molecules in two distinct conformations through hydrophobic binding with a binding affinity of -5.7 kcal/mol (Wilma scoring). The enzymatic release of MRN from the HSA nanoparticles was investigated, which also demonstrated the biodegradability of the MRN-HSA-NPs (**Figure 3.5**). Further, it was observed that fluorescently tagged MRN-HSA-NPs were taken up in a concentration-dependent manner by endothelial cells and cardiomyoblasts. Flow cytometry was performed to confirm the nanoparticle uptake by both cell lines as well (**Figures 3.8**). The MRN-HSA-NPs were also found to be safer, less cytotoxic and hence more biocompatible as compared to the MRN-Lactate, which is administered clinically to treat heart failure in patients (**Figure 3.9**). Overall, this chapter forms the rationale behind the development and characterization of MRN bound HSA-NPs.

The fourth chapter of this thesis comprises a novel scheme of synthesis of peptide-tagged HSA-NPs for MRN delivery. The angiotensin II is an 8-amino acid (Asp-Arg-Val-Tyr-Ile-His-Pro-Phe) peptide specific for the AT1 receptor present on the surface of the myocardium. During CHF, the AT1 receptor is found to be overexpressed ³²⁻³⁴. This condition has been explored for AT1-peptide mediated delivery of albumin nanoparticles carrying MRN. The AT1 peptide is attached to the HSA surface via a novel synthesis scheme using heterobifunctional crosslinkers which react with the amine and carboxylic functional groups present on HSA (**Figure 4.1**). This crosslinking was confirmed through mass spectrometry which showed that the m/z of AT1-HSA was 7000 higher than that of normal HSA, indicating that at least 3 molecules of the AT1 peptide were bound to the surface of HSA (**Figure 4.2**). The crosslinker used to bind AT1 with HSA was 5(6)-Carboxyfluorescein-NHS which comprised of the fluorescein molecule. Thus, the novel AT1-HSA-MRN-NPs developed in this study were fluorescently tagged, allowing the study of their intracellular uptake by hypoxic, hypertrophic and normal cardiomyoblasts. Hypoxic and hypertrophic cardiomyocytes simulated the conditions of MI and CHF, *in vitro*, and were found to overexpress the AT1 receptor (**Figure 4.6**). This was in alignment with a study conducted by Dvir

et al. where cardiomyocytes were tested for overexpression of the AT1 receptor followed by a study on the uptake of PEGylated liposomes conjugated with the AT1 peptide ¹⁷⁷. The AT1-HSA-MRN-NPs exhibited higher uptake in comparison to the non-targeted MRN-HSA-NPs by normal cardiomyoblasts (**Figure 4.7**). The uptake of the AT1-HSA-MRN-NPs was further increased under hypoxic and hypertrophic conditions, which indicated the targeted receptor-mediated uptake of the nanoparticles as compared to the non-targeted nanoparticles (**Figure 4.9**). The AT1-HSA-MRN-NPs were evaluated for safety and cytotoxicity and were found to be more biocompatible than the MRN-Lactate formulation.

The fifth chapter describes another synthesis scheme for binding the AT1 peptide with HSA using a PEGylated crosslinker, through covalent conjugation (Figure 5.1). The AT1-HSA is further bound with MRN and developed into AT1-HSA-MRN-NPs following the ethanol desolvation process of nanoparticle formation. Typically, PEG is known to form a biocompatible coating around the nanoparticle making it safer and reducing its cytotoxicity 141,165. The binding of AT1 with HSA was confirmed through mass spectrometry analysis, which demonstrated that the m/z of AT1-HSA was approximately 5600 higher than the HSA molecule (Figure 5.2). This was also confirmed through a UV-spectrophotometric analysis which suggested that at least 85% (approximately) of the initial amount of AT1 remained bound to the HSA post chemical modification and purification. An in vitro drug release of the AT1-HSA-MRN-NPs was performed which exhibited a slow and sustained release of MRN from the nanoparticles over time (Figure **5.4**). This is the desired release profile that was anticipated as opposed to a bolus or burst release since typically, MRN is eliminated from the body within 1-2 hours, causing the need for a continuous infusion of the drug ²²⁸. The MRN pharmacokinetics performed *in vivo* provided a clearer picture of the drug release profile of the AT1-HSA-MRN-NPs vs the MRN-Lactate (Figure **5.5**). This is the first study of its kind demonstrating that the pharmacokinetic parameters of the AT1-HSA-MRN-NPs were found to be superior than those of MRN-Lactate, justifying their advantage in overcoming the limitations of the non-targeted MRN-Lactate. The pharmacokinetic parameters of albumin nanoparticles were in alignment with those observed in other studies in combination with other drugs and in different animal models ^{229,230}. Further, the tissue distribution study at 2 hours post treatment showed that the AT1-HSA-MRN-NPs were targeted to the heart primarily, as MRN was detected majorly in the heart with some amounts in lungs, kidneys and liver (**Figure 5.6**). The treatment efficacy of the targeted nanoparticle formulation when tested in a rat model of CHF, was found to be superior than the MRN Lactate, determined by measuring the LVEF and LVFS (**Figures 5.10 and 5.11**). A previous study described the use of PLGA microcapsules to encapsulate MRN-Lactate for delivery in a rat model of CHF. However, those particles were in the micron-range particle size which is not suitable for intravenous delivery and may aggregate in the capillaries with the smallest diameters 228 . The current study was conducted to establish the effectiveness of the novel AT1-HSA-MRN-NPs in delivery of MRN to the failing heart to obtain a greater inotropic effect, recovery of heart function and contractility. There were no significant differences in the liver function tests amongst the groups (**Figure 5.8**). However, creatinine levels were found to be high in all the groups. This is not uncommon as renal dysfunction is typically indicative of myocardial injury 231,232 . An analysis of the serum cytokines IL-6, IL-10 and TNF- α indicated that the delivery of AT1-HSA-MRN-NPs lowered the levels of the proinflammatory cytokines IL-6 and TNF- α and elevated the anti-inflammatory cardioprotective cytokine IL-10 levels showing a positive and beneficial effect of the novel formulation (**Figure 5.12**).

Nanomedicine is emerging as a field with immense potential with applications in various medical disciplines ^{115,116}. So far, majority of the efforts were focused on cancer treatment and its applications and nanoparticles were being seen to interact with the cardiovascular system only in a passive manner while circulating in the body ²³³. Thus, the successful delivery of nanoparticles with their payloads needs to be readdressed when targeting the cardiovascular system ¹⁰. There may be several factors which limit the transition of a new nanoparticle formulation and therapeutics into a clinical setting. This may be separated into (i) nanomedicine development, (ii) pre-clinical testing and (iii) clinical testing and commercialization ²³⁴. The phase of nanomedicine development requires various considerations. One of the key areas of concern apart from the complexity of design is its pharmaceutical stability. The physical stability of the nanoparticles can be managed by controlling the particle size, morphology, surface charge, polydispersity, aggregation, encapsulation, purity and stability i.e. physiochemical properties which play a direct role in determining nanoparticle-cell interactions ^{138,169,226}. A multiplicity of biological barriers such as water insolubility or surface charges cause the particles to be opsonized or recognized by macrophages and monocytes, which needs to be addressed by ensuring the non-immunogenicity,

biocompatibility and biodegradability of the developed formulation ¹⁵⁷. This could be circumvented due to the presence of a PEG coating on the nanoparticle surface, which enhances the biocompatibility of the formulation ¹⁸².

The pre-clinical testing phase focuses attention on the safety and toxicity of the formulation. This would need to be analyzed in an extensive manner by assessing the interactions of the particles in physiological and physiochemical environments in the body at different concentrations. To treat cardiovascular diseases, it is crucial to ensure that the developed nanoformulation is interacting primarily with the heart, for which a dose-dependent and time-dependent tissue distribution study would be essential to understand the accumulation of the particles in various organs. A pharmacokinetics study is useful in understanding not only the absorption and distribution of the nanoparticles but also the metabolism and excretion of the particles from the system ^{229,230}. The interaction of nanoparticles at unintended sites resulting in accumulation and aggregation of the particles in different organs, also results in toxicity ^{235,236}. It is therefore important to develop more specialized and validated assays for toxicity analysis for nanomedicines. Tagging of the particles with appropriate ligands would ensure targeted and site-specific delivery ^{217,237}. Ligands may be conjugated to the surface of nanoparticles by covalent or non-covalent reactions using a variety of methods suggested in literature, which is anticipated to facilitate greater uptake of nanoparticles ^{26,173}. Enhanced therapeutic effects have been demonstrated with ligand targeted nanoparticles with lesser accumulation in unintended target organs as compared to non-targeted nanoparticles ^{175,238,239}. Apart from studying the pharmacokinetics, it would be useful to study pharmacodynamics to understand the intracellular trafficking, functionality, toxicity and degradation of the nanoparticles in the in vivo models. Also, these studies must be conducted in more than one animal model or species to have a comprehensive understanding of how the nanoparticle formulation interacts in different biological systems.

Our understanding of nano-bio interactions is rapidly expanding and with the growth in the use of nanomaterials for medical applications, the most urgent need is to develop approaches that validate both short-term and long-term health risks. A variety of nanoparticles-based nanomedicines are in the market with more in the clinical development phases ¹⁶. However, the clinical translation of the nanomedicines is an expensive and time-consuming process, a process that requires

simplification ^{233,240}. This requires an optimal clinical trial design along with reproducibility of the development procedure, infrastructure and costs of production ²³⁴. More importantly, the evaluation of safety and toxicity of nanomedicine along with understanding the appropriate dosage and therapeutic efficacy in patients would be key considerations in this process ²³⁴. Unfortunately, there is lack of clarity in the regulatory guidelines specific for the nanomedicine with greater complexity in developing patents and intellectual property associated with them ²³³. Also, understanding the biological interactions of nanomedicines in a human body environment is extremely different that those observed in pre-clinical settings. These factors impose significant hurdles, limiting the appearance of nanoparticle-based formulation in the market. However, cardiovascular drug research must be progressed to allow any drug delivery system to be effective, in future.

With an increase in the number of diseases and ailments plaguing humankind, the market for drugs and pharmaceuticals is rapidly growing. Apart from the growth in production, there is a plethora of information available to understand the complete functionality of each drug. Owing to technological advancements in recent decades, today, humans are not bound to choose from a few drugs, when selecting the best suitable option for use in prevention, diagnosis or treatment of diseases. Rather, multiple drugs are available to target one specific condition. Thus, the exponential increase in the variety of drugs being discovered and introduced, has led to research on effective drug delivery to provide lasting long-term solutions to patients. The currently known methods for drug delivery include direct administration either orally or through injection.

The majority of drugs discovered, are extremely potent as treatments for their intended use. However, upon entering the highly dynamic internal body environment through systemic circulation, a larger volume of the initial dose is eliminated within a timespan of few minutes to hours. This further necessitates administering a higher initial loading dose followed up by lower yet consistent maintenance doses to ensure a continuous rate of drug infusion to balance the rate of elimination ²⁴¹. Most drugs lack target specificity, resulting in their accumulation in off target organs and thus lowering their efficacy. The high drug dosage along with its lack of target specificity further leads to toxicity in the body along with multiple side effects ²⁴². Therefore, one of the biggest challenges faced by scientists today, is to improve upon the target specificity and

mean retention time of drugs in the body, which can help enhance other pharmacokinetic parameters such as half-life, area under the curve, volume of distribution, bioavailability ^{243,244}. Many drugs follow a biphasic-elimination profile, with an initial steep slope which indicates the initial distribution of drug in the body, and a shallow slope which shows the final excretion of the drug depending of release of the drug from tissue compartments into blood ²⁴⁵. Thus, by prolonging the initial concentration of drug in plasma and controlling the drug release, these challenges can be addressed. Here, the concept of targeted drug delivery using nanomedicine plays a crucial role.

Nanomedicine is rapidly evolving to bridge the gap in interactions between the microscopic and molecular levels, mechanisms which primarily drive the progression of any disease. It is highly likely to provide pioneering innovations in the prevention, diagnosis and treatment of diseases. Unlike other therapies, nanomedicine offers the platform for design of multi-functional and multi-component agents capable of performing multiple tasks simultaneously ²⁴⁶. The surface modification of the nanoparticles by crosslinking or binding with targeting ligands allows for modulation of their tissue distribution ²⁴⁶. Developing targeted nanoparticles for site-specific delivery of drugs has improves the pharmacokinetics and pharmacodynamics of non-targeted drugs ²⁴⁷. Nanoparticles play various roles in enhancing the overall therapeutic effect of the drug bound. They act as carriers withing the body, delivering drugs to the intended delivery site, thus not only improving their efficacy and prolonging their blood circulation time but also eliminating potential side effects and toxicity to organs ^{247,248}. Though a few nanomedicines have been approved for clinical use in cancer such as Abraxane[®] and Doxil[®] among others, cardiovascular nanomedicine is still in its primitive stages ^{249,250}. However, given the immense research for cardiovascular applications, the clinical use of these therapies can be anticipated soon.

The targeted nanoparticle formulation designed and developed in this thesis for cardiovascular applications meets the above prerequisites as a safe, non-toxic and effective therapy for drug delivery and should be characterized further for clinical translation. This new nanoformulation is the first to deliver an inotrope drug to the heart in a targeted manner. Enabled for surface-functionalization, this nanoparticle system can be used as a platform technology for binding a variety of drugs, peptides as well as other molecules for use in cardiac and non-cardiac applications such as cancer.

CHAPTER 7: SUMMARY OF OBSERVATIONS, CLAIMED ORGINAL CONTRIBUTIONS TO KNOWLEDGE AND CONCLUSIONS

7. 1 Summary of Completed Research Objectives

All the thesis specific objectives substantiate the thesis hypothesis that a novel nanoparticle formulation for targeted delivery of MRN can be developed and is beneficial for use in CVDs. In this thesis, a novel nanoparticle formulation was conceived and developed, prepared from HSA protein and chemically conjugated with the angiotensin II peptide for specific targeting to the infarcted myocardium. The ligand conjugated nanoparticle formulation was used to deliver the cardiac inotrope and vasodilator drug, MRN. This formulation was characterized *in vitro* to study binding efficiency between MRN and HSA, cumulative drug release from the nanoparticles and cellular uptake by endothelial cells and cardiomyoblasts under normal and hypoxic conditions. The pharmacokinetics, tissue distribution and treatment efficacy of the nanoparticle formulation was also evaluated *in vivo* in a rat model of CHF. A summary of the completed research objectives is presented below:

Objective 1: Based on extensive literature review, HSA-NPs were chosen as drug delivery vehicles for targeted delivery of milrinone

HSA-NPs have been widely used in various medical applications owing to their unique properties such as biocompatibility, biodegradability, non-immunogenicity and ability to undergo surface modification for binding targeting moieties and achieving target specificity. They have been used extensively for binding both hydrophobic and hydrophilic drugs which may be bound by hydrophobic, electrostatic, covalent interactions with the drug molecules. Albumin comprises of amino and carboxylate functional groups which may be covalently reacted with functional moieties present on cross-linkers for binding ligand molecules. Drugs administered into blood circulation usually lack target specificity and are rapidly cleared from the body, however, on binding with HSA-NPs, the mean circulation time is increased, thus helping in a controlled drug release effect rather than a burst release. Thus, these characteristics associated with HSA-NPs make them ideal drug carriers for use in cardiovascular therapy.

- 1. Human serum albumin nanoparticles were prepared via the ethanol desolvation process to obtain nanoparticles with size between 150-200 nm and zeta potential up to -30 mV.
- 2. The nanoparticles were optimized by varying the HSA concentration, pH of solution, amount of ethanol added, polymerization time and amount of MRN added. Notably, the particle size and surface charge are found to vary by varying the above parameters. Scanning electron microscopy shows spherical surface morphology and homogenously scattered particles.

Objective 3: Studying MRN and HSA Binding, Drug Release and Cellular Uptake Of MRN-HSA-NPs

- 3. Computational modelling suggests that MRN binds with HSA hydrophobically through lysine, arginine and tyrosine residues, with an enthalpy change of -5.7 kcal/mol (Wilma). This is also indicated by circular dichroism studies which show a change in the protein secondary structure on binding with MRN. The nanoparticle is susceptible to enzymatic degradation to release the drug, which shows its biodegradability.
- 4. The nanoparticle formulation is taken up by endothelial cells as well as cardiomyoblasts as shown by cellular uptake studies and flow cytometry. Also, the MRN-nanoformulation is safer and less cytotoxic as compared to the MRN Lactate that is administered clinically for congestive heart failure.

Objective 4: Synthesis and In Vitro Characterization of AT1-HSA-MRN-NPs

- 5. The AT1-HSA was synthesized through covalent conjugation of HSA with the AT1 peptide. Mass spectrometry analysis confirmed that at least 3 molecules of the AT1 peptide were bound per HSA.
- 6. The AT1-HSA-MRN-NPs exhibit higher safety, cell compatibility and lower cytotoxicity than the MRN Lactate formulation.
- 7. Under hypoxic and hypertrophic conditions (simulating myocardial infarction and heart failure), the uptake of the AT1-nanoparticles is greater than the non-targeted nanoformulation, indicating the specificity of the AT1-nanoparticles for the overexpressed AT1 receptor under heart failure conditions.

8. The *in vitro* drug release shows that approximately 50% of the MRN bound to AT1-HSA-MRN-NPs was released between 4-6 hours.

Objective 5: Determining the Pharmacokinetics and Tissue Distribution of AT1-HSA-MRN-NPs *In Vivo*

- 9. Pharmacokinetics analysis revealed that the blood circulation time, half life and mean residence time of MRN is improved in case of the AT1-HSA-MRN-NPs when compared with MRN Lactate.
- 10. The tissue distribution study showed that the MRN was accumulated in the heart, indicating that the AT1-HSA-MRN-NPs were effectively targeted.

Objective 6: Targeted Delivery of AT1-HSA-MRN-NPs In Vivo in a Rat Model of CHF

- 11. The AT1-HSA-MRN-NPs showed improved ejection fraction, fractional shortening and overall cardiac function compared to MRN Lactate in a rat model of CHF.
- 12. The liver function and kidney function tests of the animals administered with AT1-HSA-MRN-NPs showed improvement in comparison to the MRN Lactate animal group, suggesting the higher safety and biocompatibility of the AT1-nanoparticle formulation.
- 13. The pro-inflammatory/anti-inflammatory cytokine analysis also showed improvement in the cytokine profile in the animals treated with the AT1-HSA-MRN-NPs.

7.2 Claimed Original Contributions to Knowledge

The use of nanomedicine in cardiovascular applications has been recently established in imaging, diagnostic and therapeutic applications. However, no nanoparticle formulation has yet shown to have robust treatment efficacy and therapeutic potential. In this thesis, a novel nanoparticle system was conceived and developed by combining surface functionalized albumin nanoparticles and the cardiac inotrope, MRN to create for the first time a targeted, safe and effective formulation for use in congestive heart failure.

The claimed original contributions to knowledge are as following:

- 1. A new HSA-based delivery platform for targeted delivery of drugs and other therapeutic molecules was designed and tested using MRN as an example.
- 2. A novel targeted nanoparticle formulation was conceived and developed for drug delivery in congestive heart failure.
- 3. The targeted nanoparticle formulation can be optimized, and custom made in terms of size and surface charge.
- 4. The binding interaction of HSA with MRN was determined using molecular docking for the first time.
- The binding affinity of HSA with MRN was predicted for the first time using molecular docking.
- 6. The targeted nanoparticle formulation improved MRN pharmacokinetics and tissue distribution.
- 7. The targeted nanoparticle formulation delivers MRN specifically to the heart at the tested time condition.

- 8. The targeted nanoparticle formulation improved myocardial contractility and cardiac function, treating congestive heart failure.
- 9. The targeted nanoparticle formulation is safe, biodegradable and biocompatible.
- 10. The proposed synthesis scheme for the targeted nanoparticle formulation is highly reproducible and can be scaled up for *in vivo* applications.
- 11. The proposed nanoparticle formulation has potential for delivery of multiple drugs, peptides, genes, etc. for use in cardiovascular and other diseases.

7.3 Conclusion

Cardiovascular diseases are the leading cause of morbidity and mortality across the world today. Myocardial infarction and congestive heart failure, types of cardiovascular diseases, are responsible for more than 50% of the global cases of cardiovascular diseases with an increase in the incidences of these diseases every year. The currently known method of treating end stage congestive heart failure involves heart transplantation, however, due to donor shortages and mismatching of donor-recipient physiologies, this is not the most feasible way of treatment for the longer term. Other treatments include use of ventricular assist devices, bypass surgeries, stenting and angioplasty in cases of atherosclerosis leading to congestive heart failure. Some medical treatments include use of various drugs such as ACE inhibitors, beta blockers, inotropes or combination therapies etc. Hence, it is has become more vital than ever to develop newer technologies and therapies for the effective and efficient treatment of CHF and related CVDs.

A novel targeted nanoparticle formulation was conceived, designed and developed for targeted delivery in an animal model of congestive heart failure. The targeted nanoparticle formulation prepared from HSA protein was surface functionalized to bind the angiotensin II peptide ligand for specific targeting to the failing heart. Additionally, the HSA-NPs are bound to the cardiac inotrope and vasodilator drug, MRN. Milrinone is administered clinically to patients with CHF as it shows beneficial effects on lowering systemic resistance, capillary wedge pressure, improving the heart rate and the overall cardiac output, more than other drugs. MRN binds to HSA through

hydrophobic bonding, interacting with lysine, arginine and tyrosine residues, as revealed by molecular docking. The targeted nanoparticle formulation can be optimized to obtain particle size in the range of 150-250 nm and surface charge approximately -30 mV with spherical surface morphology.

The targeted nanoparticle formulation shows higher cellular uptake and drug delivery under heart failure conditions simulated in *in vitro*, compared to normal conditions and the non-targeted formulation. The targeted nanoparticle formulation also shows superior drug release profile *in vitro* and *in vivo*. Pharmacokinetics of the targeted nanoparticle formulation have shown to improve the mean retention time, half-life, AUC, clearance of MRN in comparison to the MRN Lactate. The drug is released in the heart as shown by the tissue distribution study along with accumulation in organs like the kidney, lungs and liver, when clearing out from the body. The novel nanoparticle formulation is also found to improve the ejection fraction, fractional shortening and the overall cardiac function when tested in a rat model of congestive heart failure. Further, this novel formulation is safe for use with least toxicity and other side effects. Overall, this thesis demonstrates the design and development of a novel nanoparticle formulation delivering MRN to the heart in a targeted manner. This formulation is biocompatible, biodegradable, non-toxic and non-immunogenic. The novel targeted nanoparticle formulation represents a paradigm shift in the management of chronic diseases such as heart failure and related CVDs that is effective, reproducible and sustainable.

CHAPTER 8: RECOMMENDATIONS

Congestive heart failure is treated using various drugs, the action of which typically causes vasodilation and changes in myocardial contractility. However, there are limitation to their use, which include poor solubility, lower blood circulation and retention time, lack of target specificity and inefficiency of treatment. In addition, the non-targeted use of these drugs results in several side effects such as hypotension, arrhythmias, toxicity, nausea among others. Thus, new preventative and therapeutic modalities for efficient treatment of CVDs must be explored and introduced. Nanomedicine has emerged as a promising field for effective delivery of drugs to the target site with tremendous potential for preparation of customized formulations.

This thesis presents the design, optimization and synthesis of a novel targeted nanoparticle formulation for drug delivery in an animal model of CHF. Despite the convincing pre-clinical data presented in this thesis, several further studies and investigations are required to improve the nanoparticle efficacy before this formulation could be recommended for clinical use.

Some limitations of the current study have been recognized. Firstly, the size of the nanoparticles was approximately 200 nm. Though with the obtained particle size, the nanoparticle formulation is suitable for intravenous delivery, a particle size less than 100 nm is considered most ideal for delivery applications, from the point of higher blood circulation time and tissue distribution. Further, for other routes of administration such as intranasal delivery, greater than 100 nm particle size would lead to capillary clogging. Thus, smaller particle sizes can be achieved through further optimization following other methods of nanoparticle preparation such as through emulsion-homogenization. Another limitation of this study is that any potential side effects associated with the use of MRN, such as arrhythmias, have not been studied in comparison to the nanoparticle formulation, when tested *in vivo*. This can be addressed by studying toxicity and cardiac function at various MRN doses. The biodistribution study must be performed in organs other than heart, liver, kidney and lungs, to understand passive targeting of the targeted nanoparticle formulation. Lastly, a long-term study is required to study the overall treatment efficacy of the targeted nanoparticle formulation and evaluate the improvement in cardiac function upon its use.

As next steps, various recommendations have been made given for future studies.

- 1) The preparation of peptide conjugated albumin nanoparticles though highly reproducible, it requires a few reaction steps to be completed. To begin with, the binding of the angiotensin II peptide with HSA is done through chemical conjugation using heterobifunctional cross-linkers. The amount of angiotensin II peptide bound to HSA could be further optimized to understand its effects on particle size, surface charge and nanoparticle uptake.
- 2) Studies on shelf-life stability of the nanoparticles should be performed for effective clinical practice and to understand the stability of the drug and peptide bound to the nanoparticles after lyophilization, over time. The stability of the nanoparticles should be tested *in vitro* and *in vivo*.
- 3) The pharmacokinetics and tissue distribution study for nanoparticles is critical in understanding their therapeutics and toxicity. An elaborative study with more animal numbers and controls should be performed to evaluate the pharmacokinetics at different nanoparticle-drug concentrations, to understand the release characteristics *in vivo*. Similarly, the time-dependent tissue distribution study of the nanoparticles would be useful in understanding their accumulation in different organs while clearing from the body
- 4) The nanoparticle system designed in this thesis could also be explored for delivery of genes, growth factors, other drugs and molecules. This system has been developed for a wide array of applications and is capable of being modified for binding with other cross-linkers, targeting moieties and payloads. The presence of active functional groups on the albumin can be utilized for loading a combination of drugs and genes etc. to have a pronounced therapeutic effect.
- 5) The pre-clinical studies indicate that the novel targeted nanoparticle formulation developed in this thesis shows immense potential as an effective drug delivery agent. As next steps, conducting clinical studies using this new nanoparticle formulation would help in addressing the urgent need to develop efficient therapeutics for CHF and other CVDs.

BIBLIOGRAPHY

- Benjamin, E. J., Muntner, P. & Bittencourt, M. S. Heart disease and stroke statistics-2019 update: A report from the American Heart Association. *Circulation* **139**, e56-e528 (2019).
- Wilson, P. W. Overview of established risk factors for cardiovascular disease.
- Arnett, D. K. *et al.* 2019 ACC/AHA guideline on the primary prevention of cardiovascular disease. *Journal of the American College of Cardiology*, 26029 (2019).
- 4 Goldgrab, D., Balakumaran, K., Kim, M. J. & Tabtabai, S. R. Updates in heart failure 30-day readmission prevention. *Heart failure reviews* **24**, 177-187 (2019).
- 5 Benjamin, E. J. *et al.* Heart disease and stroke statistics—2018 update: a report from the American Heart Association. *Circulation* **137**, e67-e492 (2018).
- Association, A. D. 10. Cardiovascular disease and risk management: standards of medical care in diabetes—2019. *Diabetes Care* **42**, S103-S123 (2019).
- 7 DREXLER, H. & FUCHS, M. Current limitations in treatment of heart failure: new avenues and treatment options. *Journal of cardiovascular electrophysiology* **13**, S53-S56 (2002).
- de Boer, R. A. & van Veldhuisen, D. J. ACE-inhibitors, Beta-blockers or the Combination in Heart Failure: Is It Just an A–B–C? *Cardiovascular Drugs and Therapy* **22**, 261-263 (2008).
- 9 Lonn, E. & McKelvie, R. Drug treatment in heart failure. *BMJ* **320**, 1188-1192, doi:10.1136/bmj.320.7243.1188 (2000).
- Martín Giménez, V. M., Kassuha, D. E. & Manucha, W. Nanomedicine applied to cardiovascular diseases: latest developments. *Therapeutic advances in cardiovascular disease* **11**, 133-142 (2017).
- Ehlerding, E. B., Grodzinski, P., Cai, W. & Liu, C. H. Big potential from small agents: nanoparticles for imaging-based companion diagnostics. *ACS nano* **12**, 2106-2121 (2018).
- Vinciguerra, D. *et al.* A facile route to heterotelechelic polymer prodrug nanoparticles for imaging, drug delivery and combination therapy. *Journal of controlled release* **286**, 425-438 (2018).
- Sahoo, S. K., Misra, R. & Parveen, S. in *Nanomedicine in Cancer* 73-124 (Pan Stanford, 2017).
- 14 Conde, J. *et al.* Revisiting 30 years of biofunctionalization and surface chemistry of inorganic nanoparticles for nanomedicine. *Frontiers in chemistry* **2**, 48 (2014).
- Mout, R., Moyano, D. F., Rana, S. & Rotello, V. M. Surface functionalization of nanoparticles for nanomedicine. *Chemical Society Reviews* **41**, 2539-2544 (2012).
- Bobo, D., Robinson, K. J., Islam, J., Thurecht, K. J. & Corrie, S. R. Nanoparticle-based medicines: a review of FDA-approved materials and clinical trials to date. *Pharmaceutical research* **33**, 2373-2387 (2016).
- Anselmo, A. C. & Mitragotri, S. Nanoparticles in the clinic. *Bioengineering & translational medicine* **1**, 10-29 (2016).
- Bagchi, M., Moriyama, H. & Shahidi, F. *Bio-nanotechnology: a revolution in food, biomedical and health sciences.* (John Wiley & Sons, 2012).

- Owens III, D. E. & Peppas, N. A. Opsonization, biodistribution, and pharmacokinetics of polymeric nanoparticles. *International journal of pharmaceutics* **307**, 93-102 (2006).
- Yoo, J.-W., Chambers, E. & Mitragotri, S. Factors that control the circulation time of nanoparticles in blood: challenges, solutions and future prospects. *Current pharmaceutical design* **16**, 2298-2307 (2010).
- Anselmo, A. C. *et al.* Elasticity of nanoparticles influences their blood circulation, phagocytosis, endocytosis, and targeting. *ACS nano* **9**, 3169-3177 (2015).
- Abbasi, S., Paul, A., Shao, W. & Prakash, S. Cationic albumin nanoparticles for enhanced drug delivery to treat breast cancer: preparation and in vitro assessment. *Journal of drug delivery* **2012** (2011).
- Dubey, P. K., Singodia, D., Verma, R. K. & Vyas, S. P. RGD modified albumin nanospheres for tumour vasculature targeting. *Journal of Pharmacy and Pharmacology* **63**, 33-40 (2011).
- Dubey, R. D. *et al.* Development and evaluation of folate functionalized albumin nanoparticles for targeted delivery of gemcitabine. *International journal of pharmaceutics* **492**, 80-91 (2015).
- Ghuman, J. *et al.* Structural basis of the drug-binding specificity of human serum albumin. *Journal of molecular biology* **353**, 38-52 (2005).
- Yu, X. *et al.* Enhanced tumor targeting of cRGD peptide-conjugated albumin nanoparticles in the BxPC-3 cell line. *Sci Rep* **6**, 31539 (2016).
- Zhao, D. *et al.* Preparation, characterization, and in vitro targeted delivery of folate-decorated paclitaxel-loaded bovine serum albumin nanoparticles. *International journal of nanomedicine* **5**, 669 (2010).
- Tang, X. *et al.* Enhanced tolerance and antitumor efficacy by docetaxel-loaded albumin nanoparticles. *Drug delivery* **23**, 2686-2696 (2016).
- Dreis, S. *et al.* Preparation, characterisation and maintenance of drug efficacy of doxorubicin-loaded human serum albumin (HSA) nanoparticles. *International journal of pharmaceutics* **341**, 207-214 (2007).
- 30 Young, R. A. & Ward, A. Milrinone. *Drugs* **36**, 158-192 (1988).
- Mudshinge, S. R., Deore, A. B., Patil, S. & Bhalgat, C. M. Nanoparticles: emerging carriers for drug delivery. *Saudi pharmaceutical journal* **19**, 129-141 (2011).
- Paradis, P., Dali-Youcef, N., Paradis, F. W., Thibault, G. & Nemer, M. Overexpression of angiotensin II type I receptor in cardiomyocytes induces cardiac hypertrophy and remodeling. *Proceedings of the National Academy of Sciences of the United States of America* **97**, 931-936 (2000).
- Rivard, K. *et al.* Overexpression of type I angiotensin II receptors impairs excitation-contraction coupling in the mouse heart. *American Journal of Physiology-Heart and Circulatory Physiology* (2011).
- 34 Xu, J. *et al.* Role of cardiac overexpression of angiotensin II in the regulation of cardiac function and remodeling post-myocardial infarction. *American Journal of Physiology-Heart and Circulatory Physiology* (2007).
- Annema, C., Luttik, M. L. & Jaarsma, T. Reasons for readmission in heart failure: Perspectives of patients, caregivers, cardiologists, and heart failure nurses. *Heart & lung : the journal of critical care* **38**, 427-434, doi:10.1016/j.hrtlng.2008.12.002 (2009).
- Endoh, M. & Hori, M. Acute heart failure: inotropic agents and their clinical uses. *Expert opinion on pharmacotherapy* **7**, 2179-2202, doi:10.1517/14656566.7.16.2179 (2006).

- 37 McAloon, C. J. *et al.* The changing face of cardiovascular disease 2000–2012: An analysis of the world health organisation global health estimates data. *International journal of cardiology* **224**, 256-264 (2016).
- Stewart, J., Manmathan, G. & Wilkinson, P. Primary prevention of cardiovascular disease: A review of contemporary guidance and literature. *JRSM Cardiovasc Dis* 6, 2048004016687211-2048004016687211, doi:10.1177/2048004016687211 (2017).
- Ziaeian, B. & Fonarow, G. C. The Prevention of Hospital Readmissions in Heart Failure. *Progress in cardiovascular diseases* **58**, 379-385, doi:10.1016/j.pcad.2015.09.004 (2016).
- Dassanayaka, S. & Jones, S. P. Recent developments in heart failure. *Circulation research* **117**, e58-e63 (2015).
- Parmley, W. W. Pathophysiology of congestive heart failure. *The American journal of cardiology* **55**, A9-A14 (1985).
- Dick, S. A. & Epelman, S. Chronic heart failure and inflammation: what do we really know? *Circulation research* **119**, 159-176 (2016).
- Degoricija, V. *et al.* Acute Heart Failure developed as worsening of Chronic Heart Failure is associated with increased mortality compared to de novo cases. *Sci Rep* **8**, 9587-9587, doi:10.1038/s41598-018-28027-3 (2018).
- Farmakis, D., Parissis, J., Lekakis, J. & Filippatos, G. Acute heart failure: epidemiology, risk factors, and prevention. *Revista Española de Cardiología (English Edition)* **68**, 245-248 (2015).
- Gheorghiade, M. *et al.* Pathophysiologic targets in the early phase of acute heart failure syndromes. *The American journal of cardiology* **96**, 11-17 (2005).
- Ramani, G. V., Uber, P. A. & Mehra, M. R. Chronic heart failure: contemporary diagnosis and management. *Mayo Clin Proc* **85**, 180-195, doi:10.4065/mcp.2009.0494 (2010).
- O'Brien, P. J. & Gwathmey, J. K. Myocardial Ca(2+)- and ATP-cycling imbalances in end-stage dilated and ischemic cardiomyopathies. *Cardiovascular research* **30**, 394-404, doi:10.1016/s0008-6363(95)00059-3 (1995).
- Sutton, M. G. S. J. & Sharpe, N. Left ventricular remodeling after myocardial infarction: pathophysiology and therapy. *Circulation* **101**, 2981-2988 (2000).
- Cleutjens, J. P., Kandala, J. C., Guarda, E., Guntaka, R. V. & Weber, K. T. Regulation of collagen degradation in the rat myocardium after infarction. *Journal of molecular and cellular cardiology* **27**, 1281-1292 (1995).
- Lew, W. Y., Chen, Z. Y., Guth, B. & Covell, J. W. Mechanisms of augmented segment shortening in nonischemic areas during acute ischemia of the canine left ventricle. *Circ Res* **56**, 351-358 (1985).
- Anversa, P., Beghi, C., Kikkawa, Y. & Olivetti, G. Myocardial response to infarction in the rat. Morphometric measurement of infarct size and myocyte cellular hypertrophy. *The American journal of pathology* **118**, 484 (1985).
- Katz, A. M. (Mass Medical Soc, 1978).
- 53 Sigurdsson, A. & Swedberg, K. The role of neurohormonal activation in chronic heart failure and postmyocardial infarction. *American heart journal* **132**, 229-234 (1996).
- Byku, M. & Mann, D. L. NEUROMODULATION OF THE FAILING HEART: LOST IN TRANSLATION? *JACC Basic Transl Sci* 1, 95-106, doi:10.1016/j.jacbts.2016.03.004 (2016).

- Ju, H., Zhao, S., Tappia, P. S., Panagia, V. & Dixon, I. M. Expression of Gq alpha and PLC-beta in scar and border tissue in heart failure due to myocardial infarction. *Circulation* **97**, 892-899 (1998).
- Verbrugge, F. H., Tang, W. W. & Mullens, W. (JACC: Heart Failure, 2015).
- Crozier, I. G., Teoh, R., Kay, R. & Nicholls, M. G. Sympathetic nervous system during converting enzyme inhibition. *The American journal of medicine* **87**, 29S-32S (1989).
- Orsborne, C., Chaggar, P. S., Shaw, S. M. & Williams, S. G. The renin-angiotensinaldosterone system in heart failure for the non-specialist: the past, the present and the future. *Postgraduate medical journal* **93**, 29-37 (2017).
- Levin, E. R., Gardner, D. G. & Samson, W. K. Natriuretic peptides. *New England journal of medicine* **339**, 321-328 (1998).
- Volpe, M., Carnovali, M. & Mastromarino, V. The natriuretic peptides system in the pathophysiology of heart failure: from molecular basis to treatment. *Clinical Science* **130**, 57-77 (2016).
- Magnussen, C. & Blankenberg, S. Biomarkers for heart failure: small molecules with high clinical relevance. *Journal of internal medicine* **283**, 530-543 (2018).
- Boularan, C. & Gales, C. Cardiac cAMP: production, hydrolysis, modulation and detection. *Frontiers in pharmacology* **6**, 203 (2015).
- Braunwald, E. The war against heart failure: the Lancet lecture. *The Lancet* **385**, 812-824 (2015).
- Feneck, R. Phosphodiesterase inhibitors and the cardiovascular system. *Continuing Education in Anaesthesia, Critical Care & Pain* **7**, 203-207 (2007).
- 65 Szappanos, H. C. *et al.* Identification of a novel cAMP dependent protein kinase A phosphorylation site on the human cardiac calcium channel. *Sci Rep* **7**, 15118 (2017).
- Bers, D. M. Calcium cycling and signaling in cardiac myocytes. *Annu. Rev. Physiol.* **70**, 23-49 (2008).
- Bedioune, I., Bobin, P., Leroy, J., Fischmeister, R. & Vandecasteele, G. in *Microdomains in the Cardiovascular System* 97-116 (Springer, 2017).
- Alousi, A. & Johnson, D. Pharmacology of the bipyridines: amrinone and milrinone. *Circulation* **73**, III10-24 (1986).
- 69 Tehrani, D. et al. THE HEMODYNAMIC EFFECTS OF INTRAVENOUS MILRINONE THERAPY IN HEART FAILURE WITH REDUCED EJECTION FRACTION PATIENTS ON BETA-BLOCKERS. Journal of the American College of Cardiology 71, A788 (2018).
- Ginwalla, M. & Tofovic, D. S. Current Status of Inotropes in Heart Failure. *Heart failure clinics* **14**, 601-616, doi:10.1016/j.hfc.2018.06.010 (2018).
- Karlsberg, R. P., DeWood, M. A., DeMaria, A. N., Berk, M. R. & Lasher, K. P. Comparative efficacy of short-term intravenous infusions of milrinone and dobutamine in acute congestive heart failure following acute myocardial infarction. Milrinone-Dobutamine Study Group. *Clinical cardiology* **19**, 21-30, doi:10.1002/clc.4960190106 (1996).
- Chong, L. Y. Z., Satya, K., Kim, B. & Berkowitz, R. Milrinone Dosing and a Culture of Caution in Clinical Practice. *Cardiol Rev* **26**, 35-42, doi:10.1097/crd.000000000000165 (2018).

- Nanayakkara, S., Mak, V., Crannitch, K., Byrne, M. & Kaye, D. M. Extended Release Oral Milrinone, CRD-102, for Advanced Heart Failure. *Am J Cardiol* **122**, 1017-1020, doi:10.1016/j.amjcard.2018.06.009 (2018).
- Chong, L. Y. Z., Satya, K., Kim, B. & Berkowitz, R. Milrinone dosing and a culture of caution in clinical practice. *Cardiology in review* **26**, 35-42 (2018).
- 75 Zhang, J. *et al.* Nebulized Phosphodiesterase III Inhibitor During Warm Ischemia Attenuates Pulmonary Ischemia–Reperfusion Injury. *The Journal of Heart and Lung Transplantation* **28**, 79-84 (2009).
- Bueltmann, M. *et al.* Inhaled milrinone attenuates experimental acute lung injury. *Intensive care medicine* **35**, 171 (2009).
- Buckley, M. S. & Feldman, J. P. Nebulized milrinone use in a pulmonary hypertensive crisis. *Pharmacotherapy: The Journal of Human Pharmacology and Drug Therapy* **27**, 1763-1766 (2007).
- Denault, A. Y. *et al.* A multicentre randomized-controlled trial of inhaled milrinone in high-risk cardiac surgical patients. *Canadian Journal of Anesthesia/Journal canadien d'anesthésie* **63**, 1140-1153 (2016).
- Laflamme, M. *et al.* Preliminary experience with combined inhaled milrinone and prostacyclin in cardiac surgical patients with pulmonary hypertension. *Journal of cardiothoracic and vascular anesthesia* **29**, 38-45 (2015).
- Hentschel, T. *et al.* Inhalation of the phosphodiesterase-3 inhibitor milrinone attenuates pulmonary hypertension in a rat model of congestive heart failure. *Anesthesiology: The Journal of the American Society of Anesthesiologists* **106**, 124-131 (2007).
- Waller, D. G. & Sampson, A. P. in *Medical Pharmacology and Therapeutics (Fifth Edition)* (eds Derek G. Waller & Anthony P. Sampson) 131-142 (Elsevier, 2018).
- Jessup, M., Ulrich, S., Samaha, J. & Helfer, D. Effects of low dose enoximone for chronic congestive heart failure. *Am J Cardiol* **60**, 80c-84c (1987).
- Metra, M. *et al.* Effects of low-dose oral enoximone administration on mortality, morbidity, and exercise capacity in patients with advanced heart failure: the randomized, double-blind, placebo-controlled, parallel group ESSENTIAL trials. *European heart journal* **30**, 3015-3026 (2009).
- Hasenfuss, G. & Teerlink, J. R. Cardiac inotropes: current agents and future directions. *European heart journal* **32**, 1838-1845 (2011).
- Group, D. I. The effect of digoxin on mortality and morbidity in patients with heart failure. *New England Journal of Medicine* **336**, 525-533 (1997).
- Currie, G. M., Wheat, J. M. & Kiat, H. Pharmacokinetic considerations for digoxin in older people. *Open Cardiovasc Med J* 5, 130-135, doi:10.2174/1874192401105010130 (2011).
- Kjeldsen, K., Nørgaard, A. & Gheorghiade, M. Myocardial Na, K-ATPase: the molecular basis for the hemodynamic effect of digoxin therapy in congestive heart failure. *Cardiovascular research* **55**, 710-713 (2002).
- Harjola, V.-P. *et al.* Use of levosimendan in acute heart failure. *European Heart Journal Supplements* **20**, I2-I10 (2018).
- Haikala, H., Nissinen, E., Etemadzadeh, E., Levijoki, J. & Lindén, I.-B. Troponin C-mediated calcium sensitization induced by levosimendan does not impair relaxation. *Journal of cardiovascular pharmacology* **25**, 794-801 (1995).
- 90 Lefkowitz, R. J., Rockman, H. A. & Koch, W. J. (Am Heart Assoc, 2000).

- Lokhandwala, M. F. & Hegde, S. S. Cardiovascular pharmacology of adrenergic and dopaminergic receptors: therapeutic significance in congestive heart failure. *The American journal of medicine* **90**, S2-S9 (1991).
- 92 Bristow, M. R., Kantrowitz, N. E., Ginsburg, R. & Fowler, M. B. β-Adrenergic function in heart muscle disease and heart failure. *Journal of molecular and cellular cardiology* **17**, 41-52 (1985).
- Goldberg, L. I. & Rajfer, S. Dopamine receptors: applications in clinical cardiology. *Circulation* **72**, 245-248 (1985).
- Goldberg, L. I., Hsieh, Y.-Y. & Resnekov, L. Newer catecholamines for treatment of heart failure and shock: an update on dopamine and a first look at dobutamine. *Progress in cardiovascular diseases* **19**, 327-340 (1977).
- 95 SCHUELKE, D. M., MARK, A. L., SCHMID, P. G. & ECKSTEIN, J. W. Coronary vasodilatation produced by dopamine after adrenergic blockade. *Journal of Pharmacology and Experimental Therapeutics* **176**, 320-327 (1971).
- 96 Sonne, J. & Lopez-Ojeda, W. in *StatPearls [Internet]* (StatPearls Publishing, 2019).
- Tuttle, R. R. & Mills, J. Dobutamine: development of a new catecholamine to selectively increase cardiac contractility. *Circulation research* **36**, 185-196 (1975).
- Saleem, S. in *Arrhythmia Induction in the EP Lab* 81-89 (Springer, 2019).
- Robie, N. W. & Goldberg, L. I. Comparative systemic and regional hemodynamic effects of dopamine and dobutamine. *American heart journal* **90**, 340-345 (1975).
- Martens, P. *et al.* Effects of intravenous home dobutamine in palliative end-stage heart failure on quality of life, heart failure hospitalization, and cost expenditure. *ESC heart failure* 5, 562-569 (2018).
- Ruffolo Jr, R. R. The pharmacology of dobutamine. *The American journal of the medical sciences* **294**, 244-248 (1987).
- Akhtar, N., Mikulic, E., Cohn, J. N. & Chaudhry, M. H. Hemodynamic effect of dobutamine in patients with severe heart failure. *The American journal of cardiology* **36**, 202-205 (1975).
- Liu, L. C., Dorhout, B., van der Meer, P., Teerlink, J. R. & Voors, A. A. Omecamtiv mecarbil: a new cardiac myosin activator for the treatment of heart failure. *Expert opinion on investigational drugs* **25**, 117-127 (2016).
- Teerlink, J. R. *et al.* Acute treatment with omecamtiv mecarbil to increase contractility in acute heart failure: the ATOMIC-AHF study. *Journal of the American College of Cardiology* **67**, 1444-1455 (2016).
- 105 Cleland, J. G. *et al.* The effects of the cardiac myosin activator, omecamtiv mecarbil, on cardiac function in systolic heart failure: a double-blind, placebo-controlled, crossover, dose-ranging phase 2 trial. *The Lancet* **378**, 676-683 (2011).
- Zimmerman, J. & Cahalan, M. in *Pharmacology and Physiology for Anesthesia* (eds Hugh C. Hemmings & Talmage D. Egan) 390-404 (W.B. Saunders, 2013).
- 107 Cavigelli-Brunner, A. *et al.* Prevention of Low Cardiac Output Syndrome After Pediatric Cardiac Surgery: A Double-Blind Randomized Clinical Pilot Study Comparing Dobutamine and Milrinone. *Pediatric Critical Care Medicine* **19**, 619-625 (2018).
- 108 Kobayashi, S. *et al.* Addition of a β1-Blocker to Milrinone Treatment Improves Cardiac Function in Patients with Acute Heart Failure and Rapid Atrial Fibrillation. *Cardiology* **142**, 1-8 (2019).

- 109 Cox, Z. L. *et al.* Elevation of plasma milrinone concentrations in stage D heart failure associated with renal dysfunction. *Journal of cardiovascular pharmacology and therapeutics* **18**, 433-438 (2013).
- 110 Xue, A., Dersch-Mills, D., Tsang, C. & Greenway, S. C. Pharmacy Support of a Pediatric Patient Receiving Milrinone at Home. *The Canadian journal of hospital pharmacy* **69**, 415 (2016).
- Lebeis, T. *et al.* Continuation of Beta Blocker Therapy Reduces Hospitalizations in Patients Treated with Milrinone as a Bridge to Transplant. *Journal of Cardiac Failure* **23**, S19-S20 (2017).
- Marius-Nunez, A. L. *et al.* Intermittent inotropic therapy in an outpatient setting: a cost-effective therapeutic modality in patients with refractory heart failure. *American heart journal* **132**, 805-808 (1996).
- 113 Ayres, J. K. & Maani, C. V. in *StatPearls [Internet]* (StatPearls Publishing, 2019).
- 114 Yang, Y. et al. in Principles of Regenerative Medicine 485-504 (Elsevier, 2019).
- 115 Kim, B. Y., Rutka, J. T. & Chan, W. C. Nanomedicine. *The New England journal of medicine* **363**, 2434-2443, doi:10.1056/NEJMra0912273 (2010).
- Freitas Jr, R. A. What is nanomedicine? *Nanomedicine: Nanotechnology, Biology and Medicine* **1**, 2-9 (2005).
- 117 Theochari, C. A. *et al.* Heart transplantation versus left ventricular assist devices as destination therapy or bridge to transplantation for 1-year mortality: a systematic review and meta-analysis. *Annals of cardiothoracic surgery* **7**, 3 (2018).
- Alraies, M. C. & Eckman, P. Adult heart transplant: indications and outcomes. *Journal of thoracic disease* **6**, 1120 (2014).
- FRoM, P. Advanced heart failure: Transplantation, LVADs, and beyond. *Cleveland Clinic journal of medicine* **80**, 33 (2013).
- Serruys, P. W., Kutryk, M. J. & Ong, A. T. Coronary-artery stents. *New England Journal of Medicine* **354**, 483-495 (2006).
- Wolff, G. *et al.* Survival benefits of invasive versus conservative strategies in heart failure in patients with reduced ejection fraction and coronary artery disease: a meta-analysis. *Circulation: Heart Failure* **10**, e003255 (2017).
- Hawranek, M. *et al.* Comparison of coronary artery bypass grafting and percutaneous coronary intervention in patients with heart failure with reduced ejection fraction and multivessel coronary artery disease. *Oncotarget* **9**, 21201 (2018).
- Miragoli, M. *et al.* Inhalation of peptide-loaded nanoparticles improves heart failure. *Science translational medicine* **10**, eaan6205 (2018).
- Shi, D., Sadat, M., Dunn, A. W. & Mast, D. B. Photo-fluorescent and magnetic properties of iron oxide nanoparticles for biomedical applications. *Nanoscale* **7**, 8209-8232 (2015).
- Dvir, T. *et al.* Nanowired three-dimensional cardiac patches. *Nature nanotechnology* **6**, 720 (2011).
- Kumar, A. *et al.* Innovative pharmaceutical development based on unique properties of nanoscale delivery formulation. *Nanoscale* **5**, 8307-8325, doi:10.1039/c3nr01525d (2013).
- 127 Anand, P. et al. (Elsevier, 2010).
- Manjunath, K. & Venkateswarlu, V. Pharmacokinetics, tissue distribution and bioavailability of clozapine solid lipid nanoparticles after intravenous and intraduodenal administration. *Journal of Controlled Release* **107**, 215-228 (2005).

- 129 Kumar, P., Lakshmi, Y. S., Bhaskar, C., Golla, K. & Kondapi, A. K. Improved safety, bioavailability and pharmacokinetics of zidovudine through lactoferrin nanoparticles during oral administration in rats. *PloS one* **10**, e0140399 (2015).
- 130 Yoo, H. S., Oh, J. E., Lee, K. H. & Park, T. G. Biodegradable nanoparticles containing doxorubicin-PLGA conjugate for sustained release. *Pharmaceutical research* **16**, 1114-1118 (1999).
- Zale, S. E., Troiano, G., Ali, M. M., Hrkach, J. & Wright, J. (Google Patents, 2016).
- Fang, R. *et al.* Sustained co-delivery of BIO and IGF-1 by a novel hybrid hydrogel system to stimulate endogenous cardiac repair in myocardial infarcted rat hearts. *International journal of nanomedicine* **10**, 4691 (2015).
- Beddoes, C. M., Case, C. P. & Briscoe, W. H. Understanding nanoparticle cellular entry: a physicochemical perspective. *Advances in colloid and interface science* **218**, 48-68 (2015).
- Murugan, K. *et al.* Parameters and characteristics governing cellular internalization and trans-barrier trafficking of nanostructures. *International journal of nanomedicine* **10**, 2191-2206, doi:10.2147/IJN.S75615 (2015).
- Shin, S., Song, I. & Um, S. Role of physicochemical properties in nanoparticle toxicity. *Nanomaterials* **5**, 1351-1365 (2015).
- Fonseca, C., Simoes, S. & Gaspar, R. Paclitaxel-loaded PLGA nanoparticles: preparation, physicochemical characterization and in vitro anti-tumoral activity. *Journal of controlled release* **83**, 273-286 (2002).
- Lundy, D. J., Chen, K.-H., Toh, E. K.-W. & Hsieh, P. C.-H. Distribution of systemically administered nanoparticles reveals a size-dependent effect immediately following cardiac ischaemia-reperfusion injury. *Sci Rep* **6**, 25613 (2016).
- García-Álvarez, R., Hadjidemetriou, M., Sánchez-Iglesias, A., Liz-Marzán, L. M. & Kostarelos, K. In vivo formation of protein corona on gold nanoparticles. The effect of their size and shape. *Nanoscale* **10**, 1256-1264 (2018).
- 139 Xu, J. et al. Dose Dependencies and Biocompatibility of Renal Clearable Gold Nanoparticles: From Mice to Non-human Primates. Angewandte Chemie International Edition 57, 266-271 (2018).
- Roh, Y. G. *et al.* Protein Nanoparticle Fabrication for Optimized Reticuloendothelial System Evasion and Tumor Accumulation. *Langmuir* **35**, 3992-3998 (2019).
- 141 Xiao, K. *et al.* The effect of surface charge on in vivo biodistribution of PEG-oligocholic acid based micellar nanoparticles. *Biomaterials* **32**, 3435-3446 (2011).
- Blanco, E., Shen, H. & Ferrari, M. Principles of nanoparticle design for overcoming biological barriers to drug delivery. *Nature biotechnology* **33**, 941 (2015).
- 143 Cho, E. C., Xie, J., Wurm, P. A. & Xia, Y. Understanding the role of surface charges in cellular adsorption versus internalization by selectively removing gold nanoparticles on the cell surface with a I2/KI etchant. *Nano letters* **9**, 1080-1084 (2009).
- Salatin, S., Maleki Dizaj, S. & Yari Khosroushahi, A. Effect of the surface modification, size, and shape on cellular uptake of nanoparticles. *Cell biology international* **39**, 881-890 (2015).
- Blanco, E., Shen, H. & Ferrari, M. Principles of nanoparticle design for overcoming biological barriers to drug delivery. *Nature biotechnology* **33**, 941-951, doi:10.1038/nbt.3330 (2015).

- Li, M.-C. *et al.* Cellulose nanoparticles: structure–morphology–rheology relationships. *ACS Sustainable Chemistry & Engineering* **3**, 821-832 (2015).
- Zhu, X., Vo, C., Taylor, M. & Smith, B. R. Non-spherical micro-and nanoparticles in nanomedicine. *Materials Horizons* (2019).
- Truong, N. P., Whittaker, M. R., Mak, C. W. & Davis, T. P. The importance of nanoparticle shape in cancer drug delivery. *Expert opinion on drug delivery* **12**, 129-142 (2015).
- Xue, J. *et al.* Cellular Internalization of Rod-Like Nanoparticles with Various Surface Patterns: Novel Entry Pathway and Controllable Uptake Capacity. *small* **13**, 1604214 (2017).
- Zhao, J. *et al.* Influence of nanoparticle shapes on cellular uptake of paclitaxel loaded nanoparticles in 2D and 3D cancer models. *Polymer Chemistry* **8**, 3317-3326 (2017).
- Vácha, R., Martinez-Veracoechea, F. J. & Frenkel, D. Receptor-mediated endocytosis of nanoparticles of various shapes. *Nano letters* **11**, 5391-5395 (2011).
- 152 Iversen, T.-G., Skotland, T. & Sandvig, K. Endocytosis and intracellular transport of nanoparticles: present knowledge and need for future studies. *Nano today* **6**, 176-185 (2011).
- Zhang, S., Gao, H. & Bao, G. Physical principles of nanoparticle cellular endocytosis. *ACS nano* **9**, 8655-8671 (2015).
- Lim, J. P. & Gleeson, P. A. Macropinocytosis: an endocytic pathway for internalising large gulps. *Immunology and cell biology* **89**, 836-843, doi:10.1038/icb.2011.20 (2011).
- Gilleron, J. *et al.* Image-based analysis of lipid nanoparticle-mediated siRNA delivery, intracellular trafficking and endosomal escape. *Nat Biotechnol* **31**, 638-646, doi:10.1038/nbt.2612 (2013).
- Wong, H. L. *et al.* A mechanistic study of enhanced doxorubicin uptake and retention in multidrug resistant breast cancer cells using a polymer-lipid hybrid nanoparticle system. *The Journal of pharmacology and experimental therapeutics* **317**, 1372-1381, doi:10.1124/jpet.106.101154 (2006).
- Aderem, A. & Underhill, D. M. Mechanisms of phagocytosis in macrophages. *Annual review of immunology* **17**, 593-623, doi:10.1146/annurev.immunol.17.1.593 (1999).
- Suen, W. L. L. & Chau, Y. Size-dependent internalisation of folate-decorated nanoparticles via the pathways of clathrin and caveolae-mediated endocytosis in ARPE-19 cells. *Journal of Pharmacy and Pharmacology* **66**, 564-573 (2014).
- Wei, X. *et al.* Mechanical cues modulate cellular uptake of nanoparticles in cancer via clathrin-mediated and caveolae-mediated endocytosis pathways. *Nanomedicine* **14**, 613-626 (2019).
- Ng, C. T. *et al.* Clathrin-Mediated Endocytosis of Gold Nanoparticles In Vitro. *The Anatomical Record* **298**, 418-427 (2015).
- Behzadi, S. *et al.* Cellular uptake of nanoparticles: journey inside the cell. *Chemical Society Reviews* **46**, 4218-4244 (2017).
- Pelkmans, L. & Helenius, A. Endocytosis via caveolae. *Traffic* **3**, 311-320 (2002).
- Wu, C. *et al.* Endosomal/lysosomal location of organically modified silica nanoparticles following caveolae-mediated endocytosis. *RSC Advances* **9**, 13855-13862 (2019).
- Wang, Z., Tiruppathi, C., Minshall, R. D. & Malik, A. B. Size and dynamics of caveolae studied using nanoparticles in living endothelial cells. *ACS nano* **3**, 4110-4116 (2009).

- Kim, H. R. *et al.* Low-density lipoprotein receptor-mediated endocytosis of PEGylated nanoparticles in rat brain endothelial cells. *Cellular and molecular life sciences* **64**, 356-364 (2007).
- Gupta, A. K., Berry, C., Gupta, M. & Curtis, A. Receptor-mediated targeting of magnetic nanoparticles using insulin as a surface ligand to prevent endocytosis. *IEEE transactions on nanobioscience* **2**, 255-261 (2003).
- Yi, X. & Gao, H. Kinetics of receptor-mediated endocytosis of elastic nanoparticles. *Nanoscale* **9**, 454-463 (2017).
- Ding, H.-m. & Ma, Y.-q. Role of physicochemical properties of coating ligands in receptor-mediated endocytosis of nanoparticles. *Biomaterials* **33**, 5798-5802 (2012).
- Yuan, H. & Zhang, S. Effects of particle size and ligand density on the kinetics of receptor-mediated endocytosis of nanoparticles. *Applied Physics Letters* **96**, 033704 (2010).
- 170 Sperling, R. A. & Parak, W. J. Surface modification, functionalization and bioconjugation of colloidal inorganic nanoparticles. *Philosophical Transactions of the Royal Society A: Mathematical, Physical and Engineering Sciences* **368**, 1333-1383 (2010).
- O'Reilly, R. K., Joralemon, M. J., Wooley, K. L. & Hawker, C. J. Functionalization of micelles and shell cross-linked nanoparticles using click chemistry. *Chemistry of materials* **17**, 5976-5988 (2005).
- Zhang, K., Fang, H., Chen, Z., Taylor, J.-S. A. & Wooley, K. L. Shape effects of nanoparticles conjugated with cell-penetrating peptides (HIV Tat PTD) on CHO cell uptake. *Bioconjugate chemistry* **19**, 1880-1887 (2008).
- Fang, Y. *et al.* Targeted glioma chemotherapy by cyclic RGD peptide-functionalized reversibly core-crosslinked multifunctional poly (ethylene glycol)-b-poly (ε-caprolactone) micelles. *Acta biomaterialia* **50**, 396-406 (2017).
- Swami, A. et al. in Multifunctional nanoparticles for drug delivery applications 9-29 (Springer, 2012).
- 175 Chen, B., He, X. Y., Yi, X. Q., Zhuo, R. X. & Cheng, S. X. Dual-peptide-functionalized albumin-based nanoparticles with ph-dependent self-assembly behavior for drug delivery. *ACS applied materials & interfaces* **7**, 15148-15153, doi:10.1021/acsami.5b03866 (2015).
- Ji, S. *et al.* RGD-conjugated albumin nanoparticles as a novel delivery vehicle in pancreatic cancer therapy. *Cancer biology & therapy* **13**, 206-215 (2012).
- Dvir, T. *et al.* Nanoparticles targeting the infarcted heart. *Nano letters* **11**, 4411-4414 (2011).
- Hennig, R., Pollinger, K., Tessmar, J. & Goepferich, A. Multivalent targeting of AT1 receptors with angiotensin II-functionalized nanoparticles. *J Drug Target* **23**, 681-689, doi:10.3109/1061186x.2015.1035276 (2015).
- Paulis, L. E. *et al.* Distribution of lipid-based nanoparticles to infarcted myocardium with potential application for MRI-monitored drug delivery. *Journal of controlled release* **162**, 276-285 (2012).
- Mavila, S., Eivgi, O., Berkovich, I. & Lemcoff, N. G. Intramolecular cross-linking methodologies for the synthesis of polymer nanoparticles. *Chemical reviews* **116**, 878-961 (2015).

- 181 Cañaveras, F., Madueño, R., Sevilla, J. M., Blázquez, M. & Pineda, T. Role of the functionalization of the gold nanoparticle surface on the formation of bioconjugates with human serum albumin. *The Journal of Physical Chemistry C* **116**, 10430-10437 (2012).
- Pelaz, B. *et al.* Surface Functionalization of Nanoparticles with Polyethylene Glycol: Effects on Protein Adsorption and Cellular Uptake. *ACS Nano* **9**, 6996-7008, doi:10.1021/acsnano.5b01326 (2015).
- Dai, Q., Walkey, C. & Chan, W. C. Polyethylene glycol backfilling mitigates the negative impact of the protein corona on nanoparticle cell targeting. *Angewandte Chemie International Edition* **53**, 5093-5096 (2014).
- Hak, S. *et al.* The effect of nanoparticle polyethylene glycol surface density on ligand-directed tumor targeting studied in vivo by dual modality imaging. *ACS nano* **6**, 5648-5658 (2012).
- Salvati, A. *et al.* Transferrin-functionalized nanoparticles lose their targeting capabilities when a biomolecule corona adsorbs on the surface. *Nature Nanotechnology* **8**, 137, doi:10.1038/nnano.2012.237
- https://www.nature.com/articles/nnano.2012.237#supplementary-information (2013).
- Maffre, P. *et al.* Effects of surface functionalization on the adsorption of human serum albumin onto nanoparticles—a fluorescence correlation spectroscopy study. *Beilstein journal of nanotechnology* **5**, 2036-2047 (2014).
- 187 Can, K., Ozmen, M. & Ersoz, M. Immobilization of albumin on aminosilane modified superparamagnetic magnetite nanoparticles and its characterization. *Colloids and Surfaces B: Biointerfaces* **71**, 154-159 (2009).
- Patil, Y. B., Toti, U. S., Khdair, A., Ma, L. & Panyam, J. Single-step surface functionalization of polymeric nanoparticles for targeted drug delivery. *Biomaterials* **30**, 859-866 (2009).
- Feng, L. *et al.* Polyethylene glycol and polyethylenimine dual-functionalized nanographene oxide for photothermally enhanced gene delivery. *Small* **9**, 1989-1997 (2013).
- 190 Elzoghby, A. O., Samy, W. M. & Elgindy, N. A. Albumin-based nanoparticles as potential controlled release drug delivery systems. *Journal of controlled release* **157**, 168-182 (2012).
- 191 Carter, D. C. & Ho, J. X. Structure of serum albumin. *Advances in protein chemistry* **45**, 153-203 (1994).
- Fasano, M. *et al.* The extraordinary ligand binding properties of human serum albumin. *IUBMB life* **57**, 787-796 (2005).
- Lomis, N. *et al.* Human Serum Albumin Nanoparticles for Use in Cancer Drug Delivery: Process Optimization and In Vitro Characterization. *Nanomaterials* **6**, 116 (2016).
- Sebak, S., Mirzaei, M., Malhotra, M., Kulamarva, A. & Prakash, S. Human serum albumin nanoparticles as an efficient noscapine drug delivery system for potential use in breast cancer: preparation and in vitro analysis. *International journal of nanomedicine* 5, 525 (2010).
- Baroni, S. *et al.* Effect of ibuprofen and warfarin on the allosteric properties of haemhuman serum albumin: a spectroscopic study. *European journal of biochemistry* **268**, 6214-6220 (2001).
- Petersen, C. E., Ha, C. E., Curry, S. & Bhagavan, N. V. Probing the structure of the warfarin-binding site on human serum albumin using site-directed mutagenesis. *Proteins: Structure, Function, and Bioinformatics* **47**, 116-125 (2002).

- Li, J. & Yao, P. Self-assembly of ibuprofen and bovine serum albumin—dextran conjugates leading to effective loading of the drug. *Langmuir* **25**, 6385-6391 (2009).
- Steiner, R., Roth, J. & Robbins, J. The binding of thyroxine by serum albumin as measured by fluorescence quenching. *Journal of Biological Chemistry* **241**, 560-567 (1966).
- 199 Petitpas, I. *et al.* Structural basis of albumin–thyroxine interactions and familial dysalbuminemic hyperthyroxinemia. *Proceedings of the National Academy of Sciences* **100**, 6440-6445 (2003).
- Schnitzer, J., Sung, A., Horvat, R. & Bravo, J. Preferential interaction of albumin-binding proteins, gp30 and gp18, with conformationally modified albumins. Presence in many cells and tissues with a possible role in catabolism. *Journal of Biological Chemistry* **267**, 24544-24553 (1992).
- Merlot, A. M., Kalinowski, D. S. & Richardson, D. R. Unraveling the mysteries of serum albumin—more than just a serum protein. *Frontiers in physiology* **5**, 299 (2014).
- Schnitzer, J. gp60 is an albumin-binding glycoprotein expressed by continuous endothelium involved in albumin transcytosis. *American Journal of Physiology-Heart and Circulatory Physiology* **262**, H246-H254 (1992).
- Tiruppathi, C., Song, W., Bergenfeldt, M., Sass, P. & Malik, A. B. Gp60 activation mediates albumin transcytosis in endothelial cells by tyrosine kinase-dependent pathway. *Journal of Biological Chemistry* **272**, 25968-25975 (1997).
- Langer, K. *et al.* Optimization of the preparation process for human serum albumin (HSA) nanoparticles. *International Journal of Pharmaceutics* **257**, 169-180 (2003).
- Von Storp, B., Engel, A., Boeker, A., Ploeger, M. & Langer, K. Albumin nanoparticles with predictable size by desolvation procedure. *Journal of microencapsulation* **29**, 138-146 (2012).
- 206 Langer, K. et al. Human serum albumin (HSA) nanoparticles: reproducibility of preparation process and kinetics of enzymatic degradation. *International journal of* pharmaceutics 347, 109-117 (2008).
- 207 Crisante, F. *et al.* Antibiotic delivery polyurethanes containing albumin and polyallylamine nanoparticles. *european journal of pharmaceutical sciences* **36**, 555-564 (2009).
- Lee, J. Y., Bae, K. H., Kim, J. S., Nam, Y. S. & Park, T. G. Intracellular delivery of paclitaxel using oil-free, shell cross-linked HSA–multi-armed PEG nanocapsules. *Biomaterials* **32**, 8635-8644 (2011).
- Yu, S., Yao, P., Jiang, M. & Zhang, G. Nanogels prepared by self-assembly of oppositely charged globular proteins. *Biopolymers: Original Research on Biomolecules* **83**, 148-158 (2006).
- Qi, J., Yao, P., He, F., Yu, C. & Huang, C. Nanoparticles with dextran/chitosan shell and BSA/chitosan core—doxorubicin loading and delivery. *International journal of pharmaceutics* **393**, 177-185 (2010).
- Lee, S. H., Heng, D., Ng, W. K., Chan, H.-K. & Tan, R. B. Nano spray drying: a novel method for preparing protein nanoparticles for protein therapy. *International journal of pharmaceutics* **403**, 192-200 (2011).
- Faheem, A. & Haggag, Y. Evaluation of nano spray drying as a method for drying and formulation of therapeutic peptides and proteins. *Frontiers in pharmacology* **6**, 140 (2015).

- Desai, N. Nanoparticle albumin bound (nab) technology: targeting tumors through the endothelial gp60 receptor and SPARC. *Nanomedicine: nanotechnology, biology, and medicine* **4**, 339 (2007).
- Cortes, J. & Saura, C. Nanoparticle albumin-bound (nabTM)-paclitaxel: improving efficacy and tolerability by targeted drug delivery in metastatic breast cancer. *European Journal of Cancer Supplements* **8**, 1-10 (2010).
- Fu, Q. et al. Nanoparticle albumin-bound (NAB) technology is a promising method for anti-cancer drug delivery. Recent patents on anti-cancer drug discovery 4, 262-272 (2009).
- Xu, R., Fisher, M. & Juliano, R. Targeted albumin-based nanoparticles for delivery of amphipathic drugs. *Bioconjugate chemistry* **22**, 870-878 (2011).
- Look, J. *et al.* Ligand-Modified Human Serum Albumin Nanoparticles for Enhanced Gene Delivery. *Molecular Pharmaceutics* **12**, 3202-3213, doi:10.1021/acs.molpharmaceut.5b00153 (2015).
- Karmali, P. P. *et al.* Targeting of albumin-embedded paclitaxel nanoparticles to tumors. *Nanomedicine: Nanotechnology, Biology and Medicine* **5**, 73-82 (2009).
- Gheorghiade, M., van Veldhuisen, D. J. & Colucci, W. S. Contemporary use of digoxin in the management of cardiovascular disorders. *Circulation* **113**, 2556-2564, doi:10.1161/circulationaha.105.560110 (2006).
- 220 Hauptman, P. J. & Kelly, R. A. Digitalis. *Circulation* **99**, 1265-1270 (1999).
- Palaparthy, R. *et al.* Relative bioavailability, food effect, and safety of the single-dose pharmacokinetics of omecamtiv mecarbil following administration of different modified-release formulations in healthy subjects. *Int J Clin Pharmacol Ther* **54**, 217-227, doi:10.5414/CP202458 (2016).
- Velazquez, E. J. *et al.* Coronary-artery bypass surgery in patients with left ventricular dysfunction. *New England Journal of Medicine* **364**, 1607-1616 (2011).
- Desai, P. P., Date, A. A. & Patravale, V. B. Overcoming poor oral bioavailability using nanoparticle formulations—opportunities and limitations. *Drug Discovery Today: Technologies* **9**, e87-e95 (2012).
- Edelson, J. *et al.* Pharmacokinetics of the bipyridines amrinone and milrinone. *Circulation* **73**, III145-152 (1986).
- Lee, E. S. & Youn, Y. S. Albumin-based potential drugs: focus on half-life extension and nanoparticle preparation. *Journal of Pharmaceutical Investigation* **46**, 305-315 (2016).
- Zhang, H., Chen, B. & Banfield, J. F. Particle size and pH effects on nanoparticle dissolution. *The Journal of Physical Chemistry C* **114**, 14876-14884 (2010).
- Hogues, H., Sulea, T. & Purisima, E. O. Exhaustive docking and solvated interaction energy scoring: lessons learned from the SAMPL4 challenge. *Journal of computer-aided molecular design* **28**, 417-427 (2014).
- Al Kindi, H. *et al.* Sustained release of milrinone delivered via microparticles in a rodent model of myocardial infarction. *The Journal of thoracic and cardiovascular surgery* **148**, 2316-2324 (2014).
- Zhang, H. *et al.* A comparison study of pharmacokinetics between bufalin-loaded bovine serum albumin nanoparticles and bufalin in rats. *Zhong xi yi jie he xue bao= Journal of Chinese integrative medicine* **10**, 674-680 (2012).

- Wang, W. *et al.* Pharmacokinetics and tissue distribution of folate-decorated human serum albumin loaded with nano-hydroxycamptothecin for tumor targeting. *Journal of pharmaceutical sciences* **105**, 1874-1880 (2016).
- Udani, S. M. & Koyner, J. L. The effects of heart failure on renal function. *Cardiology clinics* **28**, 453-465 (2010).
- Jose, P. *et al.* Increase in creatinine and cardiovascular risk in patients with systolic dysfunction after myocardial infarction. *Journal of the American Society of Nephrology* **17**, 2886-2891 (2006).
- 233 Agrahari, V. & Hiremath, P. (Future Medicine, 2017).
- 234 Min, Y., Caster, J. M., Eblan, M. J. & Wang, A. Z. Clinical translation of nanomedicine. *Chemical reviews* **115**, 11147-11190 (2015).
- 235 Cho, W.-S. *et al.* Acute toxicity and pharmacokinetics of 13 nm-sized PEG-coated gold nanoparticles. *Toxicology and applied pharmacology* **236**, 16-24 (2009).
- Kim, J. S. *et al.* Toxicity and tissue distribution of magnetic nanoparticles in mice. *Toxicological Sciences* **89**, 338-347 (2005).
- Friedman, A. D., Claypool, S. E. & Liu, R. The smart targeting of nanoparticles. *Current pharmaceutical design* **19**, 6315-6329 (2013).
- Dixit, V., Van den Bossche, J., Sherman, D. M., Thompson, D. H. & Andres, R. P. Synthesis and grafting of thioctic acid—PEG—folate conjugates onto Au nanoparticles for selective targeting of folate receptor-positive tumor cells. *Bioconjugate chemistry* 17, 603-609 (2006).
- Ferreira, M. P. *et al.* Drug-Loaded Multifunctional Nanoparticles Targeted to the Endocardial Layer of the Injured Heart Modulate Hypertrophic Signaling. *Small* **13**, 1701276 (2017).
- 240 Kamaly, N., Xiao, Z., Valencia, P. M., Radovic-Moreno, A. F. & Farokhzad, O. C. Targeted polymeric therapeutic nanoparticles: design, development and clinical translation. *Chemical Society Reviews* 41, 2971-3010 (2012).
- 241 Hill, S. Pharmacokinetics of drug infusions. *Continuing education in anaesthesia, critical care & Pain* **4**, 76-80 (2004).
- Guengerich, F. P. Mechanisms of drug toxicity and relevance to pharmaceutical development. *Drug metabolism and pharmacokinetics*, 1010210090-1010210090 (2010).
- Junyaprasert, V. B. & Morakul, B. Nanocrystals for enhancement of oral bioavailability of poorly water-soluble drugs. *asian journal of pharmaceutical sciences* **10**, 13-23 (2015).
- 244 Rodriguez-Aller, M., Guillarme, D., Veuthey, J.-L. & Gurny, R. Strategies for formulating and delivering poorly water-soluble drugs. *Journal of Drug Delivery Science and Technology* **30**, 342-351 (2015).
- 245 Maggi, L., Machiste, E. O., Torre, M. L. & Conte, U. Formulation of biphasic release tablets containing slightly soluble drugs. *European journal of pharmaceutics and biopharmaceutics* **48**, 37-42 (1999).
- Godin, B. *et al.* Emerging applications of nanomedicine for the diagnosis and treatment of cardiovascular diseases. *Trends in pharmacological sciences* **31**, 199-205 (2010).
- 247 Lombardo, D., Kiselev, M. A. & Caccamo, M. T. Smart nanoparticles for drug delivery application: development of versatile nanocarrier platforms in biotechnology and nanomedicine. *Journal of Nanomaterials* **2019** (2019).

- Patra, J. K. *et al.* Nano based drug delivery systems: recent developments and future prospects. *Journal of nanobiotechnology* **16**, 71 (2018).
- Miele, E., Spinelli, G. P., Miele, E., Tomao, F. & Tomao, S. Albumin-bound formulation of paclitaxel (Abraxane® ABI-007) in the treatment of breast cancer. *International journal of nanomedicine* **4**, 99 (2009).
- Barenholz, Y. Doxil(R)--the first FDA-approved nano-drug: lessons learned. *Journal of controlled release: official journal of the Controlled Release Society* **160**, 117-134, doi:10.1016/j.jconrel.2012.03.020 (2012).